AGH UNIVERSITY OF SCIENCE AND TECHNOLOGY

THE FACULTY OF ELECTRICAL ENGINEERING, AUTOMATICS, COMPUTER SCIENCE AND BIOMEDICAL ENGINEERING

DEPARTMENT OF POWER ELECTRONICS AND ENERGY CONTROL SYSTEMS

Ph. D. Thesis

Research on the Hex-Y Modular Multilevel Converter Topology for Low Speed Drives

Author: *M. Sc. Eng. Paweł Błaszczyk*
Degree programme: *Power Electronics*
Supervisor: *D. Sc. Ph. Eng. Stanisław Piróg*

Kraków, 2020
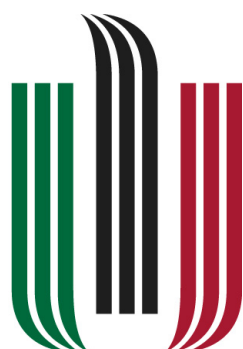
AKADEMIA GÓRNICZO-HUTNICZA IM. STANISŁAWA STASZICA W KRAKOWIE

WYDZIAŁ ELEKTROTECHNIKI, AUTOMATYKI, INFORMATYKI I INŻYNIERII BIOMEDYCZNEJ

KATEDRA ENERGOELEKTRONIKI I AUTOMATYKI SYSTEMÓW PRZETWARZANIA ENERGII

Rozprawa Doktorska

Badanie zastosowania topologii przekształtnika wielopoziomowego typu Hex-Y w aplikacji napędów bezpośrednich niskich częstotliwości.

Autor: *Mgr inż. Paweł Błaszczyk*
Dyscyplina naukowa: *Elektrotechnika*
Promotor: *Prof. dr hab. inż. Stanisław Piróg*

Kraków, 2020

Table of Content

List of Abbreviations

AC	Alternative Current
ARU	Active Rectifier Unit
BESS	Battery Energy Storage System
BRB	Branch Balancing
BRI	Branch Current Control
CCC	Circulating Current Calculation
CEC	Converter Energy Control
CS	Current Source
DC	Direct Current
DOF	Degrees of Freedom
DSP	Digital Signal Processor
EMT	Electromagnetic Transient
ESS	Energy Storage System
FB	Full Bridge
FW	Firmware
HAT	Harmonic Addition Theorem
HB	Half Bridge
HVDC	High-Voltage DC
HW	Hardware
I-MMC	Indirect AC-DC-AC MMC Topology
IGBT	Insulated Gate Bipolar Transistor
INU	Inverter Unit
IP	Intelectual Property
ISR	Interrupt Service Routine
KCL	Kirchhoff's Current Law
KVL	Kirchhoff's Voltage Law
LVRT	Low Voltage Ride Through
M3C	Modular Multilevel Matrix Converter. Also MMMC

MMC	Modular Multilevel Conversion or Modular Multilevel Converter
MOD	Scale to Modulation Index
MVDC	Medium-Voltage DC
NLM	Nearest Level Modulation
NPC	Neutral Point Clamped
PEBB	Power Electronics Building Block
PEC	Power Electronics Controller ®
PECMI	PEC Measuring Interface ®
PFC	Power Factor Correction
PLL	Phase-Locked Loop
POF	Plastic Optical Fiber
PWM	Pulse Width Modulation
REF	Reference Generator
RMS	Root Mean Square
SBI	System-Branch Current Mapping
SBV	System-Branch Voltage Mapping
SHE	Selective Harmonic Elimination
STATCOM	Static Synchronous Compensator
SVM	Space Vector Modulation
SW	Software
VS	Voltage Source

List of Symbols

N Number of series connected cells in a branch

P_s Active power component from the system s $[W]$ (see p. 75)

$P_{s,tot}$ Total active power from the system s $[W]$ (see p. 75)

$P_{x1a,b}$ Power related with current circulating with ω_1 frequency with index x in $\alpha - \beta$ referenece frame (see p. 83)

$P_{xca,b}$ Power related with current circulating with ω_c frequency with index x in $\alpha - \beta$ referenece frame (see p. 89)

Q_s Reactive power component from the system s $[Var]$ (see p. 75)

$Q_{s,tot}$ Total reactive power from the system s $[Var]$ (see p. 75)

S_s Apparent power component from the system s $[VA]$ (see p. 75)

$S_{s,tot}$ Total apparent power from the system s $[VA]$ (see p. 75)

V_{sm} Voltage amplitude (peak) on the system s $[V]$

ω Angular Frequency $[rad/s]$

ϕ Load angle $[rad]$

$\boldsymbol{A}$ In Chapter 3: Node matrix describing electrical circuit $[x \times b]$ (see p. 54)

$\boldsymbol{B}$ In Chapter 3: Mesh matrix describing electrical circuit $[n \times b]$ (see p. 54)

$\boldsymbol{E}$ Branch voltage sources vector $[b \times 1]$ (see p. 55)

$\boldsymbol{I_{c1}}$ Circulating current ω_1-frequency components $[6 \times 1]$ (see p. 85)

$\boldsymbol{I_{cc}}$ Circulating current ω_c-frequency components $[3 \times 1]$ (see p. 92)

$\boldsymbol{I}$ Branch currents vector $[b \times 1]$ (see p. 55)

$\boldsymbol{P_0}$ Constant part of the branch powers (p_b) vector $[9 \times 1]$ (see p. 78)

$\boldsymbol{P_{S,k}}$ System powers vector $[6 \times 1]$ (n varies between versions) (see p. 83)

$\boldsymbol{P_{c,k}}$ Circulating powers vector $[n \times 1]$ (n varies between versions) (see p. 83)

$\boldsymbol{P_{c1}}$ Circulating power ω_1-frequency components $[6 \times 1]$ (see p. 84)

$\boldsymbol{P_{cc}}$ Circulating power ω_c-frequency components $[3 \times 1]$ (see p. 90)

$\boldsymbol{P_{ref}}$ Reference of the constant parts in the branch powers vector $[9 \times 1]$, k-th version (see p. 83)

$\boldsymbol{T_{PS,k}}$	System power influence matrix $[9 \times 6]$ (see p. 83)
$\boldsymbol{T_{Pc,k}}$	Circulating power influence matrix $[9 \times n]$ (n varies between versions) (see p. 83)
$\boldsymbol{T_{i,\alpha\beta-br}}$	Phase-branch current mapping matrix. Phases in $\alpha-\beta$ cooridinate system $[9 \times 7]$ (see p. 67)
$\boldsymbol{T_{i,abc-br}}$	Phase-branch current mapping matrix $[9 \times 9]$ (see p. 65)
$\boldsymbol{T_{i,br-abc}}$	Branch-phase current mapping matrix $[9 \times 9]$ (see p. 65)
$\boldsymbol{T_{v,\alpha\beta-br}}$	Phase-branch voltage mapping matrix. Phases in $\alpha - \beta$ cooridinate system $[9 \times 7]$ (see p. 70)
$\boldsymbol{T_{v,abc-br}}$	Phase-branch voltage mapping matrix $[9 \times 9]$ (see p. 69)
$\boldsymbol{V}$	Branch voltage drops vector $[b \times 1]$ (see p. 55)
$\boldsymbol{Z_d}$	Diagonal impedance matrix $[b \times b]$ (see p. 55)
$\boldsymbol{Z}$	Branch impedance matrix $[b \times b]$ (see p. 55)
$\boldsymbol{i_b}$	Branch currents vector $[9 \times 1]$ (see p. 65)
$\boldsymbol{i'_o}$	Output currents vector (3 phase representation) $[7 \times 1]$ (see p. 65)
$\boldsymbol{i_o}$	Output (terminal) currents vector ($\alpha - \beta$ representation) $[9 \times 1]$ (see p. 66)
$\boldsymbol{v_b}$	Branch voltages vector $[9 \times 1]$ (see p. 122)
$\boldsymbol{v'_o}$	Output voltages vector (3 phase representation) $[6 \times 1]$ (see p. 69)
$\boldsymbol{v_o}$	Output voltages vector ($\alpha - \beta$ representation) $[8 \times 1]$ (see p. 70)
ψ	Initial phase shift $[rad]$
b	In Chapter 3: Number of branches in the electrical circuit (see p. 52)
	In all chapters: branch number ($b = 1...9$)
e_b	Branch energy
$e_{b,0}$	Branch energy contstant part
f	Frequency $[Hz]$
i_b	Branch current
i_{cx}	Circulating current ($x = 1...3$) $[A]$
j	Unit imaginary number ($j^2 = -1$)
n	Number of mesh currents in the electrical circuit (see p. 52)
p_b	Branch power
v_N	Neutral point / common mode voltage $[V]$
v_X	Star point voltage $[V]$
v_b	Branch voltage
x	Number of vertexes in the electrical circuit (see p. 52)

List of Subscripts

0	Initial value or constant component of given equation
H	Component related only for Hex part of the Hex-Y
N	Neutral point (voltage, current or power)
S	System-related quantity (inptur or output)
X	Star point (voltage, current or power)
Y	Component related only for Y part of the Hex-Y
α, β	α and β components (rotating reference frame)
b	Branch
c	Circulating. Also quantity related to the component with frequency ω_c
k, l	Counter index
m	Peak value
n	Branch index. For Hex-Y topology $n = 1...6$ for Hex branches and $n = 7...9$ for Y-branches
o	Output (terminal) quantity
p	Phase number ($p = 1...3$)
s	System index. $s = 1$ for input (terminals R, S, T), $s = 2$ for output (terminals U, V, W)
x	Circulating current index ($x = 1...3$)

Naming Convention

Following convention in symbols naming has been used in the Thesis:

x – lowercase defines function of variable x, i.e. $x \equiv x(t)$

X – uppercase symbol defines RMS value of variable x. Uppercase is also used to define constant values

X_m – uppercase symbol with subscript m defines peak (maximum) of variable x

$\boldsymbol{x}$ – bold symbol defines matrix. Complex numbers which are treated as two-element vectors are also marked bold in the Thesis.

1. Introduction

Modular Multilevel Cascaded Converters (Cascaded MMC) finds use in industry since 2010 while first commercial application using that topology has been used (HVDC transmission system)[1, 2]. The Trans Bay Cable project, USA proved that MMC converters are capable for high power transfer and has advantages over other technologies.

Currently, cascaded MMC are being studied to be used in MVDC grids, direct low and high-speed drives and renewable energy applications. Its advantages as reliability, low footprint (as voltage quality for multiple levels is high, so external bulky filters are obsolete), or high efficiency due to low switching frequency.

In this Thesis, a new converter topology called Hex-Y has been proposed. Converter's topology can couple two three-phase circuits. The topology is built with nine arms as Matrix Converter, which cascaded MMC version (M3C) was proposed by Erickson and Al-Naseem in 2001 [3]. The difference between two converter topologies is a branch arrangement.

The goal of the Thesis, is to present and analyze a new MMC converter topology and research its behavior, especially in a low output frequency operation point (up to $5\ Hz$). Given operation point is used in applications as direct drives or power generation from low-speed gearless wind generators. Given topology has been compared with M3C. Additionally, reactive power provision capability has been investigated.

The Thesis is organized as follows:

Chapter 2 contains state of the art in MMC area. Existing converter topologies has been summarized. Additionally, power module designed by ABB has been described (topology, power electronics and control components).

Chapter 3 contains description of Hex-Y topology proposed by author first time in 2018 [4]. Structural matrices for a topology has been calculated and used for phasor analysis of voltages and currents in the system. Also, circulating currents phenomenon has been explained and highlighted.

Additionally, following chapter contains a method how to „translate" voltages and currents in branches to corresponding quantities observed at converter terminals. So called branch-terminal and terminal-branch mapping has been shown.

In the **Chapter 4**, power calculations for each branch has been shown. Calculation results shows that without introduction of specific circulating current shapes, branch energies will be drifting away from each other (some branches will be discharged while others will be charged).

In following part of the chapter it is shown that specific waveform shapes prevents drifting. Required circulating currents are found and it is proved mathematically that for those waveforms, branch energies will remain constant over the fundamental time period.

In following chapter, it has been also explained how to use circulating currents to force an energy flow, what is being used for balancing in a physical (non-ideal) system.

Chapter 5 includes description of control hardware required to build the converter. Proposed by author, a control algorithm implemented on given hardware. The algorithm uses control of circulating currents to provide energy transfer between two systems and energy balancing in the same time.

At the end of this chapter, design details for branch current controller has been shown. Additionally, basic current controller simulation results are shown.

Chapter 6 includes the description of branch simulation model implementation. Additionally to description, basic simulation results are shown.

In the **Chapter 7**, use case for which most simulations were executed is being described. It has been decided to study topology in the circuit with gearless generator of the wind turbine. The case is however generic, so simulation results are applicable as well for other low speed generation or drive appliances.

Chapter contains a list of all test cases analyzed in the Thesis.

The model implemented on AC800 PEC is being described. Simulation results from given model can be found in this chapter.

In **Chapter 8**, a simplified model of Hex-Y as well as M3C converter (plant and control loop) are described. Following models has been built to be able to compare those two topologies.

Simulation results and benchmark results for chosen operation points are summarized in this chapter.

Chapter 9 contains analysis of converter behavior during supply voltage dips. It has been explained how the converter should react in that transient according to existing grid codes.

Chapter 10 contains summary. All key achievements of research are being highlighted here.

Due to the fact that MMC converters are high voltage high power devices it was not possible to perform any laboratory tests. Also tests on Real-Time Simulator (RTS) were not possible due to system complexity. Available simulator supports systems with up to six branches. Even though, a control system has been built on the control hardware which can be used in RTS and physical device (if available). Extensive simulations has been performed. Based on previous experience with computer simulations-RTS-prototype, author assumes that designed implementation is feasible for real system.

2. MMC Power Conversion Systems

Multilevel Converters are power electronics systems used for energy conversion. Power converters can be generally divided for two- and multilevel converters. In the multilevel family, different types can be identified [5]. The top-level hierarchy defines following types:

– Flying Capacitor converters,

– Neutral Point Clamped,

– H-Bridge,

– Casaded.

The Thesis is focused on Cascaded converters. Therefore MMC abbreviation will refers to this particular topology.

The Modular Multilevel Conversion (MMC) systems become more popular due to their modularity which results with a lower single module cost: the scale effect from the mass production. Another advantage of modularity is a redundancy - failed module can be bypassed and replaced during the scheduled maintenance. Another advantage of the MMC is high fault limiting capability [6] and high quality of output voltages due to the number of voltage steps in the output waveform [7].

Following chapter contains description of cascaded MMC topology. Different cell types are described. Classification depending on number of system terminals is proposed. Finally, selected MMC systems are described.

2.1. Cascaded MMC

Cascaded MMC converters are build by series (and series-parallel) connection of identical power electronics modules called cells or modules. Power Electronics Building Block (PEBB) is built with one or more cells. PEBB is an inseparable physical device, while cell can be treated as a functional module.

Each cell can provide discrete number of voltage levels (in the simplest case 0 or $+V_C$). By cascade connection of the cells, a staircase voltage can be generated.

A schematic of cascade built with two PEBBs (bordered with dashed lines), each containing two cells is presented on the Fig. 2.1. Each block in the structure is a cell which contain at least: switching

elements, energy storage elements (capacitor bank) and passive components (e.g. discharge resistor). Additionally, electronics components as gate drivers, measurement circuits and low-level protection circuits are present. In some applications, each cell contains its own low-level controller.
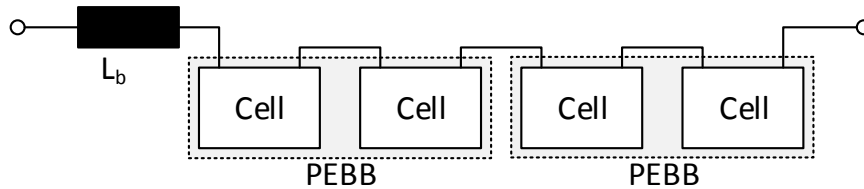
Figure 2.1. Branch high-level representation

Each module's capacitor bank can be supplied either from output of the cell (AC side) or by internal connection to the capacitor bank itself (DC side). In the first case, no extra cell power supplies are required. However balancing of the system is challenging. In the second case, each cell can be supplied separately from the DC side, e.g. by using transformer and diode rectifier [8]. In that case, balancing is not an issue, but multi winding transformer is required. Therefore this approach is not reasonable if high number of levels is required.

A complete MMC converter is built with a number of interconnected cascades to created desired topology as e.g. active rectifier or inverters. A single cascade connection of the modules together with an inductor will be called a branch[1].

2.2. Cell Types

Base building blocks of cascaded converter are cells. In most cases, power converter is built with series-parallel connection of identical modules. However, hybrid solutions can be also found [9]. In this section, most common cell types are collected.

Cell is a power converter which can be either Voltage Source (VS) or Current Source (CS). Hybrid cell realization is (VS+CS) can be also found in literature [10, 11]. Thesis is focused on VS cells. CS cell realized as Half Bridge (HB) and Full Bridge (FB) are described in [10].

Figure 2.2 presents selected cell circuits which are described e.g. in [5, 7, 12, 13]. Cell circuit is built with a capacitor symbol, which, in practice represents a capacitor bank (series-parallel connection of resistive and capacitive components). Switch symbol represents a controllable switch. In practical realization IGBT transistor is the most common, however for high powers, IGCT are found attractive [14, 15]. If higher switching frequency or lower losses are key constraints, MOSFTET transistors can be used [16, 17]. Its use however limits maximum cell voltage. Diode symbol represents an uncontrollable valve which blocks current flow in one direction.

---

[1]Term arm is also used in literature
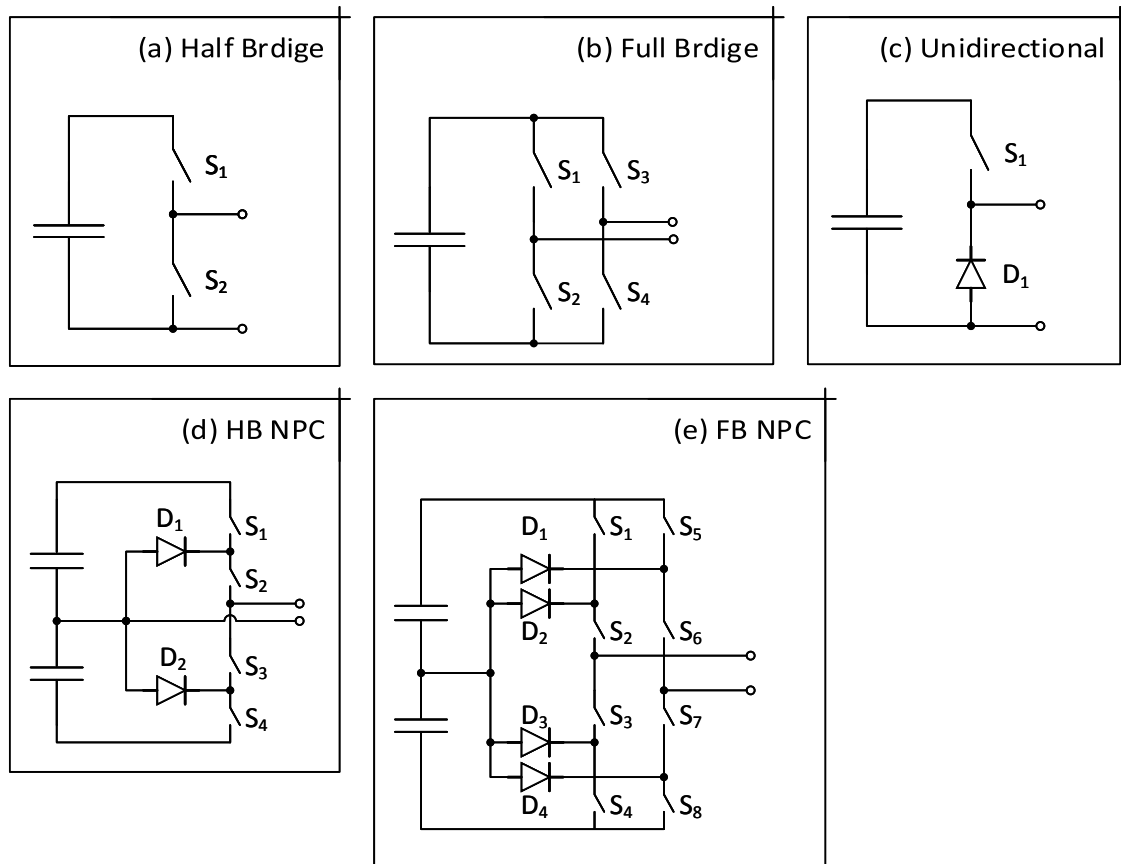
Figure 2.2. Selected cell types used as a base building blocks for cascaded MMC

Following circuit topologies are shown:

– **HB Cell** (Fig. 2.2a) is built with two controllable switches and can generate unipoloar voltage. Therefore its functionality is limited to two quadrants. Its main use is ac-dc and dc-ac conversion (e.g. HVDC grids). Converter built with HB cells is not able to limit current in case of DC link fault [18],

– **FB Cell** (Fig. 2.2b) is built with four controllable switches. It can generate bipolar voltages. It is used in ac-ac conversion systems. It can be used also for ac-dc applications if dc fault current limiting is required . In contrary to HB, current is always flowing through two instead of one switch. Therefore its losses are higher,

– **Unidirectional Cell** (Fig. 2.2c) [19, 20] is a reduced version of HB cell built with a single switch and a single diode. Replacement switch with a diode reduces the cell cost, but limits its functionality to one quadrant,

– **HB NPC** (Fig. 2.2d) [5, 7, 21] Neutral Point Clamped (NPC) HB Cell provides three voltage levels, therefore, from functional point of view it is similar to FB Cell. However, full output voltage in

that topology is limited to $\frac{1}{2}$ of full DC link voltage. Number of required controllable switches is the same as for the FB (four), however two extra diodes are required. It should be also noted that to realize this cell topology, access to the middle point of capacitor bank is required,

– **FB NPC** (Fig. 2.2e) [5, 22, 23] is an extended version of the HB NPC. An extra branch with four switches and two diodes is added. This topology provides five voltage levels. As in HB NPC, this topology can be realized only if middle point of capacitor bank is available.

Another cell types are:

– flying capacitor cells [5, 21],

– asymmetrical double commutated cell [13],

– cross- or parallel-connected cell [13, 24],

– clamped double commutated cell [13, 25],

– cell with resonant inverter for inductive power transfer [12, 26],

– current source cells as e.g. commutation cells, double commutation cell, mixed commutation cell, clamped diode or three phase commutation cells [13],

– hybrid VS/CS cells [13].

Table 2.1 summarizes each module features. Number of switches determines system complexity and can give an estimation about the module cost (which cell topology can be cheaper). Number of switches is divided into controllable and uncontrollable switches (as diodes are cheaper and does not require any gate driver circuits). Maximum number of switches in conduction path determines total module losses (more switches, higher losses). Again, this parameter can be used only for estimation / comparison between different modules.

Table 2.1. Cell topology comparison

Cell Type	Voltage levels	No. of switches [a]	Max no. of switches in conduction path	Bipolar operation (no. of quadrants)
HB	2	2	1	No (2)
FB	3	4	2	Yes (4)
Unidirectional	2	1+1	1	No (1)
HB NPC	3	4+2	2	Yes (4)
FB NPC	5	8+4	4	Yes (4)

[a]controllable + uncontrollable

Two mostly used cell types are HB and FB cells. In the Thesis only this two cell types will be used for description of converter topologies. It should be kept in mind that different cell types can be used to built presented converters as well.

Hex-Y topology proposed in the Thesis is built with FB cells as bipolar branch voltages are required to provide full functionality in direct AC-AC conversion.

2.2.1. Description of prototype PEBB with Two Full Bridge Cells

Following chapter describes prototype PEBB built by ABB. As the product is IP-protected, only an overview of the module can be presented in the Thesis. Prototype (zero-series) has been produced in batch of over 100 modules. One of customers using the module is Florida State University, Center for Advanced Power Systems. Four MMC system is used for MVDC grid simulations [27].

PEBB photo is presented on the Fig. 2.3. Size of the single module is about 40x20x60 cm, 30 kg. Modules are stacked in the cabinet to create required topology.

Figure 2.3. Photo of double FB PEBB (ABB)

Electrical schematic of the power circuit of the module is presented on the Fig. 2.4. PEBB is built with two identical FB cells. Each cell contains following components (starting from the left):

Resistors in capacitor bank are required to discharge DC link due to safety reasons. Additionally, resistors provide symmetric voltage sharing among series connection of capacitors in the capacitor bank. Value of R must provide discharge time constant of DC link (usually) on the level between 60 seconds and 6 minutes. Discharge time is trade-off between module losses and safety regulations / service time.

Capacitor bank is an energy storage of the cell. This component takes the biggest amount of volume in the PEBB (c.a. 30%). In given PEBB, electrolytic capacitors has been chosen as they provide big capacity, high energy density and low price in comparison with film capacitors. The main disadvantage of the electrolytic capacitors is its lifetime (during operation but also during the storage). Luckily,
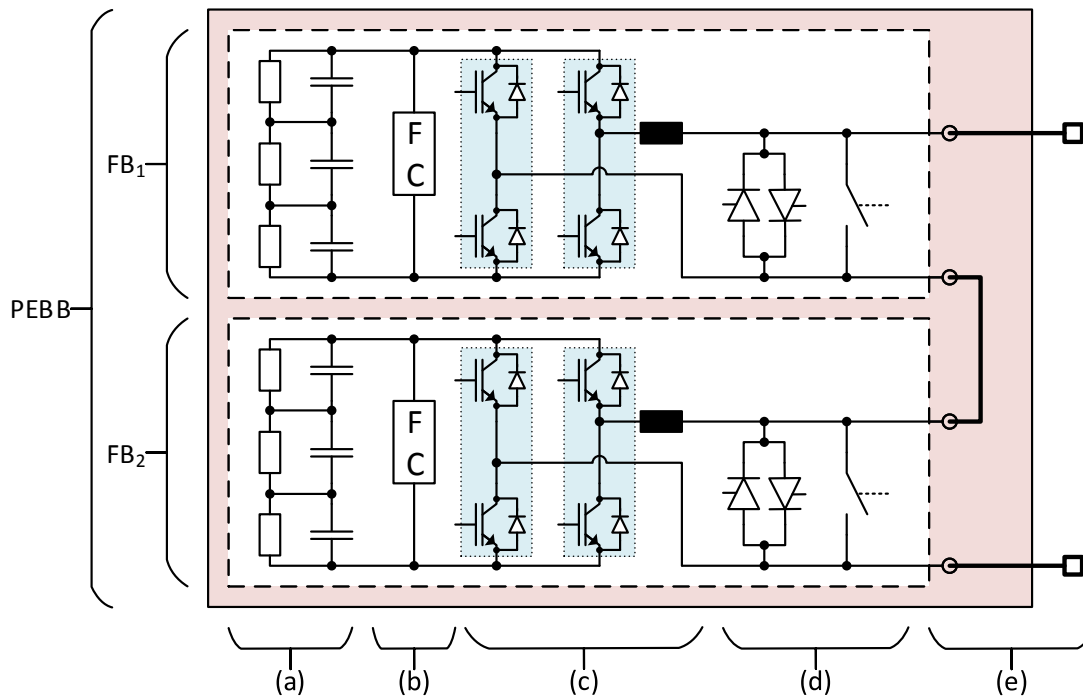
Figure 2.4. Double FB PEBB power circuit. (a) Capacitor bank, (b) Flyback converter,
(c) Full Bridge, (d) Bypass circuit, (e) Cell interconnections and PEBB output.

MMC reliability can be easily increased by adding extra modules therefore lifetime problem might be mitigated [28].

Flyback converter (FC) is a device which provides energy to auxilary PEBB circuits responsible for control, communication, measurements and driving switching devices. Flyback provides galvanic insulated low voltage. Power of the converter doesn't have to be high, but the challenge is to provide step-down operation (1000 V down to 12 V). Output voltage is in the next step step-down to the voltage required by control circuits (5 V and 3.3 V).

Insulated Gate Bipolar Transistor (IGBT) with anti-parallel diode creates a controlled switching element. In the given PEBB, 1.7 kV, 300 A HB module (two IGBT with diodes integrated in a single device) has been used. Each HB package is marked on the Figure by dotted border. As four switches are required to the FB, two HB packages are used to create a single FB cell.

Maximum switching frequency of given module is equal 2 kHz. The limitation are power losses (and resulting maximum temperature). As in MMC, output frequency is linear dependent on the number of levels, even for low number of modules (<10), switching frequency on the level of 2 kHz of the single module is high. For example, in the six cell per branch, output frequency is equal (2.1). Multiplication by two is given as FB module branches can be interleaved by 180^0 what results with double output frequency.

$$f_{out} = N \cdot 2 \cdot f = 6 \cdot 2 \cdot 2 \; kHz = 24 \; kHz \tag{2.1}$$

On the output of the bridge, small inductance (few μH) is placed. Its function is to make possible operation of parallel connected module: voltage difference between modules will cause current circulation which is suppressed by that choke. As for balanced system, voltage differences between the cells are not high, choke inductance can be relatively low. Its current rating must be however equal whole module rating.

Protection circuit is built with two components so called temporary and permanent bypasses.

Temprary bypass is built with two anti-parallel thyristors. Its function is a temporary bypassing of the cell circuit to protect it in case of the grid fault. During the fault, high current will flow through diodes what will cause its damage (due to overtemperature). To protect the module, in case of fault, thyristors are fired and start conducting the fault current. It is designed to withstand given short-circuit current for a specific time.

This protection circuit can be triggered by the Software (SW), however as short circuit current rise time is very high, software can be too slow. Therefore, each cell is equipped with a purely Hardware (HW) (analog) protection circuit which triggers thyristors in case of overcurrent detection. In that case, SW will be just informed about that event. HW circuit is designed to be triggered before damaging the diodes. In design process, minimal branch inductance is defined (as lower L causes faster fault current rise $\frac{di}{dt}$).

Thyristor bypass is designed to conduct a short circuit current for limited time (5-60 s). After that time, thyristor can be damaged due to overtemperature. Therefore if fault is not cleaned after given threshold time, a permanent bypass circuit is triggered. As its name says, this circuit can conduct current (also fault current) with no time limit.

Permanent bypass circuit is realized with a bistable relay which can be closed by protection HW circuit and by SW command. There is no possible to open the relay after the fault. The only way of doing that is to apply the voltage to the relay coil from the outside of the cell. The reason why SW is not able to open the relay is that SW is supplied from DC link of the cell. If cell is permanently bypassed, DC link is discharged and cannot be charged due to the fact that input of the cell is shorted. Therefore, cell is offline and no command can be send to it.

Permanent bypass is used also to bypass the cell in case of its fault. In that case, cell sends fault state to the top-level control and bypass itself. The system is still operational. Failed cell can be replaced during the maintenance.

It is possible to provide any level of redundancy in MMC system by adding extra cells. The only limitation is economy - more modules means higher converter cost. Another benefit of redundancy provided by extra modules is increased cells lifetime due to reduced cell DC link voltage (more cells in branch means that lower cell nominal voltage will be sufficient to provide required output voltage). It should be highlighted that redundancy in MMC doesn't mean there are spare modules waiting to be used. In MMC, all modules are working all the time, i.e. they are used during normal operation of the converter.

Each cell has two terminals. PEBB is built with two cells. If the cells are connected as on the Fig. 2.4, series connection of two FB is achieved (output PEBB terminals are marked with squares). It is possible

to rearrange internal PEBB connections and get two parallel FB cells. In that configuration, higher current rating of the PEBB is achieved.

Fig. 2.5 presents a block diagram of control circuit. It is based on DSP processor (TI F28035), which communicates with high-level control system using Plastic Optical Fiber (POF). That solution provides galvanic insulation. Higher-level system send reference for capacitor bank voltage ($U_{C,ref}$), output voltage (U_{ref}) and current (I_{ref}). As a feedback, cell sends measured capacitor bank voltage ($U_{C,meas}$) and input current (I_{meas}).

Table 2.2 contains full list of signals sent between cell and high-level control. Except aforementioned data, maximum heatsink temperature is sent from the DSP (T_{max}). Cell control mode can be changed by sending cell commands. As a feedback cell send its status and last error code (or zero in case of no fault). Protocol supports direct IGBT switching if the cell is in a given state. All cell modulators are synchronized when $Sync$ signal is sent. Correct phase shift is given as another parameter in the communication protocol. Signals A (Address) and D (Data) are used to set given cell parameters (as e.g. controller gains). As a feedback, confirmation is sent as a pair of corresponding A,D values.
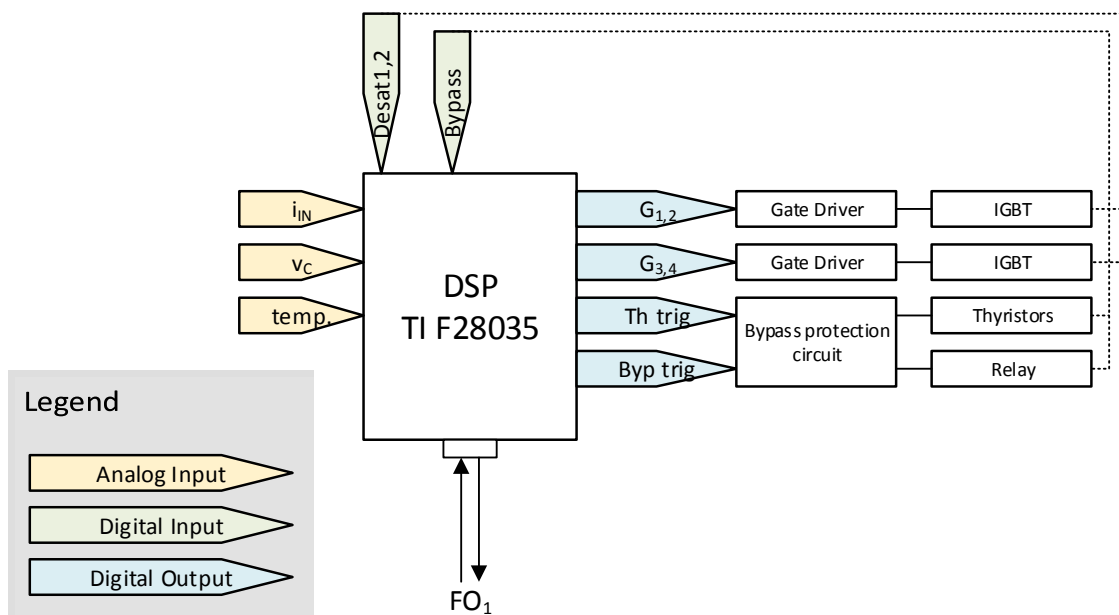
Figure 2.5. PEBB control block diagram

Control for IGBTs are PWM signals sent to gate drivers. It is possible to work in direct switching mode, where PWM modulator is not used. Instead of modulation index, control signals (ON/OFF) are sent. Switching signals are received directly from the top level control. This mode can be useful if modulation technique like Nearest Level Modulation (NLM) [7, 29, 30], Selective Harmonic Elimination (SHE) [7, 31–34] or Space Vector Modulation (SVM) [7, 35–38].

Digital outputs of the processor are being used to control bypass circuit (temporary and permanent).

Table 2.2. Data to be exchanged between cell and central controller

From DSP	To DSP
U_{ref}	
$U_{C,ref}$	$U_{C,meas}$
I_{ref}	I_{meas}
	T_{max}
Cell Command	Cell Status
	Error msg
IGBT Switch	
$Sync$, Phase shift	
A,D	A,D

Inputs for DSP processor are feedback signals from IGBTs (desaturation detection) and bypass feedback signals (triggered, or off). Analog measurements are following: capacitor bank voltage, input current (measured as a voltage drop on a shunt resistor) and temperature measurements.

Table 2.3 contains basic parameters of the single FB cell of the PEBB.

2.3. MMC Topologies

First commercial application of MMC were HVDC systems [39, 40]. An example of commercial products are: ABB HVDC Light[TM], Siemens HVDC Plus[TM] or Alstom HVDC MaxSine[TM].

Recently, a lower number of modules setup are being investigated to use the topology in a MVDC systems, e.g. on-ship MVDC grids [27].

DC-DC conversion systems [41–45] are academic and industry research topic.

A number of experiments has been performed also for ac-ac conversion systems - especially for STATCOM [46] and motor drive [15, 46–50] applications.

One of the challenging operation points for direct AC-AC MMC is a low frequency mode. In case of required non-zero torque for low speed, module oversizing is necessary. An example applications with flat torque-speed (in other words, nominal torque at low speed) characteristics are rolling / mining applications, hydro power generators [14, 15, 51, 52] or gearless wind generators [53].

In most cases, MMC converter is connected between two grids/systems. It can be connected also to a single grid as STATCOM or energy storage applications. Another possibility is to create a multiple n-phase system connections.

One possible classification of MMC systems is based on number of terminals in interconnected systems [17, 54]. This grouping shows which topologies should be taken into account during specific

Table 2.3. Full Bridge parameters

Component	Parameter	Value	Unit
Discharge Resistor	R_D	168^a	$k\Omega$
Capacitor	V_{nom}	1200^b	V
	C	2.1^c	mF
IGBT	Package	62 mm	
	V_{max}	1700	V
	I_{nom}	300	A
Inductor	L	1.2	μH
	I_{nom}	200	A
Thyristor	V_{max}	1800	V
	I_{nom}	181	A
	I_{max}	6000^d	A
Relay	I_{nom}	200^e	A

[a] two parallel branches of series connected three 112 $k\Omega$ resistors

[b] series connection of three 400 V capacitors

[c] 1.8 mF minimum capacicance due to degradation over time

[d] maximum forward surge current for 10 ms @50 Hz sine

[e] 200 A DC, 227 A AC

system design. Figure 2.6 presents mentioned classification with particular topologies in each group. Each category will be described in following subsections.

Each topology can be represented as a graph as proposed in [55]. An example graph for 3-2 topology is presented on Figure 2.7. Each node represents a connection point while each edge defines one terminal of the system (dashed line) or one branch of MMC system (continuous line). Proposed convention will be used to represent topologies in the Thesis.

To provide unification, naming convention from [56, 57] will be applied in parallel with „common" names of each topology.

Additionally, following topology naming will be used - in case of two interconnected systems, name X-Y will describe input and output system. Both X and Y can be either DC, AC or nAC. DC means 2-terminal DC system. nAC means n-phase AC system.

Input system is defined as the one which has given voltage (e.g. grid to which converter should be synchronized). Input currents are controlled to provide required active power flow in the system. It is also possible to control reactive power on the input system, but not in every topology.

Output system is the one in which voltages or currents are given as a setpoints.

For example 3AC-DC name refers to the topology which converts 3-phase AC into DC.
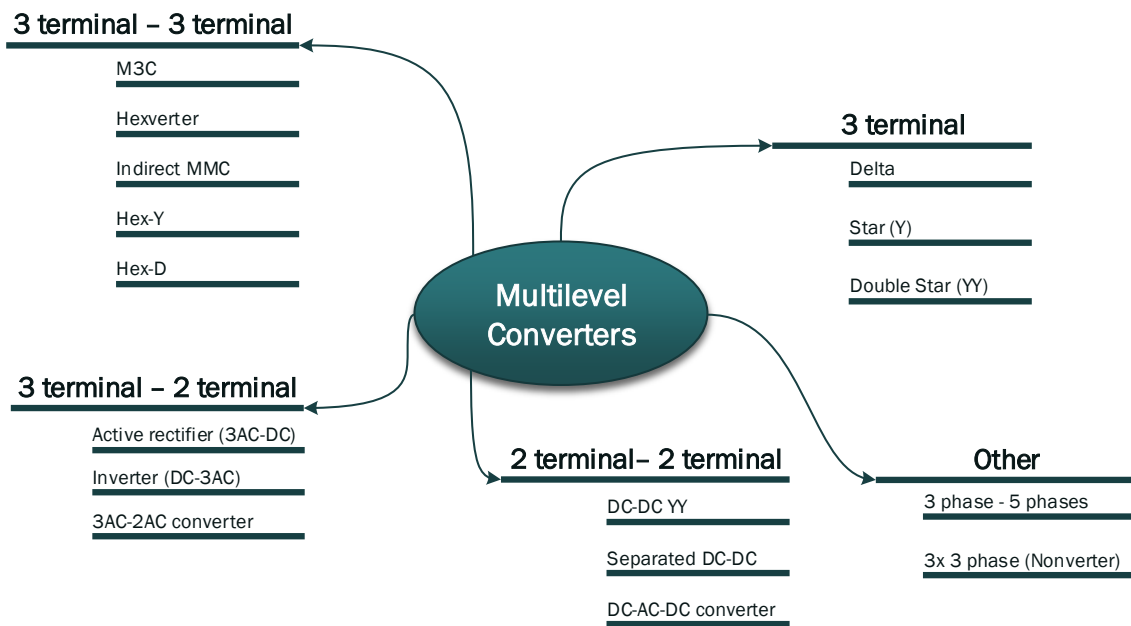
Figure 2.6. MMC system topologies. Classification based of number of terminals.

To compare different topologies, their main features as number of branches or required cell types (HB or FB) will be presented. Additionally, more detailed description of 3-3 topologies will be presented as the topology proposed in the Thesis belongs to that group. Branch to system voltage and current mapping based on Kirchhoff's Voltage Law (KVL) and Kirchhoff's Current Law (KCL) will be shown. This allows to make a basic comparison of different topologies as it was shown for 3-3 in [4].

2.3.1. 3 Terminal - 2 Terminal

3 to 2 terminal systems provide given voltage or currents at one system while the output waveforms are given as a setpoints. Following topologies are included into 3-2 group:

– Active Rectifier Unit (ARU) is an 3AC-DC converter which finds use in applications which requires controllable DC voltage. It is used also in case of systems requiring bidirectional power flow i.e. getting and returning energy to the AC grid,

– Inverter Unit (INU) is a DC-3AC converter providing given AC voltage or current,

– 1-phase power converter is an 3AC-2AC converter providing one phase AC voltage and current on the 2-terminal output side of the device. It is used e.g. in railway applications as 3 phase 50 Hz to 2 phase 16.7 Hz converter.

Fig. 2.7 presents topology graph for ARU and INU module. Arrow shows the direction from input to output for this two topologies. 3AC-2AC topology graph is identical as ARU. The only difference is
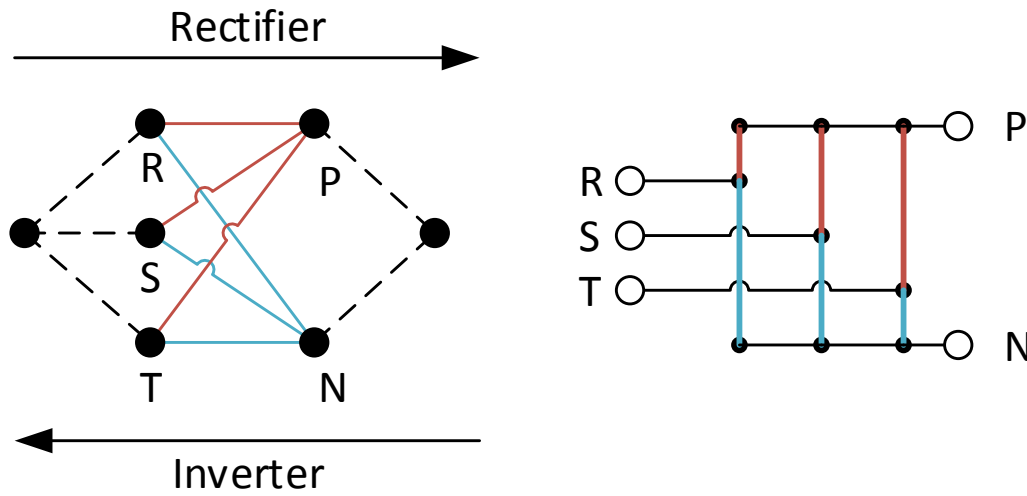
Figure 2.7. Topology graph of 3-2 converter.

that usually one phase terminals are not named P-N but e.g. A-B or U-V to highlight it is not DC output. Another important difference between 3AC-DC and 3AC-2AC is that second topology requires bipolar branch voltages therefore it must be built with FB modules while 3AC-DC can be built also with HB.

3-2 converter is built with six branches which creates two star connections (on P and N node).

For ARU and INU unit - if it is provided that DC link voltage is always positive, HB modules can be used to built the converter. It will reduce the converter cost. However, FB systems are also found [27] as they provide DC fault current limiting capability.

According to naming convention [57] topology is called Double-Star Half Bridge (DSHB) for ARU and INU or Double-Star Full Bridge (DSFB) for 3AC-2AC and Full bridge realization of ARU and INU converters.

ARU units finds use in HVDC and MVDC grids. ARU units are also a part of indirect AC-AC system which will be described in Chapter 2.3.2.1.

INU units together with diode rectifier on the input side creates two quadrant inverter. Interconnection with aforementioned ARU allows four quadrant operation.

3AC-2AC systems finds main use in railway application for $50 - 16.7Hz$ conversion [58]. Another area is one phase low frequency drives [59].

On the Figure 2.9, 3-2 topology is presented as a part of 3-2-3 system. On the left, proposed branch numbering and polarity is shown. It is used in calculation of branch voltages and currents which are required to provide specified output voltages and currents. This process will be called mapping. Mapping contains a set of simplifications, therefore it gives just an overview of voltage / current shapes in the system. The simplifications are that voltage drop on inductor is negligible, converter and grid are symmetric and there is no common mode voltage between input and output system. Therefore branch voltages are

equal [54, 60]:

$$
\begin{bmatrix} V_1 \\ V_2 \\ V_3 \\ V_4 \\ V_5 \\ V_6 \end{bmatrix} = \begin{bmatrix} -1 & 0 & 0 & 1/2 \\ 1 & 0 & 0 & 1/2 \\ 0 & -1 & 0 & 1/2 \\ 0 & 1 & 0 & 1/2 \\ 0 & 0 & -1 & 1/2 \\ 0 & 0 & 1 & 1/2 \end{bmatrix} \cdot \begin{bmatrix} V_U \\ V_V \\ V_W \\ V_{DC} \end{bmatrix} \tag{2.2}
$$

$V_{1...6}$ are the branch voltages of the rectifier unit (numbering as „$B1\cdots6$" on the Fig. 2.9), $V_{U,V,W}$ are input terminal sinusoidal voltages. V_{DC} is a DC output voltage.

Branch currents according to KCL are equal:

$$
\begin{bmatrix} I_1 \\ I_2 \\ I_3 \\ I_4 \\ I_5 \\ I_6 \end{bmatrix} = \begin{bmatrix} -1/2 & 0 & 0 & 1/3 \\ 1/2 & 0 & 0 & 1/3 \\ 0 & -1/2 & 0 & 1/3 \\ 0 & 1/2 & 0 & 1/3 \\ 0 & 0 & -1/2 & 1/3 \\ 0 & 0 & 1/2 & 1/3 \end{bmatrix} \cdot \begin{bmatrix} I_U \\ I_V \\ I_W \\ I_{DC} \end{bmatrix} \tag{2.3}
$$

Branch currents are calculated with assumption of ideal current sharing among branches. In practice, so called circulating currents are present. Detailed explanation of this phenomenon can be found in Chapter 3.2.

Presented mapping is valid for all three mentioned topologies. For 3AC-2AC V_{DC}, I_{DC} should be replaced with V_{AC} and I_{AC}. That's the only difference between ARU and 3AC-2AC[2].

In practical realization, differences between ARU and INU are following:

– ARU requires PLL module to synchronize with the 3-phase AC grid,

– ARU converter energy balancing (charging, discharging of the full system) is realized on the AC side while INU is controlling DC link current to provide balancing,

– ARU control output is DC (voltage or current) while INU control output is AC side.

2.3.2. 3 Terminal - 3 Terminal

3-3 systems are used for interconnection of two three terminal systems (as grids, loads or generators) which work with different rating i.e. frequency (cycloconverter), magnitude (transformer), phase shift (phase shifter) or combination of given parameters (inverters).

Following 3-3 topologies are described in this section:

– Indirect 3AC-DC-3AC which is a series connection of two 3-2 systems, i.e. ARU + INU,

---

[2]Expect the fact that 3AC-2AC requires FB modules what was mentioned earlier.

  – Modular Multilevel Matrix Converter (M3C) is a topology which connects each input with each
    output terminal of the system,

  – Hexverter is reduced version of M3C in which each input terminal is connected with two of three
    output terminals,

  – Hex-Y is a topology proposed in the Thesis. It can be described as rearranged M3C due to the fact
    it contains the same number of branches but in different configuration. It can be treated also as
    an extended Hexverter as six of nine branches of that topology creates classical Hexverter. Three
    remaining branches creates star connection which links input terminals,

  – Hex-D is modified version of Hex-Y in which three branches creates delta instead of start connec-
    tion.

2.3.2.1. Indirect 3AC-DC-3AC

Indirect 3AC-DC-3AC topology is constructed with a series connection of two 3-2 topologies: ARU
and INU. Topology graph is presented on Fig. 2.8. In the Thesis, I-MMC abbreviation for the topology
will be used.
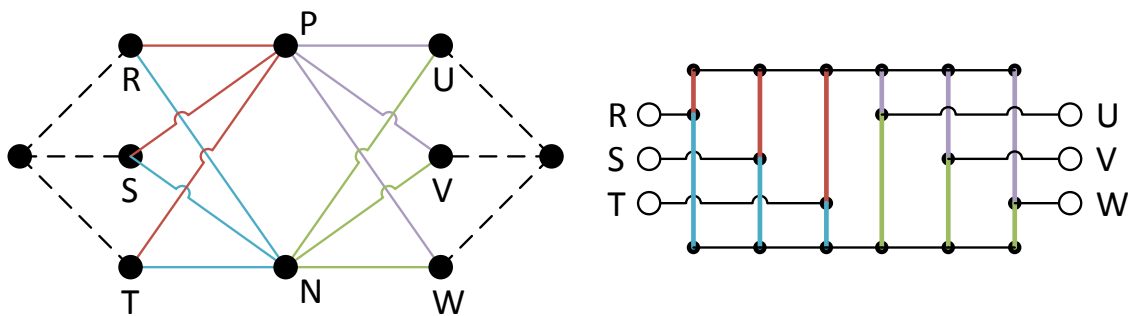
Figure 2.8. Topology graph of I-MMC

Figure 2.9 presents I-MMC converter. Components hierarchy will be explained on this example [54].
Single cell is marked as A. Series connection of cells with a branch inductor creates a single branch (B).
A group of interconnected branches which creates a functional topology (as in this example 3-2 terminal)
is called converter (C). Finally, full system which can be built with one or more converters is marked D.
In this particular system, one converter is an ARU while the second one is INU. Both together creates
3-2-3 I-MMC system.

DC link voltage (V_{PN}) can be chosen arbitrary. To provide positive branch voltage in each operation
point, DC link voltage must be higher that defined by Eq. (2.4). That voltage level allows to use HB
modules in converter construction. It will reduce the system cost significantly.
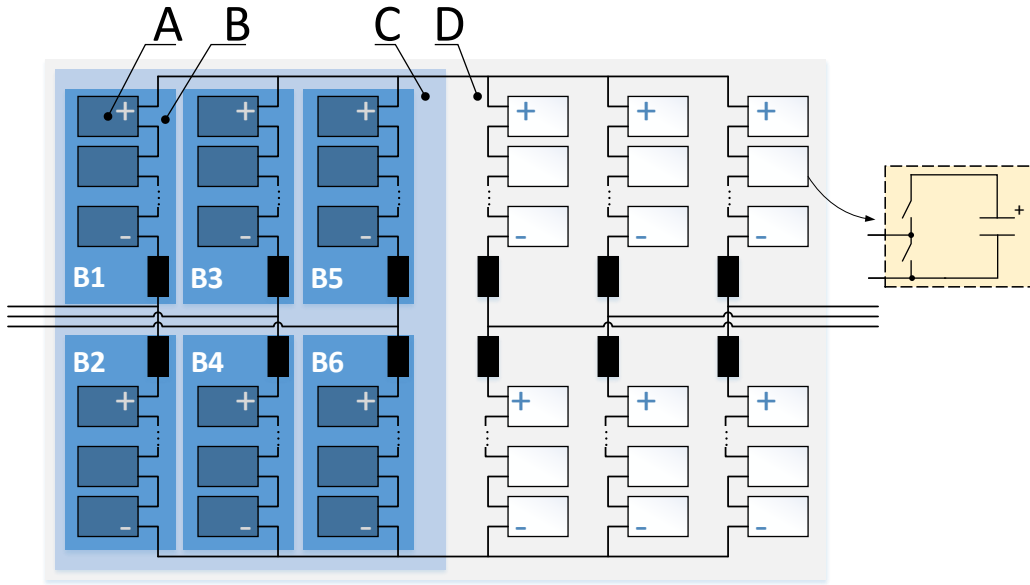
Figure 2.9. Indirect MMC converter.

It must be noted, that MMC systems has no DC link in classical meaning - i.e. DC link does not contain any capacitors, therefore it is usually called virtual.

$$V_{DC} \geq 2 \cdot \max\left(V_{1m}, V_{2m}\right) \tag{2.4}$$

As higher DC link voltage causes converter oversizing (higher peak branch voltage), minimal required DC link voltage is usually chosen as a setpoint. Of course, margin for control, grid voltage swell etc. must be taken into account. Otherwise AC voltage saturation will be observed.

Mapping matrices for voltages and currents of ARU/INU has been presented in Chapter 2.3.1, Eq. (2.2) and (2.3).

Maximum branch voltage and current for ARU and INU are equal [60]:

$$\begin{cases} V_{b,max,ARU} = \frac{V_{DC}}{2} + V_{1m} = \max\left(V_{1m}, V_{2m}\right) + V_{1m} \\ V_{b,max,INU} = \frac{V_{DC}}{2} + V_{2m} = \max\left(V_{1m}, V_{2m}\right) + V_{2m} \end{cases} \tag{2.5}$$

$$\begin{cases} I_{b,max,ARU} = \left(\frac{1}{2} + \frac{V_{1m}}{4 \cdot \max(V_{1m}, V_{2m})}\right) I_{1m} \\ I_{b,max,INU} = \left(\frac{1}{2} + \frac{V_{2m}}{4 \cdot \max(V_{1m}, V_{2m})}\right) I_{2m} \end{cases} \tag{2.6}$$

Following quantities are useful in the topology comparison as it is stated in [4, 61].

Maximum branch currents are calculated with an assumption that input power is equal output power, there is no reactive power in both systems ($\cos(\phi) = 1$) and circulating currents are zero. Another important assumption is that there is no common mode voltage between two systems. Minimal DC link voltage providing positive branch voltages has been chosen.

It should be noted that in practical realization, sizing takes into account actual control algorithm: are circulating currents suppressed or controlled? If they are controlled what is its shape? What is resulting peak branch current? For peak branch voltage and DC link voltage, calculations include minimum and maximum AC voltage magnitude defined by the grid codes. Capacitor bank fluctuations and margin for current control are taken into account as well.

2.3.2.2. M3C Topology

Direct AC-AC - M3C (known also as MMMC) [62] origins from the Matrix Converter topology [63]. In M3C topology, 3AC-3AC conversion is performed without any intermediate circuit by direct connection of every input with every output phase. In total there are 9 branches built with full bridge modules as required branch voltage is bipolar. Details about the current/voltage mapping for the M3C topology can be found in [64].

Figure 2.10 presents topology graph of M3C. It can be noted that converter is built with nine branches which creates three star connections. Therefore according to naming convention [57] topology is called Triple Star Full Bridge (TSFB). To simplify the analysis, topology can be represented as three separate clusters containing three branches each [65]. Every cluster is a 3AC-1AC converter.
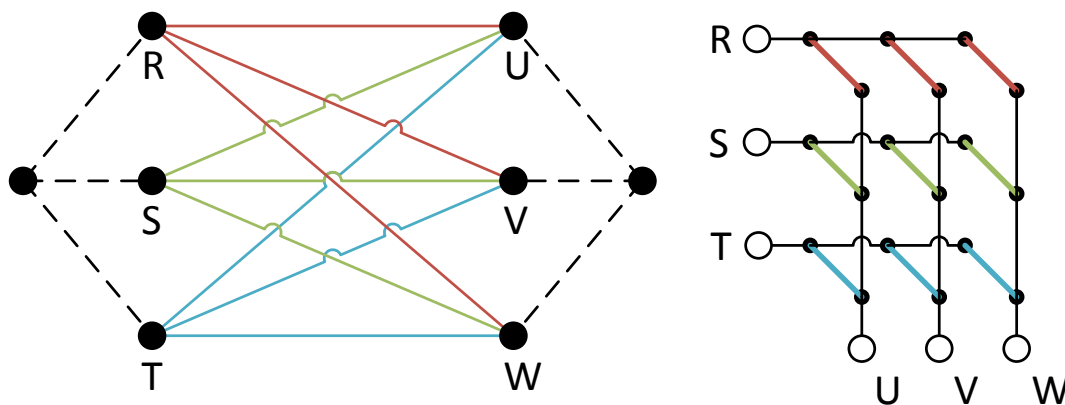
Figure 2.10. Topology graph of M3C.

Converter topology with proposed branch numbering is presented on Figure 8.10. Branch voltage and current mapping is defined in Eq. (2.7) and (2.8) [4]. For current mapping, circulating currents are not included. As branch voltages can be negative, FB modules are being used to built a converter. Detailed topology analysis can be found in [64]. Mapping process on Hex-Y example is also fully explained in Chapter 3.
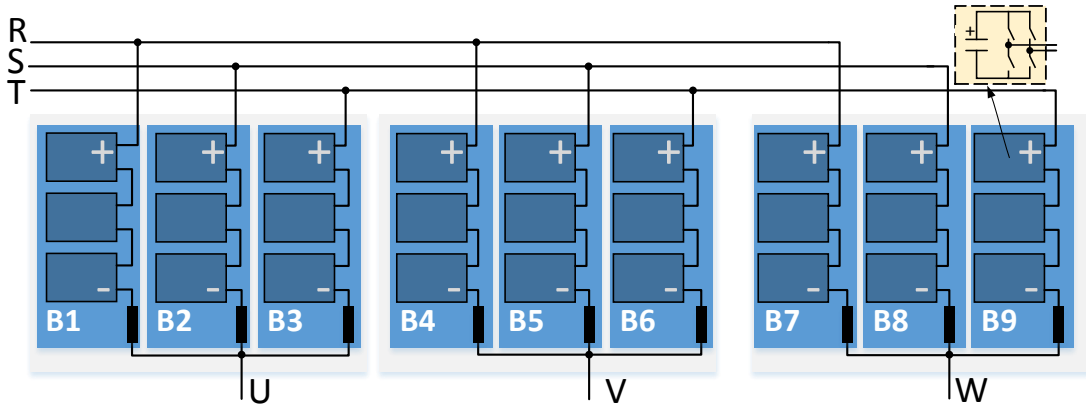
Figure 2.11. M3C converter

$$
\begin{bmatrix} V_1 \\ V_2 \\ V_3 \\ V_4 \\ V_5 \\ V_6 \\ V_7 \\ V_8 \\ V_9 \end{bmatrix} = \begin{bmatrix} 1 & 0 & 0 & -1 & 0 & 0 \\ 0 & 1 & 0 & -1 & 0 & 0 \\ 0 & 0 & 1 & -1 & 0 & 0 \\ 1 & 0 & 0 & 0 & -1 & 0 \\ 0 & 1 & 0 & 0 & -1 & 0 \\ 0 & 0 & 1 & 0 & -1 & 0 \\ 1 & 0 & 0 & 0 & 0 & -1 \\ 0 & 1 & 0 & 0 & 0 & -1 \\ 0 & 0 & 1 & 0 & 0 & -1 \end{bmatrix} \cdot \begin{bmatrix} V_R \\ V_S \\ V_T \\ V_U \\ V_V \\ V_W \end{bmatrix}
\tag{2.7}
$$

$$
\begin{bmatrix} I_1 \\ I_2 \\ I_3 \\ I_4 \\ I_5 \\ I_6 \\ I_7 \\ I_8 \\ I_9 \end{bmatrix} = \frac{1}{3} \begin{bmatrix} 1 & 0 & 0 & 1 & 0 & 0 \\ 0 & 1 & 0 & 1 & 0 & 0 \\ 0 & 0 & 1 & 1 & 0 & 0 \\ 1 & 0 & 0 & 0 & 1 & 0 \\ 0 & 1 & 0 & 0 & 1 & 0 \\ 0 & 0 & 1 & 0 & 1 & 0 \\ 1 & 0 & 0 & 0 & 0 & 1 \\ 0 & 1 & 0 & 0 & 0 & 1 \\ 0 & 0 & 1 & 0 & 0 & 1 \end{bmatrix} \cdot \begin{bmatrix} I_R \\ I_S \\ I_T \\ I_U \\ I_V \\ I_W \end{bmatrix}
\tag{2.8}
$$

Maximum branch voltage (as a difference between input and output phase) - assuming there is no common mode voltage and branch inductor voltage drop is neglected is equal:

$$
V_{b,max} = V_{1m} + V_{2m}
\tag{2.9}
$$

where V_{1m} and V_{2m} are peak phase-to-neutral voltages in input and output system respectively.

If there are no circulating currents nor asymmetry in the system, peak branch currents are equal:

$$I_{b,max} = \frac{1}{3} \left(I_{1m} + I_{2m} \right) \tag{2.10}$$

2.3.2.3. Hexverter

Reduced version of the M3C is so-called Hexverter [66] which can be described as Double Delta Full Bridge (DDFB). In the Hexverter, each phase is connected to the two phases of the other grid (system). Graphically it can be presented as a hexagon when each edge is a branch and each vertex is a phase terminal. Reduced number of branches limits the converter's cost, but it might cause non-ideal behavior during the transients as e.g. asymmetric grid faults. Additionally, to operate in given frequency range, reactive power is used as a control variable. Therefore reactive power cannot be given as a reference value. Similarly to M3C, the topology has no intermediate DC link and requires full bridge modules for operation.

On the Fig. 2.12 topology graph is presented. It can be noticed that Hexverter is a reduced version of M3C as three branches are removed (compare with Fig. 2.10).
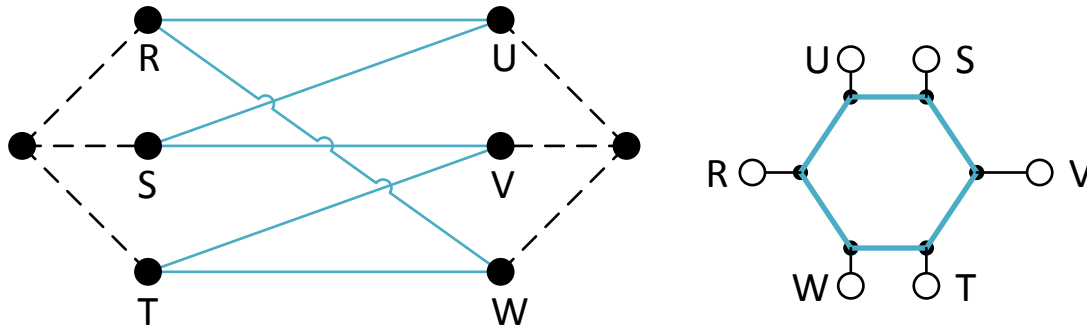
Figure 2.12. Topology graph of Hexverter

Figure 2.13 presents topology realization. Converter branches creates a hexagon in which vertexes are input and output phase connection points (alternately).

System-branch mapping for voltages and currents has been explained in [66, 67]:

$$\begin{bmatrix} V_1 \\ V_2 \\ V_3 \\ V_4 \\ V_5 \\ V_6 \end{bmatrix} = \begin{bmatrix} 1 & 0 & 0 & -1 & 0 & 0 \\ 0 & -1 & 0 & 1 & 0 & 0 \\ 0 & 1 & 0 & 0 & -1 & 0 \\ 0 & 0 & -1 & 0 & 1 & 0 \\ 0 & 0 & 1 & 0 & 0 & -1 \\ -1 & 0 & 0 & 0 & 0 & 1 \end{bmatrix} \cdot \begin{bmatrix} V_R \\ V_S \\ V_T \\ V_U \\ V_V \\ V_W \end{bmatrix} \tag{2.11}$$
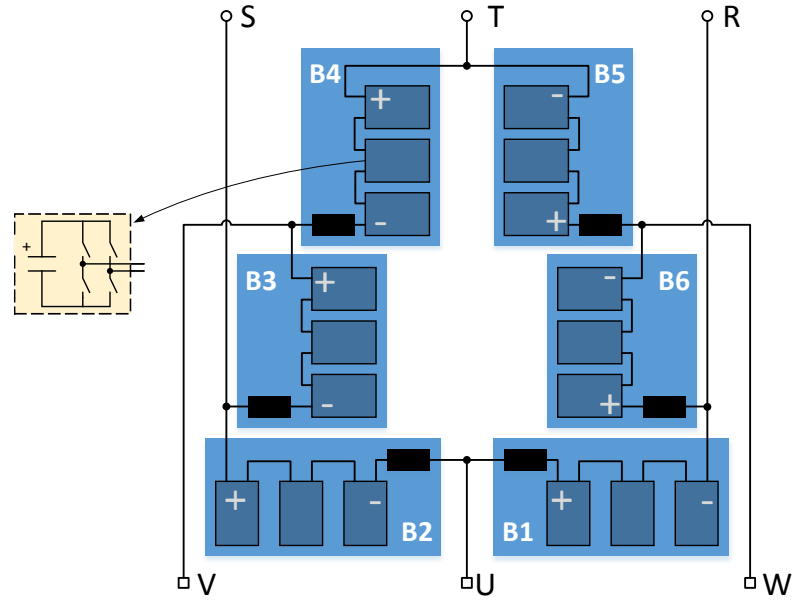
Figure 2.13. Hexverter

$$
\begin{bmatrix} I_1 \\ I_2 \\ I_3 \\ I_4 \\ I_5 \\ I_6 \end{bmatrix} = \frac{1}{3} \begin{bmatrix} -1 & 1 & 0 & 1 & 0 & -1 \\ -1 & 1 & 0 & -1 & 1 & 0 \\ 0 & -1 & 1 & -1 & 1 & 0 \\ 0 & -1 & 1 & 0 & -1 & 1 \\ 1 & 0 & -1 & 0 & -1 & 1 \\ 1 & 0 & -1 & 1 & 0 & -1 \end{bmatrix} \cdot \begin{bmatrix} I_R \\ I_S \\ I_T \\ I_U \\ I_V \\ I_W \end{bmatrix}
\tag{2.12}
$$

Peak branch voltage ($V_{b,max}$) and current ($I_{b,max}$) which defines converter dimensioning are equal [64]:

$$
V_{b,max} = V_{1m} + V_{2m}
\tag{2.13}
$$

$$
I_{b,max} = \frac{\sqrt{3}}{3} \left(I_{1m} + I_{2m} \right)
\tag{2.14}
$$

Circulating current influence is not included in the Eq. (2.12). In contrary to M3C, Hexverter topology has one (instead of four) independent circulating currents which can be used for branch energy balancing or capacitor ripple reduction. Therefore, as an external degree of freedom, common mode voltage (between neutral points of two systems) is being used. It will increase branch voltage, what is not included in the Eq. (2.11). Unfortunately, a common mode voltage is not allowed or not welcome in some applications as it might cause e.g. bearing failures in motor drive applications [19, 68]. Therefore, a Hexverter topology is not feasible for that systems.

Another degree of freedom used in control of Hexverter is reactive power. Therefore, proposed topology can be not applicable in the systems which requires reactive power control.

On the other hand, a big advantage of that topology is its size - only six branches are required to provide 3-3 conversion.

It should be also noted that as reduced version of M3C, Hexverter control can be applied for M3C system in case of failed branches. In other words: M3C with damaged branch can be "rearranged" to work as a Hexverter [69].

2.3.2.4. Hex-Y

In the Thesis, a new asymmetric topology (grid and load side can be distinguished) is presented.

Hex-Y is a topology proposed in [4]. It can be treated as connection of Hexverter and three additional branches building star connection. Due to its origin it has been called a Hex-Y as it is combination of the Hexverter and start connected Static Synchronous Compensator (STATCOM). According to the naming convention [57], the topology can be named Double Delta Single Start Full Bridge (DDSS-FB).

Topology graph is presented on the Fig. 2.14. X is a star point of the Y-connection of three branches. It is floating and its potential can be used as one of Degrees of Freedom (DOF) in control algorithm. It is also possible to reduce its potential to zero (reference ground on input side). This allows to minimize branch voltages in the Y-part of converter.

Similar to M3C, topology contains nine branches. Therefore it can be treated also as rearranged M3C. Due to similarities with M3C (number of branches) proposed Hex-Y topology will use M3C as a reference topology is benchmarking.
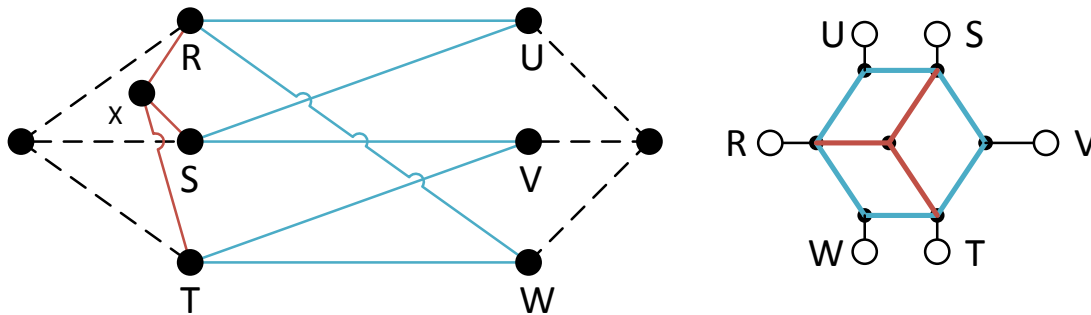
Figure 2.14. Topology graph of Hex-Y

Fig. 2.15 shows topology realization. In blue, Hexverter branches are shown. Orange branches creates Y-connection on the input grid side. It is possible to treat a system as combination of two converters coupled by circulating currents flowing between branches.

Maximum branch voltages are equal [4]:

$$\begin{cases} V_{b,max,HEX} = V_{1m} + V_{2m} \\ V_{b,max,Y} = V_{1m} \end{cases} \tag{2.15}$$
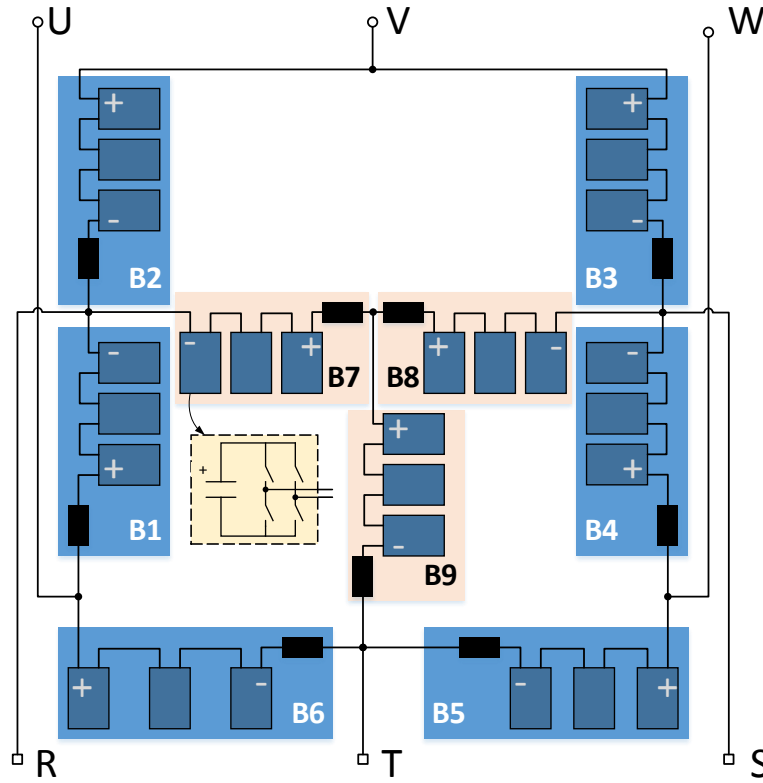
Figure 2.15. Hex-Y converter

It should be noted that it was assumed that $V_X = 0$. Also zero common mode voltage is defined.

Maximum branch currents (with circulating currents included) are equal (2.16) [4]. As resulting current shape is a function of phase shift between two systems, circulating current frequency and so on, the worst case is shown. To highlight that fact, $\leq$ sign is used. In given operation point, peak branch current might be lower. I_{Cm} is a peak circulating current.

$$\begin{cases} I_{b,max,HEX} \leq \frac{\sqrt{3}}{5}I_{1m} + \frac{\sqrt{7}}{5}I_{2m} + \frac{4}{5}I_{Cm} \\ I_{b,max,Y} \leq \frac{2}{5}I_{1m} + \frac{1}{5}I_{2m} + \frac{4\sqrt{3}}{5}I_{Cm} \end{cases} \tag{2.16}$$

2.3.2.5. Hex-D

Hex-D is a modified version of Hex-Y which topology graph is presented on Fig. 2.16. Three branches of that topology creates delta instead of star connection.

This topology has not been deeply analyzed yet. It is out of the scope of the Thesis.

2.3.3. 2 Terminal - 2 Terminal

2-2 systems are mainly DC-DC converters which finds increasing use as HVDC and MVDC systems are growing. Following converters provides voltage level conversion and may separate individual grid segments. Beyond galvanic insulation it is possible to use MMC converters to isolate grid faults.
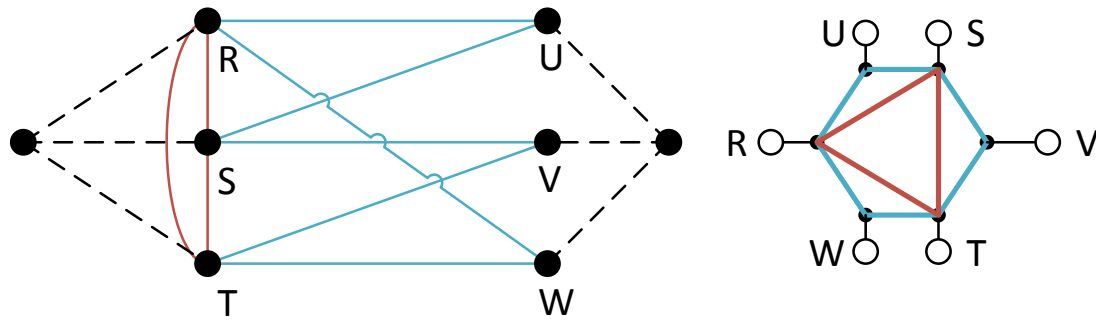
Figure 2.16. Topology graph of Hex-D

Detailed overview of different DC-DC MMC systems can be found in [70]. Following 2-2 topologies will be mentioned in the chapter:

– Separated DC-DC converter built with eight branches and separating transformer,

– Indirect DC-DC (I-DCDC) converter with intermediate 3-phase AC link (DC-3AC-DC topology),

– Double Y (YY) converter built with six branches.

Separated DC-DC [41] is built with two 4-branch converters connected with one phase transformer. Topology graph is presented on Fig. 2.17.
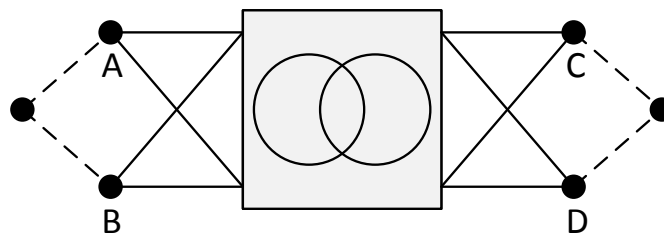
Figure 2.17. Topology graph of Separated DC-DC

Transformer provides galvanic insulation and voltage level adaptation (transfer ratio). Depending on chosen frequency, either standard 1-phase transformer (50 or 60 Hz) or medium/high frequency transformer can be used. Benefit of low frequency transformer is that it usually a standard product so the lead time may be lower. Its volume is however not applicable for high power applications. For medium frequency transformer, its volume and weight is significantly lower. Also the noise level and vibrations are lower than in low frequency systems. The limitations for maximum frequency are: control loop time step, switching frequency of modules and wiring impedance.

Indirect DC-DC is a system built as a series connection of two 3-2 converters [71]. Topology is similar to I-MMC: while I-MMC is a series connection of ARU and INU, I-DCDC is a series connection of INU and ARU. Interconnection is done on 3-phase AC side. Topology graph is presented on Fig. 2.18.
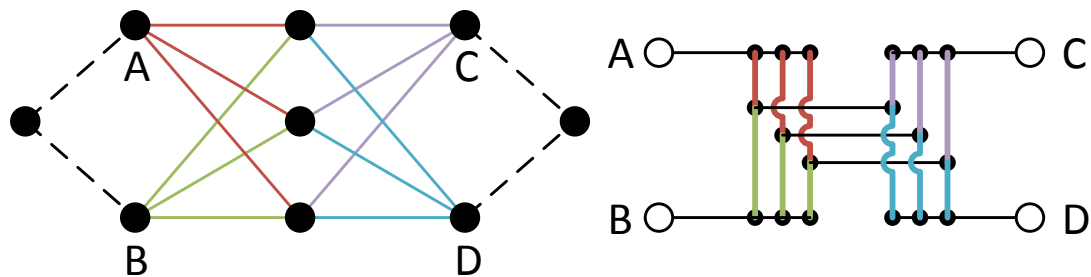
Figure 2.18. Topology graph of Indirect DC-DC

In case of galvanic insulation requirement, of if high transfer ratio is requested, a 3 phase transformer can be placed on the internal AC link [44]. Similar to I-MMC, topology can be realized with HB modules (for correctly defined AC and DC voltage magnitudes).

As in separated DC-DC, AC frequency can vary. Lowest frequency is defined by allowed capacitor bank voltage ripple and highest by control loop speed, switching frequency and impedances.

YY topology [45, 72] is built with six branches creating two star connections. Star points potential is used as a control variable for branch balancing. Fig. 2.19 presents topology graph.
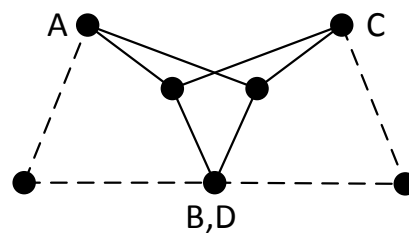
Figure 2.19. Topology graph of YY

System can be built either with HB or FB modules. As there is no any intermediate circuit, the topology can be named direct DC-DC. One disadvantage of that solution is no possibility to introduce transformer which provides galvanic insulation and high transfer ratio between two DC grids. Therefore its usage is limited to systems with low ratio [71]. Voltage scaling is possible only by branch voltages.

A great advantage of that topology is its size. Converter is built only with six branches and no any extra passive components.

2.3.4. 3 Terminal

3 terminal systems are connected to a single 3-phase grid. They are used to provide grid stability as so called STATCOM. Converter provides reactive power in case of voltage dips or swells.

The second common application is Energy Storage System (ESS). ESS systems are energy banks used in case of grid faults or higher energy consumption. An example of ESS is Battery Energy Storage System (BESS) which uses batteries to store the energy and supply the grid in case of lost power. ESS systems can also use supercaps to store the energy which provides lower energy density but faster response in case of faults.

Systems designed for grid stability provision does not require high energy capability in contrary to ESS. Therefore they can be built with classical cells with capacitor bank only. ESS systems with higher energy storage capability are built with modules containing extra components: battery and intermediate circuit (DC/DC converter). As a result, split-battery energy storage system is realized.

Intermediate DC/DC power conversion stage is required to provide optimal operation point for the battery. Depending on the voltage rating, buck or boost converter is required. DC/DC converter should have high efficiency and must provide bidirectional power flow. An example FB cell with battery and HB DC/DC (buck) converter is presented on the Fig. 2.20.
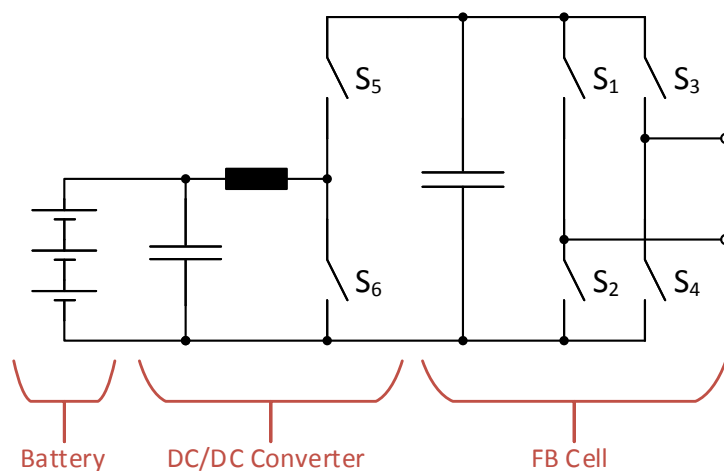
Figure 2.20. Cell for distributed BESS

Independently of the application (ESS or STATCOM), there is no difference on the level of topology graph. Following 3-phase system are described in this section:

– Single Delta (D) built with three branches connected in triangle

– Single Star (Y) built with three branches connected in star

– Double Star (YY) built with six branches, creating two star connections

Detailed analysis of presented topologies can be found in [16, 56, 73].

Single Delta (SDFB) is a topology built with three branches as it is shown on Fig. 2.21a. Branches create a closed loop what allows to use the current circulating among them as a control variable used for energy balancing. As each branch is connected between two phases, its rating (minimum voltage) must be higher than phase to phase voltage.

In Single Star (SSFB) topology, branches creates star connection as it is shown of Fig. 2.21b. Voltage of point X can be controlled to be zero (in reference to system ground) or can be used as a control variable for energy balancing. Advantage of SSFB is that branch voltage rating is reduced by $\sqrt{3}$ if star point voltage is controlled to be zero.

(a) (b)
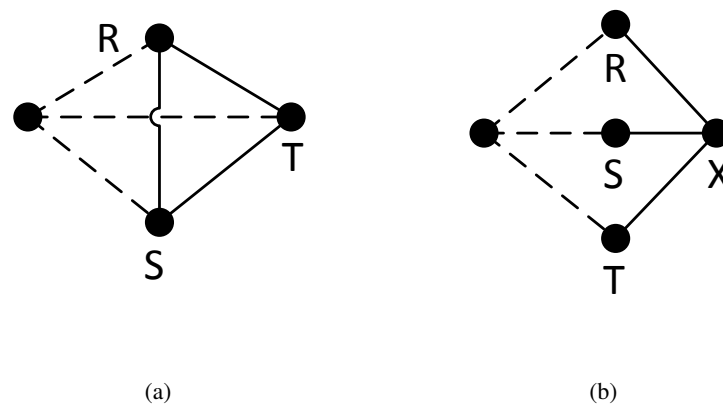
Figure 2.21. Topology graph of SDFB (a) and SSFB (b)

Double Star (DSHB) topology is built with HB modules. Its graph is identical as 3-2 ARU topology presented on the Fig. 2.7. The only difference is that for 3-phase system, P-N terminals are not used, i.e. its voltage doesn't have to be controlled for a given setpoint. It can be used as an internal control variable instead.

2.3.5. Other

Depending on application, special topologies might be found required. In the Thesis, two examples are shown.

One non-classical use case is a triple three-phase system (3-3-3) which couples three different systems. It can be realized as a so-called Nonverter [74]. Topology is built with nine branches as is shown of Fig. 2.22. It connects each system phase with another system terminal in a sequence. As a result, a circular topology is received.

Second topology is 3-5 converter which can be used as e.g. five phase drive for a motor / generator. It can be realized either as an indirect or direct topology. Direct (matrix) topology graph is presented on the Fig. 2.23. System is built with 15 branches which connects every input with every output phase.
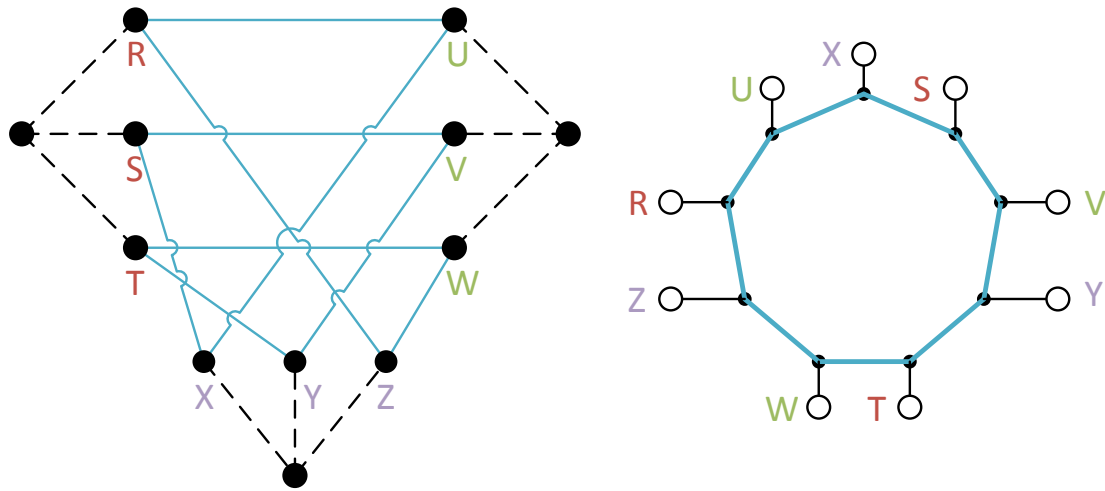
Figure 2.22. Topology graph of Nonverter

Another realization of 3-5 is an indrect topology (3-2-5) which uses virtual DC link between the phases. Fig. 2.24 presents topology graph. Similar to I-MMC, HB modules can be used to built the converter. There are 16 branches in total.

In the [75], topologies 3-5 are described, but not as MMC. Instead, classical switches are present in each branch. However there is no contradictions to replace a switch with a full MMC branch.
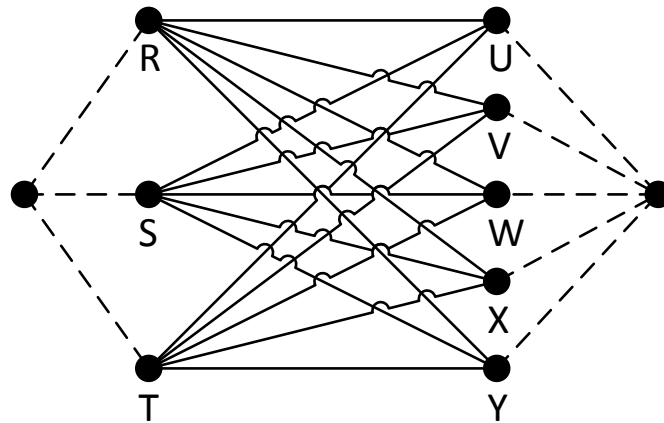
Figure 2.23. Topology graph of direct 3-5 converter
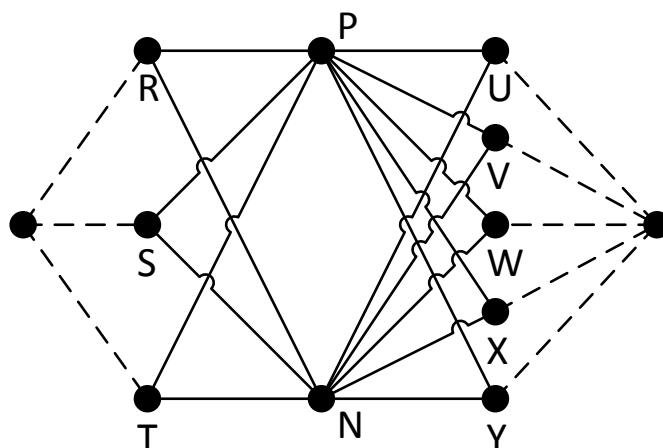
Figure 2.24. Topology graph of indirect 3-5 converter

3. Hex-Y Topology

Chapter 3.1 describes the Hex-Y topology. It includes nodal and mesh equations which allows to calculate branch currents for a given voltages and impedances.

Chapter 3.2 presents how to „translate" branch currents into output (line) currents using KCL. Three Degrees of Freedom (DOF): so called circulating currents has been identified. Full system equations in $\alpha - \beta$ coordinate system has been presented. Additionally an example waveform is being plotted.

In the Chapter 3.3 terminal to branch voltage mapping is shown. There are two voltages independent on terminal quantities: neutral point voltage between two systems (V_N) and the star point voltage of the Y-branch (V_X). Example waveforms are plotted.

3.1. Hex-Y Topology

Hex-Y topology is used for interconnection of two three-phase systems. Figure 3.1 presents an equivalent circuit of the converter and two AC grids. Dashed line separates circuit into three sections. On the bottom, first AC system (so called input) is shown. In the middle, a converter built with nine branches is present. As it is shown, each branch is represented as series connection of voltage source E_b and branch impedance Z_b. On the top of the Figure, second system (so called output) is shown. Second system can be either another grid or load (e.g. motor). It has been assumed that system is symmetrical, i.e. each phase impedance Z_{gs} is equal (but can be different between input and output systems).

3.1.1. Structural Matrices

To calculate currents flow in a given system, a first step is to built topology graph as it is suggested in [76]. Basing on the Figure 3.1, the graph has been constructed. Graph is directed (oriented), what means it includes arrows which defines positive current flow direction. According to given directions of terminal currents I_{gsp} ($s = 1, 2$, $p = 1, 2, 3$), current is positive if it flows into the converter. For given definition, positive current will cause converter charging (positive energy balance). Negative power cause energy flow from converter to the grid or load.
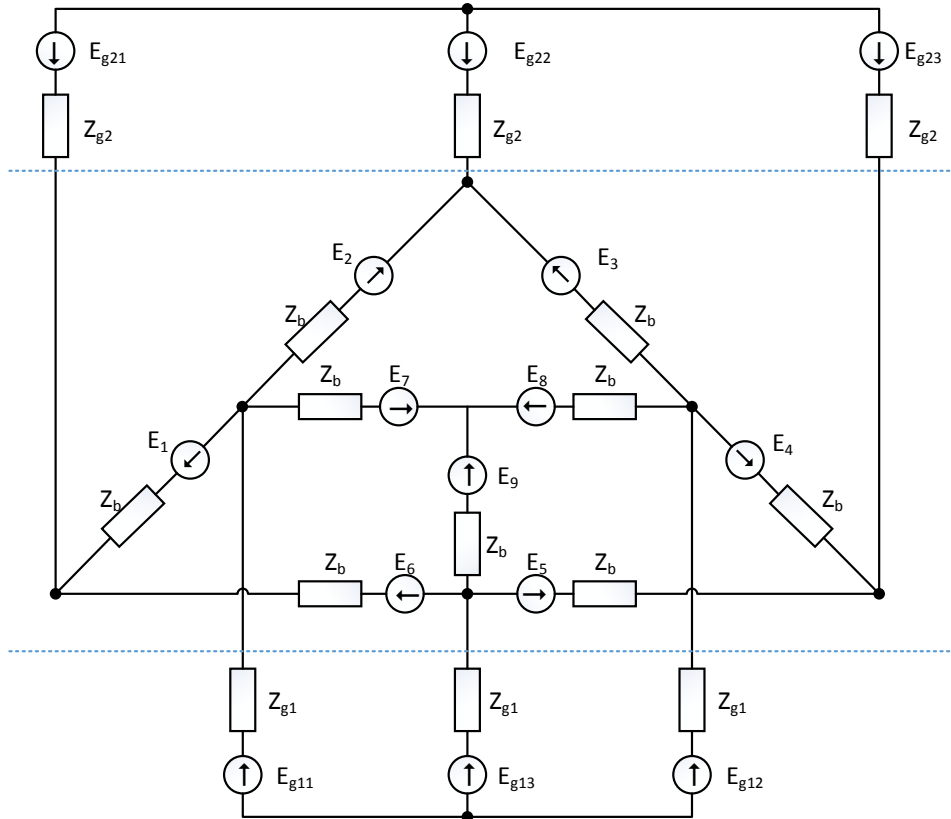
Figure 3.1. Hex-Y converter connected to two grids

Figure 3.2a presents an oriented topology graph of the system. Graph vertices (nodes) are numbered with a **Bold** font. There are $x = 9^1$ nodes. Graph edges are marked *Italic*. There are $b = 15$ edges in a given circuit.

Number of independent graph loops (circuits) is defined by Equation (3.1):

$$n = b - x + 1 = 15 - 9 + 1 = 7 \tag{3.1}$$

Symbol n defines how many independent currents should be known to fully determine current flow in the circuit. In other words n defines number of degrees of freedom (DOF) in the circuit.

Currents can be chosen in any way. The only restriction is that they have to by linear independent one to each other. In this chapter, it has been decided to choose currents which are flowing through given graph edges. Edges has been selected by building a spanning tree from a graph in following iterative process: first, define a current loop. Next, remove one edge belonging to that loop. Current in that edge is one of chosen currents. The process repeats until graph does not contain any loop.

---

[1]Usually, in graph theory, number of nodes is marked with symbol v. In the Thesis, it has been decided to use x symbol instead due to the fact that v letter is used to define voltage.
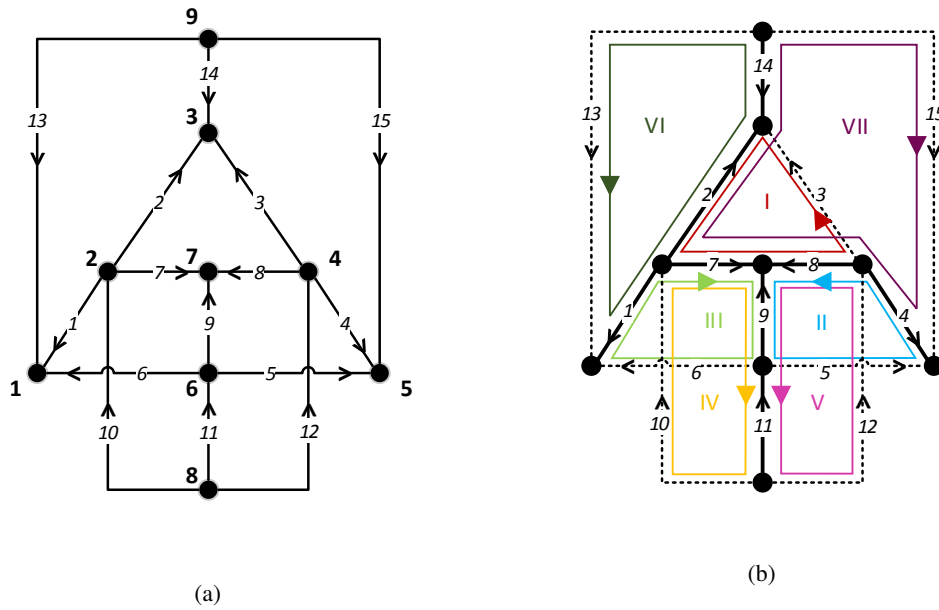
Figure 3.2. (a) Hex-Y topology graph , (b) Chosen current loops

As a result of given procedure, a graph spanning tree and a set of fulfilling branches - marked with a dashed lines on the Figure 3.2b is obtained.

Having defined and enumerated graph vertices and edges, highlighted current loops and defined tree and fulfilling edges, structural matrices of given circuit can be built. Those matrices will fully describe given topology.

Incidence matrix [76, 77], $\boldsymbol{A}$ defined as (3.2) includes information about interconnections between graph nodes. Each row describes a single node by description whether given edge connects with that node or not. If given node has no connection with given edge, 0 is used. For oriented graph, if given node has connection with corresponding edge,1 or -1 is used. 1 means that edge starts at this node. -1 that edge ends in that node.

Matrix size is $x \times b$. First 8 columns corresponds to a defined spanning tree edges (see Fig. 3.2b). Following 7 columns corresponds to conspanning graph edges (chords).

Matrix rank is $x - 1$. It means that current in one of the nodes can be defined as a linear combination of all other currents. It is in line with Kirchhoff Current Law which says that sum of all currents flowing into a given node must be equal zero. For matrix $\boldsymbol{A}$, it means that sum of elements in each column should be equal zero.

$$
A =
\begin{array}{c}
\begin{array}{ccccccccccccccc}
1 & 2 & 4 & 7 & 8 & 9 & 11 & 14 & 3 & 5 & 6 & 10 & 12 & 13 & 15
\end{array} \\
\left[
\begin{array}{ccccccccccccccc}
-1 & 0 & 0 & 0 & 0 & 0 & 0 & 0 & 0 & 0 & -1 & 0 & 0 & -1 & 0 \\
1 & 1 & 0 & 1 & 0 & 0 & 0 & 0 & 0 & 0 & 0 & -1 & 0 & 0 & 0 \\
0 & -1 & 0 & 0 & 0 & 0 & 0 & -1 & -1 & 0 & 0 & 0 & 0 & 0 & 0 \\
0 & 0 & 1 & 0 & 1 & 0 & 0 & 0 & 1 & 0 & 0 & 0 & -1 & 0 & 0 \\
0 & 0 & -1 & 0 & 0 & 0 & 0 & 0 & 0 & -1 & 0 & 0 & 0 & 0 & -1 \\
0 & 0 & 0 & 0 & 0 & 1 & -1 & 0 & 0 & 1 & 1 & 0 & 0 & 0 & 0 \\
0 & 0 & 0 & -1 & -1 & -1 & 0 & 0 & 0 & 0 & 0 & 0 & 0 & 0 & 0 \\
0 & 0 & 0 & 0 & 0 & 0 & 1 & 0 & 0 & 0 & 0 & 1 & 1 & 0 & 0 \\
0 & 0 & 0 & 0 & 0 & 0 & 0 & 1 & 0 & 0 & 0 & 0 & 0 & 1 & 1
\end{array}
\right]
\begin{array}{c}
1 \\ 2 \\ 3 \\ 4 \\ 5 \\ 6 \\ 7 \\ 8 \\ 9
\end{array}
\end{array}
$$

$$(3.2)$$

Circuit matrix (loop incidence matrix) B describes which graph edges are present in a given loop. Its size is $n \times b$. Each matrix row describes one current loop. Each column corresponds with a single edge. As in the matrix A, first columns contains edges which belongs to a tree.

If edge is not present in given loop, number 0 is used. Number 1 means that the edge is within a loop and its direction is the same as chosen loop direction. In case of opposite directions, number -1 is being used. Loop and edge directions are marked on the Fig. 3.2b.

B matrix for given topology is defined by Equation (3.3). It should be noted, that matrix part built with chords (edges which does not belong to a spanning tree) is an identity matrix.

$$
B =
\begin{array}{c}
\begin{array}{ccccccccccccccc}
1 & 2 & 4 & 7 & 8 & 9 & 11 & 14 & 3 & 5 & 6 & 10 & 12 & 13 & 15
\end{array} \\
\left[
\begin{array}{ccccccccccccccc}
0 & -1 & 0 & 1 & -1 & 0 & 0 & 0 & 1 & 0 & 0 & 0 & 0 & 0 & 0 \\
0 & 0 & -1 & 0 & 1 & -1 & 0 & 0 & 0 & 1 & 0 & 0 & 0 & 0 & 0 \\
-1 & 0 & 0 & 1 & 0 & -1 & 0 & 0 & 0 & 0 & 1 & 0 & 0 & 0 & 0 \\
0 & 0 & 0 & 1 & 0 & -1 & -1 & 0 & 0 & 0 & 0 & 1 & 0 & 0 & 0 \\
0 & 0 & 0 & 0 & 1 & -1 & -1 & 0 & 0 & 0 & 0 & 0 & 1 & 0 & 0 \\
-1 & 1 & 0 & 0 & 0 & 0 & 0 & -1 & 0 & 0 & 0 & 0 & 0 & 1 & 0 \\
0 & 1 & -1 & -1 & 1 & 0 & 0 & -1 & 0 & 0 & 0 & 0 & 0 & 0 & 1
\end{array}
\right]
\begin{array}{c}
\text{I} \\ \text{II} \\ \text{III} \\ \text{IV} \\ \text{V} \\ \text{VI} \\ \text{VII}
\end{array}
\end{array}
\qquad (3.3)
$$

To confirm that matrices are correctly defined, i.e. they describe the same oriented graph, theorem described by Equation (3.4) has been checked.

$$
A \cdot B^T = 0 \qquad (3.4)
$$

3.1.2. Edge Current Calculation

Structural matrices A and B describes circuit topology as an oriented graph. To make an analysis of electric circuit, each graph edge represents an electric branch built with series connection of voltage source E and impedance Z (see Fig. 3.1).

Ohm's law in matrix form is following:

$$V + E = Z_d \cdot I \tag{3.5}$$

where

$V^{[b \times 1]}$ – branch voltage matrix,

$E^{[b \times 1]}$ – branch voltage source matrix,

$Z_d^{[b \times b]}$ – branch impedance matrix (diagonal),

$I^{[b \times 1]}$ – branch current matrix.

It should be noted that Ohm's law can be applied also in phasor circuit analysis. In that case, all numbers in equation will be complex and they defines both - amplitude and initial phase in case of voltages and currents and complex impedance in case of Z_d.

One way how to calculate current flow in the circuit is a loop method which uses Equation (3.6).

$$I = B^T \cdot Z^{-1} \cdot E \tag{3.6}$$

where

$Z^{[b \times b]}$ – Impedance matrix (branch and mutual impedances)

Matrix Z can be calculated with an Equation (3.1.2):

$$Z = B \cdot Z_d \cdot B^T \tag{3.7}$$

For a topology defined on the Figure 3.1, assuming aforementioned edge and node numbering, given matrices are equal:

$$V = \begin{bmatrix} V_{21} \\ V_{23} \\ V_{45} \\ V_{27} \\ V_{47} \\ V_{67} \\ V_{68} \\ V_{39} \\ V_{43} \\ V_{65} \\ V_{61} \\ V_{28} \\ V_{48} \\ V_{19} \\ V_{59} \end{bmatrix} \quad (3.8) \qquad E = \begin{bmatrix} E_1 \\ E_2 \\ E_4 \\ E_7 \\ E_8 \\ E_9 \\ E_{g13} \\ E_{g22} \\ E_3 \\ E_5 \\ E_6 \\ E_{g11} \\ E_{g12} \\ E_{g21} \\ E_{g23} \end{bmatrix} \quad (3.9) \qquad I = \begin{bmatrix} I_1 \\ I_2 \\ I_4 \\ I_7 \\ I_8 \\ I_9 \\ I_{g13} \\ I_{g22} \\ I_3 \\ I_5 \\ I_6 \\ I_{g11} \\ I_{g12} \\ I_{g21} \\ I_{g23} \end{bmatrix} \quad (3.10)$$

$$\boldsymbol{Z_d}^{[b \times b]} = diag(Z_b, Z_b, Z_b, Z_b, Z_b, Z_b, Z_{g1}, Z_{g2}, Z_b, Z_b, Z_b, Z_{g1}, Z_{g1}, Z_{g2}, Z_{g2}) \tag{3.11}$$

$$\boldsymbol{Z}^{[b \times b]} = \begin{bmatrix} 4Z_b & -Z_b & Z_b & Z_b & -Z_b & -Z_b & -3Z_b \\ -Z_b & 4Z_b & Z_b & Z_b & 2Z_b & 0 & 2Z_b \\ Z_b & Z_b & 4Z_b & 2Z_b & Z_b & Z_b & -Z_b \\ Z_b & Z_b & 2Z_b & 2Z_b + 2Z_{g1} & Z_b + Z_{g1} & 0 & -Z_b \\ -Z_b & 2Z_b & Z_b & Z_b + Z_{g1} & 2Z_b + 2Z_{g1} & 0 & Z_b \\ -Z_b & 0 & Z_b & 0 & 0 & 2Z_b + 2Z_{g2} & Z_b + Z_{g2} \\ -3Z_b & 2Z_b & -Z_b & -Z_b & Z_b & Z_b + Z_{g2} & 4Z_b + 2Z_{g2} \end{bmatrix} \tag{3.12}$$

By use of Equation (3.6), edge currents as function of source voltages and circuit impedances can been calculated. It should be noted that given equations can be used for current flow calculation in a phasor domain only if input and output system voltages are symmetric, has the same frequency and no high level harmonics are present.

3.1.3. Edge Currents for an Example System Voltages

Definition of system matrices is required to calculate branch currents in an electric circuit. Following section contain analysis of current waveforms in a case when input and output frequencies are equal. With taken assumption, phasor circuit analysis is possible.

On the output system, only impedance is present. There are no voltage sources present, i.e. $E_{g2p} = 0$ (where $p = 1...3$ defines phase index). Therefore only converter is forcing current flow from source to the load through impedances.

Given example shows only how to map voltages and calculate current flow within a converter. Control algorithms are out of scope in this part. Current is not controlled. Its flow is forced by given selection of voltage in the sources E.

Input system voltages are equal (3.13a). Required (setpoint) output voltages are equal (3.13b).

$$v_{1p}(t) = V_{1m}cos\left(\omega t - \frac{2(p-1)}{3}\pi\right) \tag{3.13a}$$

$$v_{2p}(t) = V_{2m}cos\left(\omega t - \frac{2(p-1)}{3}\pi - \psi_2\right) \tag{3.13b}$$

Voltages in a phasor (complex) domain are equal (3.14). Complex numbers are marked **Bold** in the Thesis.

$$\begin{aligned} \boldsymbol{V_{g11}} &= V_{1m}e^{j0} & \boldsymbol{V_{g12}} &= V_{1m}e^{j\frac{2\pi}{3}} & \boldsymbol{V_{g13}} &= V_{1m}e^{j\frac{4\pi}{3}} \\ \boldsymbol{V_{g21}} &= V_{2m}e^{j\psi_2} & \boldsymbol{V_{g22}} &= V_{2m}e^{j\left(\frac{2\pi}{3}+\psi_2\right)} & \boldsymbol{V_{g23}} &= V_{2m}e^{j\left(\frac{4\pi}{3}+\psi_2\right)} \end{aligned} \tag{3.14}$$

Assuming that voltage drop on branch impedances is relatively low (i.e. $V_b \approx E_b$), and having given system voltages (supply and required output voltages), it is possible to define what are required voltages E_b in each branch. To obtain those values, Equation (3.40) is being used. Details about full mapping process can be found in Chapter 3.3.

Voltages V_N and V_X are set to zero. Branch voltage source vector E is equal (3.15).

$$\boldsymbol{E} = \begin{bmatrix} E_1 \\ E_2 \\ E_4 \\ E_7 \\ E_8 \\ E_9 \\ E_{g13} \\ E_{g22} \\ E_3 \\ E_5 \\ E_6 \\ E_{g11} \\ E_{g12} \\ E_{g21} \\ E_{g23} \end{bmatrix} = \begin{bmatrix} -\boldsymbol{V_{g11}} + \boldsymbol{V_{g21}} \\ -\boldsymbol{V_{g11}} + \boldsymbol{V_{g22}} \\ -\boldsymbol{V_{g12}} + \boldsymbol{V_{g23}} \\ -\boldsymbol{V_{g11}} \\ -\boldsymbol{V_{g12}} \\ -\boldsymbol{V_{g13}} \\ \boldsymbol{V_{g13}} \\ 0 \\ -\boldsymbol{V_{g12}} + \boldsymbol{V_{g22}} \\ -\boldsymbol{V_{g13}} + \boldsymbol{V_{g23}} \\ -\boldsymbol{V_{g13}} + \boldsymbol{V_{g21}} \\ \boldsymbol{V_{g11}} \\ \boldsymbol{V_{g12}} \\ 0 \\ 0 \end{bmatrix} \tag{3.15}$$

Matrix B has been defined by Equation (3.3). Matrix Z is defined by Equation (3.12).

Currents has been calculated with an Equation (3.6). After rearrangement to have natural order (branches from 1 to 15 instead of spanning and conspanning tree branches order), currents are equal (3.16).

$$I' = \begin{bmatrix} I_1 \\ I_2 \\ I_3 \\ I_4 \\ I_5 \\ I_6 \\ I_7 \\ I_8 \\ I_9 \\ I_{g11} \\ I_{g12} \\ I_{g13} \\ I_{g21} \\ I_{g22} \\ I_{g23} \end{bmatrix} = \begin{bmatrix} -\dfrac{\boldsymbol{V_{g23}}(Z_b+Z_{g1})+\boldsymbol{V_{g22}}(Z_b+4Z_{g1})-\boldsymbol{V_{g21}}(2Z_b+5Z_{g1})}{3Z_{r1}} \\ -\dfrac{\boldsymbol{V_{g21}}Z_b-2\boldsymbol{V_{g22}}Z_b+\boldsymbol{V_{g23}}Z_b+4\boldsymbol{V_{g21}}Z_{g1}-5\boldsymbol{V_{g22}}Z_{g1}+\boldsymbol{V_{g23}}Z_{g1}}{3Z_{r1}} \\ -\dfrac{-2\boldsymbol{V_{g22}}Z_b+\boldsymbol{V_{g23}}Z_b-5\boldsymbol{V_{g22}}Z_{g1}+4\boldsymbol{V_{g23}}Z_{g1}+\boldsymbol{V_{g21}}(Z_b+Z_{g1})}{3Z_{r1}} \\ -\dfrac{\boldsymbol{V_{g22}}Z_b-2\boldsymbol{V_{g23}}Z_b+4\boldsymbol{V_{g22}}Z_{g1}-5\boldsymbol{V_{g23}}Z_{g1}+\boldsymbol{V_{g21}}(Z_b+Z_{g1})}{3Z_{r1}} \\ -\dfrac{\boldsymbol{V_{g21}}Z_b+\boldsymbol{V_{g22}}Z_b-2\boldsymbol{V_{g23}}Z_b+4\boldsymbol{V_{g21}}Z_{g1}+\boldsymbol{V_{g22}}Z_{g1}-5\boldsymbol{V_{g23}}Z_{g1}}{3Z_{r1}} \\ -\dfrac{\boldsymbol{V_{g22}}(Z_b+Z_{g1})+\boldsymbol{V_{g23}}(Z_b+4Z_{g1})-\boldsymbol{V_{g21}}(2Z_b+5Z_{g1})}{3Z_{r1}} \\ \dfrac{\boldsymbol{V_{g23}}Z_{g1}}{Z_{r1}} \\ \dfrac{\boldsymbol{V_{g21}}Z_{g1}}{Z_{r1}} \\ \dfrac{\boldsymbol{V_{g22}}Z_{g1}}{Z_{r1}} \\ -\dfrac{\boldsymbol{V_{g23}}Z_b}{Z_{r1}} \\ -\dfrac{\boldsymbol{V_{g21}}Z_b}{Z_{r1}} \\ -\dfrac{\boldsymbol{V_{g22}}Z_b}{Z_{r1}} \\ -\dfrac{\boldsymbol{V_{g21}}(2Z_b+5Z_{g1})}{Z_{r1}} \\ -\dfrac{\boldsymbol{V_{g22}}(2Z_b+5Z_{g1})}{Z_{r1}} \\ -\dfrac{\boldsymbol{V_{g23}}(2Z_b+5Z_{g1})}{Z_{r1}} \end{bmatrix} \tag{3.16}$$

Symbol $Zr1$ has been defined to simplify given equations. It is equal (3.17):

$$Z_{r1} = Z_b^2 + 3Z_b Z_{g1} + 2Z_b Z_{g2} + 5Z_{g1}Z_{g2} \tag{3.17}$$

Table 3.1 contains numerical values for an example test case. In this operation point, converter works as a phase shifter. Phase between two waveforms is equal ϕ_2. For given numbers, branch currents has been calculated with an equation (3.16).

Table 3.1. Waveform parameters

Parameter	Value	Unit
V_1	4.16	kV
V_2	4.16	kV
ω	$2\pi \cdot 50$	rad/s
ψ_2	$\pi/6$	rad
R_{g1}	0.001	Ω
L_{g1}	0	mH
R_{g2}	10	Ω
L_{g2}	0	mH
R_b	0.001	Ω
L_b	1.25	mH

Graphical phasor representation of grid and load voltages is presented on the Figure 3.3.. It should be noted that grid voltage vectors are equal to given references, i.e. voltages are symmetrical, with given phase shifts. Load currents are phase shifted by about π what is correct for a given load type (resistive). Vector direction is according to given convention - current and voltage has opposite direction if the energy is coming out from the converter.

For a grid side, currents are phase shifted by about $\pi/2$. Its magnitudes are relatively low[2]. It is caused by relatively low grid impedance. In real system, grid currents are regulated by voltage drop control on the converter at input side. Without control applied, only some reactive power is fed from the grid.

Control algorithm target it provide required active power to keep converter energy at the given level. Additionally, reactive power can be controlled to meet given requirements, e.g. to provide $cos\phi = 0$ or to provide grid support in case of voltage dips or swells.

| (a) System 1 | (b) System 2 |
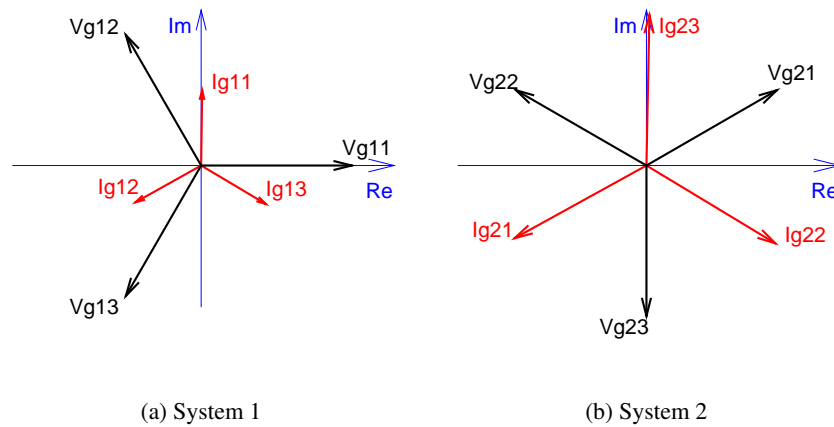
Figure 3.3. Grid side phasors of voltages (black) and currents (red)

On the Figure 3.4 (a,b) voltage and current phasors in the converter branches are shown. It should be noted that for given setpoint, current is flowing only through Hex branches. Y-branches does not take part in active power transfer. It can be also noted that current has the same magnitude and phase for branch pairs 1-6, 2-3 and 4-5. It means that current is symmetrically shared among all branches.

Identical voltages and currents on the converter's output terminals can be obtained for a different voltage source vector E. It will introduce so called circulating currents. Phenomenon description and mathematical model is presented in Chapter 3.2. In this section an example circulating currents are being introduced to show its influence on branch currents. As it was mentioned, output currents are identical as in the case with zero circulating current.

Circulating current flow is forced by modification of voltages in the Equation (3.15). By modification of voltage source in a branch, additional current flow is forced. Voltage and current phasors are

---

[2]It cannot be noticed on a picture, as there is no scale on it.

presented on the Figure 3.4 (c,d). Given waveforms has been made by voltage source vector defied by Equation (3.18).

$$\boldsymbol{E} = \begin{bmatrix} E_1 \\ E_2 \\ E_4 \\ E_7 \\ E_8 \\ E_9 \\ E_{g13} \\ E_{g22} \\ E_3 \\ E_5 \\ E_6 \\ E_{g11} \\ E_{g12} \\ E_{g21} \\ E_{g23} \end{bmatrix} = \begin{bmatrix} -V_{g11} + V_{g21} - Z_b \cdot I_{c1} \\ -V_{g11} + V_{g22} + Z_b \cdot I_{c2} \\ -V_{g12} + V_{g23} + Z_b \cdot I_{c3} \\ -V_{g11} + Z_b \cdot (I_{c1} - I_{c2}) \\ -V_{g12} + Z_b \cdot (I_{c2} - I_{c3}) \\ -V_{g13} + Z_b \cdot (I_{c3} - I_{c1}) \\ V_{g13} \\ 0 \\ -V_{g12} + V_{g22} - V_{g23} - Z_b \cdot I_{c2} \\ -V_{g13} + V_{g23} - V_{g23} - Z_b \cdot I_{c3} \\ -V_{g13} + V_{g21} + V_{g23} + Z_b \cdot I_{c1} \\ V_{g11} \\ V_{g12} \\ 0 \\ 0 \end{bmatrix} \tag{3.18}$$

Where:

$$\boldsymbol{I_{c1}} = I_{c0}e^{j0} \quad \boldsymbol{I_{c2}} = I_{c0}e^{j\frac{2\pi}{3}} \quad \boldsymbol{I_{c2}} = I_{c0}e^{j\frac{4\pi}{3}} \tag{3.19}$$

I_{c0} is a magnitude of circulating current which has been set to $100\ A$ in presented example case.

As it was expected, circulating current introduction forced current flow through Y branches. Also its introduction causes asymmetry in Hex branch pairs in contrary to zero circulating current case.

3.2. Current Mapping

To calculate branch powers in given system, branch currents must be know. It should be also noted that system currents are given. Therefore mapping what branch currents provide given system currents is required. To simplify the analysis, it has been assumed that each branch can be represented as an ideal current source. In that case, current flow can be calculated with use of KCL.

Topology graph analysis presented in a Chapter 3.1 shows that in a system, seven independent currents are present (as the graph is built with 9 nodes and 15 edges). Those independent currents can be chosen in many ways. In the previous analysis, specific loop currents has been chosen.

In following section, independent currents are defined by circulating currents and system's output currents. Chose following variables makes energy and power analysis in the branches more natural. Currents are being defined as output currents (given setpoints) and circulating currents (used as Degree of Freedom in a system). Given choice is also important as those values are directly references for a closed loop current control system [78].

(a) Hex branches; No circulating currents   (b) Y branches; No circulating currents

(c) Hex branches incl. circulating currents   (d) Y branches incl. circulating currents
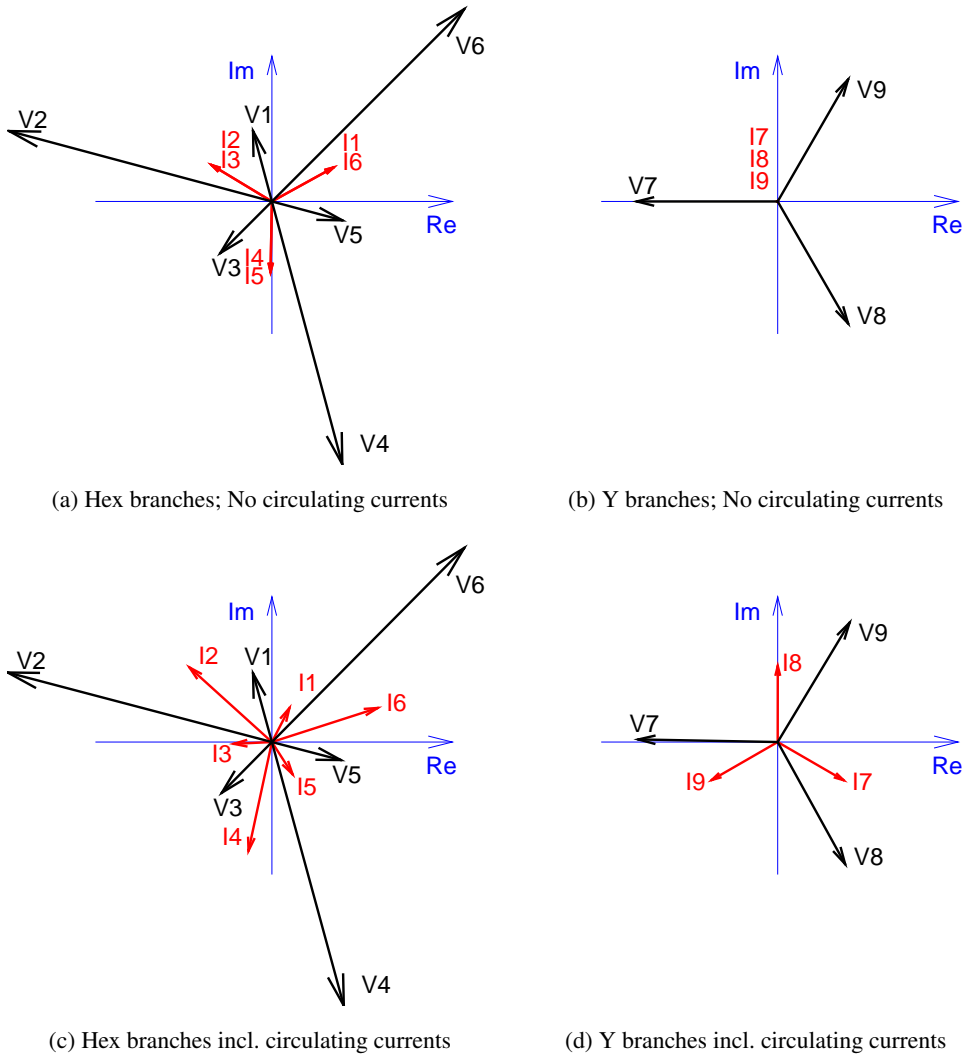
Figure 3.4. Branch phasors of voltages (black) and currents (red). (a,b) voltages defined by Eq. (3.15), (c,d) voltages with extra voltage drops introducing circulating currents.

Currents polarity and symbols are presented on the Figure 3.5.

To distinguish different coordinate systems, following naming convention is being used. Quantities with index o (output) refers to input/output values, circulating currents and star point voltage. Index b refers to nine branch quantities.

3.2.1. Circulating Currents

Circulating currents are feature for Modular Multilevel Converter (MMC) technology [79]. Its existence is linked to closed loops in the converter's topology. It is important, that circulating currents can be controlled in a control system.
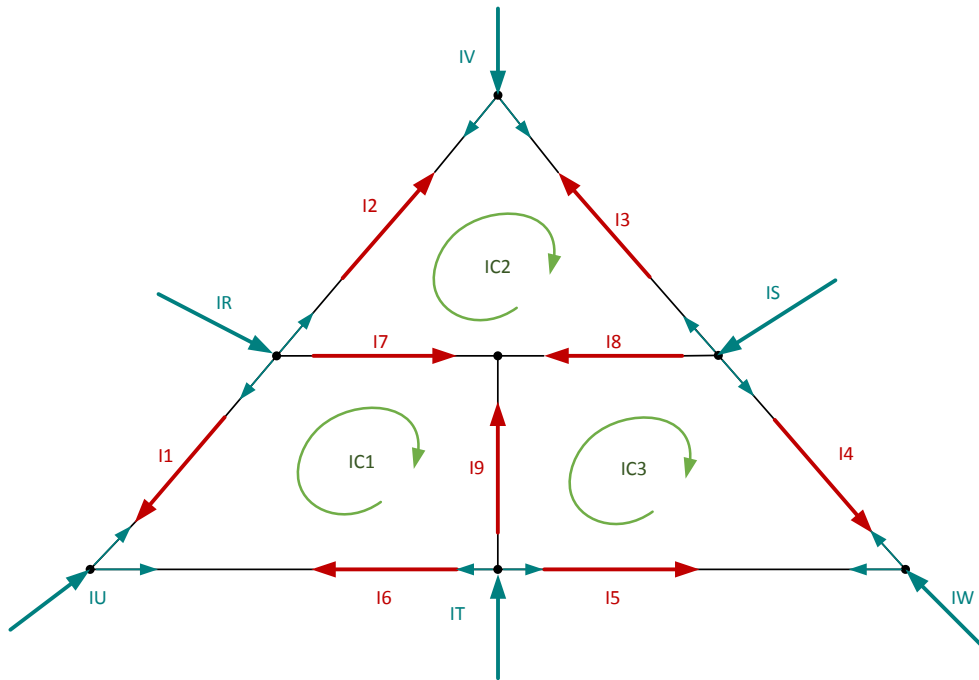
Figure 3.5. Terminal and branch currents definition. In red - branch currents. In blue
- terminal currents. In green - circulating currents.

Circulating current is defined as a current flowing in closed loop built with converter branches. This current has no influence on converter's output. Therefore it is treated as an internal quantity of the MMC system.

Number of circulating currents is equal to number of loops in a converter. Currents can be defined in a different ways. However it must be provided that chosen quantities are linear independent of each other.

An example way to define circulating currents is building a tree from converter graph. In that method, closed loop is chosen and one edge of that loop is being removed from the graph. This is repeated until there are no more closed loops in the graph i.e. graph tree is obtained.

For a topology presented on the Figure 3.5, circulating currents has been defined as currents flowing through following loops: 1-7-9-6 (i_{c1}), 2-3-8-7 (i_{c2}) and 4-5-9-8 (i_{c3}). Another possible definition is to use e.g. following paths: 1-2-3-4-5-6, 1-7-8-4-5-6 and 1-7-9-6.

3.2.1.1. Circulating current for a single converter arm

To explain circulating currents following section contains the simplest example in which two branches and one output phase are present.

Circulating currents are defined as a function of branch currents. To make this process more clear, two branch system is presented on the Figure 3.6.
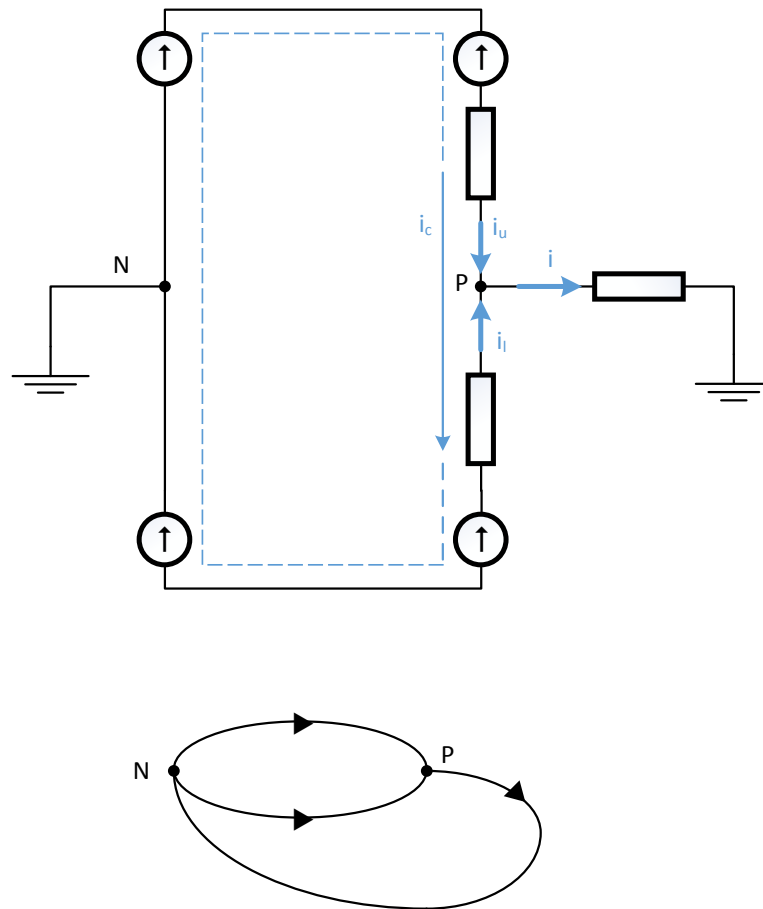
Figure 3.6. Single arm circuit schematic (top) plus topology graph (bottom)

According to topology graph, circuit contains two nodes and three edges what gives $3 - 2 + 1 = 2$ independent currents [see Eq. (3.1)]. Two of three any currents (top branch i_u, bottom branch i_l or output i) can be chosen.

Another way to choose linear independent currents is to define circulating current, i.e. current flowing in a closed loop between two branches. To use this approach, top and bottom branch current is represented as a sum of output current component and circulating current component. Equation (3.20) presents given definition.

$$\begin{cases} i_u = \frac{i}{2} + i_c \\ i_l = \frac{i}{2} - i_c \end{cases} \tag{3.20}$$

Sum of upper and lower branch current is equal output current what is in line with KCL:

$$i_u + i_l = i \tag{3.21}$$

Difference defines circulating current:

$$i_c = \frac{i_u - i_l}{2} \tag{3.22}$$

In further system analysis, quantities i_c and i can be used to fully describe currents in the system. Top and bottom branch currents can be calculated by use of Equation (3.20).

3.2.1.2. Circulating Currents in Hex-Y Topology

Previous shows how to define circulating current flowing through given branches. It is equal half of the difference between two branch currents. For each circulating current, an equation can be written down. Equation is valid to any chosen node. However, for Hex-Y topology and given circulating currents definition, in case of more than two converter branches in a single node, circulating current can be treated also as a sum of two circulating currents (see Figure 3.5).

Current i_{c1} will be defined on the node 1 (Figure 3.2a). Following equation is obtained:

$$i_{c1} = \frac{i_6 - i_1}{2} \tag{3.23}$$

Similarly, circulating currents i_{c2} and i_{c3} are defined on nodes 3 and 5 respectively.

$$i_{c2} = \frac{i_2 - i_3}{2} \tag{3.24a}$$

$$i_{c3} = \frac{i_4 - i_5}{2} \tag{3.24b}$$

Knowledge of currents $i_{c1,2,3}$ and two currents in the input and output system (e.g. two current phases, or $\alpha - \beta$ three phase components), all branch currents can be calculated.

Following section shows how to perform this calculation. The process will be named mapping, as it allows to map (or transform) quantities from one reference system to the other one. Output (o) system (circulating and phase currents) is useful for top-level control where phase current references are given. Branch (b) system (branch currents) is useful for low-level control when given branch current references are given for current controllers on the branch and cell level.

3.2.2. Output-Branch Mapping

Branch currents are calculated in following way: in the first step, mapping output currents in a matrix form has been defined. Use of three output currents for both systems and three circulating currents gives a 9×9 matrix. In the next step, an inverted matrix has been calculated. Finally three phase currents has been mapped into $\alpha - \beta$ reference frame.

Branch-phase mapping is given as:

$$\boldsymbol{i'_o} = \boldsymbol{T_{i,br-abc}} \cdot \boldsymbol{i_b} \tag{3.25}$$

In the equation (3.25) Current vectors $\boldsymbol{i'_o}$ and $\boldsymbol{i_b}$ defines currents in a following way:

$$\boldsymbol{i'_o}^{[9\times 1]} = \begin{bmatrix} i_R & i_S & i_T & i_U & i_V & i_W & i_{c1} & i_{c2} & i_{c3} \end{bmatrix}^T \tag{3.26}$$

$$\boldsymbol{i_b}^{[9\times 1]} = \begin{bmatrix} i_1 & i_2 & i_3 & i_4 & i_5 & i_6 & i_7 & i_8 & i_9 \end{bmatrix}^T \tag{3.27}$$

To calculate inverted matrix, nine equations are required (square matrix must be built). Therefore, 9-element current vector $\boldsymbol{i'_o}$ has been chosen even though only 7 degrees of freedom are present in the system. Given matrix will be reduced in the next step by use of $\alpha - \beta$ Clarke transformation [80].

So called branch-terminal matrix $\boldsymbol{T_{i,br-abc}}$ represents linear transformation between branch and terminal coordinate systems. It has been constructed by use of KCL for given nodes (first six equations). Remaining three equations describes circulating currents as it has been defined by Equations (3.23) and (3.24). Complete mapping matrix is equal (3.28):

$$\boldsymbol{T_{i,br-abc}^{[9\times 9]}} = \begin{bmatrix} 1 & 1 & 0 & 0 & 0 & 0 & 1 & 0 & 0 \\ 0 & 0 & 1 & 1 & 0 & 0 & 0 & 1 & 0 \\ 0 & 0 & 0 & 0 & 1 & 1 & 0 & 0 & 1 \\ -1 & 0 & 0 & 0 & 0 & -1 & 0 & 0 & 0 \\ 0 & -1 & -1 & 0 & 0 & 0 & 0 & 0 & 0 \\ 0 & 0 & 0 & -1 & -1 & 0 & 0 & 0 & 0 \\ -0.5 & 0 & 0 & 0 & 0 & 0.5 & 0 & 0 & 0 \\ 0 & 0.5 & -0.5 & 0 & 0 & 0 & 0 & 0 & 0 \\ 0 & 0 & 0 & 0.5 & -0.5 & 0 & 0 & 0 & 0 \end{bmatrix} \tag{3.28}$$

Terminal-branch matrix describes opposite transformation. It can be calculated as an inversion of aforementioned $\boldsymbol{T_{i,br-abc}}$ matrix as it is shown in an Equation (3.25):

$$\boldsymbol{i_b} = \boldsymbol{T_{i,br-abc}^{-1}} \cdot \boldsymbol{i'_o} = \boldsymbol{T_{i,abc-br}} \cdot \boldsymbol{i'_o} \tag{3.29}$$

Inverted matrix, named $\boldsymbol{T_{i,abc-br}}$ ie equal (3.30):

$$\boldsymbol{T_{i,abc-br}^{[9\times 9]}} = \begin{bmatrix} 0 & 0 & 0 & -0.5 & 0 & 0 & -1 & 0 & 0 \\ 0 & 0 & 0 & 0 & -0.5 & 0 & 0 & 1 & 0 \\ 0 & 0 & 0 & 0 & -0.5 & 0 & 0 & -1 & 0 \\ 0 & 0 & 0 & 0 & 0 & -0.5 & 0 & 0 & 1 \\ 0 & 0 & 0 & 0 & 0 & -0.5 & 0 & 0 & -1 \\ 0 & 0 & 0 & -0.5 & 0 & 0 & 1 & 0 & 0 \\ 1 & 0 & 0 & 0.5 & 0.5 & 0 & 1 & -1 & 0 \\ 0 & 1 & 0 & 0 & 0.5 & 0.5 & 0 & 1 & -1 \\ 0 & 0 & 1 & 0.5 & 0 & 0.5 & -1 & 0 & 1 \end{bmatrix} \tag{3.30}$$

As it was mentioned before, in physical system, there are 7 DOF's (assuming that there is no zero sequence component in phase currents). Those DOF can be coupled with input (2), output (2) and circulating currents (3).

To reduce terminal-branch mapping, three phase to $\alpha - \beta$ reference frame Clarke transformation defined as (3.31) will be used.

$$\boldsymbol{x_{\alpha\beta}} = \frac{2}{3}\left(x_a + \boldsymbol{a}x_b + \boldsymbol{a}^2 x_c\right) \tag{3.31}$$

In a matrix form:

$$\begin{bmatrix} x_\alpha \\ x_\beta \end{bmatrix} = \frac{2}{3} \begin{bmatrix} 1 & -\frac{1}{2} & -\frac{1}{2} \\ 0 & \frac{\sqrt{3}}{2} & \frac{-\sqrt{3}}{2} \end{bmatrix} \cdot \begin{bmatrix} x_a \\ x_b \\ x_c \end{bmatrix} \tag{3.32}$$

where

a – Rotation operator ($a = e^{j\frac{2}{3}\pi}$),

x – Voltage or Current component in three-phase reference frame (a, b, c), or in 2-phase (α, β) reference frame.

Inverse Clark transformation is given as (3.33).

$$\begin{bmatrix} x_a \\ x_b \\ x_c \end{bmatrix} = \begin{bmatrix} 1 & 0 \\ -\frac{1}{2} & \frac{\sqrt{3}}{2} \\ -\frac{1}{2} & \frac{-\sqrt{3}}{2} \end{bmatrix} \cdot \begin{bmatrix} x_\alpha \\ x_\beta \end{bmatrix} \tag{3.33}$$

Terminal-branch current mapping matrix defines dependence between current vector i_o and branch vector i_b (3.34).

$$\boldsymbol{i_b} = \boldsymbol{T_{i,\alpha\beta-br}} \cdot \boldsymbol{i_o} \tag{3.34}$$

Reduced output current is given as (3.35):

$$\boldsymbol{i_o}^{[7\times1]} = \begin{bmatrix} i_{\alpha1} & i_{\beta1} & i_{\alpha2} & i_{\beta2} & i_{c1} & i_{c2} & i_{c3} \end{bmatrix}^T \tag{3.35}$$

where:

$i_{\alpha1}, i_{\beta1}$ – input current components,

$i_{\alpha2}, i_{\beta2}$ – output current components,

i_{c1}, i_{c2}, i_{c3} – circulating currents.

Substituting into equation (3.29) currents from i_o' vector transformed by Equation (3.33) into $\alpha - \beta$ reference frame, $\boldsymbol{T_{i,\alpha\beta-br}}$ mapping matrix is obtained:

$$T_{i,\alpha\beta-br}^{[9\times 7]} = \begin{bmatrix} 0 & 0 & -\frac{1}{2} & 0 & -1 & 0 & 0 \\ 0 & 0 & \frac{1}{4} & -\frac{\sqrt{3}}{4} & 0 & 1 & 0 \\ 0 & 0 & \frac{1}{4} & -\frac{\sqrt{3}}{4} & 0 & -1 & 0 \\ 0 & 0 & \frac{1}{4} & \frac{\sqrt{3}}{4} & 0 & 0 & 1 \\ 0 & 0 & \frac{1}{4} & \frac{\sqrt{3}}{4} & 0 & 0 & -1 \\ 0 & 0 & -\frac{1}{2} & 0 & 1 & 0 & 0 \\ 1 & 0 & \frac{1}{4} & \frac{\sqrt{3}}{4} & 1 & -1 & 0 \\ -\frac{1}{2} & \frac{\sqrt{3}}{2} & -\frac{1}{2} & 0 & 0 & 1 & -1 \\ -\frac{1}{2} & -\frac{\sqrt{3}}{2} & \frac{1}{4} & -\frac{\sqrt{3}}{4} & -1 & 0 & 1 \end{bmatrix} \tag{3.36}$$

3.2.3. Branch current waveforms for given phase currents

As branch-output mapping is defined it is possible to calculate branch currents for given phase currents. In this section, an example waveforms will be presented. The example shows branch currents for symmetric sinusoidal currents with different frequencies for input and output system.

Phase currents transformed into $\alpha - \beta$ (3.32) are equal:

$$\begin{bmatrix} i_{\alpha s} \\ i_{\beta s} \end{bmatrix} = \begin{bmatrix} \frac{2}{3} & -\frac{1}{3} & -\frac{1}{3} \\ 0 & \frac{\sqrt{3}}{2} & -\frac{\sqrt{3}}{2} \end{bmatrix} \cdot \begin{bmatrix} I_{sm}cos(\omega_s t - \phi_s - \psi_s) \\ I_{sm}cos(\omega_s t - \phi_s - \frac{2}{3}\pi - \psi_s) \\ I_{sm}cos(\omega_s t - \phi_s - \frac{4}{3}\pi - \psi_s) \end{bmatrix} = \begin{bmatrix} I_{sm}cos(\omega_s t - \phi_s - \psi_s) \\ I_{sm}sin(\omega_s t - \phi_s - \psi_s) \end{bmatrix} \tag{3.37}$$

where

$$s \quad - \text{ system } (s = 1 \text{ or } 2),$$

$$I_{sm} \quad - \text{ current amplitude,}$$

$$\omega_s \quad - \text{ angular frequency } (\omega_s = 2\pi f_s),$$

$$\phi_s \quad - \text{ load angle of the system s,}$$

$$\psi_s \quad - \text{ initial phase shift of the system s } (\psi_1 = 0).$$

An example system parameters are given in Table 3.2. Circulating currents are equal zero to make mapping simper. I_t vector is equal (3.38):

$$\boldsymbol{i_o} = \begin{bmatrix} i_{\alpha 1} \\ i_{\beta 1} \\ i_{\alpha 2} \\ i_{\beta 2} \\ i_{c1} \\ i_{c2} \\ i_{c3} \end{bmatrix} = \begin{bmatrix} cos(\omega_1 t) \\ sin(\omega_1 t) \\ -cos(\omega_2 t) \\ -sin(\omega_2 t) \\ 0 \\ 0 \\ 0 \end{bmatrix} \tag{3.38}$$

Table 3.2. Waveform parameters

Parameter	Value	Unit
V_{1m}	1	$p.u.$
I_{1m}	1	$p.u.$
V_{2m}	1	$p.u.$
I_{2m}	-1	$p.u.$
ω_1	$2\pi \cdot 50$	rad/s
ω_2	$2\pi \cdot 25$	rad/s
ϕ_1	0	rad
ϕ_2	0	rad
ψ_1	0	rad
ψ_2	0	rad

For predefined vector, according to Equation (3.34) branch currents are equal (3.39).

$$
\boldsymbol{i_b} = \begin{bmatrix} i_1 \\ i_2 \\ i_3 \\ i_4 \\ i_5 \\ i_6 \\ i_7 \\ i_8 \\ i_9 \end{bmatrix} = \begin{bmatrix} \frac{1}{2}cos(\omega_2 t) \\ \frac{1}{4}\left[-cos(\omega_2 t) + \sqrt{3}sin(\omega_2 t)\right] \\ \frac{1}{4}\left[-cos(\omega_2 t) + \sqrt{3}sin(\omega_2 t)\right] \\ \frac{1}{4}\left[-cos(\omega_2 t) - \sqrt{3}sin(\omega_2 t)\right] \\ \frac{1}{4}\left[-cos(\omega_2 t) - \sqrt{3}sin(\omega_2 t)\right] \\ \frac{1}{2}cos(\omega_2 t) \\ cos(\omega_1 t) - \frac{1}{4}cos(\omega_2 t) - \frac{1}{4}\sqrt{3}sin(\omega_2 t) \\ \frac{1}{2}\left[-cos(\omega_1 t) + cos(\omega_2 t) + \sqrt{3}sin(\omega_1 t)\right] \\ \frac{1}{4}\left[-2cos(\omega_1 t) - cos(\omega_2 t) + \sqrt{3}\left[-2sin(\omega_1 t) + sin(\omega_2 t)\right]\right] \end{bmatrix} \tag{3.39}
$$

Branch current for a branch 1 (Hex) and branch 7 (Y) has been presented on the Figure 3.7.

3.3. Voltage Mapping

Voltage mapping is a process of mathematical transformation branch voltage waveforms into voltages present on the system output terminals. Mapping can be described by a matrix equation. Following section explains how the mapping matrix is calculated.

Figure 3.8 presents system voltages with its naming and polarity. Following nomenclature has been used: voltages are marked with arrows showing higher potential or equivalent $+/-$ symbols.

Based on Figure 3.8 dependencies between branch and output voltages can be written down. Inverted process is possible as well. Branch-phase mapping transformation is given as (3.40).

$$
\boldsymbol{v_b} = \boldsymbol{T_{v,abc-br}} \cdot \boldsymbol{v_o'} \tag{3.40}
$$
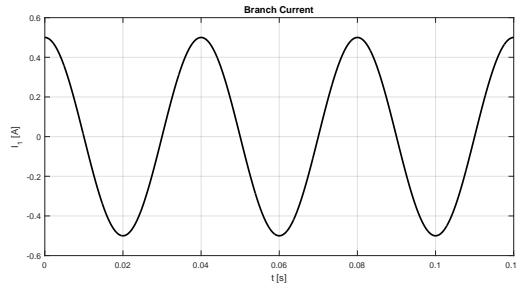
(a) Branch 1
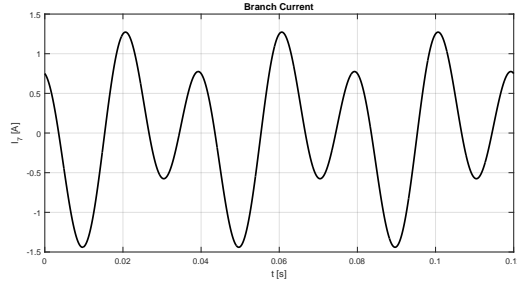
(b) Branch 7

Figure 3.7. Branch currents

In given equation, V_b vector contains branch voltages. V_o' vector contains output terminal voltages and two extra voltages i.e. star point of Y (marked X in the Figure) and common mode voltage between two systems. Vectors are equal:

$$\boldsymbol{v_b}^{[9\times1]} = \begin{bmatrix} v_1 & v_2 & v_3 & v_4 & v_5 & v_6 & v_7 & v_8 & v_9 \end{bmatrix}^T \tag{3.41}$$

$$\boldsymbol{v_o'}^{[8\times1]} = \begin{bmatrix} v_R & v_S & v_T & v_U & v_V & v_W & v_N & v_X \end{bmatrix}^T \tag{3.42}$$

Matrix $\boldsymbol{T_{v,abc-br}}$ is equal (3.43).

$$\boldsymbol{T_{v,abc-br}^{[9\times8]}} = \begin{bmatrix} -1 & 0 & 0 & 1 & 0 & 0 & 1 & 0 \\ -1 & 0 & 0 & 0 & 1 & 0 & 1 & 0 \\ 0 & -1 & 0 & 0 & 1 & 0 & 1 & 0 \\ 0 & -1 & 0 & 0 & 0 & 1 & 1 & 0 \\ 0 & 0 & -1 & 0 & 0 & 1 & 1 & 0 \\ 0 & 0 & -1 & 1 & 0 & 0 & 1 & 0 \\ -1 & 0 & 0 & 0 & 0 & 0 & 0 & 1 \\ 0 & -1 & 0 & 0 & 0 & 0 & 0 & 1 \\ 0 & 0 & -1 & 0 & 0 & 0 & 0 & 1 \end{bmatrix} \tag{3.43}$$

Three phase input and output voltages can be transformed by Clarke transformation (3.32). Finally, Equation (3.44) is obtained.
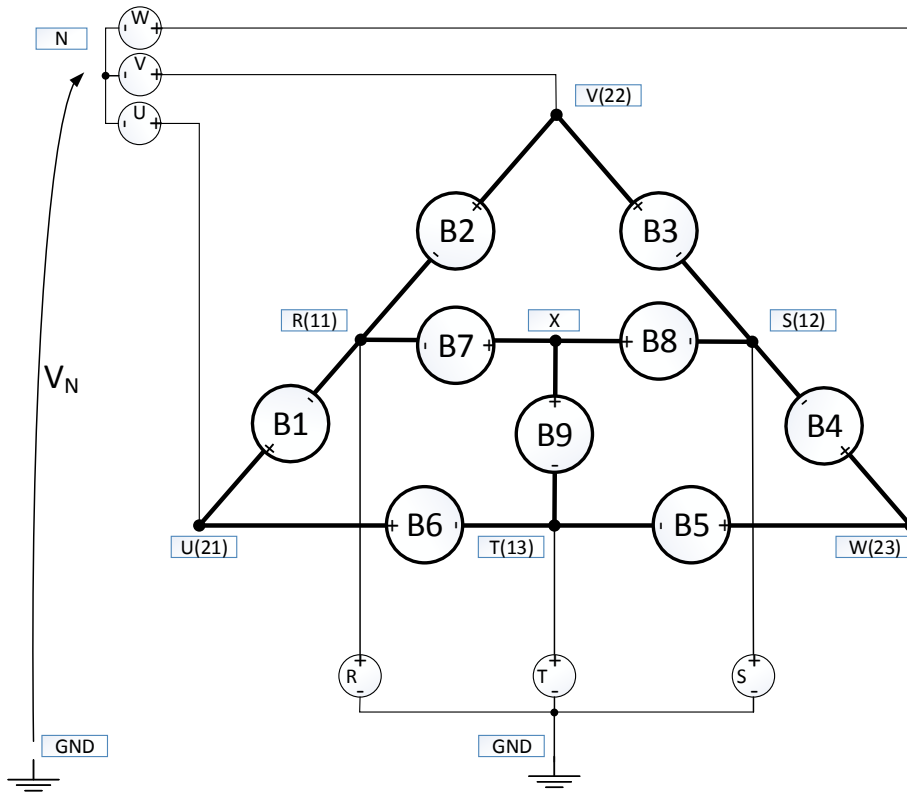
Figure 3.8. Voltage mapping for Hex-Y topology.

$$v_b = T_{v,\alpha\beta-br} \cdot v_o \tag{3.44}$$

Vector v_o is defined as:

$$v_o^{[6\times 1]} = \begin{bmatrix} v_{\alpha 1} & v_{\beta 1} & v_{\alpha 2} & v_{\beta 2} & v_N & v_X \end{bmatrix}^T \tag{3.45}$$

Transformation matrix is equal:

$$T_{v,\alpha\beta-br}^{[9\times 6]} = \begin{bmatrix} -1 & 0 & 1 & 0 & 1 & 0 \\ -1 & 0 & -\frac{1}{2} & \frac{\sqrt{3}}{2} & 1 & 0 \\ \frac{1}{2} & -\frac{\sqrt{3}}{2} & -\frac{1}{2} & \frac{\sqrt{3}}{2} & 1 & 0 \\ \frac{1}{2} & -\frac{\sqrt{3}}{2} & -\frac{1}{2} & -\frac{\sqrt{3}}{2} & 1 & 0 \\ \frac{1}{2} & \frac{\sqrt{3}}{2} & -\frac{1}{2} & -\frac{\sqrt{3}}{2} & 1 & 0 \\ \frac{1}{2} & \frac{\sqrt{3}}{2} & 1 & 0 & 1 & 0 \\ -1 & 0 & 0 & 0 & 0 & 1 \\ \frac{1}{2} & -\frac{\sqrt{3}}{2} & 0 & 0 & 0 & 1 \\ \frac{1}{2} & \frac{\sqrt{3}}{2} & 0 & 0 & 0 & 1 \end{bmatrix} \tag{3.46}$$

3.3.1. Branch voltage waveforms for given phase voltages

An example branch voltage waveforms has been calculated for given phase voltages. As for an example with currents, symmetric sinusoidal waveforms has been chosen. Common mode and star point voltages has been set to zero. Table 3.2 contains system parameters. $\boldsymbol{v_o}$ vector is equal (3.47).

$$\boldsymbol{v_o} = \begin{bmatrix} v_{\alpha 1} \\ v_{\beta 1} \\ v_{\alpha 2} \\ v_{\beta 2} \\ v_N \\ v_X \end{bmatrix} = \begin{bmatrix} cos(\omega_1 t) \\ sin(\omega_1 t) \\ cos(\omega_2 t) \\ sin(\omega_2 t) \\ 0 \\ 0 \end{bmatrix} \tag{3.47}$$

For given waveforms, branch voltages are equal (3.48).

$$\begin{bmatrix} v_1 \\ v_2 \\ v_3 \\ v_4 \\ v_5 \\ v_6 \\ v_7 \\ v_8 \\ v_9 \end{bmatrix} = \begin{bmatrix} -cos(\omega_1 t) + cos(\omega_2 t) \\ \frac{1}{2}\left[-2cos(\omega_1 t) - cos(\omega_2 t) + \sqrt{3}sin(\omega_2 t) \right] \\ \frac{1}{2}\left[cos(\omega_1 t) - cos(\omega_2 t) - \sqrt{3}(sin(\omega_1 t) - sin(\omega_2 t)) \right] \\ \frac{1}{2}\left[cos(\omega_1 t) - cos(\omega_2 t) + \sqrt{3}(-sin(\omega_1 t) - sin(\omega_2 t)) \right] \\ \frac{1}{2}\left[cos(\omega_1 t) - cos(\omega_2 t) + \sqrt{3}(sin(\omega_1 t) - sin(\omega_2 t)) \right] \\ \frac{1}{2}\left[cos(\omega_1 t) + 2cos(\omega_2 t) + \sqrt{3}sin(\omega_1 t) \right] \\ -cos(\omega_1 t) \\ \frac{1}{2}\left[cos(\omega_1 t) - \sqrt{3}sin(\omega_1 t) \right] \\ \frac{1}{2}\left[cos(\omega_1 t) + \sqrt{3}sin(\omega_1 t) \right] \end{bmatrix} \tag{3.48}$$

Waveforms for branch 1 (Hex) and branch 7 (Y) are presented on the Figure 3.9.

It should be noted that in contrary to branch currents which contains only ω_2 components [Equation (3.39)], voltage contains both frequency components - ω_1 and ω_2.

In Y part, the situation is opposite, i.e. currents contain both frequency components while voltage contains only ω_1 frequency.
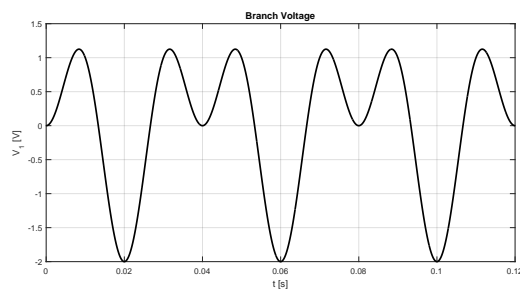
(a) Branch 1
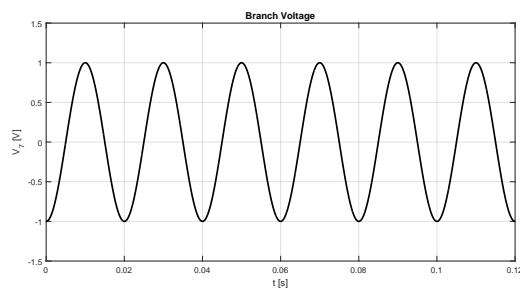
(b) Branch 7

Figure 3.9. Branch voltages

4. Branch Powers

In Chapter 4,it is presented how the branch powers are calculated and what is the necessary condition to have the stable system. The special operation points are identified and distinguished from a normal operation points. An example branch powers and corresponding energies are presented to highlight that the system without introduction of circulating currents is not stable even in normal operation points.

Having given branch voltages and currents, it is possible to calculate instantaneous branch powers by using an Equation (4.1).

$$p = v \cdot i \tag{4.1}$$

Branch energy corresponds to branch power and losses. Losses are neglected in the analysis as it is assumed they are equal for each branch and they can be compensated with power balancing module in further analysis.

The energy is an integral of branch power as it is stated in the Equation (4.2).

$$e_b(t) = \int_0^t p_b \cdot dt + E_{b,0} = \int_0^t v_b \cdot i_b \cdot dt + E_{b,0} \tag{4.2}$$

where

$$b \quad - \quad \text{branch number } (b = 1...9),$$

$$E_{b,0} \quad - \quad \text{initial branch energy.}$$

To provide that energy not drift to $\pm\infty$ it must be guaranteed that constant component in the branch power p_b is equal zero in each branch. In the next step of control loop algorithm design, a constant component will be non-zero to provide required energy flow within a converter: to compensate power losses and provide charging/discharging capabilities for a converter.

4.1. Branch power for zero circulating current and common mode voltage

In the first step of analysis, it will be checked if in case of zero circulating currents and no common mode voltage and star point voltages (v_N, v_X), constant components in branch powers are present. If

they are, it means, that branch energies will drift during the converter operation. To achieve the steady state of a converter, energies must not contain constant components.

First, powers for an operation point with sinusoidal waveforms with different input and output frequency has been calculated. Currents and voltages are represented as $\boldsymbol{i_o}$ and $\boldsymbol{v_o}$ - see Equations (4.3) and (4.4).

$$
\boldsymbol{i_o} = \begin{bmatrix} i_{\alpha 1} \\ i_{\beta 1} \\ i_{\alpha 2} \\ i_{\beta 2} \\ i_{c1} \\ i_{c2} \\ i_{c3} \end{bmatrix} = \begin{bmatrix} I_{1m}cos(\omega_1 t) \\ I_{1m}sin(\omega_1 t) \\ I_{2m}cos(\omega_2 t - \psi_2) \\ I_{2m}sin(\omega_2 t - \psi_2) \\ 0 \\ 0 \\ 0 \end{bmatrix} \tag{4.3}
$$

$$
\boldsymbol{v_o} = \begin{bmatrix} v_{\alpha 1} \\ v_{\beta 1} \\ v_{\alpha 2} \\ v_{\beta 2} \\ v_N \\ v_X \end{bmatrix} = \begin{bmatrix} V_{1m}cos(\omega_1 t - \phi_1) \\ V_{1m}sin(\omega_1 t - \phi_1) \\ V_{2m}cos(\omega_2 t - \psi_2 - \phi_2) \\ V_{2m}sin(\omega_2 t - \psi_2 - \phi_2) \\ 0 \\ 0 \end{bmatrix} \tag{4.4}
$$

Branch powers for that case are presented in Appendix A, Equations (A.1). In calculated powers, following frequency components can be identified:

$$
p_b(t) = P_{b,0} + p_b(2\omega_1 t) + p_b(2\omega_2 t) + p_b((\omega_1 - \omega_2)t) + p_b((\omega_1 + \omega_2)t) \tag{4.5}
$$

$P_{b,0}$ is a constant component. Additionally components related with double input and double output frequencies are visible. Also components with sum/difference of input/output frequencies are present.

From an equation 4.5 following conclusion can be drawn: constant component $P_{b,0}$ defines whether the branch power is in equilibrium point or not. Additional constant components can also appear when:

> **Special operation points for Hex-Y topolog**
>
> – $\omega_1 = 0$ makes an extra constant component in the $p_b(2\omega_1 t)$ part
>
> – $\omega_2 = 0$ makes an extra constant component in the $p_b(2\omega_2 t)$ part
>
> – $\omega_1 = \omega_2$ makes an extra constant component in the $p_b((\omega_1 - \omega_2)t)$ part
>
> – $\omega_1 = -\omega_2$ makes an extra constant component in the $p_b((\omega_1 + \omega_2)t)$ part

As it was mentioned, constant part in the branch power is critical because for non-zero value, branch charging/discharging is observed. In the steady state it should be equal zero to provide constant capacitor bank voltage (average).

In further analysis it was assumed that $\omega_1 \neq 0$ for every operation point (grid connected converter). For $\omega_1 \neq \pm\omega_2 \neq 0$, *normal operation point* is defined. In case of $\omega_2 = \pm\omega_1$ or $\omega_2 = 0$, a *special operation point* is defined.

Normal operation point study will start with energy flow analysis. It will be performed by finding constant component in each branch power. They are equal:

$$P_{b,0} = \begin{cases} -\frac{1}{4}P_2 & \text{for } b = 1...6 \\ -\frac{1}{2}P_1 & \text{for } b = 7...9 \end{cases} \tag{4.6}$$

where

$$b \quad - \quad \text{Branch number } (b = 1...9),$$

$$P_s \quad - \quad \text{Active power corresponding to system } s, \text{ equal (4.7a)},$$

$$Q_s \quad - \quad \text{Reactive power corresponding to system } s \text{ equal (4.7b)}[1].$$

Powers used in the equation above are defined as (4.7):

$$P_s = V_{sm} \cdot I_{sm} \cdot cos(\phi_s) \tag{4.7a}$$

$$Q_s = V_{sm} \cdot I_{sm} \cdot sin(\phi_s) \tag{4.7b}$$

$$S_s = V_{sm} \cdot I_{sm} \tag{4.7c}$$

Total, 3-phase system powers are equal (4.8).

$$P_{s,tot} = \frac{3}{2}V_{sm} \cdot I_{sm} \cdot cos(\phi_s) = \frac{3}{2}P_s \tag{4.8a}$$

$$Q_{s,tot} = \frac{3}{2}V_{sm} \cdot I_{sm} \cdot sin(\phi_s) = \frac{3}{2}Q_s \tag{4.8b}$$

$$S_{s,tot} = \frac{3}{2}V_{sm} \cdot I_{sm} = \frac{3}{2}S_s \tag{4.8c}$$

According to Equations (4.6), in normal operation point, constant components are non-zero. It means that branch energy will drift over time.

> **Power flow in a system**
>
> – Active power flows between Hex and Y branches
>
> – For $P_1 = -P_2$, total power is equal zero. It means that converter transfers full energy between two systems. Total converter energy remains constant

---

[1]Reactive power is not used in the Equation (4.6), but it is defined here to keep definitions in one place.

4.1.1. An Example Branch Power and Energy Waveforms

In this section, power and energy waveforms for a chosen example are shown. Test case parameters are summarized in the Table 3.2. For zero reactive power and equal input and output active powers for both systems, it is supposed to observe energy flow between Hex and Y branches. Total converter energy remains constant (as input power is equal output power).

As constant components are equal for each branch (but different for Hex and Y), it should be observed that drift is similar for each Hex and for each Y branch respectively.

Branch powers are product of currents defined by Equation (3.39) and voltages defined by Equation (3.48). Complete power equations are included in Appendix, Equation (A.1).

(a) Hex Power

(b) Hex Energy

(c) Y Power

(d) Y Energy
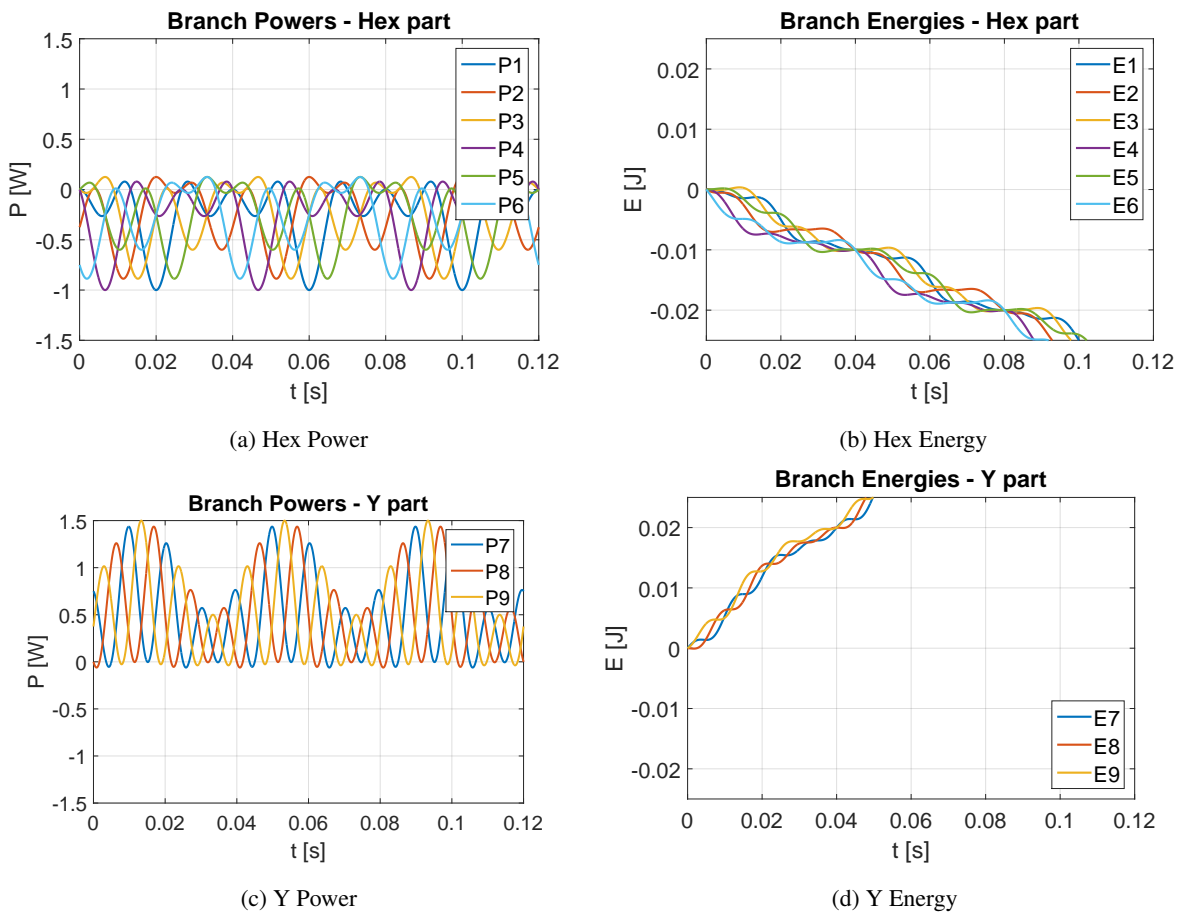
Figure 4.1. Branch powers and energies for an example case. Branches 1 through 6 belongs to Hex, 7 through 9 belongs to Y part of the converter.

On the Figures 4.1a and 4.1c branch power waveforms are shown. It can be noted that each Hex branch has negative average value while each Y branch has positive average.

On the Figures 4.1b and 4.1d branch energy waveforms are presented. Plot has been obtained by integration of branch powers. As it was supposed, it can be noted that all Hex and all Y branches drifts to either $-\infty$ (Hex) or $+\infty$ (Y). Hex branches are being discharged (all equally together) and Y branches are being charged (also all together).

Based on observed dependencies, it can be assumed that to provide steady state operation of the converter, circulating currents i_{cx} and (or) voltages v_X, v_N should be introduced.

4.2. Branch power for introduced circulating current and common mode voltage

In the previous section it has been justified that introduction of non-zero circulating current is required to provide steady state operation of a converter. Without circulating currents, energy divergence is observed. It is possible that also introduction of non-zero voltages v_N and v_X is required. Following sections contains analysis of different waveforms and its influence on the branch powers.

Analysis is performed for symmetric voltages and currents in both, input and output system.

In the first step, voltage and current vectors $\boldsymbol{v_o}$ and $\boldsymbol{i_o}$ are redefined. Voltage vector contains v_N and v_X components (4.9).

$$
\boldsymbol{v_o} = \begin{bmatrix} v_{\alpha 1} \\ v_{\beta 1} \\ v_{\alpha 2} \\ v_{\beta 2} \\ v_N \\ v_X \end{bmatrix} = \begin{bmatrix} V_{1m}cos(\omega_1 t - \phi_1) \\ V_{1m}sin(\omega_1 t - \phi_1) \\ V_{2m}cos(\omega_2 t - \psi_2 - \phi_2) \\ V_{2m}sin(\omega_2 t - \psi_2 - \phi_2) \\ v_N(t) \\ v_X(t) \end{bmatrix} \tag{4.9}
$$

Currents vector $\boldsymbol{i_o}$ contains non-zero circulating currents (4.10):

$$
\boldsymbol{i_o} = \begin{bmatrix} i_{\alpha 1} \\ i_{\beta 1} \\ i_{\alpha 2} \\ i_{\beta 2} \\ i_{c1} \\ i_{c2} \\ i_{c3} \end{bmatrix} = \begin{bmatrix} I_{1m}cos(\omega_1 t) \\ I_{1m}sin(\omega_1 t) \\ I_{2m}cos(\omega_2 t - \psi_2) \\ I_{2m}sin(\omega_2 t - \psi_2) \\ i_{c1}(t) \\ i_{c2}(t) \\ i_{c3}(t) \end{bmatrix} \tag{4.10}
$$

For given symbols, branch voltages, currents and powers are presented in Appendix A, Equations A.2. Further analysis will be performed for constant components in obtained power equations.

The goal in a Thesis is to define circulating currents and voltages which provides steady state operation of the converter. Following target is to have enough DOF to control each converter branch energy separately. Given problem has more than one solution. Therefore in further study, optimization of chosen waveforms can be performed (however it is out of the scope of the Thesis).

Section 4.3 contains analysis for normal operation point, i.e. $\omega_1 \neq \pm\omega_2 \neq 0$. Special operation point in which output frequency is zero ($\omega_2 = 0$) is analyzed in the Section 4.7.

4.3. Branch powers for normal operation point

Equations (A.2) shows powers for each branch. As it was mentioned in the Section 4.1, branch energies will go to $\pm\infty$ if there is constant component it a branch power. Integral from harmonic components will be zero for given period T.

Constant components in Equations (A.2) are coupled with circulating currents and powers in a system.

Using nomenclature defined in Equations (4.7a) and (4.7b), constant power components in each branch are equal (4.11).

$$
\boldsymbol{P_0} = \begin{bmatrix} P_{1,0} \\ P_{2,0} \\ P_{3,0} \\ P_{4,0} \\ P_{5,0} \\ P_{6,0} \\ P_{7,0} \\ P_{8,0} \\ P_{9,0} \end{bmatrix} = \begin{bmatrix} -i_{c1}v_N - \frac{1}{4}P_2 \\ i_{c2}v_N - \frac{1}{4}P_2 \\ -i_{c2}v_N - \frac{1}{4}P_2 \\ i_{c3}v_N - \frac{1}{4}P_2 \\ -i_{c3}v_N - \frac{1}{4}P_2 \\ i_{c1}v_N - \frac{1}{4}P_2 \\ \left(i_{c1} - i_{c2}\right)v_X - \frac{1}{2}P_1 \\ \left(i_{c2} - i_{c3}\right)v_X - \frac{1}{2}P_1 \\ \left(i_{c3} - i_{c1}\right)v_X - \frac{1}{2}P_1 \end{bmatrix} \tag{4.11}
$$

First target in control design is to chose that circulating currents i_{cx} and voltages v_N, v_X to cancel out all constant components in branch powers, i.e. make $\boldsymbol{P_0}$ vector equal zero (4.12). In the next step, control loop design target is to make vector $\boldsymbol{P_0}$ equals given non-zero setpoint what allows for example to charge the converter.

$$
\boldsymbol{P_0}^{[9\times1]} = \boldsymbol{0} \tag{4.12}
$$

In the first step it has been analyzed if constant values provides a solution of given problems. Corresponding waveforms are defined:

$$
i_{cx}(t) = I_{cx} = const \tag{4.13a}
$$

$$
v_N(t) = V_N = const \tag{4.13b}
$$

$$
v_X(t) = V_X = const \tag{4.13c}
$$

Substituting functions, branch power constant components are equal (4.14).

$$
\boldsymbol{P_0} =
\begin{bmatrix}
P_{1,0} \\
P_{2,0} \\
P_{3,0} \\
P_{4,0} \\
P_{5,0} \\
P_{6,0} \\
P_{7,0} \\
P_{8,0} \\
P_{9,0}
\end{bmatrix}
=
\begin{bmatrix}
-I_{c1}V_N - \frac{1}{4}P_2 \\
I_{c2}V_N - \frac{1}{4}P_2 \\
-I_{c2}V_N - \frac{1}{4}P_2 \\
I_{c3}V_N - \frac{1}{4}P_2 \\
-I_{c3}V_N - \frac{1}{4}P_2 \\
I_{c1}V_N - \frac{1}{4}P_2 \\
(I_{c1} - I_{c2})V_X - \frac{1}{2}P_1 \\
(I_{c2} - I_{c3})V_X - \frac{1}{2}P_1 \\
(I_{c3} - I_{c1})V_X - \frac{1}{2}P_1
\end{bmatrix}
=
\begin{bmatrix}
0 \\
0 \\
0 \\
0 \\
0 \\
0 \\
0 \\
0 \\
0
\end{bmatrix}
\tag{4.14}
$$

Unfortunately, for those waveform shapes, it is not possible to meet (4.12). It can be easily noted that, for example, equations for branch 1 and 6 are contradictory for $I_{c1} \neq 0$ and $V_N \neq 0$ if $P_2 \neq 0$. Adding equations (4.15), $-\frac{P_2}{2} = 0$ is obtained for any I_{c1} or V_N.

$$
\begin{cases}
P_{1,0}: & -I_{c1}V_N - \frac{1}{4}P_2 = 0 \\
P_{6,0}: & +I_{c1}V_N - \frac{1}{4}P_2 = 0
\end{cases}
\tag{4.15}
$$

Similarly, equations for branches 2-3 and 4-5 are contradictory.

4.4. Branch power stabilization by sinusoidal circulating currents

As constant components are not enough to cancel out all constant power components in power equations, different waveform should be analyzed. In this section, sinusoidal components with frequency ω_c will be introduced. It has been assumed that $\omega_c \neq \omega_1 \neq \pm\omega_2 \neq 0$.

As in previous case, power components for given waveform are calculated. Sinusoidal components are added to constant component to keep consistency and not loose generality of solution. In case constant components are not required, they can be removed.

Sinusoidal components can be represented as a single value with a phase shift i.e. $A sin(\omega t + \phi)$. However, in the Thesis, it has been decided to represent each component in $\alpha - \beta$ reference frame. In other words, each frequency component is represented as a sum of two $\pi/2$-shifted waveforms with the same frequency.

Therefore, circulating currents and voltages are defined as:

$$
i_{cx}(t) = I_{cx} + I_{cxc\alpha}cos(\omega_c t) + I_{cxc\beta}sin(\omega_c t)
\tag{4.16a}
$$

$$
v_N(t) = V_N + V_{Nc\alpha}cos(\omega_c t) + V_{Nc\beta}sin(\omega_c t)
\tag{4.16b}
$$

$$
v_X(t) = V_X + V_{Xc\alpha}cos(\omega_c t) + V_{Xc\beta}sin(\omega_c t)
\tag{4.16c}
$$

> ### Circulating components nomenclature
>
> Component amplitude in circulating currents are presented in the form $I_{cxc\alpha,\beta}$, where following symbols means:
>
> $$c \quad - \quad \text{information that it is circulating component}$$
> $$x \quad - \quad \text{index of circulating current } (x = 1...3)$$
> $$c \quad - \quad \text{circulating current angular frequency. In that case } \omega_c$$
> $$\alpha, \beta \quad - \quad \alpha \; (cos) \text{ or } \beta \; (sin) \text{ component of the current}$$
>
> In the same way, voltages and currents are being described in following sections of the Thesis.

For given functions, branch powers has been calculated in the same way as it is described in Section 4.3. For normal operation point, constant components for each branch are equal (4.17).

$$\boldsymbol{P_0} = \begin{bmatrix} P_{1,0} \\ P_{2,0} \\ P_{3,0} \\ P_{4,0} \\ P_{5,0} \\ P_{6,0} \\ P_{7,0} \\ P_{8,0} \\ P_{9,0} \end{bmatrix} = \begin{bmatrix} -I_{c1}V_N - \frac{1}{2}I_{c1c\alpha}V_{Nc\alpha} - \frac{1}{2}I_{c1c\beta}V_{Nc\beta} - \frac{1}{4}P_2 \\ I_{c2}V_N + \frac{1}{2}I_{c2c\alpha}V_{Nc\alpha} + \frac{1}{2}I_{c2c\beta}V_{Nc\beta} - \frac{1}{4}P_2 \\ -I_{c2}V_N - \frac{1}{2}I_{c2c\alpha}V_{Nc\alpha} - \frac{1}{2}I_{c2c\beta}V_{Nc\beta} - \frac{1}{4}P_2 \\ I_{c3}V_N + \frac{1}{2}I_{c3c\alpha}V_{Nc\alpha} + \frac{1}{2}I_{c3c\beta}V_{Nc\beta} - \frac{1}{4}P_2 \\ -I_{c3}V_N - \frac{1}{2}I_{c3c\alpha}V_{Nc\alpha} - \frac{1}{2}I_{c3c\beta}V_{Nc\beta} - \frac{1}{4}P_2 \\ I_{c1}V_N + \frac{1}{2}I_{c1c\alpha}V_{Nc\alpha} + \frac{1}{2}I_{c1c\beta}V_{Nc\beta} - \frac{1}{4}P_2 \\ (I_{c1} - I_{c2})V_X + \frac{1}{2}(I_{c1c\alpha}V_{Xc\alpha} - I_{c2c\alpha}V_{Xc\alpha} + I_{c1c\beta}V_{Xc\beta} - I_{c2c\beta}V_{Xc\beta}) - \frac{1}{2}P_1 \\ (I_{c2} - I_{c3})V_X + \frac{1}{2}(I_{c2c\alpha}V_{Xc\alpha} - I_{c3c\alpha}V_{Xc\alpha} + I_{c2c\beta}V_{Xc\beta} - I_{c3c\beta}V_{Xc\beta}) - \frac{1}{2}P_1 \\ (I_{c3} - I_{c1})V_X + \frac{1}{2}(I_{c3c\alpha}V_{Xc\alpha} - I_{c1c\alpha}V_{Xc\alpha} + I_{c3c\beta}V_{Xc\beta} - I_{c1c\beta}V_{Xc\beta}) - \frac{1}{2}P_1 \end{bmatrix}$$
$$(4.17)$$

It can be noted, that given solution also do not provide possibility to cancel out a constant component in each branch. For example, equations for branch 1 and 6 are still contradictory. To clear constant component in those branches it must be provided that:

$$\begin{cases} P_{1,0}: & -I_{c1}V_N - \frac{1}{2}I_{c1c\alpha}V_{Nc\alpha} - \frac{1}{2}I_{c1c\beta}V_{Nc\beta} - \frac{1}{4}P_2 = 0 \\ P_{6,0}: & I_{c1}V_N + \frac{1}{2}I_{c1c\alpha}V_{Nc\alpha} + \frac{1}{2}I_{c1c\beta}V_{Nc\beta} - \frac{1}{4}P_2 = 0 \end{cases} \qquad (4.18)$$

Adding those equation, it can be noted that equation has no solution for $P_2 \neq 0$:

$$-\frac{1}{2}P_2 = 0 \qquad (4.19)$$

It should be highlighted that product $I_{cx}V_N$ is present only in Hex branches. Product $I_{cx}V_X$ is present only in Y branches. This observation will be used in further analysis when energy transfer between and within Hex and Y part will be analyzed.

4.5. Branch power stabilization by harmonic sinusoidal circulating currents

In this section it will be checked if sinusoidal circulating currents with frequency equal to input system's frequency can be used to cancel out constant parts from branch powers.

In total there are five physical quantities which can be controlled (two voltages plus three currents). By introducing different components (constant, sinusoidal and so on), we end up with sufficient number of degrees of freedom to keep the system on the fixed energy power point reference. Equations (4.20) presents proposed waveforms. They give in total 15 DOF. All voltages and currents are composed with constant plus sinusoidal components with frequency ω_1. Instead of introducing phase shift, sinusoidal component is being built with two 90-deg phase shifted waveforms ($\alpha - \beta$):

$$i_{cx}(t) = I_{cx} + I_{cx1\alpha}cos(\omega_1 t) + I_{cx1\beta}sin(\omega_1 t) \tag{4.20a}$$

$$v_N(t) = V_N + V_{N1\alpha}cos(\omega_1 t) + V_{N1\beta}sin(\omega_1 t) \tag{4.20b}$$

$$v_X(t) = V_X + V_{X1\alpha}cos(\omega_1 t) + V_{X1\beta}sin(\omega_1 t) \tag{4.20c}$$

where

x – Circulating current index ($x = 1...3$)

ω_1 – System 1 (supply) frequency

In the first step some assumptions has been made to find a „base" solution which can be later on expanded to give a generic solution valid for normal operation points:

– There is no reactive power flow ($\phi_1 = 0$, $\phi_2 = 0$)

– Input power is equal output power with opposite sign ($P_1 = V_1 \cdot I_1 = -V_2 \cdot I_2 = -P_2$)

– Calculations are given for zero phase shift of System 1 voltage ($\psi_1 = 0$)

4.5.1. Constant components for given waveforms

If voltages and currents are defined by equations (4.20), the branch powers constant parts are equal (for previously defined simplifications):

$$\boldsymbol{P_0} = \begin{bmatrix} \frac{I_{c11\alpha}V_1}{2} - I_{c1}V_N - \frac{I_{c11\alpha}V_{N1\alpha}}{2} - \frac{I_{c11\beta}V_{N1\beta}}{2} - \frac{1}{4}I_2V_2cos(\phi_2) \\ -\frac{I_{c21\alpha}V_1}{2} + I_{c2}V_N + \frac{I_{c21\alpha}V_{N1\alpha}}{2} + \frac{I_{c21\beta}V_{N1\beta}}{2} - \frac{1}{4}I_2V_2cos(\phi_2) \\ -\frac{I_{c21\alpha}V_1}{4} + \frac{1}{4}\sqrt{3}I_{c21\beta}V_1 - I_{c2}V_N - \frac{I_{c21\alpha}V_{N1\alpha}}{2} - \frac{I_{c21\beta}V_{N1\beta}}{2} - \frac{1}{4}I_2V_2cos(\phi_2) \\ \frac{I_{c31\alpha}V_1}{4} - \frac{1}{4}\sqrt{3}I_{c31\beta}V_1 + I_{c3}V_N + \frac{I_{c31\alpha}V_{N1\alpha}}{2} + \frac{I_{c31\beta}V_{N1\beta}}{2} - \frac{1}{4}I_2V_2cos(\phi_2) \\ -\frac{I_{c31\alpha}V_1}{4} - \frac{1}{4}\sqrt{3}I_{c31\beta}V_1 - I_{c3}V_N - \frac{I_{c31\alpha}V_{N1\alpha}}{2} - \frac{I_{c31\beta}V_{N1\beta}}{2} - \frac{1}{4}I_2V_2cos(\phi_2) \\ \frac{I_{c11\alpha}V_1}{4} + \frac{1}{4}\sqrt{3}I_{c11\beta}V_1 + I_{c1}V_N + \frac{I_{c11\alpha}V_{N1\alpha}}{2} + \frac{I_{c11\beta}V_{N1\beta}}{2} - \frac{1}{4}I_2V_2cos(\phi_2) \\ P_{7,0} \\ P_{8,0} \\ P_{9,0} \end{bmatrix} \qquad (4.21)$$

$P_{7...9,0}$ are equal:

$$P_{7,0} = -\frac{I_{c11\alpha}V_1}{2} + \frac{I_{c21\alpha}V_1}{2} + I_{c1}V_X - I_{c2}V_X + \frac{I_{c11\alpha}V_{X1\alpha}}{2} - \frac{I_{c21\alpha}V_{X1\alpha}}{2} + \frac{I_{c11\beta}V_{X1\beta}}{2}$$
$$-\frac{I_{c21\beta}V_{X1\beta}}{2} - \frac{1}{2}I_1V_1cos(\phi_1) + \frac{1}{2}I_1V_{X1\alpha}cos(\phi_1) + \frac{1}{2}I_1V_{X1\beta}sin(\phi_1) \qquad (4.22a)$$

$$P_{8,0} = \frac{I_{c21\alpha}V_1}{4} - \frac{1}{4}\sqrt{3}I_{c21\beta}V_1 - \frac{I_{c31\alpha}V_1}{4} + \frac{1}{4}\sqrt{3}I_{c31\beta}V_1 + I_{c2}V_X - I_{c3}V_X + \frac{I_{c21\alpha}V_{X1\alpha}}{2} -$$
$$\frac{I_{c31\alpha}V_{X1\alpha}}{2} + \frac{I_{c21\beta}V_{X1\beta}}{2} - \frac{I_{c31\beta}V_{X1\beta}}{2} - \frac{1}{2}I_1V_1cos(\phi_1) - \frac{1}{4}I_1V_{X1\alpha}cos(\phi_1) + \qquad (4.22b)$$
$$\frac{1}{4}\sqrt{3}I_1V_{X1\beta}cos(\phi_1) - \frac{1}{4}\sqrt{3}I_1V_{X1\alpha}sin(\phi_1) - \frac{1}{4}I_1V_{X1\beta}sin(\phi_1)$$

$$P_{9,0} = -\frac{I_{c11\alpha}V_1}{4} - \frac{1}{4}\sqrt{3}I_{c11\beta}V_1 + \frac{I_{c31\alpha}V_1}{4} + \frac{1}{4}\sqrt{3}I_{c31\beta}V_1 - I_{c1}V_X + I_{c3}V_X$$
$$-\frac{I_{c11\alpha}V_{X1\alpha}}{2} + \frac{I_{c31\alpha}V_{X1\alpha}}{2} - \frac{I_{c11\beta}V_{X1\beta}}{2} + \frac{I_{c31\beta}V_{X1\beta}}{2} - \frac{1}{2}I_1V_1cos(\phi_1) - \frac{1}{4}I_1V_{X1\alpha}cos(\phi_1) \qquad (4.22c)$$
$$-\frac{1}{4}\sqrt{3}I_1V_{X1\beta}cos(\phi_1) + \frac{1}{4}\sqrt{3}I_1V_{X1\alpha}sin(\phi_1) - \frac{1}{4}I_1V_{X1\beta}sin(\phi_1)$$

The goal of feed-forward control is to choose the control variables (DOF in the system) to satisfy (4.23):

$$\boldsymbol{P_0} = \boldsymbol{P_{ref}} \qquad (4.23)$$

For a steady state $\boldsymbol{P_{ref}} = \boldsymbol{0}$ as it was stated in the Eq. (4.12). Following DOF are identified:

Degrees of freedom which can be used to define constant components of the branch powers

$\boldsymbol{P_0}$ vector given as (4.21) has following DOF's:

- $I_{cx1\alpha,\beta}$ - in total six circulating current sinusoidal magnitudes with frequency ω_1

- I_{cx} - three constant circulating current components

- $V_{N1\alpha,\beta}$ - two phase shifted neutral point voltage sinusoidal components with frequency ω_1

- V_N - constant DC voltage offset between two systems (neutral point voltage)

- $V_{X1\alpha,\beta}$ - two phase shifted star point voltage sinusoidal components with frequency ω_1

- V_X - star point voltage constant component

As some values are coupled with each other (constant components) it is wise to reduce number of DOF in the first step. If it will lead to no solution due to missing DOF, those parts can be introduced back.

4.5.2. Solution for no common mode voltage

In the first step it will be assumed that both neutral point and star point voltages are equal zero. This leads to vector P_0 defined in (4.24)

$$
\boldsymbol{P_0} = \begin{bmatrix}
\frac{I_{c11\alpha}V_1}{2} - \frac{1}{4}I_2V_2\cos\left(\phi_2\right) \\
-\frac{I_{c21\alpha}V_1}{2} - \frac{1}{4}I_2V_2\cos\left(\phi_2\right) \\
-\frac{I_{c21\alpha}V_1}{4} + \frac{1}{4}\sqrt{3}I_{c21\beta}V_1 - \frac{1}{4}I_2V_2\cos\left(\phi_2\right) \\
\frac{I_{c31\alpha}V_1}{4} - \frac{1}{4}\sqrt{3}I_{c31\beta}V_1 - \frac{1}{4}I_2V_2\cos\left(\phi_2\right) \\
-\frac{I_{c31\alpha}V_1}{4} - \frac{1}{4}\sqrt{3}I_{c31\beta}V_1 - \frac{1}{4}I_2V_2\cos\left(\phi_2\right) \\
\frac{I_{c11\alpha}V_1}{4} + \frac{1}{4}\sqrt{3}I_{c11\beta}V_1 - \frac{1}{4}I_2V_2\cos\left(\phi_2\right) \\
-\frac{I_{c11\alpha}V_1}{2} + \frac{I_{c21\alpha}V_1}{2} - \frac{1}{2}I_1V_1\cos\left(\phi_1\right) \\
\frac{I_{c21\alpha}V_1}{4} - \frac{1}{4}\sqrt{3}I_{c21\beta}V_1 - \frac{I_{c31\alpha}V_1}{4} + \frac{1}{4}\sqrt{3}I_{c31\beta}V_1 - \frac{1}{2}I_1V_1\cos\left(\phi_1\right) \\
-\frac{I_{c11\alpha}V_1}{4} - \frac{1}{4}\sqrt{3}I_{c11\beta}V_1 + \frac{I_{c31\alpha}V_1}{4} + \frac{1}{4}\sqrt{3}I_{c31\beta}V_1 - \frac{1}{2}I_1V_1\cos\left(\phi_1\right)
\end{bmatrix} \tag{4.24}
$$

To simplify and unify notation, $V \cdot I$ terms will be defined as powers. System-related powers are defined by (4.7). Circulating current components are coupled with V_{1m} voltage. Following notation will be used:

$$P_{11\alpha} = I_{c11\alpha}V_{1m} \tag{4.25}$$

$$P_{11\beta} = I_{c11\beta}V_{1m} \tag{4.26}$$

$$P_{21\alpha} = I_{c21\alpha}V_{1m} \tag{4.27}$$

$$P_{21\beta} = I_{c21\beta}V_{1m} \tag{4.28}$$

$$P_{31\alpha} = I_{c31\alpha}V_{1m} \tag{4.29}$$

$$P_{31\beta} = I_{c31\beta}V_{1m} \tag{4.30}$$

Equation (4.23) can be written as:

$$\boldsymbol{P_0} = \boldsymbol{T_{Pc,1}P_{c,1}} + \boldsymbol{T_{PS,1}P_S} = \boldsymbol{P_{ref,1}} \tag{4.31}$$

$\boldsymbol{P_{c,1}}$ [eq. (4.32)] is a circulating power vector which contains all constant power components. Currently it build only with ω_1 frequency. In the next steps, vector will be expanded. Therefore, its name contain an index equal 1. Values in $\boldsymbol{P_{c,1}}$ can be changed with no affect on the system powers.

$\boldsymbol{P_S}$ [eq. (4.33)] is a system powers vector. $\boldsymbol{P_S}$ vector has redundant elements as the power can be described by any two of P, Q, S power component. It will be kept in that form, as the notation can be simplified (e.g. if the apparent power is present in the equation it is not required to recalculate it for active/reactive components).

$$\boldsymbol{P_{c,1}} = \boldsymbol{P_{c1}} = \begin{bmatrix} P_{11\alpha} & P_{11\beta} & P_{21\alpha} & P_{21\beta} & P_{31\alpha} & P_{31\beta} \end{bmatrix}^T \tag{4.32}$$

$\boldsymbol{P_{c1}}$ symbol defines components coupled with ω_1 frequency while $\boldsymbol{P_{c,1}}$ defines all frequency components. As it was explained, in this case both vectors are equal as there is no any other frequency components present.

$$\boldsymbol{P_S} = \begin{bmatrix} P_1 & Q_1 & S_1 & P_2 & Q_2 & S_2 \end{bmatrix}^T \tag{4.33}$$

Matrices $\boldsymbol{T_{Pc,1}}$ and $\boldsymbol{T_{PS,1}}$ describes each power's influence on a specific branch. They are equal (4.34) and (4.35) respectively.

$$\boldsymbol{T_{Pc,1}}^{[9\times6]} = \begin{bmatrix} \frac{1}{2} & 0 & 0 & 0 & 0 & 0 \\ 0 & 0 & -\frac{1}{2} & 0 & 0 & 0 \\ 0 & 0 & -\frac{1}{4} & \frac{\sqrt{3}}{4} & 0 & 0 \\ 0 & 0 & 0 & 0 & \frac{1}{4} & -\frac{\sqrt{3}}{4} \\ 0 & 0 & 0 & 0 & -\frac{1}{4} & -\frac{\sqrt{3}}{4} \\ \frac{1}{4} & \frac{\sqrt{3}}{4} & 0 & 0 & 0 & 0 \\ -\frac{1}{2} & 0 & \frac{1}{2} & 0 & 0 & 0 \\ 0 & 0 & \frac{1}{4} & -\frac{\sqrt{3}}{4} & -\frac{1}{4} & \frac{\sqrt{3}}{4} \\ -\frac{1}{4} & -\frac{\sqrt{3}}{4} & 0 & 0 & \frac{1}{4} & \frac{\sqrt{3}}{4} \end{bmatrix} \tag{4.34}$$

$$\boldsymbol{T_{PS,1}}^{[9\times6]} = \begin{bmatrix} 0 & 0 & 0 & -\frac{1}{4} & 0 & 0 \\ 0 & 0 & 0 & -\frac{1}{4} & 0 & 0 \\ 0 & 0 & 0 & -\frac{1}{4} & 0 & 0 \\ 0 & 0 & 0 & -\frac{1}{4} & 0 & 0 \\ 0 & 0 & 0 & -\frac{1}{4} & 0 & 0 \\ 0 & 0 & 0 & -\frac{1}{4} & 0 & 0 \\ -\frac{1}{2} & 0 & 0 & 0 & 0 & 0 \\ -\frac{1}{2} & 0 & 0 & 0 & 0 & 0 \\ -\frac{1}{2} & 0 & 0 & 0 & 0 & 0 \end{bmatrix} \tag{4.35}$$

The goal of a feed forward control defined by (4.31) can be achieved by proper chose of the vector $\boldsymbol{P_{c,1}}$. In the first step, Hex-part of the system equations will be satisfied. Next, proposed $P_{c,1}$ vector will be used to calculate power's components for the Y-part. If the $\boldsymbol{P_{ref,1}}$ for Y-part won't be satisfied, non-zero v_X voltage will be introduced. The equation, for the Hex part only is given as (4.36). All vectors with H index are the first six rows of previously defined matrices.

$$\boldsymbol{P_{0,H}} = \boldsymbol{T_{Pc,1H}}\boldsymbol{P_{c,1}} + \boldsymbol{T_{PS,1H}}\boldsymbol{P_S} = \boldsymbol{P_{ref,1H}} \tag{4.36}$$

As the $\boldsymbol{T_{Pc,1H}}$ is a square matrix with a rank of 6, an inverted matrix exists. Therefore it is possible to write an equation for $\boldsymbol{P_{c,1}}$:

$$P_{c,1} = T_{Pc,1H}{}^{-1} \left(P_{ref,1H} - T_{PS,1H} P_S \right) \tag{4.37}$$

$T_{Pc,1H}{}^{-1}$ matrix is equal (4.38):

$$T_{Pc,1H}{}^{-1} = \begin{bmatrix} 2 & 0 & 0 & 0 & 0 & 0 \\ -\frac{2}{\sqrt{3}} & 0 & 0 & 0 & 0 & \frac{4}{\sqrt{3}} \\ 0 & -2 & 0 & 0 & 0 & 0 \\ 0 & -\frac{2}{\sqrt{3}} & \frac{4}{\sqrt{3}} & 0 & 0 & 0 \\ 0 & 0 & 0 & 2 & -2 & 0 \\ 0 & 0 & 0 & -\frac{2}{\sqrt{3}} & -\frac{2}{\sqrt{3}} & 0 \end{bmatrix} \tag{4.38}$$

To satisfy Eq. (4.12), $P_{ref,1H}$ vector is equal zero. It can be also noted that for Hex branches $T_{PS,1H} P_S$ vector elements are equal $-\frac{P_2}{4}$ each. Therefore, circulating power components can be calculated from the Eq. (4.39):

$$P_{c,1} = -T_{Pc,1H}{}^{-1} \cdot T_{PS,1H} P_S \tag{4.39}$$

This leads to following $P_{c,1}$ vector:

$$P_{c,1} = P_2 \cdot \begin{bmatrix} \frac{1}{2} & \frac{1}{2\sqrt{3}} & -\frac{1}{2} & \frac{1}{2\sqrt{3}} & 0 & -\frac{1}{\sqrt{3}} \end{bmatrix}^T \tag{4.40}$$

In the next step, calculated vector $P_{c,1}$ (4.40) is substituted to the Y-part of the system to check if this part is satisfied. To not introduce a new symbols (with Y subscript), the total power for all branches will be calculated starting from Eq. (4.31):

$$P_0 = T_{Pc,1} P_{c,1} + T_{PS,1} P_S = \begin{bmatrix} 0 & 0 & 0 & 0 & 0 & 0 & -\frac{P_1+P_2}{2} & -\frac{P_1+P_2}{2} & -\frac{P_1+P_2}{2} \end{bmatrix}^T \tag{4.41}$$

For $P_1 = -P_2$, P_0 vector is equal zero what was the target of the feed forward control defined by the Eq. (4.12).

The total energy in the system (sum of all elements in the P_0 vector) is equal $-\frac{3}{2}\left(P_1 + P_2\right)$ what satisfy energy conservation rule: that's the amount of energy taken from the both systems ($P_{s,tot} = \frac{3}{2} P_s$) [see Eq. (4.8a)].

Powers vector $P_{c,1}$ defines required circulating currents. Assuming that $P_2 = -P_1$ for steady state, circulating currents are equal:

$$I_{c1} = \frac{1}{V_{1m}} \cdot P_{c,1} = -I_{1m} cos(\phi_1) \cdot \begin{bmatrix} \frac{1}{2} & \frac{1}{2\sqrt{3}} & -\frac{1}{2} & \frac{1}{2\sqrt{3}} & 0 & -\frac{1}{\sqrt{3}} \end{bmatrix}^T \tag{4.42}$$

Vector I_{c1} includes all circulating current components related with ω_1 frequency i.e.:

$$I_{c1} = \begin{bmatrix} I_{11\alpha} & I_{11\beta} & I_{21\alpha} & I_{21\beta} & I_{31\alpha} & I_{31\beta} \end{bmatrix}^T \tag{4.43}$$

In the final step, $\alpha - \beta$ components of each current can be combined into a single function using Harmonic Addition Theorem (HAT) [81]. That simplifies its analysis as determination of phase shifts

and magnitudes. It allows also to make more generic solution by introducing initial phase shift for the system 1.

A simplified theorem valid for two sinusoidal functions is defined as (4.44):

$$a \cdot sin(x) + b \cdot cos(x) = c \cdot sin(x + \phi) \tag{4.44}$$

where:

$c = Sign(a)\sqrt{a^2 + b^2}$

$\phi = atan\left(-\frac{b}{a}\right)$

Therefore i_{cx} functions defined in Eq. (4.20a), with introduced initial phase shift ψ_1 are equal:

$$i_{c1} = \frac{I_{1m}cos(\phi_1)}{\sqrt{3}}cos\left(\omega_1 t + \frac{5\pi}{6} - \psi_1\right) \tag{4.45a}$$

$$i_{c2} = \frac{I_{1m}cos(\phi_1)}{\sqrt{3}}cos\left(\omega_1 t + \frac{\pi}{6} - \psi_1\right) \tag{4.45b}$$

$$i_{c3} = \frac{I_{1m}cos(\phi_1)}{\sqrt{3}}cos\left(\omega_1 t + \frac{9\pi}{6} - \psi_1\right) \tag{4.45c}$$

4.5.3. Solution check

Waveforms for given solution has been generated using equation for branch currents (3.34) for given terminal/circulating current vector are calculated in the Eq. (4.46). HAT has been used to combine sine/cosine functions. Table 3.2 includes used waveform parameters.

$$\boldsymbol{I_b} = \boldsymbol{T_{i,\alpha\beta-br}} \cdot \begin{bmatrix} cos(\omega_1 t) \\ sin(\omega_1 t) \\ -cos(\omega_2 t) \\ -sin(\omega_2 t) \\ \frac{\sqrt{3}}{3}cos\left(\omega_1 t + \frac{5\pi}{6}\right) \\ \frac{\sqrt{3}}{3}cos\left(\omega_1 t + \frac{\pi}{6}\right) \\ \frac{\sqrt{3}}{3}cos\left(\omega_1 t + \frac{9\pi}{6}\right) \end{bmatrix} = \begin{bmatrix} \frac{cos\left(\frac{\pi}{6}-\omega_1 t\right)}{\sqrt{3}} + \frac{1}{2}cos(\omega_2 t) \\ \frac{cos\left(\frac{\pi}{6}+\omega_1 t\right)}{\sqrt{3}} - \frac{1}{2}sin\left(\frac{\pi}{6} - \omega_2 t\right) \\ -\frac{cos\left(\frac{\pi}{6}+\omega_1 t\right)}{\sqrt{3}} - \frac{1}{2}sin\left(\frac{\pi}{6} - \omega_2 t\right) \\ \frac{sin(\omega_1 t)}{\sqrt{3}} - \frac{1}{2}sin\left(\frac{\pi}{6} + \omega_2 t\right) \\ -\frac{sin(\omega_1 t)}{\sqrt{3}} - \frac{1}{2}sin\left(\frac{\pi}{6} + \omega_2 t\right) \\ -\frac{cos\left(\frac{\pi}{6}-\omega_1 t\right)}{\sqrt{3}} + \frac{1}{2}cos(\omega_2 t) \\ -\frac{1}{2}sin\left(\frac{\pi}{6} + \omega_2 t\right) \\ \frac{1}{2}cos(\omega_2 t) \\ -\frac{1}{2}sin\left(\frac{\pi}{6} - \omega_2 t\right) \end{bmatrix} \tag{4.46}$$

Branch voltages are not affected by introduced balancing method: neither v_X nor v_N voltage has been used. Therefore they are expressed as in the Eq. (3.48).

Complete branch power equations are presented in Appendix A, Eq. (A.3). The main conclusion is that the powers does not contain any constant term: there are built with only sine waveforms. Therefore its integral (branch energy) remains constant over the waveform period.

(a) Hex Power

(b) Hex Energy

(c) Y Power

(d) Y Energy
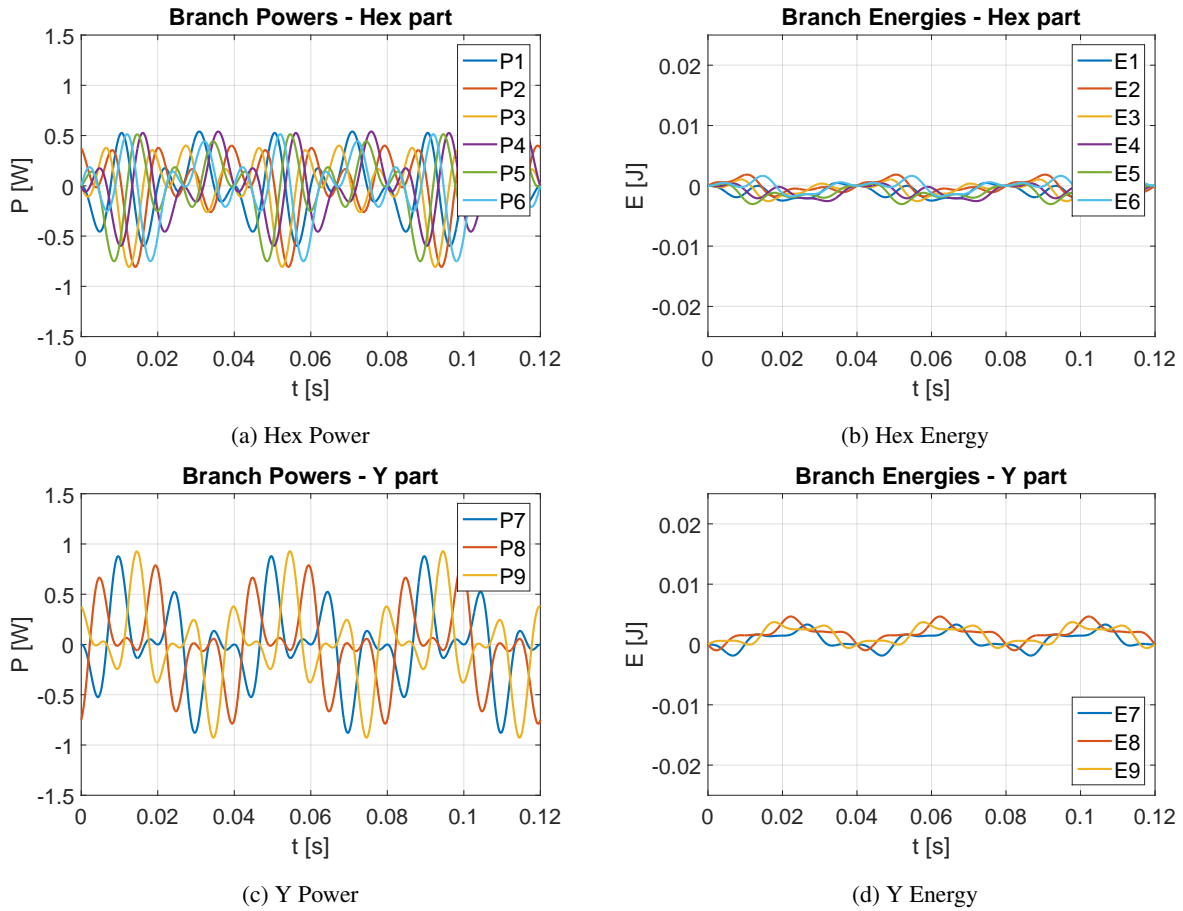
Figure 4.2. Branch powers and energies for an example case with introduced circulating currents. Branches 1 through 6 belongs to Hex, 7 through 9 belongs to Y part of the converter. Y scale as in the Fig. 4.1

Fig. 4.2 presents branch powers and energies for introduces circulating currents. In contrary to waveforms on the Fig. 4.1, the system remains stable what proves that circulating currents with harmonic frequency ω_1 can be used to keep the system 1 in a steady state.

Fig. 4.3 shows one Hex and one Y branch currents. Additionally RMS current for the waveform has been calculated. As it is shown, circulating current introduction increases RMS current of the Hex branches and reduces RMS current value of Y-branches.

4.6. Branch power stabilization by harmonic and non-harmonic sinusoidal circulating currents

Previous section presented the workflow how to identify and use non-coupled DOF (ω_1-component circulating currents) to cancel out constant components in the power equations. Proposed scheme can be expanded to support the generic case in which each branch power constant component can be non-zero
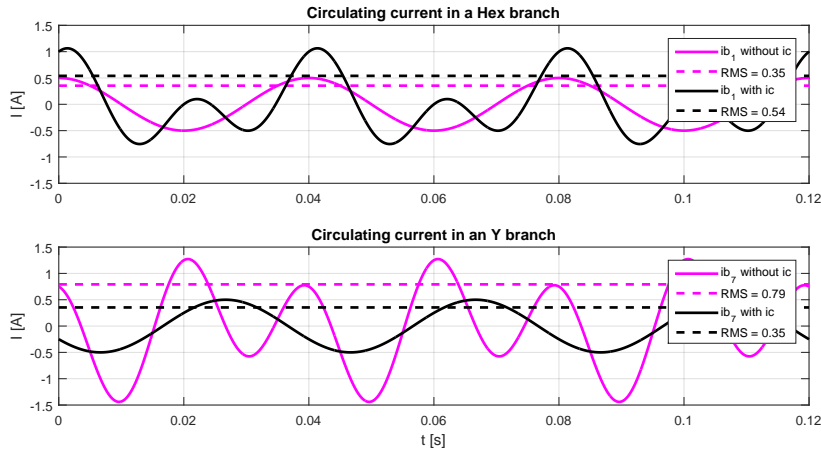
Figure 4.3. Branch currents affected by introduced circulating currents. Representative example of branch 1 (Hex) and branch 7 (Y)

value. This will lead for branch charging/discharging possibility. It is used also for power transfer among branches to provide branch energy balancing.

Usage only ω_1-circulating currents gives six DOF. It is required to have eight DOF's to be able to control all the branch powers. The last branch power must satisfy energy conversation rule of the system: sum of external active powers and branch powers is equal zero, what (for given power flow directions) can be written as (4.47).

$$\sum_{b=1}^{9} p_b + \frac{3}{2}\left(P_1 + P_2\right) = 0 \tag{4.47}$$

It has been decided to introduce an extra three DOF's by applying non-zero star point voltage v_X which will give a constant power components in the Y-branches if its frequency will be equal to the frequency of circulating current.

Star point voltage will be given as (4.48). It is possible to expand it with $V_{Xc\beta}$ component (90 deg phase shifted) if it will be required.

$$v_X(t) = V_{Xc\alpha}cos\left(\omega_c t\right) \tag{4.48}$$

Circulating currents previously defined as (4.20a) will be now expanded with an extra component to interfere whith v_X voltage:

$$i_{cx}(t) = I_{cx} + I_{cx1\alpha}cos(\omega_1 t) + I_{cx1\beta}sin(\omega_1 t) + I_{cxc\alpha}cos(\omega_c t) \tag{4.49}$$

where

  x – Circulating current index ($x = 1_{...}3$)

  ω_1 – System 1 (supply) frequency

  ω_c – Circulating current angular frequency

It must be provided that $\omega_c \neq \omega_{1,2}$. Otherwise, extra constant components will be visible in the power equations.

To summarize, it can be noted that:

– circulating current $I_{cx1\alpha,\beta}$ element introduces extra constant power components in Hex and Y branches. It gives six DOF's,

– circulating current $I_{cxc\alpha,\beta}$ element introduces extra constant power components only in Y branches. It gives three DOF's (for cosine-component used only),

– in the physical system energy conservation rule must be satisfied. It means that for N branches, system has $N - 1$ independent variables,

– 9 DOF and 8 variables means the system is undetermined (there are infinite number of solutions).

It is possible to introduce any extra equation to make the system determined. It should be only provided that extra equation is a linear function of the Y-branch powers. It should be also provided that the equation is linear independent from the three Y-branch power equations.

In the thesis, an extra equation is given as (4.50). In the future work instead of that condition, an optimization algorithm (e.g. for circulating current magnitude minimization) can be used.

$$I_{c1c\alpha} + I_{c2c\alpha} + I_{c3c\alpha} = 0 \tag{4.50}$$

Assuming that circulating currents are functions defined as (4.49), star point voltage is defined as (4.48) and the neutral point voltage (between two systems) is set to be zero, constant power components in each branch are equal (4.51):

$$\boldsymbol{P_0} = \begin{bmatrix} \frac{1}{4}(2P_{11\alpha} - P_2) \\ -\frac{P_2}{4} - \frac{P_{21\alpha}}{2} \\ -\frac{P_2}{4} - \frac{P_{21\alpha}}{4} + \frac{\sqrt{3}P_{21\beta}}{4} \\ -\frac{P_2}{4} + \frac{P_{31\alpha}}{4} - \frac{\sqrt{3}P_{31\beta}}{4} \\ -\frac{P_2}{4} - \frac{P_{31\alpha}}{4} - \frac{\sqrt{3}P_{31\beta}}{4} \\ \frac{P_{11\alpha}}{4} + \frac{\sqrt{3}P_{11\beta}}{4} - \frac{P_2}{4} \\ -\frac{P_1}{2} - \frac{P_{11\alpha}}{2} + \frac{P_{1c\alpha}}{2} + \frac{P_{21\alpha}}{2} - \frac{P_{2c\alpha}}{2} \\ -\frac{P_1}{2} + \frac{P_{21\alpha}}{4} - \frac{\sqrt{3}P_{21\beta}}{4} + \frac{P_{2c\alpha}}{2} - \frac{P_{31\alpha}}{4} + \frac{\sqrt{3}P_{31\beta}}{4} - \frac{P_{3c\alpha}}{2} \\ -\frac{P_1}{2} - \frac{P_{11\alpha}}{4} - \frac{\sqrt{3}P_{11\beta}}{4} - \frac{P_{1c\alpha}}{2} + \frac{P_{31\alpha}}{4} + \frac{\sqrt{3}P_{31\beta}}{4} + \frac{P_{3c\alpha}}{2} \end{bmatrix} \tag{4.51}$$

Similarly as in the previous section, all $V \cdot I$ components are represented as specific powers. System powers $P_{1,2}$ are defined by (4.7a). Equations (4.25) - (4.30) defines ω_1-circulating current power components. ω_c-circulating current components are defined by Eq. (4.52) - (4.54).

$$P_{1c\alpha} = I_{c1c\alpha}V_{Xc\alpha} \tag{4.52}$$

$$P_{2c\alpha} = I_{c2c\alpha}V_{Xc\alpha} \tag{4.53}$$

$$P_{3c\alpha} = I_{c3c\alpha}V_{Xc\alpha} \tag{4.54}$$

Similarly to the previous section, the equation (4.23) can be written as (4.55).

$$P_0 = T_{Pc,2}P_{c,2} + T_{PS,2}P_S = P_{ref,2} \tag{4.55}$$

The key difference between the Eq. (4.55) and the Eq. (4.31) is the $T_{Pc,2}P_{c,2}$ term. $P_{c,2}$ is a circulating current vector with extra elements compared to $P_{c,1}$ vector defined in (4.32). $P_{c,2}$ is defined as (4.56). First six components belongs to P_{c1} vector. Last three to P_{cc} vector.

$$P_{c,2} = \begin{bmatrix} P_{c1} & P_{cc} \end{bmatrix}^T = \begin{bmatrix} P_{11\alpha} & P_{11\beta} & P_{21\alpha} & P_{21\beta} & P_{31\alpha} & P_{31\beta} & P_{1c\alpha} & P_{2c\alpha} & P_{3c\alpha} \end{bmatrix}^T \tag{4.56}$$

Element of the matrices $T_{PS,2}$ and $P_{ref,2}$ are also different than $T_{PS,1}$ and $P_{ref,1}$ due to the introduced extra equation.

Before defining aforementioned matrices, one of the branch power equation will be removed to make the determined system of nine equations. It can be noted that sum of all branch power constant components is equal the sum of active powers on the both systems what satisfies energy conservation rule (4.47). It also means that any of the power equations can be removed as one is redundant. It has been decided to remove the last power equation. The ninth equation is replaced with (4.50).

Therefore matrices $T_{Pc,2}$, $T_{PS,2}$ and $P_{ref,2}$ are equal:

$$T_{Pc,2}{}^{[9\times9]} = \begin{bmatrix} \frac{1}{2} & 0 & 0 & 0 & 0 & 0 & 0 & 0 & 0 \\ 0 & 0 & -\frac{1}{2} & 0 & 0 & 0 & 0 & 0 & 0 \\ 0 & 0 & -\frac{1}{4} & \frac{\sqrt{3}}{4} & 0 & 0 & 0 & 0 & 0 \\ 0 & 0 & 0 & 0 & \frac{1}{4} & -\frac{\sqrt{3}}{4} & 0 & 0 & 0 \\ 0 & 0 & 0 & 0 & -\frac{1}{4} & -\frac{\sqrt{3}}{4} & 0 & 0 & 0 \\ \frac{1}{4} & \frac{\sqrt{3}}{4} & 0 & 0 & 0 & 0 & 0 & 0 & 0 \\ -\frac{1}{2} & 0 & \frac{1}{2} & 0 & 0 & 0 & \frac{1}{2} & -\frac{1}{2} & 0 \\ 0 & 0 & \frac{1}{4} & -\frac{\sqrt{3}}{4} & -\frac{1}{4} & \frac{\sqrt{3}}{4} & 0 & \frac{1}{2} & -\frac{1}{2} \\ 0 & 0 & 0 & 0 & 0 & 0 & 1 & 1 & 1 \end{bmatrix} \tag{4.57}$$

$$T_{PS,2}{}^{[9\times6]} = \begin{bmatrix} 0 & 0 & 0 & -\frac{1}{4} & 0 & 0 \\ 0 & 0 & 0 & -\frac{1}{4} & 0 & 0 \\ 0 & 0 & 0 & -\frac{1}{4} & 0 & 0 \\ 0 & 0 & 0 & -\frac{1}{4} & 0 & 0 \\ 0 & 0 & 0 & -\frac{1}{4} & 0 & 0 \\ 0 & 0 & 0 & -\frac{1}{4} & 0 & 0 \\ -\frac{1}{2} & 0 & 0 & 0 & 0 & 0 \\ -\frac{1}{2} & 0 & 0 & 0 & 0 & 0 \\ 0 & 0 & 0 & 0 & 0 & 0 \end{bmatrix} \tag{4.58}$$

$$P_{ref,2} = \begin{bmatrix} p_1 & p_2 & p_3 & p_4 & p_5 & p_6 & p_7 & p_8 & 0 \end{bmatrix}^T \tag{4.59}$$

$p_{1...8}$ are corresponding branch power constant component references. p_9 satisfies the Eq. (4.47). For a steady state, power references are $p_{1...9} = 0$.

To reach specified setpoint (defined by $\boldsymbol{P_{ref,2}}$ vector), specific circulating current are being applied. It is possible to calculate currents by solving the Eq. (4.55) for the $\boldsymbol{P_{c,2}}$ vector.

Eq. (4.55) can be transformed to (4.60) if $rank\left(\boldsymbol{T_{Pc2}}\right) = 9$. The correct matrix rank has been provided by removing redundant equation and introducing linear independent Eq. (4.50).

$$\boldsymbol{P_{c,2}} = \boldsymbol{T_{Pc,2}}^{-1}\left(-\boldsymbol{T_{PS,2}}\boldsymbol{P_S} + \boldsymbol{P_{ref,2}}\right) \tag{4.60}$$

It should be noted that $\boldsymbol{T_{Pc,2}}$ matrix has been defined for a given topology: its elements doesn't depend on the system powers nor power reference values. It can be assumed that $\boldsymbol{T_{Pc,2}} = const$. It is very important conclusion as it means the inverted matrix $\boldsymbol{T_{Pc,2}}^{-1}$ doesn't have to be calculated in real time for the control system.

Matrix $\boldsymbol{T_{Pc,2}}^{-1}$ is equal:

$$\boldsymbol{T_{Pc,2}}^{-1} = \begin{bmatrix} 2 & 0 & 0 & 0 & 0 & 0 & 0 & 0 & 0 \\ -\frac{2}{\sqrt{3}} & 0 & 0 & 0 & 0 & \frac{4}{\sqrt{3}} & 0 & 0 & 0 \\ 0 & -2 & 0 & 0 & 0 & 0 & 0 & 0 & 0 \\ 0 & -\frac{2}{\sqrt{3}} & \frac{4}{\sqrt{3}} & 0 & 0 & 0 & 0 & 0 & 0 \\ 0 & 0 & 0 & 2 & -2 & 0 & 0 & 0 & 0 \\ 0 & 0 & 0 & -\frac{2}{\sqrt{3}} & -\frac{2}{\sqrt{3}} & 0 & 0 & 0 & 0 \\ \frac{4}{3} & \frac{4}{3} & \frac{2}{3} & \frac{2}{3} & 0 & 0 & \frac{4}{3} & \frac{2}{3} & \frac{1}{3} \\ -\frac{2}{3} & -\frac{2}{3} & \frac{2}{3} & \frac{2}{3} & 0 & 0 & -\frac{2}{3} & \frac{2}{3} & \frac{1}{3} \\ -\frac{2}{3} & -\frac{2}{3} & -\frac{4}{3} & -\frac{4}{3} & 0 & 0 & -\frac{2}{3} & -\frac{4}{3} & \frac{1}{3} \end{bmatrix} \tag{4.61}$$

Solving Eq. (4.60) gives required power values. Circulating currents are calculated using required powers and corresponding voltages. For ω_1-related powers (vector $\boldsymbol{P_{c1}}$), the power is proportional to the V_{1m} voltage. Therefore:

$$\boldsymbol{I_{cx1\alpha,\beta}} = \frac{P_{x1\alpha,\beta}}{V_{1m}} \tag{4.62}$$

For ω_c-related powers (vector $\boldsymbol{P_{cc}}$), the power is proportional to the $V_{Xc\alpha}$ voltage which can be chosen as a trade off between required Y-branch voltage rating and maximum branch current. Higher voltage means lower current and vice versa:

$$\boldsymbol{I_{cxc\alpha}} = \frac{P_{xc\alpha}}{V_{Xc\alpha}} \tag{4.63}$$

4.6.1. Solution check

For the first check, the steady state circulating currents will be calculated. It is expected to get the same results as in the Section 4.5.2, Eq. (4.42). ω_c-related components should be equal zero. Next, charging scenario will be presented. Finally, the energy transfer between two branches will be demonstrated.

4.6.1.1. Steady state

For the steady state, the reference power vector is equal zero:

$$\boldsymbol{P_{ref,2}} = \boldsymbol{0} \tag{4.64}$$

System active powers are equal but with opposite sign: energy transfer between input and output with no energy aggregation in the converter's branches. No reactive power is transferred. Therefore, system powers vector defined in the Eq. (4.33) is given as (4.65):

$$\boldsymbol{P_S} = \begin{bmatrix} P_1 & 0 & P_1 & -P_1 & 0 & -P_1 \end{bmatrix}^T \tag{4.65}$$

Circulating powers defined by the Eq. (4.60), for given $\boldsymbol{P_{ref,2}}$ and $\boldsymbol{P_s}$ vectors are equal:

$$\boldsymbol{P_{c,2}} = P_1 \begin{bmatrix} -\frac{1}{2} & -\frac{1}{2\sqrt{3}} & \frac{1}{2} & -\frac{1}{2\sqrt{3}} & 0 & \frac{1}{\sqrt{3}} & 0 & 0 & 0 \end{bmatrix}^T \tag{4.66}$$

From the calculated power, circulating currents can be extracted and divided into two groups. First six components are used to calculate the circulating current using Eq. (4.62). For the three last, scaling using $V_{Xc\alpha}$ voltage is used [Eq. (4.62)].

ω_1-circulating currents can be written in the $\boldsymbol{I_{c1}}$ vector defined in (4.43), which is equal:

$$\boldsymbol{I_{c1}} = I_{1m}cos(\phi_1) \begin{bmatrix} -\frac{1}{2} & -\frac{1}{2\sqrt{3}} & \frac{1}{2} & -\frac{1}{2\sqrt{3}} & 0 & \frac{1}{\sqrt{3}} \end{bmatrix}^T \tag{4.67}$$

ω_c-circulating currents written in the $\boldsymbol{I_{cc}}$ vector are equal zero:

$$\boldsymbol{I_{cc}} = \begin{bmatrix} 0 & 0 & 0 \end{bmatrix}^T \tag{4.68}$$

where $\boldsymbol{I_{cc}}$ is defined as

$$\boldsymbol{I_{cc}} = \begin{bmatrix} I_{c1c\alpha} & I_{c2c\alpha} & I_{c3c\alpha} \end{bmatrix}^T \tag{4.69}$$

Vector $\boldsymbol{I_{c1}}$ is the same as the vector calculated in the Section 4.5.2, Eq. (4.42). The same results means that the steady-state solution calculated by the Eq. (4.60) is valid (see Section 4.5.3). Zero $\boldsymbol{I_{cc}}$ vector means that no ω_c components are introduced in the steady state.

4.6.1.2. Charging

Proposed generic solution can be used for full feed-forward energy control of the system. One of important aspects of the MMC converter operation is an internal energy control used e.g. for charging the converter during the startup procedure.

In this subsection it will be analyzed what are the required circulating currents to provide symmetric charging of the converter. Symmetric word means that all the branches will be charged up together (no energy/power divergence between the branches should be observed).

For symmetric charging, valid, equal power references for each branch must be given. The energy conservation rule provides that the total power in the system remains the same. Modification of the

Eq. (4.47) leads to:

$$\sum_{b=1}^{9} p_b = -\frac{3}{2}\left(P_1 + P_2\right) \tag{4.70}$$

Each branch power should be equal what means that:

$$p_b = -\frac{1}{9} \cdot \frac{3}{2}\left(P_1 + P_2\right) \tag{4.71}$$

Power reference vector is equal:

$$\boldsymbol{P_{ref,2}} = -\frac{P_1 + P_2}{6}\begin{bmatrix} 1 & 1 & 1 & 1 & 1 & 1 & 1 & 1 & 0 \end{bmatrix}^{T} \tag{4.72}$$

System power vector is equal

$$\boldsymbol{P_S} = \begin{bmatrix} P_1 & 0 & P_1 & P_2 & 0 & P_2 \end{bmatrix}^{T} \tag{4.73}$$

Circulating powers defined by the Eq. (4.60), for given $\boldsymbol{P_{ref,2}}$ and $\boldsymbol{P_S}$ vectors are equal:

$$\boldsymbol{P_{c,2}} = \begin{bmatrix} \frac{P_2-2P_1}{6} & \frac{P_2-2P_1}{6\sqrt{3}} & -\frac{P_2-2P_1}{6} & \frac{P_2-2P_1}{6\sqrt{3}} & 0 & -\frac{P_2-2P_1}{3\sqrt{3}} & 0 & 0 & 0 \end{bmatrix}^{T} \tag{4.74}$$

As in the previous case, circulating power vector is used to calculate circulating current vectors $\boldsymbol{I_{c1}}$ (4.43) and $\boldsymbol{I_{cc}}$ (4.69).

$$\boldsymbol{I_{c1}} = \frac{P_2 - 2P_1}{6V_{1m}}\begin{bmatrix} 1 & \frac{1}{\sqrt{3}} & -1 & \frac{1}{\sqrt{3}} & 0 & -\frac{2}{\sqrt{3}} \end{bmatrix}^{T} \tag{4.75}$$

$$\boldsymbol{I_{cc}} = \begin{bmatrix} 0 & 0 & 0 \end{bmatrix}^{T} \tag{4.76}$$

Found solution will be checked by the calculation of the powers in the system with terminal parameters defined as in the Table 3.2. The only parameter which is changed is the I_{1m} current which will be equal $I_{1m} = 1.5$ to allow charging of the converter. As the V_X voltage is not required ($\boldsymbol{I_{cc}}$ vector is zero), branch voltages are the same as (3.48).

Circulating currents $\boldsymbol{I_{c1}}$ leads to branch currents equal (4.77). HAT rule has been used to combine $\alpha - \beta$ components of circulating currents

$$
\boldsymbol{I_b} = \boldsymbol{T_{i,\alpha\beta-br}} \cdot
\begin{bmatrix}
cos(\omega_1 t) \\
sin(\omega_1 t) \\
-cos(\omega_2 t) \\
-sin(\omega_2 t) \\
\frac{P_2-2P_1}{3\sqrt{3}} cos\left(\omega_1 t - \frac{\pi}{6}\right) \\
\frac{P_2-2P_1}{3\sqrt{3}} cos\left(\omega_1 t + \frac{7\pi}{6}\right) \\
\frac{P_2-2P_1}{3\sqrt{3}} cos\left(\omega_1 t + \frac{3\pi}{6}\right)
\end{bmatrix} =
$$

$$
\begin{bmatrix}
-I_{c1m}cos\left(\frac{\pi}{6} - \omega_1 t\right) + \frac{1}{2}cos(\omega_2 t) \\
\frac{1}{4}\left[-4I_{c1m}cos\left(\frac{\pi}{6} + \omega_1 t\right) - 2sin\left(\frac{\pi}{6} - \omega_2 t\right)\right] \\
\frac{1}{4}\left[4I_{c1m}cos\left(\frac{\pi}{6} + \omega_1 t\right) - 2sin\left(\frac{\pi}{6} - \omega_2 t\right)\right] \\
-I_{c1m}sin(\omega_1 t) - \frac{1}{2}sin\left(\frac{\pi}{6} + \omega_2 t\right) \\
\frac{1}{4}\left[4I_{c1m}sin(\omega_1 t) - 2sin\left(\frac{\pi}{6} + \omega_2 t\right)\right] \\
I_{c1m}cos\left(\frac{\pi}{6} - \omega_1 t\right) + \frac{1}{2}cos(\omega_2 t) \\
\frac{3}{2}cos(\omega_1 t) + I_{c1m}cos\left(\frac{\pi}{6} - \omega_1 t\right) + I_{c1m}cos\left(\frac{\pi}{6} + \omega_1 t\right) - \frac{1}{2}sin\left(\frac{\pi}{6} + \omega_2 t\right) \\
\frac{1}{2}\left[-2I_{c1m}cos\left(\frac{\pi}{6} + \omega_1 t\right) + cos(\omega_2 t) + 2I_{c1m}sin(\omega_1 t) - 3sin\left(\frac{\pi}{6} - \omega_1 t\right)\right] \\
\frac{1}{4}\left[-4I_{c1m}cos\left(\frac{\pi}{6} - \omega_1 t\right) - 4I_{c1m}sin(\omega_1 t) - 6sin\left(\frac{\pi}{6} + \omega_1 t\right) - 2sin\left(\frac{\pi}{6} - \omega_2 t\right)\right]
\end{bmatrix}
\tag{4.77}
$$

Where I_{c1m} defines ω_1 circulating currents amplitude (equal for all three currents):

$$
I_{c1m} = \frac{P_2 - 2P_1}{3\sqrt{3}}
\tag{4.78}
$$

Branch power equations for given voltage and current shapes are given in Appendix A, Eq. (A.5). Fig. 4.4 shows the waveforms. It can be noticed that all branch energies are increasing together.

4.6.1.3. Energy transfer between two branches

Presented solution allows to control each energy branch / power independently. The only restriction is an energy conversation rule (4.47). $\boldsymbol{P_{ref,2}}$ vector contains only eight branch powers so the ninth branch power will be calculated to always satisfy the rule.

Due to increasing complexity of power and energy equations, a simple simulation model has been built. It is used for power integration and verification of the mapping (if the terminal voltages are correct).

In actual control algorithm each branch power will be controlled to keep its energies (capacitor bank voltages) at similar level. In this section an example showing energy transfer among two branches will be demonstrated. $\boldsymbol{P_{ref,2}}$ vector is given as (4.79). It should be observed that branch 1 is charged up (positive value of $\boldsymbol{P_{1,0}}$) and branch 9 is discharged ($\Sigma P_{k,0} = 0$) for first 100 ms of the simulation. After that time, branch energies should remain at the same average level as the $\boldsymbol{P_{ref,2}}$ vector is set to zero.

$$
\begin{cases}
\boldsymbol{P_{ref,2}} = \begin{bmatrix} 0.2 & 0 & 0 & 0 & 0 & 0 & 0 & 0 & 0 \end{bmatrix}^T & \text{for } t < 100ms \\
\boldsymbol{P_{ref,2}} = \begin{bmatrix} 0 & 0 & 0 & 0 & 0 & 0 & 0 & 0 & 0 \end{bmatrix}^T & \text{for } t \geq 100ms
\end{cases}
\tag{4.79}
$$

(a) Hex Power

(b) Hex Energy

(c) Y Power

(d) Y Energy
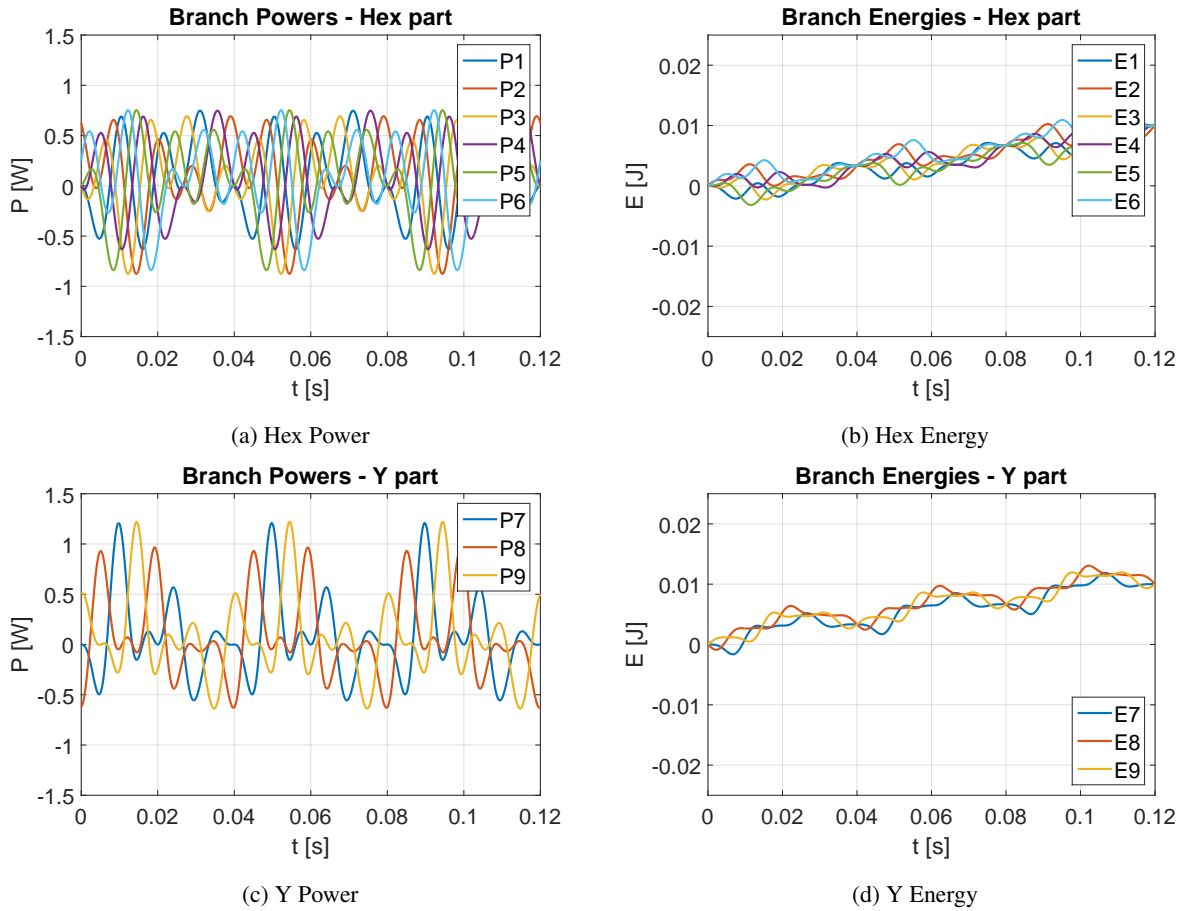
Figure 4.4. Branch powers and energies for a charging sequence. Branches 1 through 6 belongs to Hex, 7 through 9 belongs to Y part of the converter

Fig. 4.5 shows the simulation results - branch energies for a given example. $\omega_c = 2\pi 100 \ [rad/s]$ circulating power frequency has been chosen. It can be noticed that for the first 100 ms energy of the branch 1 is falling while the energy of branch 9 i rising. All other branch average energies remains constant. After 100 ms each branch average energy remains constant.

Figure 4.6 shows circulating currents decomposition for ω_1 and ω_c components for a given test case. It can be observed that ω_c components are used only during the power transfer among the branches. It is also visible that ω_1 circulating current component magnitude remains constant over a whole simulation. During the power transfer only the phase shift is changed.

4.7. Branch Powers for $\omega_2 = 0$

Following test case is a boundary condition for the low frequency mode which is critical especially for motor startup and for all applications with low output frequency (as milling, rolling, hydro power generation and so on).

(a) Hex Energy

(b) Y Energy
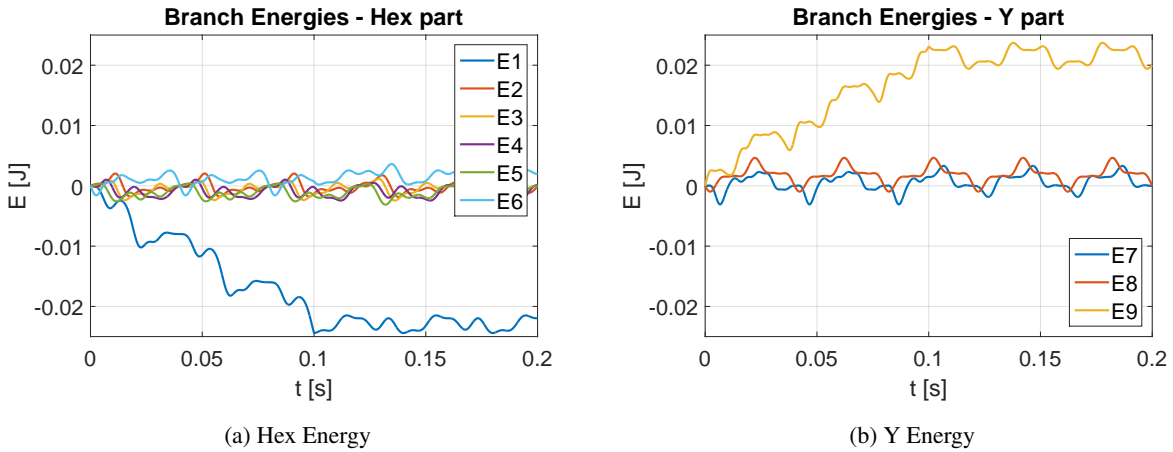
Figure 4.5. Branch energies for an example of power transfer between branches 1 and 9. Branches 1 through 6 belongs to Hex, 7 through 9 belongs to Y part of the converter
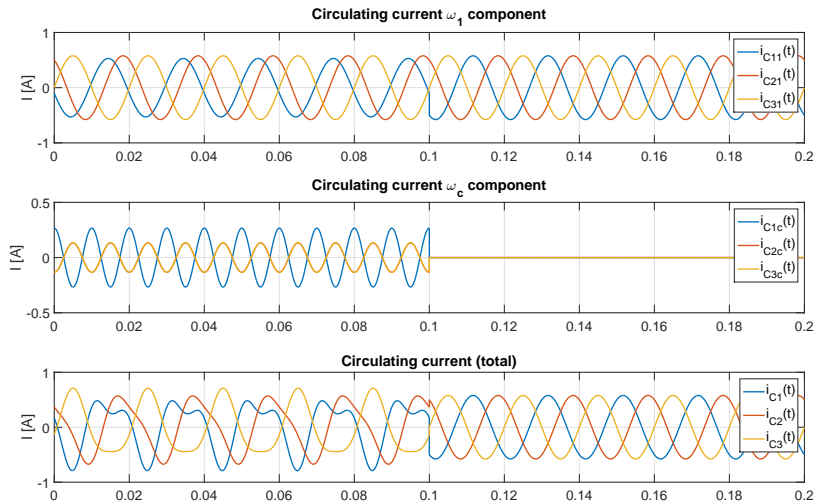
Figure 4.6. Circulating current components

If the output frequency is zero, extra components in the branch powers can appear as it was stated in the Chapter 4.1. Therefore, $\omega_2 = 0$ case is called a special operation point and it has to be investigated separately.

Conclusions drawn from that case will apply as well for the low frequency mode in which ω_2 is close to zero.

Case study analysis will be performed in the same way as for a normal operation point. Therefore, a workflow is following:

– define circulating currents and neutral point / star point voltages,

– identify constant components in branch powers,

– build a power equation for each branch,

   – create a system of nine linear independent equations ($\boldsymbol{P_0} = \boldsymbol{P_{ref}}$),

   – find a solution in a matrix form,

   – validate the solution.

Based on the previous experience, following current and voltage shapes has been chosen:

$$i_{cx}(t) = I_{cx} + I_{cx1\alpha}cos(\omega_1 t) + I_{cx1\beta}sin(\omega_1 t) + I_{cxc\alpha}cos(\omega_c t) \tag{4.80}$$

$$v_X(t) = V_{Xc\alpha}cos\left(\omega_c t\right) \tag{4.81}$$

$$v_N(t) = 0 \tag{4.82}$$

For given waveforms, constant components in power equations are equal:

$$\boldsymbol{P_0} = \begin{bmatrix} \frac{P_{11\alpha}}{2} - \frac{P_2}{4} - \frac{1}{4}S_2 \cdot cos(\phi_2 + 2\psi_2) \\ -\frac{P_2}{4} - \frac{P_{21\alpha}}{2} + \frac{1}{4}S_2 \cdot sin\left(\frac{\pi}{6} - \phi_2 - 2\psi_2\right) \\ -\frac{P_2}{4} - \frac{P_{21\alpha}}{4} + \frac{\sqrt{3}P_{21\beta}}{4} + \frac{1}{4}S_2 \cdot sin\left(\frac{\pi}{6} - \phi_2 - 2\psi_2\right) \\ -\frac{P_2}{4} + \frac{P_{31\alpha}}{4} - \frac{\sqrt{3}P_{31\beta}}{4} + \frac{1}{4}S_2 \cdot sin\left(\frac{\pi}{6} + \phi_2 + 2\psi_2\right) \\ -\frac{P_2}{4} - \frac{P_{31\alpha}}{4} - \frac{\sqrt{3}P_{31\beta}}{4} + \frac{1}{4}S_2 \cdot sin\left(\frac{\pi}{6} + \phi_2 + 2\psi_2\right) \\ \frac{P_{11\alpha}}{4} + \frac{\sqrt{3}P_{11\beta}}{4} - \frac{P_2}{4} - \frac{1}{4}S_2 \cdot cos(\phi_2 + 2\psi_2) \\ -\frac{P_1}{2} - \frac{P_{11\alpha}}{2} + \frac{P_{1c\alpha}}{2} + \frac{P_{21\alpha}}{2} - \frac{P_{2c\alpha}}{2} \\ -\frac{P_1}{2} + \frac{P_{21\alpha}}{4} - \frac{\sqrt{3}P_{21\beta}}{4} + \frac{P_{2c\alpha}}{2} - \frac{P_{31\alpha}}{4} + \frac{\sqrt{3}P_{31\beta}}{4} - \frac{P_{3c\alpha}}{2} \\ -\frac{P_1}{2} - \frac{P_{11\alpha}}{4} - \frac{\sqrt{3}P_{11\beta}}{4} - \frac{P_{1c\alpha}}{2} + \frac{P_{31\alpha}}{4} + \frac{\sqrt{3}P_{31\beta}}{4} + \frac{P_{3c\alpha}}{2} \end{bmatrix} \tag{4.83}$$

Where system powers (P_s, S_s) are defined by (4.7) and circulating powers are defined by Eq. (4.25)-(4.30) for ω_1 and (4.52)-(4.54) for ω_c components.

Constant components defined in Eq. (4.83) are used to create an equation $\boldsymbol{P_0} = \boldsymbol{P_{ref}}$. As for the normal operation point, there are 8 linear independent equations. Therefore, the ninth equation will be (4.50) which replace branch 9 power equation.

Matrix form of the equation is identical as (4.55). Index for the matrices is incremented to keep the consistency.

$$\boldsymbol{P_0} = \boldsymbol{T_{Pc,3}}\boldsymbol{P_{c,3}} + \boldsymbol{T_{PS,3}}\boldsymbol{P_S} = \boldsymbol{P_{ref,3}} \tag{4.84}$$

It can be noticed that $\boldsymbol{T_{Pc,3}} = \boldsymbol{T_{Pc,2}}$, $\boldsymbol{P_{c,3}} = \boldsymbol{P_{c,2}}$ and $\boldsymbol{P_{ref,3}} = \boldsymbol{P_{ref,2}}$. The only difference is a $\boldsymbol{T_{PS,3}}$ matrix which will contain non-zero elements for the $S2$ column:

$$\boldsymbol{T_{PS,3}}^{[9\times6]} = \begin{bmatrix} 0 & 0 & 0 & -\frac{1}{4} & 0 & -\frac{1}{4}a_1 \\ 0 & 0 & 0 & -\frac{1}{4} & 0 & \frac{1}{4}a_2 \\ 0 & 0 & 0 & -\frac{1}{4} & 0 & \frac{1}{4}a_2 \\ 0 & 0 & 0 & -\frac{1}{4} & 0 & \frac{1}{4}a_3 \\ 0 & 0 & 0 & -\frac{1}{4} & 0 & \frac{1}{4}a_3 \\ 0 & 0 & 0 & -\frac{1}{4} & 0 & -\frac{1}{4}a_1 \\ -\frac{1}{2} & 0 & 0 & 0 & 0 & 0 \\ -\frac{1}{2} & 0 & 0 & 0 & 0 & 0 \\ 0 & 0 & 0 & 0 & 0 & 0 \end{bmatrix} \tag{4.85}$$

$a_{1\ldots3}$ symbols are introduced to shorten notation. They are equal:

$$a_1 = cos\left(\phi_2 + 2\psi_2\right) \tag{4.86a}$$

$$a_2 = sin\left(\frac{\pi}{6} - \phi_2 - 2\psi_2\right) \tag{4.86b}$$

$$a_3 = sin\left(\frac{\pi}{6} + \phi_2 + 2\psi_2\right) \tag{4.86c}$$

It should be noted that $\phi_2 = 0$. For zero frequency current is in phase with voltage. Inductor impedance is equal zero and capacitor impedance is ∞.

As each matrix is defined, it is possible to make an equation and calculate required currents for a given setpoint.

Required circulating powers are equal (4.87). Resulting circulating powers vector defines circulating currents: $\boldsymbol{I_{c1}}$ (4.43) and $\boldsymbol{I_{cc}}$ (4.69).

$$\boldsymbol{P_{c,3}} = \boldsymbol{T_{Pc,3}^{-1}}\left(-\boldsymbol{T_{PS,3}}\boldsymbol{P_S} + \boldsymbol{P_{ref,3}}\right) \tag{4.87}$$

System powers vector $\boldsymbol{P_s}$ is defined in (4.33). Matrices $\boldsymbol{T_{PC,3}^{-1}}$ and $\boldsymbol{P_{ref,3}}$ are equal:

$$\boldsymbol{T_{PC,3}^{-1}}^{[9\times9]} = \begin{bmatrix} 2 & 0 & 0 & 0 & 0 & 0 & 0 & 0 & 0 \\ -\frac{2}{\sqrt{3}} & 0 & 0 & 0 & 0 & \frac{4}{\sqrt{3}} & 0 & 0 & 0 \\ 0 & -2 & 0 & 0 & 0 & 0 & 0 & 0 & 0 \\ 0 & -\frac{2}{\sqrt{3}} & \frac{4}{\sqrt{3}} & 0 & 0 & 0 & 0 & 0 & 0 \\ 0 & 0 & 0 & 2 & -2 & 0 & 0 & 0 & 0 \\ 0 & 0 & 0 & -\frac{2}{\sqrt{3}} & -\frac{2}{\sqrt{3}} & 0 & 0 & 0 & 0 \\ \frac{4}{3} & \frac{4}{3} & \frac{2}{3} & \frac{2}{3} & 0 & 0 & \frac{4}{3} & \frac{2}{3} & \frac{1}{3} \\ -\frac{2}{3} & -\frac{2}{3} & \frac{2}{3} & \frac{2}{3} & 0 & 0 & -\frac{2}{3} & \frac{2}{3} & \frac{1}{3} \\ -\frac{2}{3} & -\frac{2}{3} & -\frac{4}{3} & -\frac{4}{3} & 0 & 0 & -\frac{2}{3} & -\frac{4}{3} & \frac{1}{3} \end{bmatrix} \tag{4.88}$$

$$\boldsymbol{P_{ref,3}} = \begin{bmatrix} p_1 & p_2 & p_3 & p_4 & p_5 & p_6 & p_7 & p_8 & 0 \end{bmatrix}^T \tag{4.89}$$

4.7.1. Solution Check

Proposed solution will be checked for two cases. In the first case, $\psi_2 = const$. It will prove if given currents provide equal average branch powers for a given phase angle ψ_2.

For the second test case ψ_2 will be a low-frequency sine function. This will show that average power remains constant for different angles. It will also show that proposed solution can be used in low frequency mode.

Test case parameters are defined in the Table 4.1. Both cases with different ω_2 frequency are defined. $\psi_2 = 0$ has been chosen, however solution can be checked for any angle.

Table 4.1. Waveform parameters for zero output frequency (1) and low frequency (2)

Parameter	Value		Unit
V_{1m}	1		$p.u.$
I_{1m}	1		$p.u.$
V_{2m}	1		$p.u.$
I_{2m}	-1		$p.u.$
ω_1	$2\pi \cdot 50$		rad/s
ω_2	0	(1)	rad/s
	$2\pi \cdot 1$	(2)	rad/s
ω_c	$2\pi \cdot 100$		rad/s
ϕ_1	0		rad
ϕ_2	0		rad
ψ_1	0		rad
ψ_2	0		rad

In case of the zero frequency, required circulating powers calculated with Eq. (4.87) are equal:

$$\boldsymbol{P_{c,3}} = \begin{bmatrix} \boldsymbol{P_{c1}} \\ \boldsymbol{P_{cc}} \end{bmatrix} = \begin{bmatrix} P_{11\alpha} \\ P_{11\beta} \\ P_{21\alpha} \\ P_{21\beta} \\ P_{31\alpha} \\ P_{31\beta} \\ P_{1c\alpha} \\ P_{2c\alpha} \\ P_{3c\alpha} \end{bmatrix} = \begin{bmatrix} -\frac{1+a_1}{2}P_1 \\ -\frac{1+a_1}{2\sqrt{3}}P_1 \\ \frac{(1-a_2)}{2}P_1 \\ \frac{-1+a_2}{2\sqrt{3}}P_1 \\ 0 \\ \frac{1-a_3}{\sqrt{3}}P_1 \\ \frac{-2a_1+3a_2+a_3}{6}P_1 \\ \frac{a_1+a_3}{6}P_1 \\ \frac{a_1-3a_2-2a_3}{6}P_1 \end{bmatrix} \tag{4.90}$$

Circulating currents components calculated from given powers using (4.62) for ω_1 components and (4.62) for ω_c components are equal: (4.91). $V_{Xc\alpha} = 1$ has been chosen.

$$\boldsymbol{I_{c,3}} = \begin{bmatrix} I_{11\alpha} \\ I_{11\beta} \\ I_{21\alpha} \\ I_{21\beta} \\ I_{31\alpha} \\ I_{31\beta} \\ I_{1c\alpha} \\ I_{2c\alpha} \\ I_{Ic\alpha} \end{bmatrix} = \begin{bmatrix} -\frac{1}{2}(1+a_1)I_1 \\ -\frac{(1+a_1)I_1}{2\sqrt{3}} \\ \frac{1}{2}(P_1 - a_2 I_1) \\ \frac{(-1+a_2)I_1}{2\sqrt{3}} \\ 0 \\ \frac{I_1 - a_3 I_1}{\sqrt{3}} \\ \frac{1}{6}(-2a_1 + 3a_2 + a_3)I_1 \\ \frac{1}{6}(a_1 + a_3)I_1 \\ \frac{1}{6}(a_1 - 3a_2 - 2a_3)I_1 \end{bmatrix} \tag{4.91}$$

Each of three circulating currents is build with three components according to Eq. (4.80). After combining given components and using HAT rule for $\alpha-\beta$ components, following currents are obtained:

$$i_{c1}(t) = \frac{-1 - a_1}{\sqrt{3}} I_{1m} cos\left(\frac{\pi}{6} - \omega_1 t\right) + \frac{-2a_1 + 3a_2 + a_3}{6} I_{1m} cos\left(\omega_c t\right) \tag{4.92a}$$

$$i_{c2}(t) = \frac{-1 + a_2}{\sqrt{3}} I_{1m} cos\left(\frac{\pi}{6} + \omega_1 t\right) + \frac{a_1 + a_3}{6} I_{1m} cos\left(\omega_c t\right) \tag{4.92b}$$

$$i_{c3}(t) = \frac{1 - a_3}{\sqrt{3}} I_{1m} sin\left(\omega_1 t\right) + \frac{a_1 - 3a_2 - 2a_3}{6} I_{1m} cos\left(\omega_c t\right) \tag{4.92c}$$

It should be noted that reduction using HAT rule is used only to simplify the equation. In the real control loop it is much easier to calculate α and β components separately and simply add them.

For a given example angle $\psi_2 = 0$, following currents are obtained:

$$i_{c1}(t) = -\frac{2}{\sqrt{3}} I_{1m} cos\left(\frac{\pi}{6} - \omega_1 t\right) \tag{4.93a}$$

$$i_{c2}(t) = \frac{1}{2\sqrt{3}} I_{1m} cos\left(\frac{\pi}{6} + \omega_1 t\right) + \frac{1}{4} I_{1m} cos\left(\omega_c t\right) \tag{4.93b}$$

$$i_{c3}(t) = \frac{1}{2\sqrt{3}} I_{1m} sin\left(\omega_1 t\right) - \frac{1}{4} I_{1m} cos\left(\omega_c t\right) \tag{4.93c}$$

Branch voltage and current waveforms are presented on the Figure 4.7.

Figure 4.8 pretenses branch energies which are calculated by integration of instantaneous branch powers.

Figure 4.9 presents terminal voltages and currents. It should be noted that for $\psi_2 = 0$ two system voltages are equal $(cos(\frac{2\pi}{3}) = cos(\frac{4\pi}{3}) \rightarrow V_V = V_W)$.

Following conclusion can be drawn: It is possible to keep branch average energy constant also for the special operation point $\omega_2 = 0$. Common mode voltage introduction is not required. Hex branch voltages contains only ω_1 frequency component. For Y branches also ω_c component is present.

It is possible to optimize shapes of the waveforms (e.g. reduce the energy ripple) by introducing extra current components with frequency ω_c but 90 deg phase shifted in relation to already introduced I_{Cxca} component.

(a) Hex Power

(b) Hex Energy

(c) Y Power

(d) Y Energy
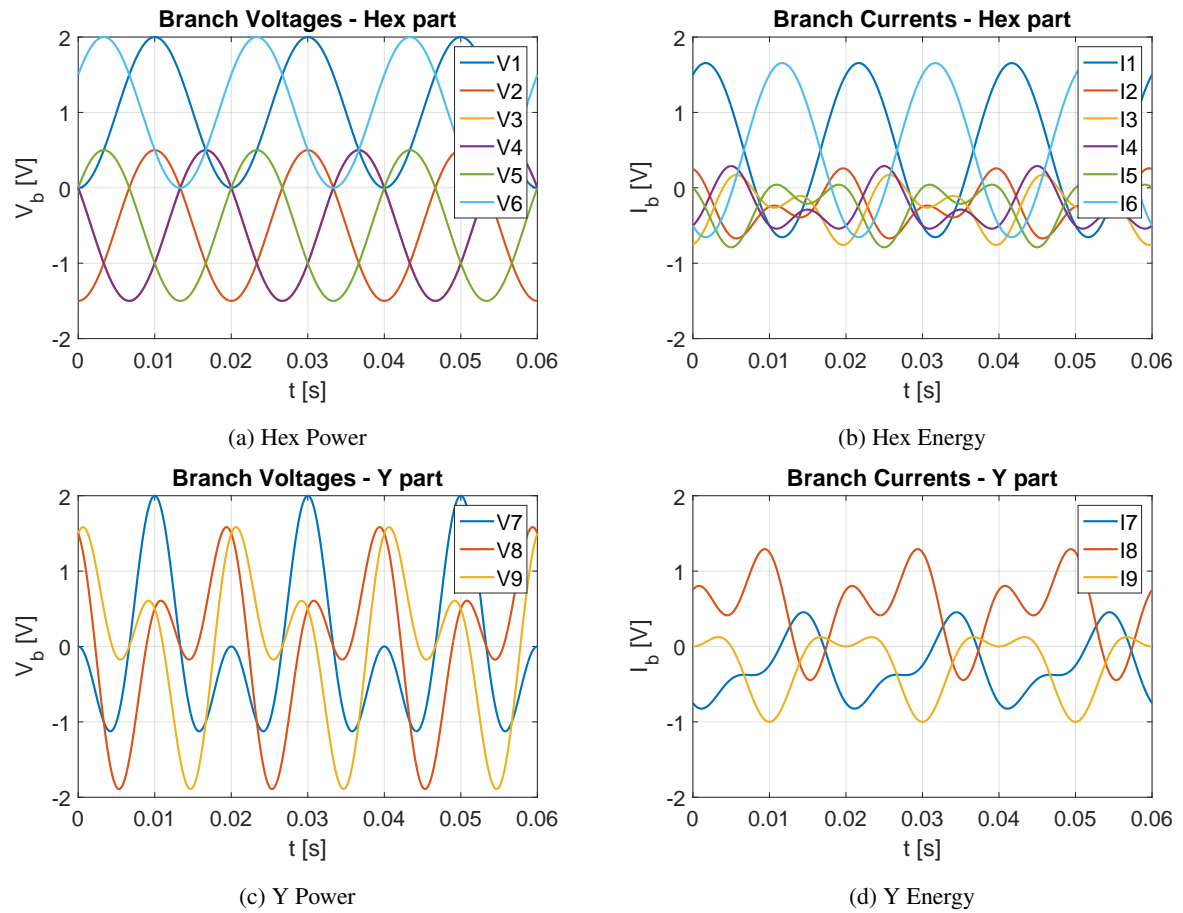
Figure 4.7. Branch Voltages for Hex (a) and Y (b) part. Branch Currents for Hex (c) and Y (d) part. Zero output frequency

(a) Hex Energy

(b) Y Energy
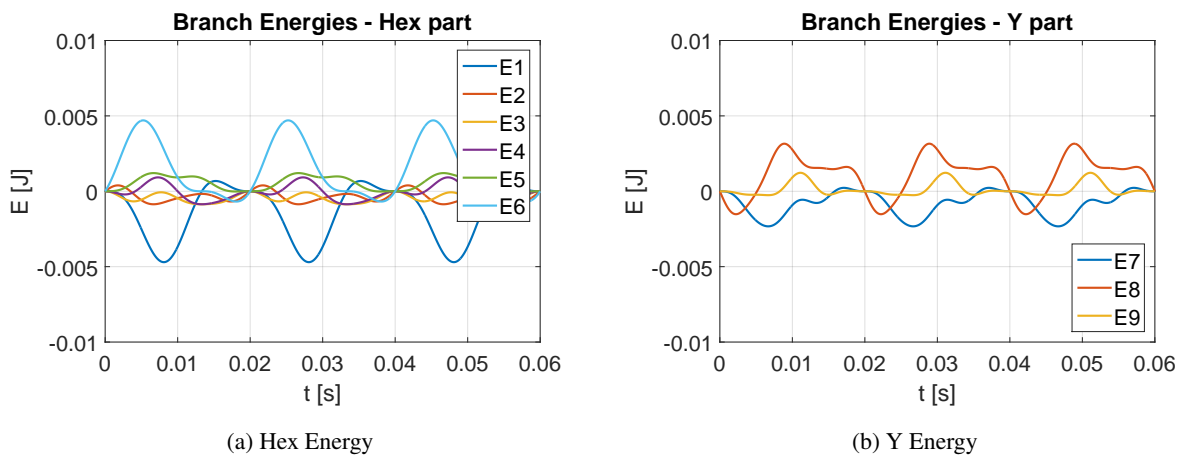
Figure 4.8. Branch energies for zero output frequency in Hex (a) and Y (b) branches

Proposed solution has been checked also for the low frequency mode (1 Hz). Waveform parameters are defined in the Table 4.1, case (2). Fig. 4.10 shows terminal voltages and currents for given test case.

(a) Hex Power

(b) Hex Energy

(c) Y Power

(d) Y Energy
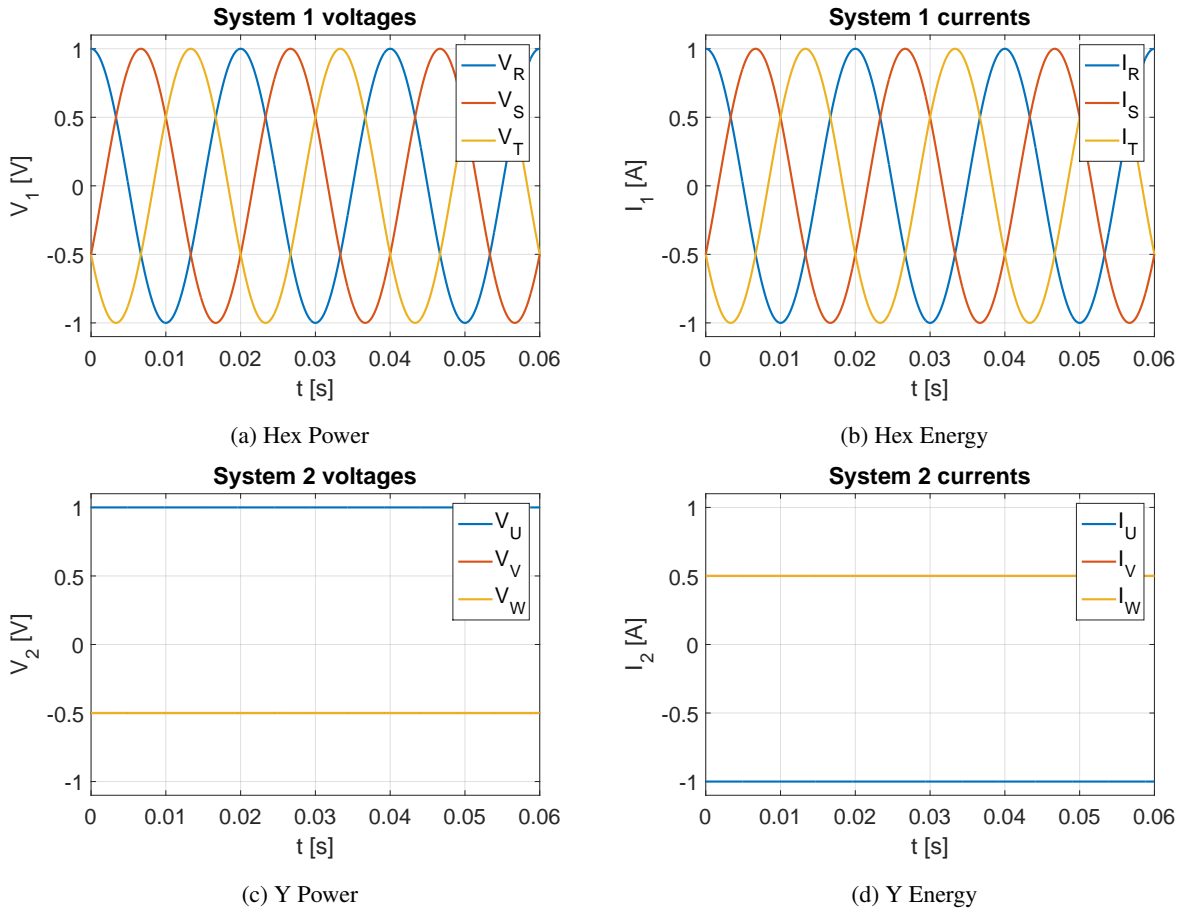
Figure 4.9. System 1 Voltages (a) and Currents (b), System 2 Voltages (c) and Currents (d) for zero output frequency

Branch energies are shown on the Fig. 4.11. Average branch powers remains constant what proves that proposed circulating currents can be used for both zero and low output frequency. It can be noticed that depending on the current phase angle ψ_2, different branch ripples can be observed.

Corresponding circulating currents (ω_1 and ω_c components) are shown on the Fig. 4.12 (a,b). Fig. 4.12 (c) shows total circulating currents $i_{c1...3}$.

(a) Hex Power

(b) Hex Energy

(c) Y Power

(d) Y Energy
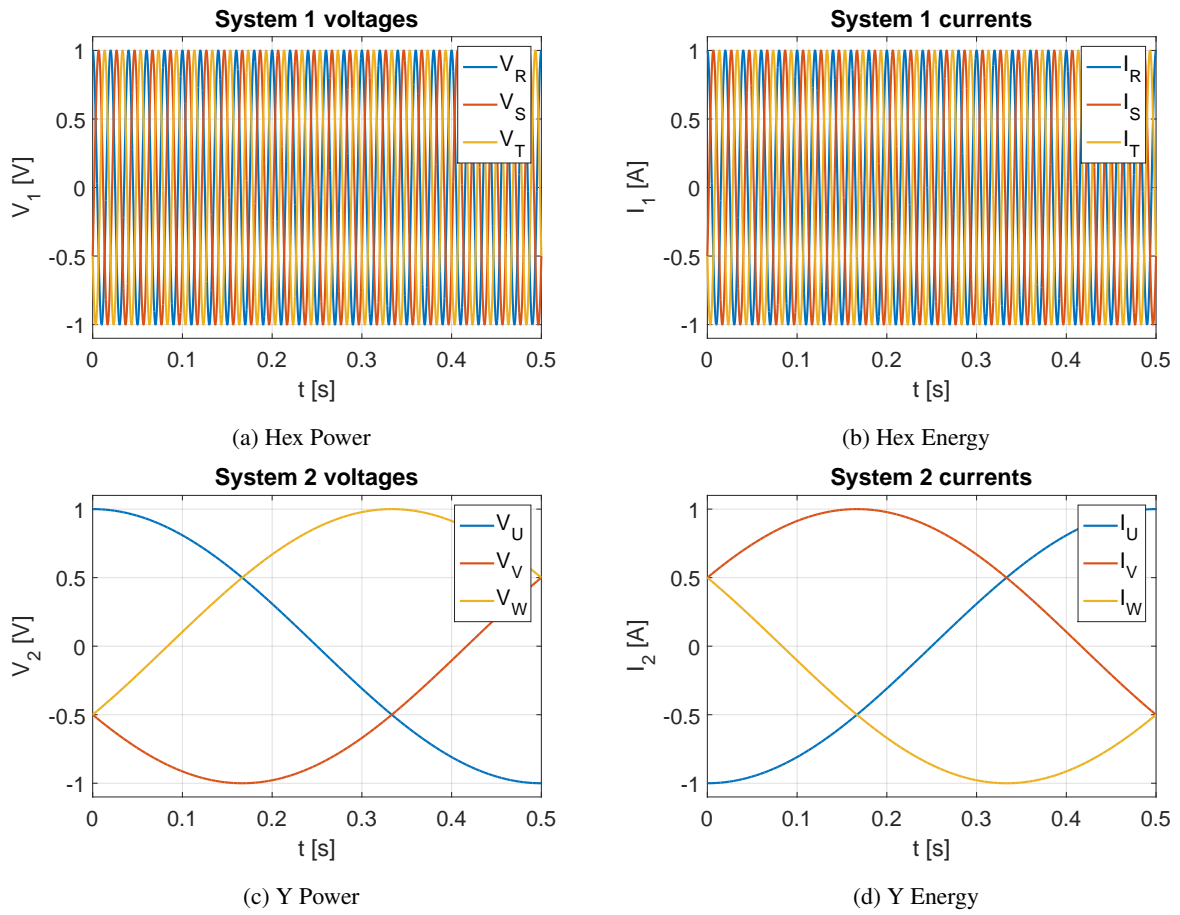
Figure 4.10. System 1 Voltages (a) and Currents (b), System 2 Voltages (c) and Currents (d) for low output frequnency

(a) Hex Energy

(b) Y Energy
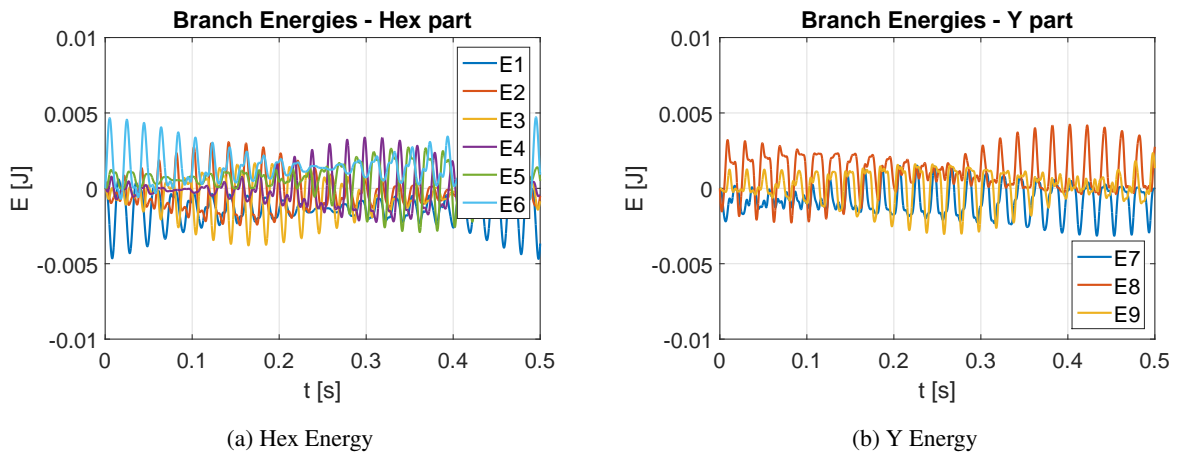
Figure 4.11. Branch energies for low output frequency in Hex (a) and Y (b) branches
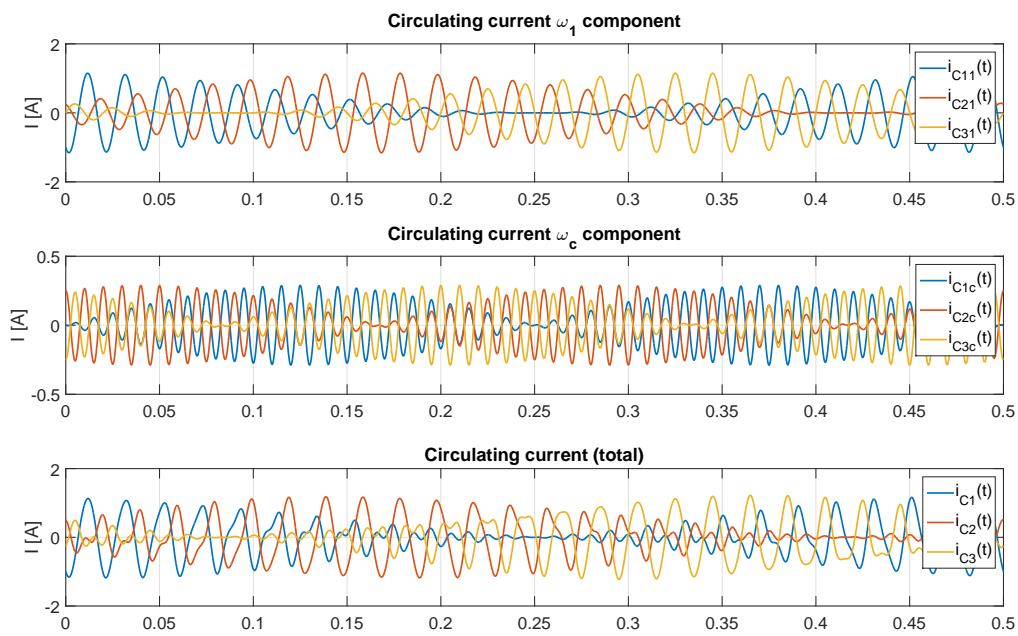
Figure 4.12. Circulating current components for low output frequency

5. Hex-Y Control

In following chapter, a control algorithm of Hex-Y MMC converter is being presented. Implementation of the control is distributed among different hardware components what is also explained. Depending on the final application, high-level control modules (as e.g. reference generation) can be implemented differently. In the Thesis, a use case with low-speed drive / generator defines high-level control algorithm. On the low-level, different controllers can be also used, e.g. resonant controller instead of classical PI.

A short overview of the control concept can be found in [82]. Paper includes also a comparison of Hex-Y and M3C topology for given operation points.

5.1. Control Hardware Overview

Fig. 5.1 presents control hardware components which are used to build a system. Hierarchy from top to bottom represents also control loop speed, i.e. bottom modules are used for fast control loops as the delay of feedback signal (measurements) is the smallest. In case of top-levels, delays are higher.

Black dashed lines represents electrical connections. Red dashed line separates control and power system (MMC converter and grid). Blue lines represents fiber optic connections between specific modules. Bold blue lines represents communication based on 10 Mbit/s Multilink, thin lines represents 5 Mbit/s UART link. Multilink supports Fast/Mid/Slow data exchange. Parameters are shown in the Table 5.1.

Table 5.1. Multilink Capability in 16-bit words

Type	No	Update time
Fast	8	$125\,\mu s$
Mid	4	$500\,\mu s$
Slow	64	$3.2\,ms$

Due to the fact that used control hardware supports only six branches in total, to built Hex-Y nine-branch controller, two base modules are used. One is controlling six Hex branches while the other one
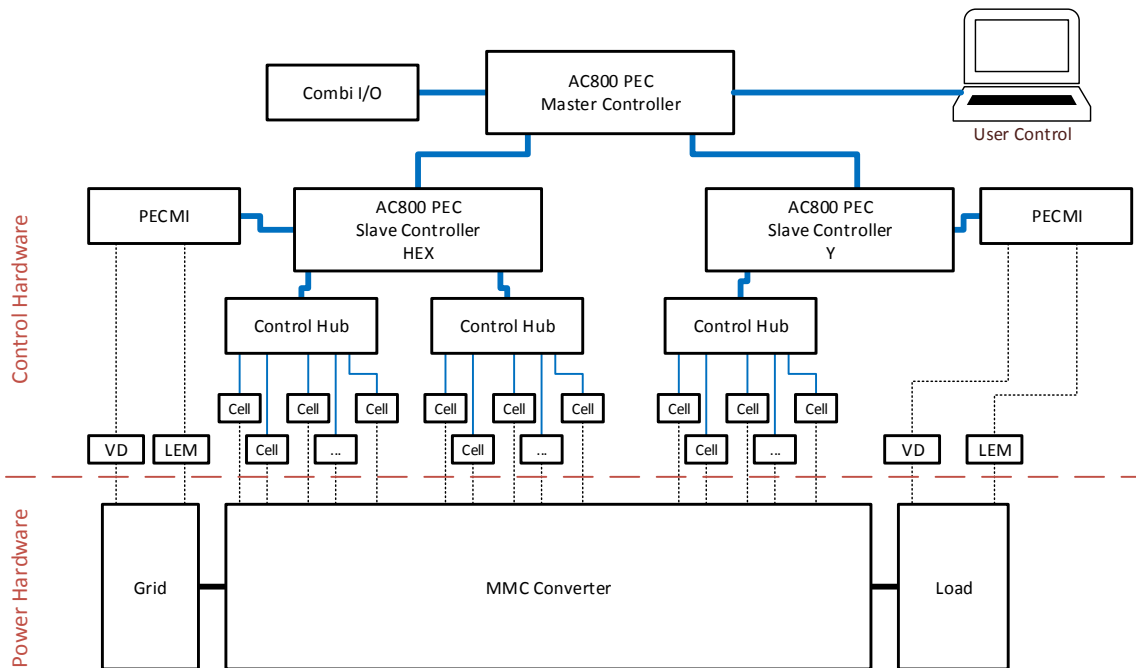
Figure 5.1. Power and control hardware overview.

is controlling three Y branches. Above, a Master controller is present. Below each module, a distribution unit (hub) is required to distribute given references among each cell. At the bottom, a set of cell controllers (each controller for a single cell) is placed.

Master and Slaves are implemented on ABB AC800 PEC platform [83, 84] which is described in the section 5.1.1. Both controllers are connected to the peripheral module providing voltage and current measurements (PECMI). Voltage measurements are read from the voltage divider (VD on the Figure). Currents are measured with LEM sensors.

I/O control for auxiliaries (e.g. control of the main breaker or temperature measurements) is provided by Combi IO module which is connected directly to Master. If it is required to have an extra I/O control locally (on the Slave PEC level), it is possible to connect extra Combi IO modules.

Distribution unit (so called Control HUB) is ABB custom product. FPGA on board is used to minimize the delay of data routing between Slave and Cell controllers. Its main function is reduction of amount of data between cells and system e.g. by calculating and sending over average branch voltage and currents instead of every cell measurements.

On the cell level, DSP controller is being used. Details about the cell control hardware can be found in Chapter 2.2.1 which describes PEBB module id detail.

Figure 5.2. AC 800 PEC PP D113 [84].

5.1.1. AC 800 PEC Controller

AC 800 PEC [83, 84] is an industrial controller characterized by high computational power and integration of three-level control layers which allows to work with fast and slow processes with a single device.

AC 800 PEC is a modular solution to which a number of extensions is available. Example modules are PECMI and Combi IO described in following sections.
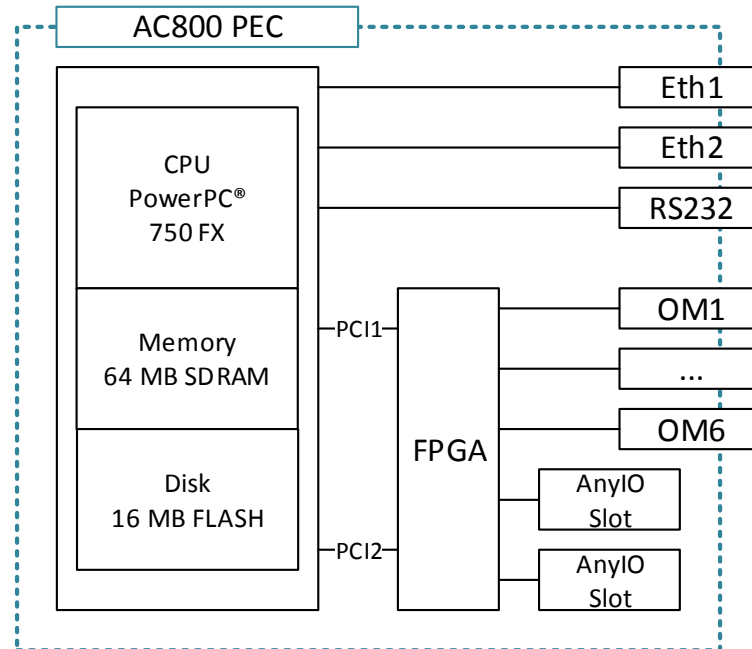
Figure 5.3. AC 800 PEC Hardware Block Diagram.

Block diagram of the device is presented on the Figure 5.3. Module communicates with external world by:

– two Ethernet ports used for connection with plant control network, other processor modules or for programming,

– RS232 port used for a service purposes and for local process panel,

– two on-board AnyIO ports which can be used to install extension communication modules, as Modbus, Profibus or CANopen,

– six optical module (OM) boards. Each board contain six fiber optic connectors used for fast and robust communication with peripheral modules.

Example peripheral devices connected by optical modules with PEC controller are PECMI, Combi IO or S800 module which works as a regular PLC controller (slow process control with virtually unlimited number of I/Os). Additionally, application-specific modules can be found. For example: PEBB Interface module used for 2x6-pulse IGBT converters or PINT module for control of two independent 6-pulse thyristor converter bridges.

Controller is built with PowerPC 750 FX processor running at 600 MHz. Processor contains 64-bit Floating Point Unit (FPU).

16 MB FLASH memory is used to store application and data and configuration. Application is loaded and running from 64 MB SDRAM memory.

The fastest calculations are performed on FPGA. Controller is available in three configurations: 10, 20 and 30 kB FPGA.

PEC controller contains three software layers as it is presented on the Figure 5.4. The slowest one (Level 1) is executed with frequency below 1 kHz. In this layer functionality as slow process control, monitoring, data export and display panel service is realized. This layer is programmed with structural text according to industrial standard IEC 61131-3.

Level 2 layer is executed with frequency in range 1-10 kHz. It contains main control algorithm, main state machine and fast protection. This layer is programmed in Matlab/Simulink with use of automated code generation (code is generated to Native C).

Level 3 layer is executed with frequency above 100 kHz. It includes time-critical functionality as ultra fast protection and hardware specific functions, e.g. PWM modulator. It is programmed in VHDL, however controller is delivered with generic packages what means that for standard application, VHDL knowledge (and generation tools) are not required.

5.1.2. PECMI

PEC Measuring Interface (PECMI UA D140) presented on Figure 5.5 is a peripheral device used for voltage and current measurements in AC and DC power circuits [83, 85]. Board contains following interfaces:

– three differential voltage inputs with 10 $k\Omega$ impedance,
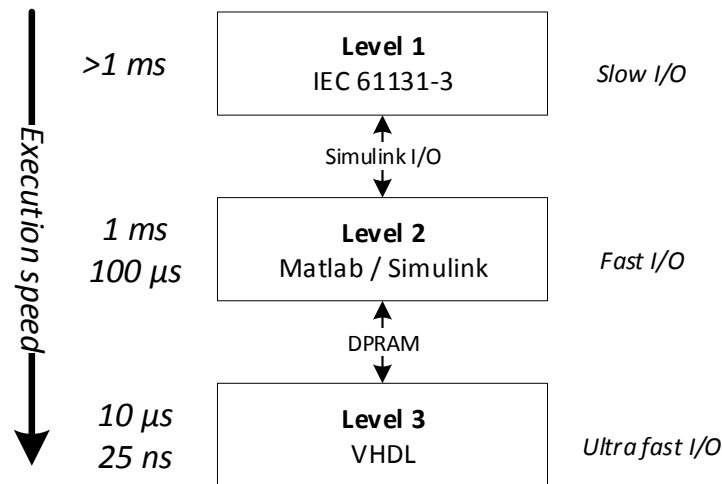
Figure 5.4. AC 800 PEC Software Programming Layers.
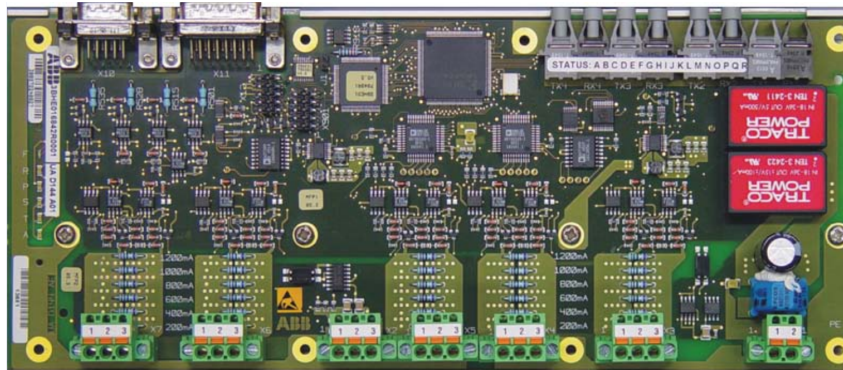
Figure 5.5. PECMI UA D140 [85].

– five scalable interfaces for current measurement with LEM sensors.

Additionally to current measurements, the board is equipped with five fast analog inputs for overcurrent detection (with configurable threshold). Its reaction time is below $3\ \mu s$.

Measurements are performed by 14-bit, 8-channel ADC with simultaneous sampling.

Board contains interfaces to connect voltage divider - either low voltage divider (LVD) feasible for applications up to $1\ kVrms$ or high voltage divider (HVD) feasible for applications up to $6\ kVrms$. For higher voltages, HVD with extension modules can be used. It is possible to connect also current and voltage transducers (CT,VT).

Inputs for current measurement are scalable from $200\ mA$ to $1200\ mA$ with $200\ mA$ step.

On the board, voltages $\pm\ 15\ V$ and $\pm\ 24\ V$ are available. They can be used to supply sensors. Communication with AC 800 PEC is realized via optical links with cycle time $25\ \mu s$.

The board has FPGA which is used for protection, communication and measurements preprocessing. It is possible to enable filtering on specific inputs. If required, extra functionality can be also implemented on the FPGA unit.

5.1.3. Combi IO

Combi IO module is built with a base module UA D141 and attached one or two sub-modules containing measurement circuits. The base module is responsible for providing power supply, communication with AC 800 PEC and data processing (filtering, configuration etc.) [86].

An extension of base module can be a single traction sub-module (DA D143) which provides 13 analog inputs and 18 digital inputs.

Another sub-module is UA D142 Mixed IO presented on the Figure 5.6. Combi IO can be equipped with two of that boards. In the test setup used in Thesis, both modules are available, however a single board would be enough.
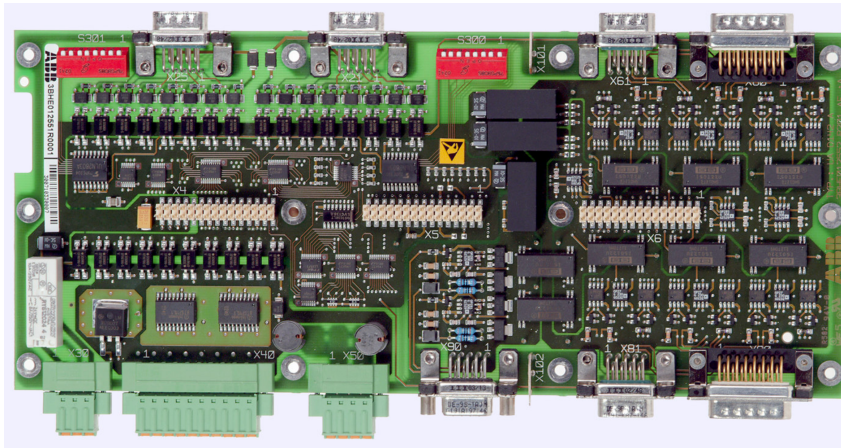
Figure 5.6. Combi IO Mixed Module UA D142 [87].

Single module contains [87]:

– 6 analog inputs (AI), which can work as a voltage or current inputs rated with $\pm 10\ V$ or $\pm 20\ mA$. Input bandwidth: $25\ kHz$,

– 2 analog outputs (AO), rated $\pm 10\ V$ or $\pm 20\ mA$. Output bandwidth: $10\ kHz$,

– 16 digital inputs (DI), $24\ V$, isolated,

– 8 digital outputs (DO), $24\ V$, max $0.5\ A$ per output,

– hardware trip output (interlock), realized with a trip relay.

Analog inputs are divided into two three-channel sections. Sections are separated and independently configured. By use of low voltage divider (LVD) it is possible to use AIs to take measurements up to $1\ kVrms$.

Analog outputs are galvanicaly separated (test voltage $500\ V$).

5.1.4. Control Hub

Figure 5.7. Control Hub with four Fiber Optic boards. $4 \cdot 9 = 36$ cells connected. Photo taken at ABB Corporate Technology Center.

Control Hub is non-standard (not available for external sale) ABB product which is responsible for communication between central controller (AC 800 PEC) and cell controllers.

Control Hub is built with base unit containing power supply, FPGA and fiber optic links to communicate with central controller. To the base unit, up to 10 fiber optic (FO) extension boards is connected. Each FO extension contains 10 FO pairs. Therefore single Control Hub can control up to 100 cells. In practice however, it is easier to use multiple control hubs instead of a single device controlling all the boards. It is much easier to route FO within a single cabinet, so if the system is built with n-cabinets, n-Control Hubs are used.

Limit of Control Hubs is determined by AC 800 PEC capability. Central controller can support up to 16 Control Hubs what gives 1600 cells as a limit[1].

Control Hub contains following interfaces:

– PEC - Control Hub redundant optical link. Communication with native *MMCLink* protocol. Baud rate: 10 Mbit/s,

– communication with up to 100 cell controllers based on UART protocol. Baud rate: 5 Mbit/s,

– 4 digital inputs (DI),

– 2 digital output (DO),

– 2 PWM outputs with configurable frequency (0-2kHz) and duty cycle (0-100%),

– single pressure drop sensor input (for detection of air filters wear out),

– trip line circuit (interlock).

---

[1]Current firmware unfortunately supports only two control hubs. As Hex-Y requires three Control Hubs, hierarchical control with Master and two Slave PEC controllers is used.

Main functions of the module are to provide communication and protection between central controller and cell controllers. Additionally, module provides IO service on the single cabinet level (e.g. check the door status, door lock, fan control, etc.).

Control Hub provides message broadcasting from central controller. Each Control Hub has information about cell mapping i.e. to which branch belongs which cell connected to a given optical link. Mapping is sent by central controller during startup. It can be also updated during runtime to provide bypassing of failed cell[2]. Table 2.2 presents data which is exchanged.

Control Hub is also responsible for cell PWM generators synchronization, which is realized by sending *Sync* command every 100 ms[3]. Cell, after receiving this command resets its counter and set to given initial value.

To reduce amount of data sent to the central controller, Hub is calculating average branch voltage and current and send only those numbers upstream. This is possible as cell balancing is realized on cell controllers, not on the central controller.

5.2. Control of Hex-Y Converter

Fig. 5.8 presents interconnections between MMC control system. Colors on the Figure shows physical location of given module in a control hardware. As it was highlighted in previous section, proposed control system is hierarchical and distributed. The most time-critical modules are realized on the low-level DSPs placed directly on each power module. High-level references are calculated on the master modules and feed further.

Control algorithm has three key functions. First, it must provide given output voltage and current setpoints. Second, it must provide adequate energy level in all modules (energy control and balancing is required). Finally, it must provide that currents and voltages does not exceed given limits.

Phase-Locked Loop (PLL) and Reference Generator (REF) modules are responsible for generation of voltage reference setpoints at converter output terminals.

Converter Energy Control (CEC) module provides given energy level of the whole converter. Branch Balancing (BRB) module is responsible for energy sharing among converter branches.

For given branch energy setpoints, Circulating Current Calculation (CCC) module calculates required circulating currents and and star point voltage. Also this module provides saturation for the references to not exceed system limits.

System voltages and currents are next mapped into corresponding branch quantities. It is realized in modules System-Branch Voltage Mapping (SBV) and System-Branch Current Mapping (SBI).

Branch current reference is next compared with branch measurements. Error is feed into Branch Current Control (BRI) module which contains controllers. Output from the module is added to given branch

---

[2]This function is however not implemented in a current firmware version.

[3]This number is parameterized
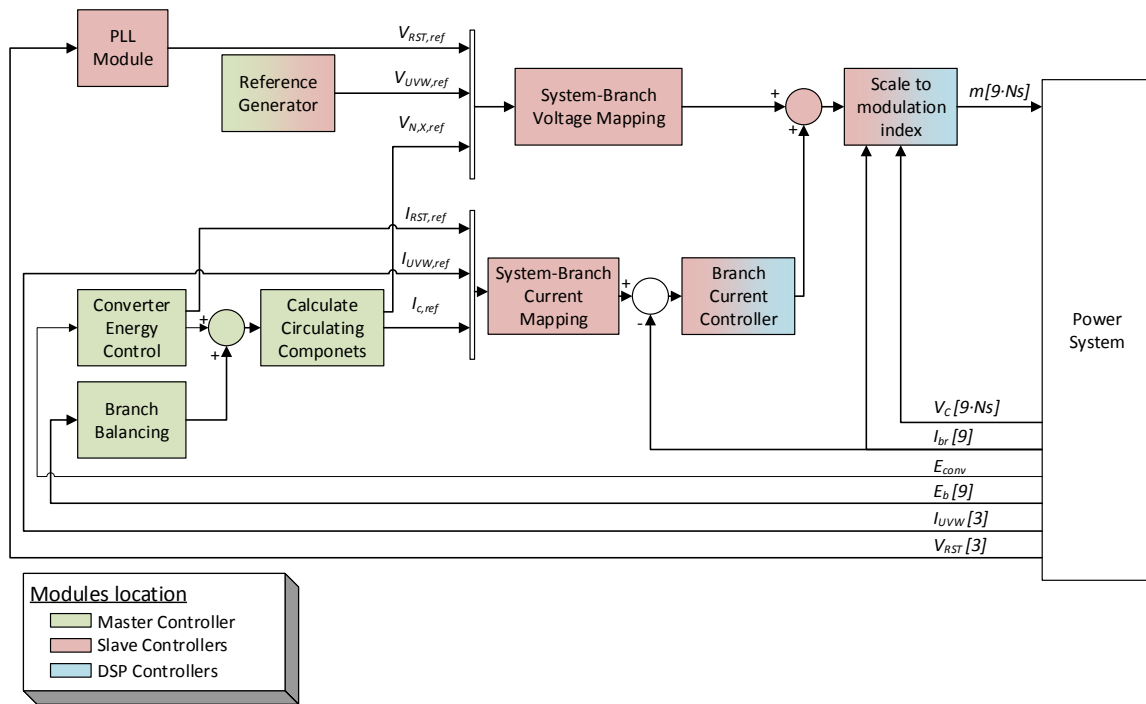
Figure 5.8. Control loop overview.

voltage setpoints and feed to Scale to Modulation Index (MOD) module which calculates modulation index of each module.

Details of each module are presented in following subsections.

5.2.1. Phase-Locked Loop Module (PLL)

PLL is a module responsible for input grid synchronization. Output of PLL is a phase angle and voltage magnitude (RMS or peak). In this module, also voltage change detection mechanism can be included. It will be used to detect voltage dips and swells. Detection is crucial if grid support functionality is required. In that case, voltage magnitude can be tuned by reactive current injection.

The module synchronizes with a voltage in dq reference frame[4] by controlling (setting to zero) voltage in one axis (q). It is realized by angle modification.

Fig. 5.9 shows a block diagram of the module which is implemented in a Thesis. Input voltage is transferred into $\alpha\beta$ and next into dq reference frame. q-axis voltage is compared with a reference equal zero. Error is fed into PI controller which output is angular frequency ω. Its value is added to the nominal grid frequency ω_0. Integrated sum is a phase angle of the voltage (θ).

As soon as q-voltage is below threshold, it can be assumed that PLL module is synchronized. Phase θ is an output signal of the module. Synchronization signal is also passed as it is used in a state machine and protection modules (synchronization loss detection).

---

[4]For dq reference frame, voltage transformation is being used in the Thesis.

d-voltage is filtered with a low-pass filter and feed as an output of the PLL module. Its value is equal peak voltage magnitude.
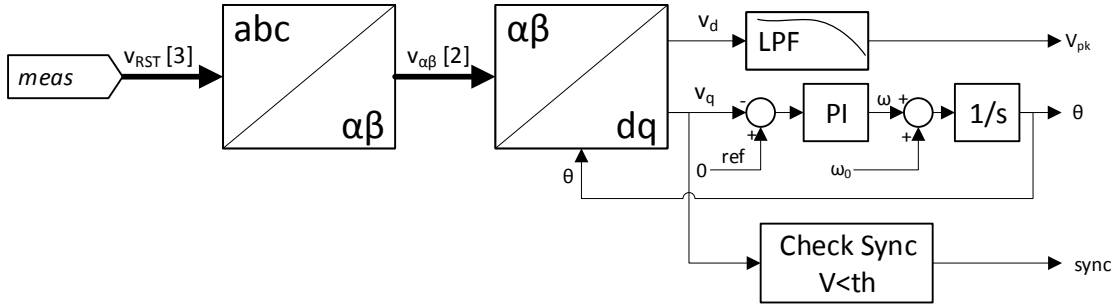
Figure 5.9. PLL Module

5.2.2. Reference Generator (REF)

REF module generates three phase voltage reference at converter's output. When on the output generator or motor is present, specific algorithm as e.g. constant V/f is used. When on the output side, electric grid is connected then reference generator has to use a second PLL module to synchronize with.

Following module is fully application dependent. In the Thesis, it is assumed that motor with flat torque-speed characteristics is present. Therefore reference generator contains simple speed controller which generates three-phase voltage reference with given magnitude and frequency. Frequency determines angular speed of the motor while magnitude determines a torque.

Fig. 5.10 shows a block diagram of the module which generates a symmetric three-phase voltage reference.
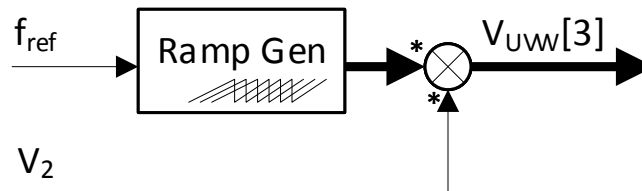
Figure 5.10. REF module

5.2.3. Converter Energy Control (CEC)

Following module provides required energy flow between input and output systems. Additionally it provides given energy level of the converter itself. Its energy is stored in distributed capacitor banks (each cell contains its own bank).

Energy flow is provided by control of active power at the input system.

Additionally, module can provide given level of reactive power on the input grid side. To keep $cos(\phi) = 0$, zero reactive current is provided. Non-zero reactive current is required by grid support modules (e.g. to boost voltage in case of dip detection).

The module is also crucial in converter charging process. In that phase, energy reference given to the module is ramping up from low to nominal value. More steep ramp means charging will be faster, however input current will be higher. On the Fig. 5.11 energy reference for charging and nominal operation is present. Angle α defines charging speed.
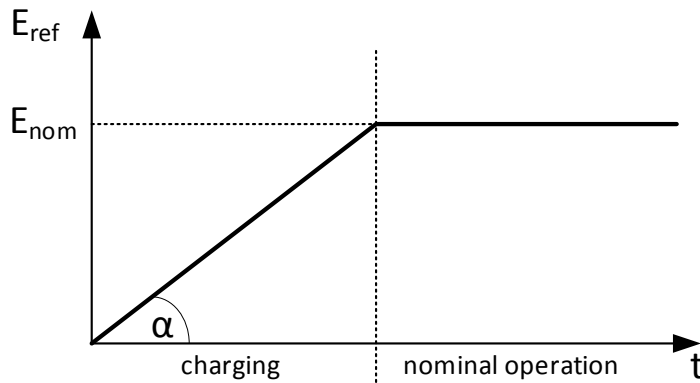
Figure 5.11. Energy reference for CEC module

Fig 5.12 shows block diagram of the module. It should be noted that in practice, CEC module can either control converter energy or average capacitor voltage as $E \sim V_C^2$. Capacitor voltage control is more accurate and easier to design as each capacitor voltage is measured quantity. For energy, it is being calculated using measured voltage and nominal cell capacitance which, in fact can fluctuate due to manufacturing process. Additionally, during the lifetime of the module, capacitance degradation is observed. Therefore, cell energy estimation is less accurate than direct voltage measurement.

E_{ref} is the reference value of the energy (see Fig. 5.11). E_{conv} is measured converter energy which is sum of each capacitor bank energy as it is defined in the Eq. (5.1).

$$E_{conv} = \frac{1}{2} \sum_{k=1}^{all\ cells} C_k \cdot V_{C,k}^2 \qquad (5.1)$$
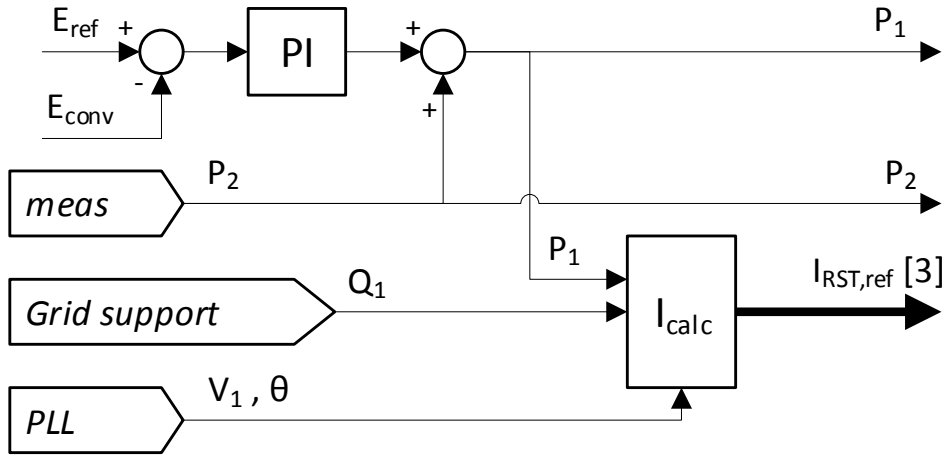
Figure 5.12. CEC module

PI controller output is an active power reference required to keep given reference. Total input active power is a sum of controller output and power feed to the output system (P_2). Powers P_1 and P_2 are also used in the Circulating Current Calculation (CCC) module.

Input currents are calculated in I_{calc} block which is presented on the Fig. 5.13. This module gets active power reference from CEC. Reactive power reference is get from grid support module or set to zero in case of $cos(\phi) = 1$ provision.

Powers are scaled into currents by input voltage magnitude from PLL module. Currents are next multiplied by $cos(\theta_1)$ (active) and $sin(\theta_1)$ (reactive). Angle θ_1 is get from PLL module. As a result, 3-phase current references are obtained. Summed up currents are feed as an input current reference into next module - Current Mapping (SBI)

5.2.4. Branch Balancing (BRB)

Branch Balancing module (BRB) is responsible for uniform energy distribution among converter branches. In ideal case, the balance is provided by correct selection of circulating currents - to provide that $\int_0^T v_b \cdot i_b \, dt = 0$.

In practice however, waveforms of branch voltages and current are not equal reference values. Therefore imbalance can be observed. As a result some branches are charged up while others are discharged. Even if total branch energy is equal to given setpoint (what in provided by CEC module), the converter can go into fault mode due to branch energy drift.

To compensate that, a closed loop control is implemented. Fig. 5.14 shows a block diagram of the module. Energy measurement from each branch is used as a feedback signal while setpoint is equal average branch energy (from all branches). Error is feed to nine PI controllers (one for each branch).

$$\cos(\theta_1+[0;2\pi/3;4\pi/3])$$

P_1 → $1/V_1$ → ⊗ → ⊕ → $I_{1,ref}$

$$\sin(\theta_1+[0;2\pi/3;4\pi/3])$$

Q_1 → $1/V_1$ → ⊗
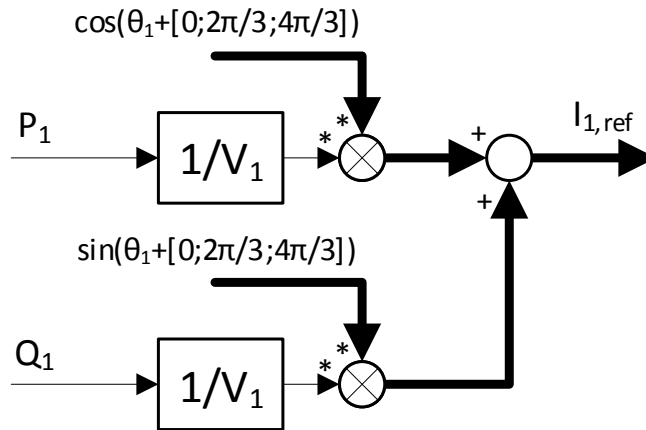
Figure 5.13. CEC module, Icalc

The output of the controller is a required power change in the branch Δp_b. Following power should be delivered to a given branch to charge/discharge it.

Input for the module is a vector of nine branch powers (or average branch capacitor bank voltages). Output from BRB module is a vector of nine Δp_b values used in CCC module.

meas → $e_b[9]$ → Σ → $1/9$ → e_{avg} → ⊕ → PI → $\Delta p_x[9]$
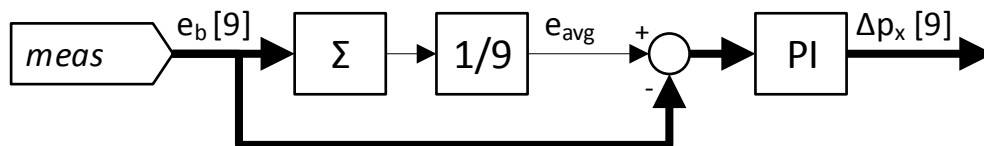
Figure 5.14. BRB module

It should be noted that $\sum_{b=1}^{9} \Delta p_b = 0$. Total branch power is controlled by CEC module as it was mentioned earlier.

5.2.5. Circulating Current Calculation (CCC)

Following module is crucial in energy control process. It calculates what circulating current waveforms are required to provide given average power for each converter's branch. Consequently, branch energy is increased or decreased as it is required by BRB and CEC modules.

Fig. 5.15 presents a block diagram of the module. It is built with no controllers. It calculates given currents and voltages of neutral and star point. Calculations are based on predefined functions (from the topology itself).

Inputs for the module are system powers from CEC module (P_1 and P_2) and branch balancing powers from BRB module (Δp_b). All quantities combined together provides that converter branch energies are equal and total energy is equal to given setpoint.

Sum of system powers P_1 and P_2 is shared evenly among each branch what explains $1/9$ coefficient in the block diagram. Δp_b is for contrary different for each branch what is clear as each branch has its own energy controller (within BRB module).

Functions $i = f(p)$ defining circulating current shapes are discussed in paragraph 4.7. Circulating current contains constant part and two different frequency harmonic components (ω_1 and ω_c) as it is shown in the Eq. (4.80). Power components are calculated using Eq. (4.87).

Next, power components are scaled to currents and fed to Current Mapping Module (SBI). Meanwhile, voltages defined by Eq. (4.81) and (4.82) are fed to Voltage Mapping Module (SBV).
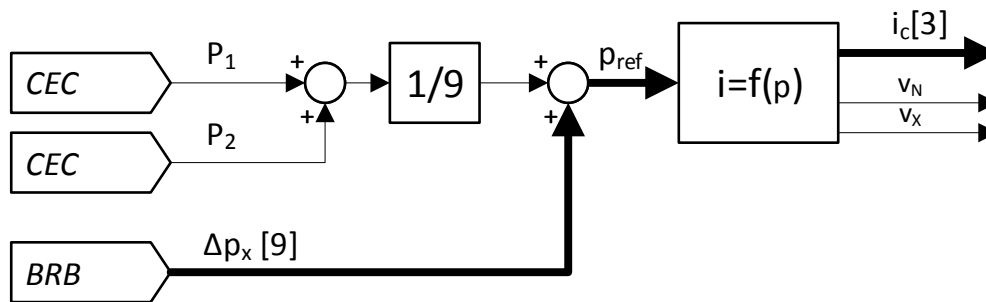
Figure 5.15. CCC module

5.2.6. System-Branch Voltage Mapping (SBV)

Following module transforms previously defined system and internal voltages into branch voltages as it is shown on the Fig. 5.16. Mapping is defined by the T_V matrix which has been calculated in the Chapter 3, Eq. (3.46). Inputs for the mapping are following: direct measurement, or filtered measurement from PLL module for input voltages; reference voltage from the REF module and neutral with star point voltage reference from CCC module.

Three phase references are transformed into $\alpha - \beta$ components. Output from the module is 9-element vector with branch voltages.
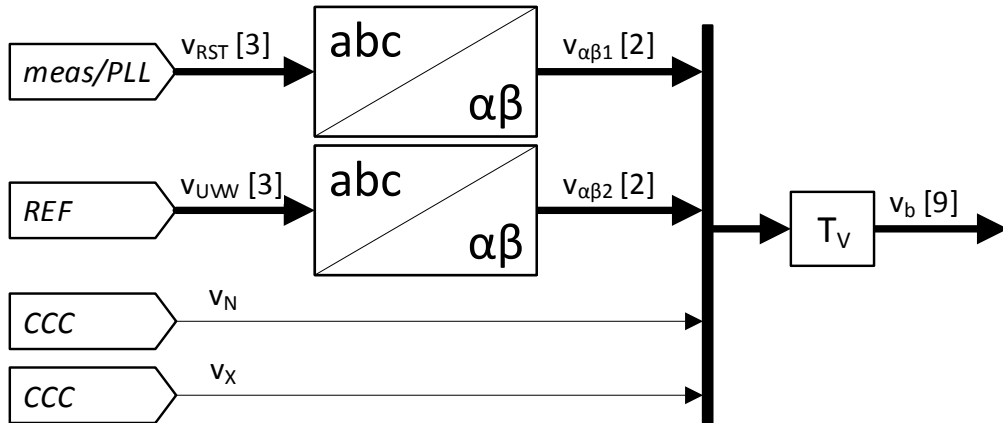
Figure 5.16. SBV module

5.2.7. System-Branch Current Mapping (SBI)

Following module is similar to SBV. The difference is that it transforms currents instead of voltages. Fig. 5.17 shows a block diagram of the module.

Inputs for the module are following: input currents from CEC module, output currents either from direct measurements or from REF generator and circulating currents from CCC module. Branch currents are being mapped using T_I matrix defined in Chapter 3, Eq. (3.36).

Three phase references are transformed into $\alpha - \beta$ components. Output from the module is 9-element vector with branch currents.
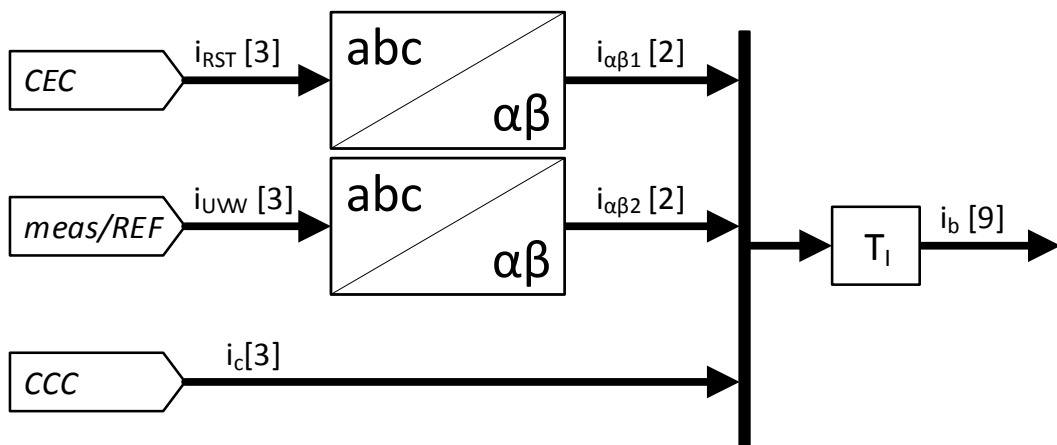
Figure 5.17. SBI module

5.2.8. Branch Current Controller (BRI)

Following module controls branch currents in the converter. Current control is possible as each branch has an inductor in which current flow can be forced.

Cells are voltage sources, therefore current flow is forced by introduction of voltage drops.

Block diagram of the module is presented on the Fig. 5.18. As it is shown it includes PI controller for each branch.
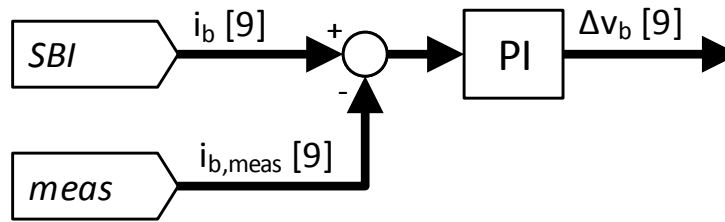
Figure 5.18. BRI module

In practical realization, a distributed controller has been implemented. Due to the fact, current control is critical for a stability, fast control loop on the cell controller is implemented. In parallel, slower control loop on the slave controller is present.

At the cell level (cell controller), only proportional controller is used. On the branch level (slave controller), PI is being used. Instead of PI, other controllers as resonant P+R [88] can be used.

5.2.9. Scale to modulation index (MOD)

Following module calculates modulation index given for each cell.

Fig. 5.19 shows a block diagram of the module. Voltage reference from SBV module modified by voltage drop from BRI module is scaled by an average branch voltage. Resulting value must be in range $-1...1$ as overmodulation does not increase resulting voltage. It should be noted that if HB modules are used, modulation index must be limited to the range from 0 to 1.

As a result of scaling, an average branch modulation index is obtained. In case of averaged simulation model, this value is used. In practice however, a cell balancing is also required.

The cell balancing module is presented on the Fig. 5.20. There are in total $9 \cdot N$ controllers - each for every single cell. To sake of simplicity, below a single branch is being described.

Given module is built with N of proportional controllers (one for each cell within a branch). Only proportional controller can be used as it must be provided that total branch modulation index is not affected. In case of integral parts or other controllers it cannot be easily provided.
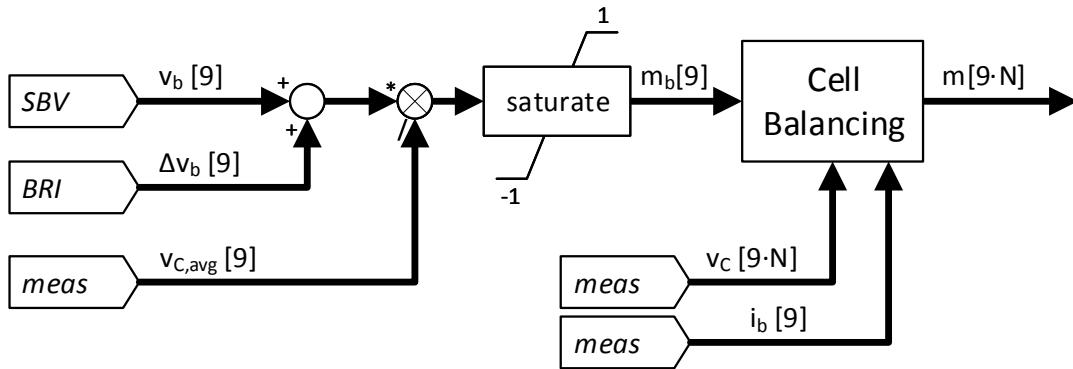
Figure 5.19. MOD module

The reference for a controller is an average branch capacitor bank voltage. Error is multiplied by branch current sign (branch current measurement is also possible). The reason is that if the current polarity determines whether cells are being charged or discharged. E.g. in case of negative current, cell capacitor banks are being discharged. Therefore, cells with too high voltage should be active longer time than the others. In case of positive current, situation is opposite.

Calculated modulation index is a change of the average branch modulation index calculated previously.
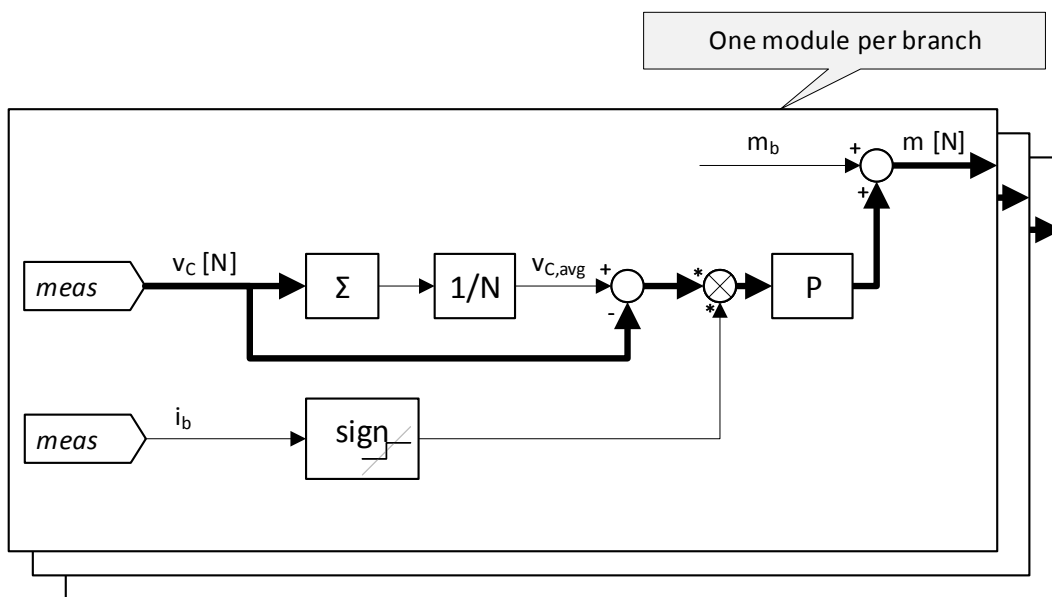
Figure 5.20. Cell balancing

Following module provides that cells within a branch are being balanced. Together with BRB module which provides that each branch is balanced with each other and with CEC which provides that total converter energy is equal given setpoints, those three modules are responsible for equal distribution of given power among the converter cells.

Different balancing levels are being summarized in [54]. In given paper, also one more top-level is being presented: a system energy balancing which is required in multiple-converter systems as e.g. four converter series-parallel system described in [60].

5.3. Branch Current Control Design

As BRI module is critical due to stability, details about its design are presented in this section. The module is divided into two sub-modules: feed-forward voltage drop calculation and a feedback control.

Design process will use a simplified, averaged branch model presented on the Fig. 5.21. The branch is modeled as an ideal voltage source in series with branch resistance and a branch inductor.
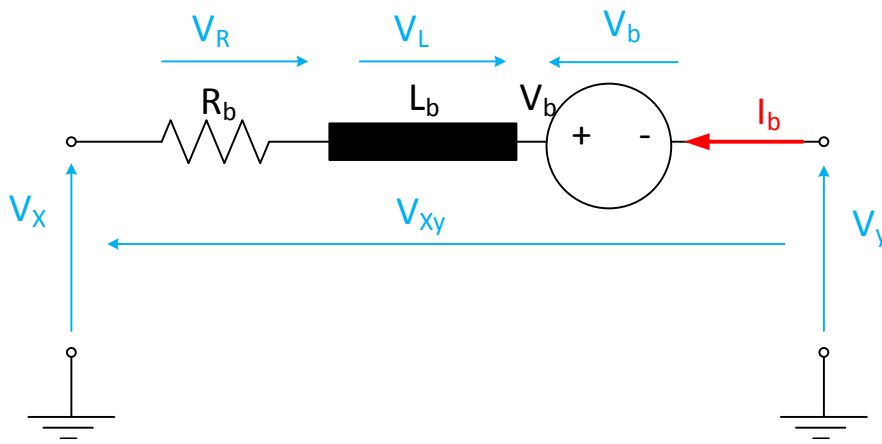
Figure 5.21. Simplified branch model. Branch between phases X and y built with R and L plus voltage source

5.3.1. Feed-forward voltage drop calculation

As it can be deduced the current is controlled through a voltage source which must also provide correct terminal voltages. It can be assumed that V_X is a measured input voltage and V_y is an output voltage from the controller. Therefore in a steady state the branch voltage must be equal (for neglected resistor voltage drop):

$$V_{Xy} = V_X - V_y = V_{b,v} \tag{5.2}$$

Where $V_{b,v}$ is a branch voltage required to achieve specific voltage drop (generate V_y having given V_X voltage).

The current is controlled through the branch voltage modification which can be described as (5.3). Where $V_{b,v}$ is a branch voltage from the voltage control module and ΔV_b is an extra voltage drop required

to force the current flowing through the branch.

$$V_b = V_{b,v} - \Delta V_b \tag{5.3}$$

The voltage across the branch according to Fig. 5.21) is equal:

$$V_{Xy} = V_b - \left(L \cdot \frac{di}{dt} + Ri \right) \tag{5.4}$$

Therefore the voltage drop from a current flowing in the branch is equal (5.5).

$$\Delta V_b = L \cdot \frac{di}{dt} + Ri \tag{5.5}$$

Following voltage drop can be included in the branch voltage reference calculation and it will force the required current flow. This way of current control is named feed-forward path as it doesn't need any feedback signal. The voltage drop calculation is calculated directly from the given current reference and known branch parameters. Its accuracy depends on the knowledge of the R and L values.

5.3.2. Feedback Current Control Scheme

A feed-forward control is not enough to building a correct branch voltage due to the fact that branch resistance and inductance are not exactly known.

In real cases, especially for discrete controllers, feed-forward voltage drop calculation is not satisfactory and can be used only as a support for feedback controller which controls the current using the feedback loop (including current measurement). In this section, a full control loop is described. Simulation results are presented. Additionally the comparison of feedback controller only versus tandem controller (feedback+feed-forward) is shown.

The feedback control loop is supported by the feed-forward signal. Due to the fact that feed-forward signal is given, the current controller operation point is always close to zero.

The full control loop (including branch voltage generation plus current control) is presented on the Fig. 5.22. As is shown, for current control, a P-controller has been chosen due to its simplicity and fast response. The zero steady state error in the system is already provided by the higher-level control which is out of scope of this section.

A top line is a branch voltage reference which is defined by Eq. (5.2). Combined Feed-Forward and Feedback outputs gives a voltage drop (ΔV_b) required to force the current flow.

In the given model the-feed forward generation is being implemented with sample rate 125 μs and feedback with 25 μs. Following timing is determined by hardware used in the Thesis: cell controllers sample time is fixed to 25 μs and higher level control (PEC) is fixed to 125 μs.

5.3.3. Simulation results

Simulations in the following section has been performed in Matlab/Simulink R2016b with SimScape blockset. Branch has been modeled as a voltage source with series connected resistance and inductance as is shown on Fig. 5.23.
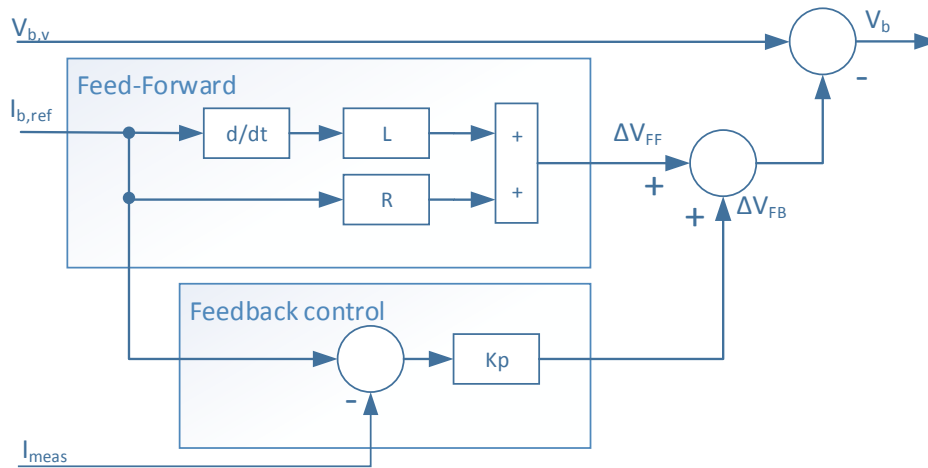
Figure 5.22. Current Control Loop

Fig. 5.24. presents simulation model of the voltage generator including feedback control loop. Both modules can be turned on and off independently so theirs influence on the output can be checked in this section.

When feedback path is disabled, feed-forward calculation provides zero current error only in case of continuous control with well known R and L of the branch. In case of discrete control and errors in resistance and inductance estimation, an error is observed. As it is obvious conclusion, simulation results are not included in the Thesis.

More interesting aspect is the influence of the feed-forward path in case of enabled feedback control loop. Figure 5.25 presents simulation results for a two test cases. In the first test, feed-forward has been disabled. For the second test, feed-forward has been enabled. As it can be observed, for enabled feed-forward, feedback controller reference is lower (as the operation point of the controller is closer to zero). As a result, for the same controller gain, an error in the output current is significantly lower (red lines on bottom plots).

In following simulation, feedback controller gain has been chosen by trial and error method ($K_P = 10.0$). In the next section, proportional gain will be tuned.

5.3.4. Controller design

To calculate the stability region and tune the proportional gain a simplified schematic of the system is required. A current control closed loop is presented as on the Fig. 5.26.

As the feed-forward path is introduced the disturbance will be ignored in the controller design. Following transfer functions are presented: (5.6) — proportional controller, (5.7) — Branch voltage to current transfer function ($I = G_O(s)V$), (5.8) — Measurement loop transfer function defined as a delay (τ):
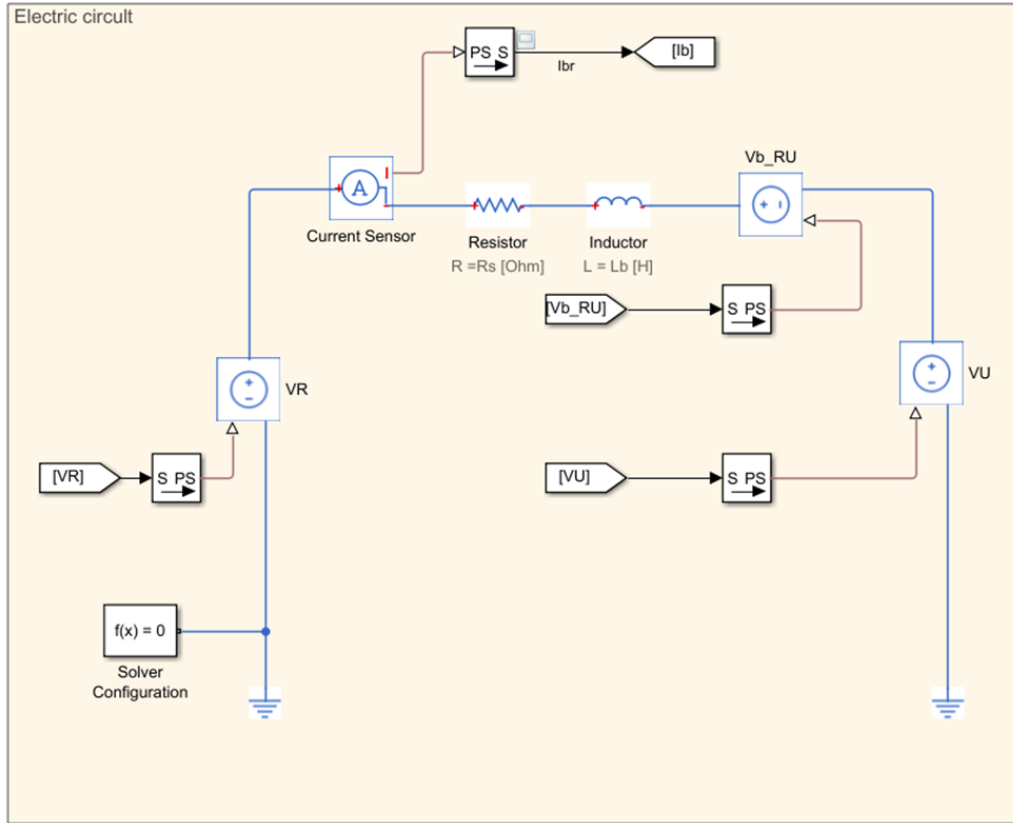
Figure 5.23. Simulation electrical circuit

$$G_P(s) = Kp \tag{5.6}$$

$$G_O(s) = \frac{\frac{1}{R}}{\frac{L}{R} \cdot s + 1} = \frac{K}{Ts + 1} \tag{5.7}$$

$$G_M(s) = e^{-s\tau} \tag{5.8}$$

The measurement delay can be neglected if the current controller is realized on the cell level (PEBB module). Taking this assumption into account and including discrete/continuous (analog) nature of specific components, the block diagram of the control is presented on Fig. 5.27. As it is shown, extra modules to transfer from continuous to discrete domain and vice versa are required.

As it is hybrid system there are two ways of the controller design – the discrete part (controller) can be transferred to the continuous part or the continuous part (branch electric circuit) into discrete part.

In the Thesis, RL branch model has been transferred to the discrete Z plane. Using that approach, the characteristic function of the control loop can be calculated and the Kp stability range can be defined.
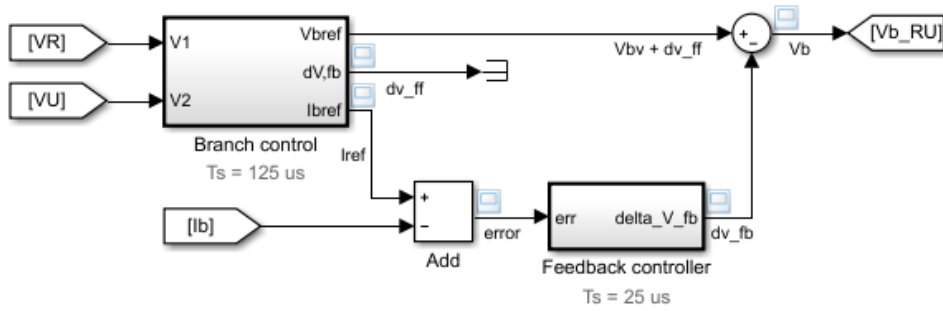
Figure 5.24. Branch voltage and current control model overview

(a) feed-forward OFF   (b) feed-forward ON
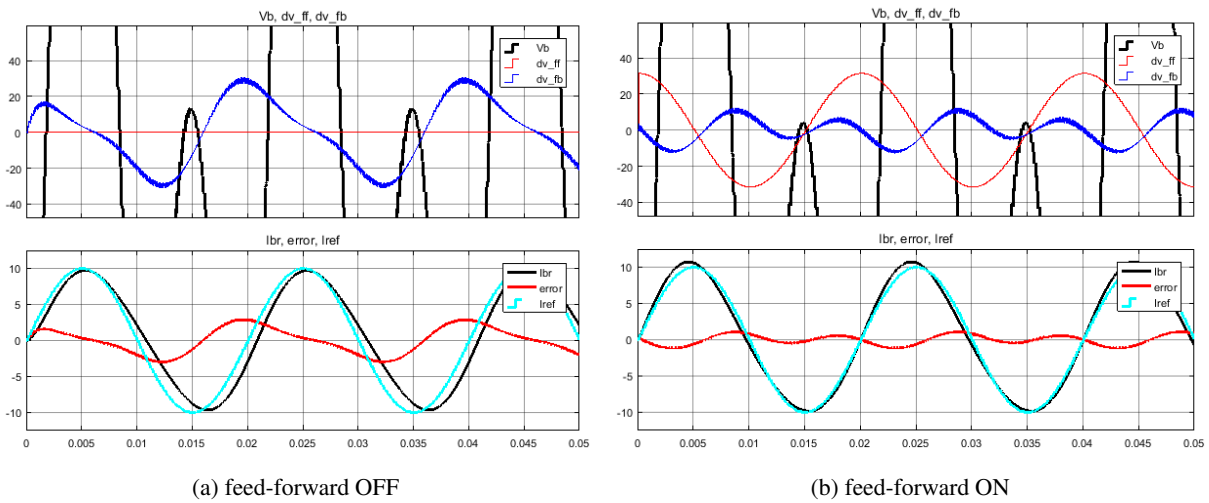
Figure 5.25. Feed-forward voltage drop calculation influence on branch current. Top plots: black - branch voltage, red - feed forward voltage reference, blue - feedback voltage reference. Bottom plots: black - branch current, cyan - branch current reference, red - error.

5.3.4.1. System discrete representation

To transfer electric circuit into discrete space an extra phenomenon must be considered – Digital to Analog and Analog to Digital conversion. For the D/A Zero Order Hold (ZOH) can be used. For the A/D conversion sample & hold can be used. For that specific A/D and D/A conversions so called Zero-Hold equivalent of the transfer function is determined:

$$G(z) = \left(1 - z^{-1}\right) \cdot \mathcal{Z}\left\{\frac{G(s)}{s}\right\} \tag{5.9}$$

Where $\mathcal{Z}\{\ \}$ is a continuous to discrete Z-Transform. For the analog circuit defined in (5.7), the Z-equivalent is equal (5.10).

$$G(z) = \left(1 - z^{-1}\right) \cdot \mathcal{Z}\left\{\frac{K}{s(Ts + 1)}\right\} \tag{5.10}$$
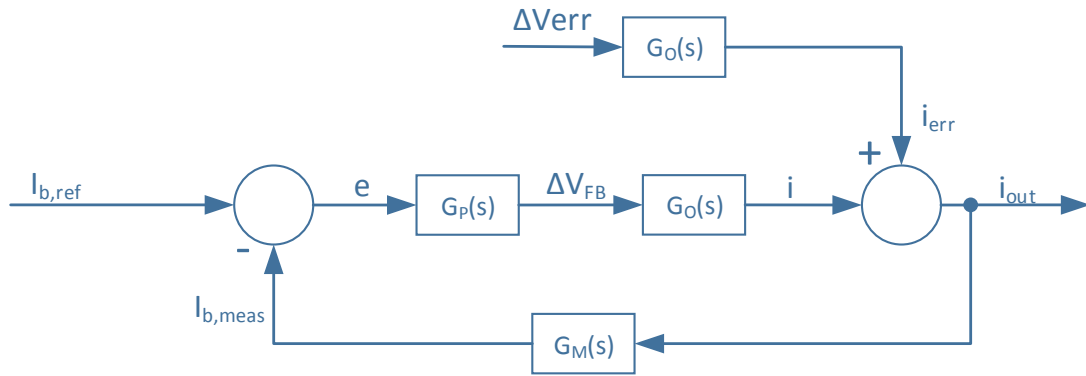
Figure 5.26. Current control loop with disturbance (on top). Continuous system
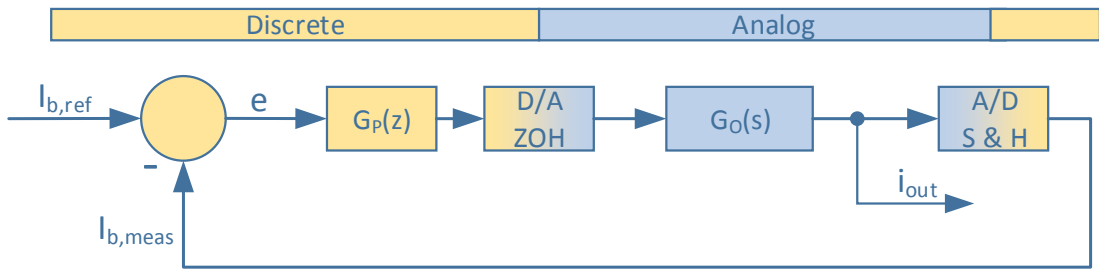
Figure 5.27. Current control closed loop - discrete/continuous blocks

Knowing that Z-transform of asymptotic exponential function is equal (5.11) for sampling time Ts, it it possible get Z-transfer function of the G_O using superposition (linearity) property of the transform. Therefore $G_O(z)$ is equal (5.12).

$$G(z) = \mathcal{Z}\left\{\frac{1}{s(s+a)}\right\} = \frac{\left(1 - e^{-aTs}\right)z^{-1}}{a\left(1 - z^{-1}\right)\left(1 - e^{-aTs}z^{-1}\right)} \tag{5.11}$$

$$G_O(z) = \frac{1}{R} \cdot \frac{1 - e^{-\frac{R}{L}\cdot Ts}}{z - e^{-\frac{R}{L}\cdot Ts}} \tag{5.12}$$

For proportional controller Z-transfer function is identical as in the Laplace space:

$$G_P(z) = K_P \tag{5.13}$$

5.3.4.2. Stability region calculation

The closed loop system transfer function $G_C(z)$ is equal (5.14).

$$G_C(z) = \frac{G_P(z) \cdot G_O(z)}{1 + G_P(z) \cdot G_O(z)} \tag{5.14}$$

The characteristic equation of (5.14) is defined as:

$$1 + \frac{K_P}{R} \cdot \frac{1 - e^{-\frac{R}{L}\cdot Ts}}{z - e^{-\frac{R}{L}\cdot Ts}} = 0 \tag{5.15}$$

For given branch parameters (10 $m\Omega$ and 2.5 mH) and defined sample time `Ts=25`μ`s` the equation (5.15) yields to:

$$\frac{z - 0.9999 + 0.01 \cdot K_P}{0.01z - 0.01} = 0 \tag{5.16}$$

The system is stable when all poles of characteristic equation are in the unity circle on the Z-pane. Therefore the system is stable for K_P within a range:

$$\begin{cases} -0.9999 + 0.01K_P < 1 \\ -0.9999 + 0.01K_P > -1 \end{cases} \Rightarrow -0.01 < K_P < 200 \tag{5.17}$$

Table 5.2 presents allowed maximum K_P for different sampling times and different inductances. Branch resistance is constant as it has no significant influence on the results.

According to the Table it can be said that controller can be more aggressive (higher K_P) if it is faster (lower `Ts`) or when there is higher inductance in the system.

Table 5.2. Maximum K_P for defined sample time and inductance

		Ts		
		$25\mu s$	$125\mu s$	$500\mu s$
	2.5 mH	200	40	10
L	1.25 mH	100	20	5
	0.20 mH	16.7	3.3	0.83

5.3.4.3. Simulation results for different Kp

To summarize, simulation with two proportional gains has been performed. Figure 5.28 shows results for two proportional gains. Both are in the stability region. It can be noted that for higher proportional gain, current error is lower. However, branch voltage reference is in that case much higher and high frequency oscillations can be observed. Therefore, gain tuning is a trade-off between output current accuracy and branch voltage shape.

Given analysis shows control loop refresh rate and impedance influence. Both parameters should be taken into account during controller design. Calculated gain can be used as a starting point in laboratory testing when it can be fine tuned. Stability margin defines also maximum gain which should be allowed.

(a) Kp = 10

(b) Kp = 100
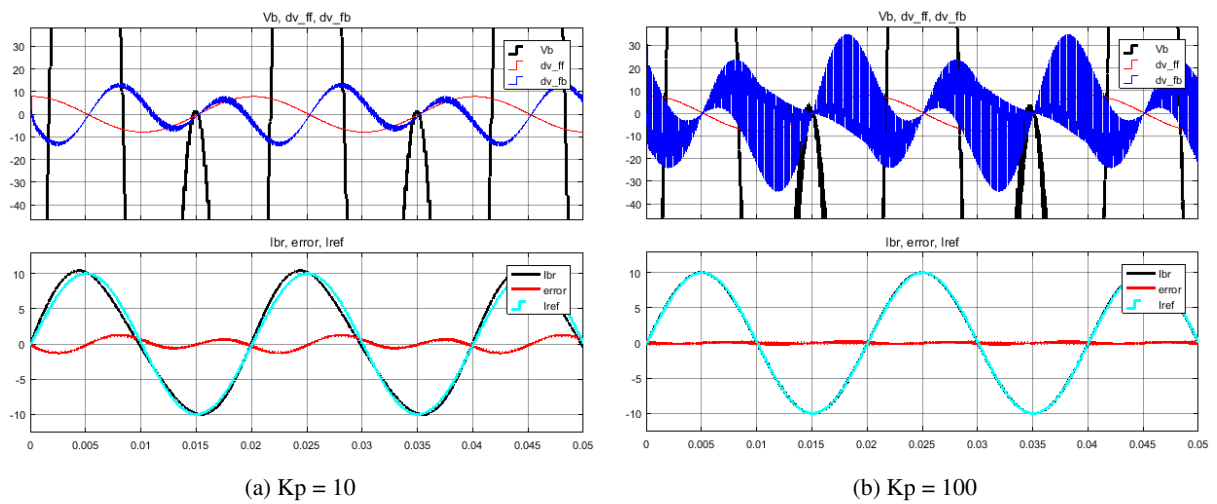
Figure 5.28. Simulation for two proportional gains within stability region. Top plots: black - branch voltage, red - feed forward voltage reference, blue - feedback voltage reference. Bottom plots: black - branch current, cyan - branch current reference, red - error.

6. Branch Modeling

In following chapter cell and branch model is presented. Representation of the module is based on equivalent circuit for given switch configurations. In the next step, proposed cell model is adapted to represent averaged model. Final step is to average the branch build with series connection of n-modules with a single one. The analysis is given for a FB cell type.

Additionally, modulation scheme which can be used for HB and FB control is described.

Cell and branch are modeled as it was proposed in [89]. Given paper describes workflow for the HB module and final parameters for the FB module. In the Thesis, full workflow for a FB module is presented. Additionally, given branch model is used to build an equivalent arm averaged model which in contrary to arm switching model does not require modulator implementation and can be used with a higher simulation step time

Given model is tested for defined test-cases covering all operation modes, i.e. passive state without any switch active and modulation (active state).

6.1. Equivalent circuit models for given states

Equivalent circuit method for modeling of MMC has been proposed by Li and Belanger in [89]. It has been shown how to model HB cell. It is also mentioned that this workflow is applicable for other cell types (as FB or double-clamp module). In this section, a model for the FB module is built. Final model parameters are compliant with the ones given in [89][1].

Figure 6.1 presents FB cell model to be used in the analysis. More detailed module description can be found in Chapter 2.2.1. For equivalent circuit analysis, the cell is build with four ideal switches and anti-parallel diodes. To make the system closer to reality, voltage drops for switch and diode will be included in the analysis.

Module DC link is built with a capacitor and discharge resistor. Series resistance is neglected.

To build an equivalent circuit, all module operation modes should be defined and analyzed. The operation mode is defined as a specific switch configuration. As the FB module has 4 switches: therefore it is $2^4 = 16$ switch combinations. Proposed switch numbering can be found on the Fig. 6.1.

Each configuration can be treated as an operation mode, however it is possible that more than one configuration is treated as the same operation mode (e.g. zero switching state can be achieved by closing

---

[1]One voltage polarity (diode voltage drop) has been found different
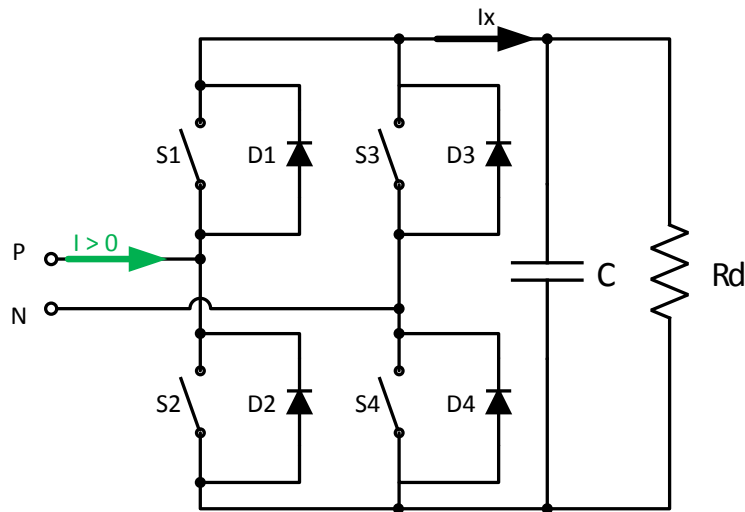
Figure 6.1. Cell model used for building equivalent circuit model

S1 and S3 or S2 and S4). Most of the configurations are also not useful or not possible to reach with use of standard gate drivers which produces only complementary switching signals for a half bridge. Table 6.1 shows all useful switch configurations and its given operation mode acronyms used by author.

Table 6.1. Operation modes for given switch configuration

Switch State				Operation Mode
S1	S2	S3	S4	
0	0	0	0	FW
0	1	0	1	ZD
0	1	1	0	NEG
1	0	0	1	POS
1	0	1	0	ZU

Following functional operation modes are identified:

– free-wheeling (FW). All switches are off. The module beehives as a diode rectifier,

– zero-up (ZU). Zero state constructed with top switches,

– zero-down (ZD). Zero state constructed with bottom switches,

– positive output voltage (POS),

– negative output voltage (NEG).

In following subsections each state is analyzed and an equivalent circuit for positive and negative current flow direction is built. Both subciruits are next merged. The merge process is realized by connection of two circuits (for positive and negative current flow) with adding ideal diodes which are blocking opposite current flow direction for given circuit branch what is shown as an example on Fig. 6.2. To increase the model accuracy, voltage drop on diode and switch is added in series to capacitor bank voltage.
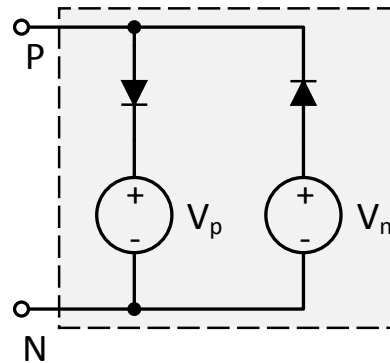
Figure 6.2. Equivalent circuit of the system providing different voltages for opposite current direction

It must be noted that following circuit should be analyzed as a system with borders shown on the Figure 6.2. The reason is that output voltage and current is correct but inside the model, there can be an extra current circulating between two sources (if $V_n > V_p$). This current does not exist in the real system and should be neglected in the analysis.

Full equivalent model has two roles: First, it should ensure correct terminal voltage for given current and switch configuration. Second, it should calculate capacitor bank voltage. Schematic diagram of an equivalent circuit fulfilling given functions is presented on Figure 6.3. Left side of the circuit provides terminal voltage which is present on the cell terminals. Right side is responsible for capacitor dynamics (charging / discharging). Discharge resistor is being used as well in that part of the circuit.

The missing part is a definition of the voltage V_p, V_n and internal DC link current I_x. As it is shown its values depend on the circuit states (input current and capacitor voltage) but also on the control signal for the switches which can be translated into previously defined operation modes. Following subsections shows what are values of voltages and current for each operation mode.

6.1.1. Free wheeling state

In the FW, all switches are off. It means that the only possible current path is through diodes. Output voltage depends on the current direction. Another names of that state which can be found in the literature are passive and diode state.
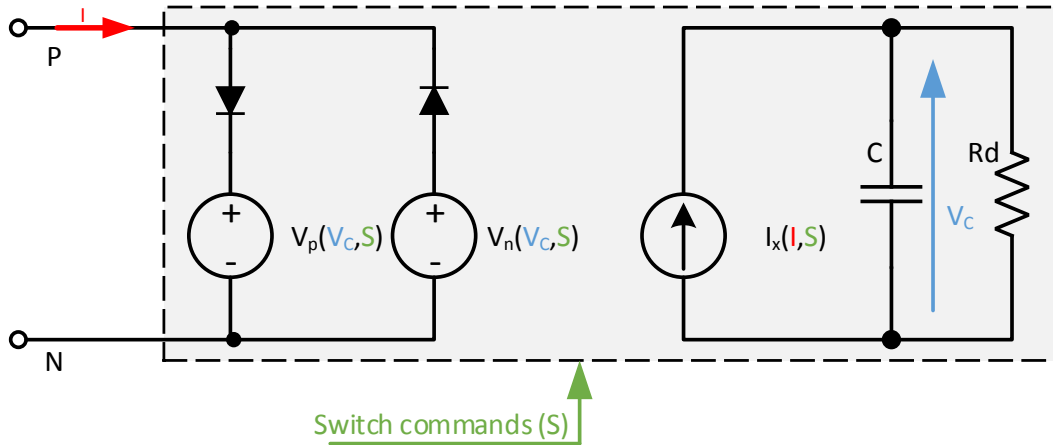
Figure 6.3. Full equivalent circuit of the cell

Figure 6.4a shows the current path in case of positive current flow (red,dashed) and negative current flow (green, continuous). When current is flowing through a diode or a switch, a voltage drop occurs. It will be defined as V_D for diode and V_S for a switch.

Equivalent circuits of the cell for positive and negative current direction is show on Figure 6.4b. Voltages V_p, V_n and current I_x are equal:

$$V_p = V_C + 2V_D \tag{6.1a}$$

$$V_n = -V_C - 2V_D \tag{6.1b}$$

$$I_x = abs\,(I) \tag{6.1c}$$

6.1.2. Fundamental switching states

States in which two switches are turned on (closed) are referred as the Fundamental Switching States and they are used in modulation to provide given voltage on the output terminals. It is also possible to use the states with only one switch active (marked as N/A in Table 6.1) however it is out of the scope of the Thesis.

Fundamental Switching States provide positive (POS), negative (NEG) or zero (ZU, ZD) output voltage irrespective of current flow direction. Current path for all four states for positive (red) and negative (green) current flow is shown on Figure 6.5.

Table 6.2 presents equivalent circuit parameters for all operation states. Parameters can be retrieved from the circuits from the Fig. 6.5 by building equivalent circuits as in the Fig. 6.4. For sake of versatility,

(a) Current path

(b) Equivalent circuits
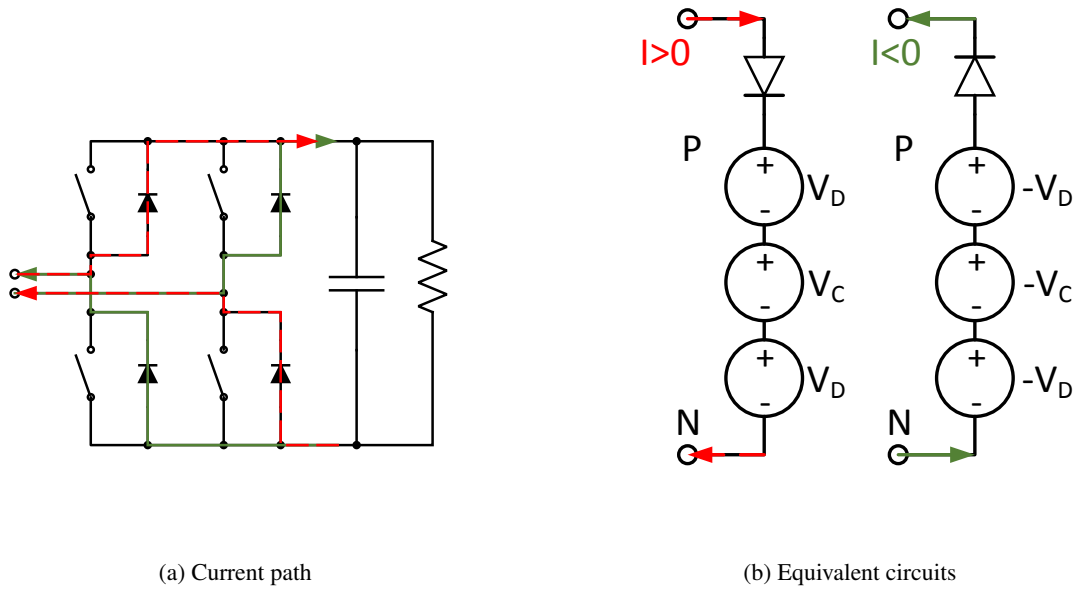
Figure 6.4. Free Wheeling state

FW state is also included. ZU/ZD state results in the same model voltage and current so they can be merged into one equivalent circuit. In practice however both switching states should be used interchangeably to provide equal heat dissipation among full bridge components.

Table 6.2. Equivalent circuit parameters

	FW	POS	NEG	ZU/ZD
V_p	$V_C + 2V_D$	$V_C + 2V_D$	$-V_C + 2V_S$	$V_S + V_D$
V_n	$-V_C - 2V_D$	$V_C - 2V_S$	$-V_C - 2V_D$	$-V_S - V_D$
I_x	$abs(I)$	I	$-I$	0

Voltages V_p, V_n defines module behavior on the output terminals. Current I_x is an internal variable which has influence on the capacitor voltage. Looking at the equivalent circuit from Fig. 6.3, the equation linking current with the capacitor voltage is obtained:

$$V_C = \frac{1}{C} \int \left(I_x(t) - \frac{V_C}{Rd} \right) dt + V_{C0} \tag{6.2}$$

Parameters from the Table 6.2 allows to build the cell switching model. Practical implementation (Matlab/Simulink model) is presented in the section 6.4.

The single cell model is used to build a branch by making a series connection of the cells. The process is described in the next section.

(a) POS

(b) NEG

(c) ZU

(d) ZD
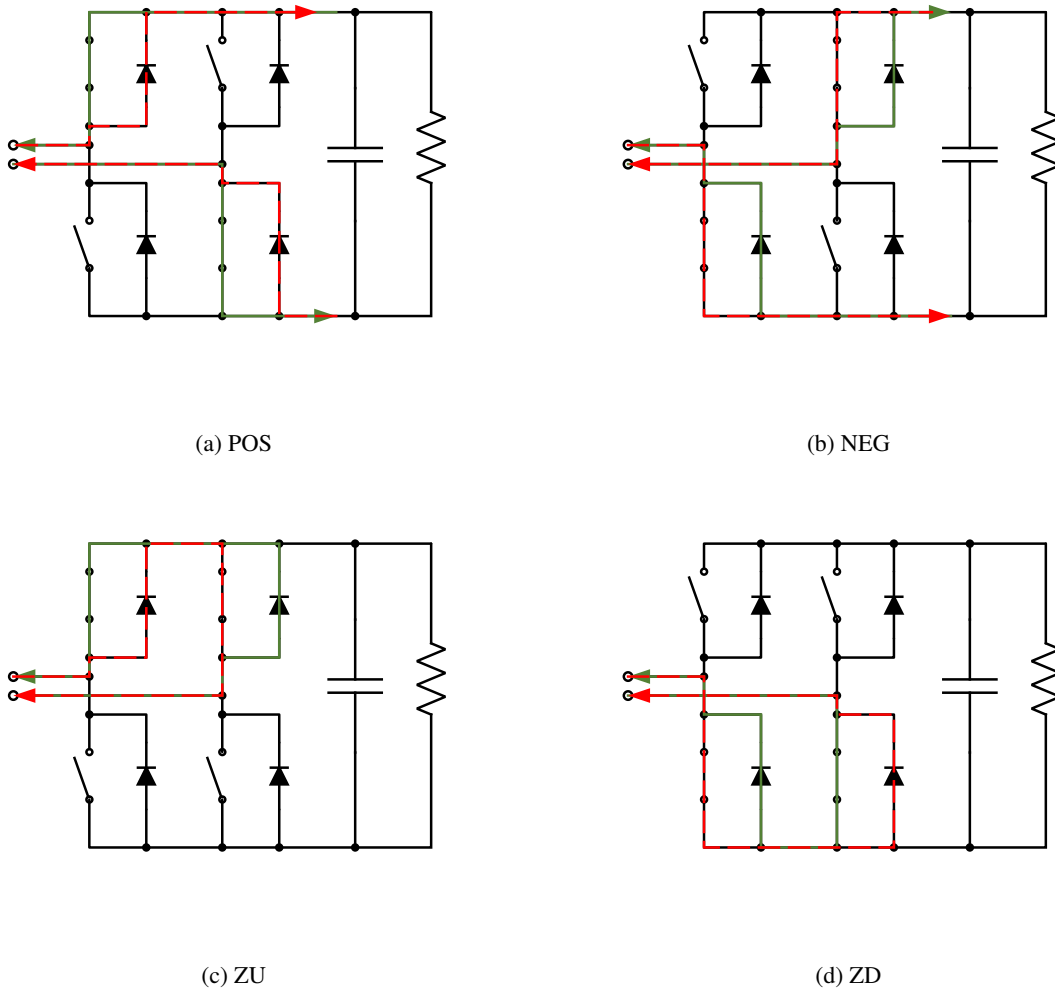
Figure 6.5. Current paths for Fundamental Switching States for positive (red) and negative (green) current flow direction

6.2. Branch switching model

MMC branch is build with a series connection of the cells. Usually each cell structure is identical. There are also a hybrid topologies which uses different cell types, e.g. middle cell [9], but it is out of the scope of the Thesis.

In case of N-series connection of identical cell, the branch model can be build by simplifying a series connection by a single voltage source. As each cell is build with two sources with opposite diodes, each source can be treated separately what results with equivalent circuit as on the Fig. 6.6.

Series connection of N-ideal diodes can be replaced with a single ideal diode.

Equivalent voltages are the sum of corresponding module voltages:

$$V_{p\Sigma} = \sum_{k=1}^{N} V_{p,k} \tag{6.3a}$$
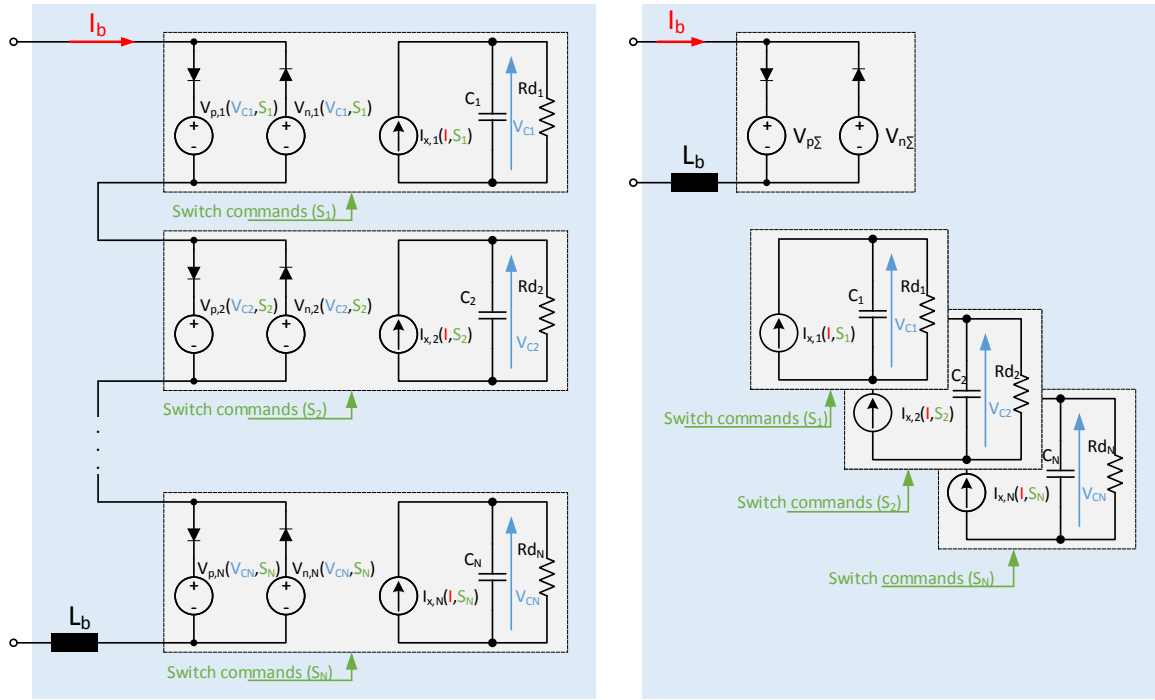
Figure 6.6. Branch build with series connections of cells (left) and full equivalent circuit of the branch (right)

$$V_{n\Sigma} = \sum_{k=1}^{N} V_{n,k} \tag{6.3b}$$

Each capacitor voltage (V_{Ck}) is being calculated using a separate RC-circuit. Cell voltage depends on the current which is identical for every cell. It depends also on the switching state which is different for every cell. Therefore separate circuits are required. The second reason why those circuits cannot be merged is the fact that each cell parameters (like resistance or capacitance) might differ.

Resulting output voltages ($V_{p,k}$, $V_{n,k}$) are calculated using individual capacitor voltage V_{Ck} and switches state S_k as it has been summarized in the Table 6.1.

Cell capacitor bank circuits are fully decoupled from the each other. Therefore it is possible to solve them independently, also in parallel manner what provides real-time execution of the simulation model irrespective of number of the modules in a branch (in case of FPGA implementation increase number of modules results with rise of amount of required resources, not computation time).

In case of continuous averaged model following circuits can be merged into a single one by assumption of identical cell parameters and identical average modulation index (switching states) what is shown in the next section.

6.3. Averaged cell and branch model

There are test cases in which switching events are not critical and more important is to run a longer simulation in a reasonable time (e.g. load flow simulations or RMS simulations). For that cases, a detailed model implementing cell switching (so called Electromagnetic Transient (EMT)) in not feasible – its maximum simulation step time is too low. For example in case of 1kHz switching frequency, 0.1% PWM resolution requires sample time of $1\mu s$.

For longer simulations, μs-time step is not acceptable. Therefore an averaged model is preferable. This section shows how this model is received starting from switching model presented in the Section 6.1. Section 6.4 shows the model practical implementation. Additionally accuracy analysis for increasing simulation step time is presented.

An averaged model has lower level of complexity as the switching transient is not implemented. It means however that following model can be used only with assumption that switching frequency is much higher than system's frequencies. E.g. 1kHz switching frequency for 50 Hz system can be modeled with satisfying accuracy. If it can be assumed that switching event is immediate and switching frequency is so high that all states can be „averaged out", a simplified model is required.

The idea of averaging is that for one cycle each switch can stay in two different states i.e. ON and OFF. It leads to a number of different converter equivalent circuits. Assuming that every circuit is valid for specific time, the average value of all required quantities can be calculated by taking weighted average over all states where weight is a time section of given state.

As it was shown in the section 6.1 there are five fundamental states named FW, ZU, ZD, POS, NEG.

FW state is used only during the faults and in the converter startup sequence. An averaged model will not cover that state. It is also not required to build an averaged model for the FW mode as there are no switching events in that state.

For functional operation only fundamental switching states are being used. Depending on the modulation index ZU,ZD states are combined with POS and NEG states as it is shown in the Fig. 6.7. As ZU and ZD stated are modeled in the same way, both are merged into ZERO state.
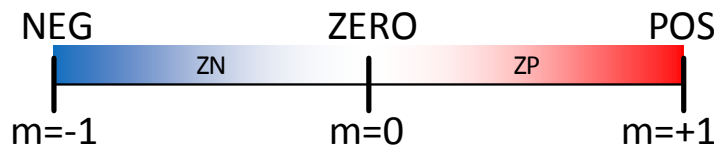
Figure 6.7. Switching states used for given modulation index m

To build an averaged model, averaged parameters for equivalent circuit (from the Fig. 6.3) should be calculated. Aforementioned parameters are voltages V_p, V_n and current I_x.

To be able to calculate averaged values, a time period in given state should be known. Linear dependency of modulation index m and duty cycle D is presented on the Fig. 6.8. It should be noted that $\Sigma D = 1$ for each modulation index value (what means no any other state is utilized).
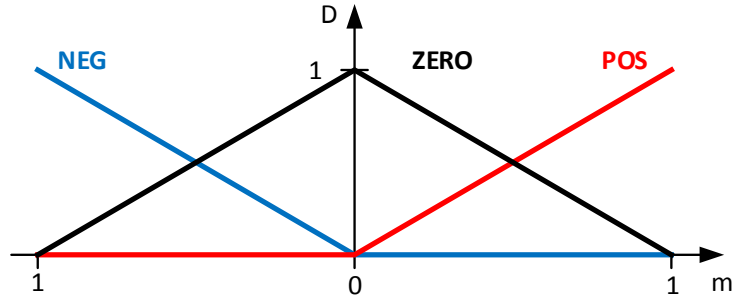
Figure 6.8. Duty cycle for a given modulation index for fundamental switching states

For $0 \leq m \leq 1$, ZERO and POS states are utilized. Taking values from the Table 6.2 and duty cycle from the Figure 6.8 following averaged values are calculated:

$$
\begin{aligned}
V_p &= (1 - m) \cdot V_{p,ZERO} + m \cdot V_{p,POS} = (1 - m) \cdot (V_S + V_D) + m \cdot (V_C + 2V_D) \\
&= m \cdot V_C + (1 - m)V_S + (1 + m)V_D
\end{aligned} \tag{6.4a}
$$

$$
\begin{aligned}
V_n &= (1 - m) \cdot V_{n,ZERO} + m \cdot V_{n,POS} = (1 - m) \cdot (-V_S - V_D) + m \cdot (V_C - 2V_S) \\
&= m \cdot V_C - (1 + m)V_S + (m - 1)V_D
\end{aligned} \tag{6.4b}
$$

$$
\begin{aligned}
I_x &= (1 - m) \cdot I_{x,ZERO} + m \cdot I_{x,POS} = (1 - m) \cdot 0 + m \cdot I \\
&= m \cdot I
\end{aligned} \tag{6.4c}
$$

Analogously for the m in range $-1 \leq m \leq 0$, ZERO and NEG states are utilized. Averaged voltages and current are equal:

$$
\begin{aligned}
V_p &= (1 + m) \cdot V_{p,ZERO} - m \cdot V_{p,NEG} = (1 + m) \cdot (V_S + V_D) - m \cdot (-V_C + 2V_S) \\
&= m \cdot V_C + (1 - m)V_S + (1 + m)V_D
\end{aligned} \tag{6.5a}
$$

$$
\begin{aligned}
V_n &= (1 + m) \cdot V_{n,ZERO} - m \cdot V_{n,NEG} = (1 + m) \cdot (-V_S - V_D) - m \cdot (-V_C - 2V_D) \\
&= m \cdot V_C - (1 + m)V_S + (m - 1)V_D
\end{aligned} \tag{6.5b}
$$

$$
\begin{aligned}
I_x &= (1 + m) \cdot I_{x,ZERO} - m \cdot I_{x,NEG} = (1 + m) \cdot 0 - m \cdot (-I) \\
&= m \cdot I
\end{aligned} \tag{6.5c}
$$

It can be noticed that for both operation areas, averaged voltages and current are identical. It means that the system is symmetrical and there is no any discontinuity at $m = 0$.

It should be highlighted that following equations can be used in an averaged model but also for discrete switching model if it will be provided that $m \in \{-1, 0, 1\}$ what corresponds to NEG, ZERO and POS switching states.

6.3.1. Averaged branch model

Proposed averaged model can be expanded from a single cell to the branch. One possible implementation is identical with generalization shown in a section 6.2.

Making the switching function continuous allows to assume that every cell has the same modulation index. Additional assumption that every cell capacitor bank parameters (C, Rd) are equal, an averaged model can be simplified even more: a single RC circuit can be used to model a branch (as each capacitor's voltage is identical).

Total capacitor voltage from N cells in branch is equal:

$$V_C = \frac{N}{C} \int \left(I_x(t) - \frac{V_C}{Rd} \right) dt + V_{C0} \tag{6.6}$$

The same model can be derived by building an equivalent branch circuit composed with N series connected capacitors in parallel with discharge resistors what gives:

$$V_C = \frac{1}{C_e} \int \left(I_x(t) - \frac{N V_C}{R_e} \right) dt + V_{C0} \tag{6.7}$$

where

C_e – Equivalent capacitance $C_e = \frac{C}{N}$

R_e – Equivalent resistance $R_e = N \cdot Rd$

Substituting C_e and R_e into Eq. (6.7), equation (6.6) is obtained.

6.3.2. Simplified cell model

Assuming that V_S and V_D are relatively low, following circuit parameters are given:

$$V_p = m \cdot V_C \tag{6.8a}$$

$$V_n = m \cdot V_C \tag{6.8b}$$

$$I_x = m \cdot I \tag{6.8c}$$

As both voltages are equal, model can be further simplified. Opposite polarity diodes can be removed from the circuit and a single voltage source is enough to model the cell as it has been shown on the Fig. 6.9.
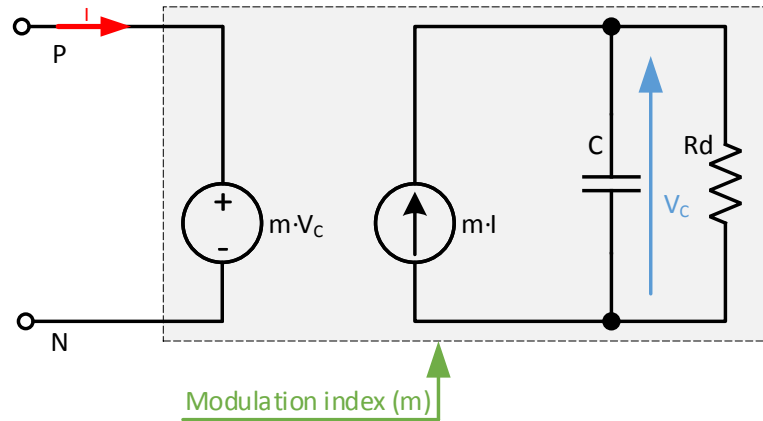
Figure 6.9. Simplified equivalent circuit

6.4. Model implementation

Simulation model has been implemented in Matlab/Simulink environment[2]. For electric circuit part, Simscape blockset has been used.

An average cell model which can be used as a switching model by replacing continuous[3] modulation index m with discrete switching command S which valid values $\{-1, 0, 1\}$.

Cell structure has been presented on Fig. 6.3. It can be divided into two functional modules (separate, but coupled electric circuits). Following component naming is being used: circuit part containing V_p and V_n voltage sources plus diodes is an interface module as it contains output terminals. A part with current source I_x and RC circuit is an internal module. Both modules are coupled by input current I and capacitor voltage V_C.

It has been decided to model two working modes. In the first working mode neither switch is active. The cell works in a diode mode. Following state will be named passive. In the second working mode (active), cell switches are providing given modulation index. Table 6.3 summarizes what operation modes are used in a given work mode.

Simulink model of the module (top level) is shown on Fig. 6.10. Specific components will be described with in following subsections.

Module can be used in different simulations. Therefore it has been encapsulated into library block. Inputs, outputs and module parameters are summarized in a Table 6.4.

---

[2]Matlab R2015a, win64 release has been used to build all models in the Thesis

[3]In practice due to computer limitations each represented signal is discretized. However it can be assumed that given signal is close enough to continuous if single or double precision number representation is being used

Table 6.3. Operation mode states in use for given working modes

Passive	Active
FW	POS
	NEG
	ZERO

(a)

(b)
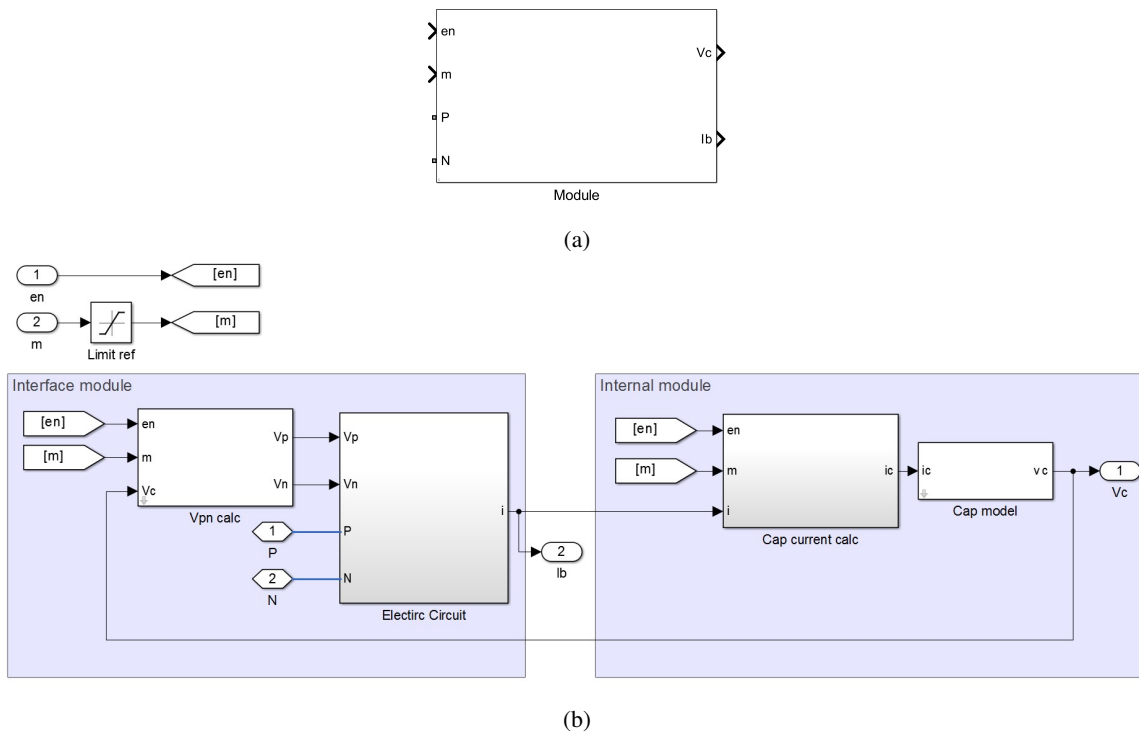
Figure 6.10. Cell module subsystem used in the simulation (a), Module content (b)

6.4.1. Interface Module

The interface module function is to create correct voltage on the cell output terminals. It is built with two electric circuit branches, each with a voltage source plus a diode as is shown on Fig. 6.3, left side.

Electric circuit has been built using Simscape building blocks. Output terminals (P, N) are electric terminals which are being used as an interface to connect with external circuits (grid and load models). In electric circuit block two parallel ideal voltage source blocks in series with two anti-parallel diodes can be found. Additionally, current measurement block is used to measure branch current. Following measurement is used in capacitor voltage calculation but can be also used in a top level control if required. Fig. 6.11 shows an electric circuit implementation. S / PS blocks are used for conversion between physical signals and Simulink signals.

Table 6.4. Cell simulation model inputs, outputs and parameters

	No	Name	Description	Unit
Input	1	en	PWM enable signal	—
			0 for passive mode,	
			1 for active mode	
	2	m	Modulation index $m \in< -1, 1 >$,	—
			Operation mode if $m \in \{-1, 0, 1\}$	
	3	P	Positive output terminal	Simscape El.
	4	N	Negative output terminal	Simscape El.
Output	1	Vc	Capacitor bank voltage	V
	2	Ib	Cell input current	A
Parameter	1	R	Discharge resistance	Ω
	2	C	Module capacitance	H
	3	Vs	Switch voltage drop	V
	4	Vd	Diode voltage drop	V
	5	Vc0	Initial capacitor voltage	V

Implementation of that module includes V_p and V_n voltage calculation. Both voltages are calculated for given modulation index and operation mode (passive or active). Modulation index for passive mode is ignored. Switch and diode voltage drops are included.

For passive mode, Table 6.2 shows equations for calculation of aforementioned voltages. In case of active mode, averaged values as defined in Eq. (6.4) are being used.

6.4.2. Internal Module

Internal module is responsible for capacitor modeling. Based on modulation index and operation mode, capacitor current defined as a function of input current is calculated. As for the voltages, Table 6.2 and Eq. (6.4) are being used to calculate current for passive and active mode respectively.

Capacitor current is an input for RC circuit which is represented as differential equation - see Eq. (6.2). As it is internal (decoupled from the grid) system it has been represented as ordinary differential equation as shown on Fig. 6.12. Continuous implementation has been chosen. In future work this part can be easily replaced with discrete model if required.

Vc0 parameter defines initial capacitor voltage. In case Vc0 will be set negative it means, capacitor voltage is not calculated using aforementioned equation. Instead, capacitor voltage is forced to be equal given value (with positive sign). Following functionality is useful in the first step of control loop development when a grid interface is implemented and there is no balancing nor energy control implemented.
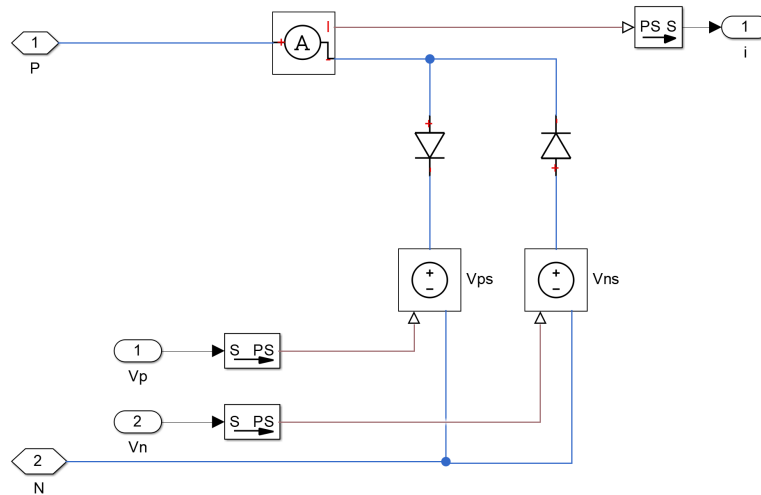
Figure 6.11. Electirc circuit of the cell model
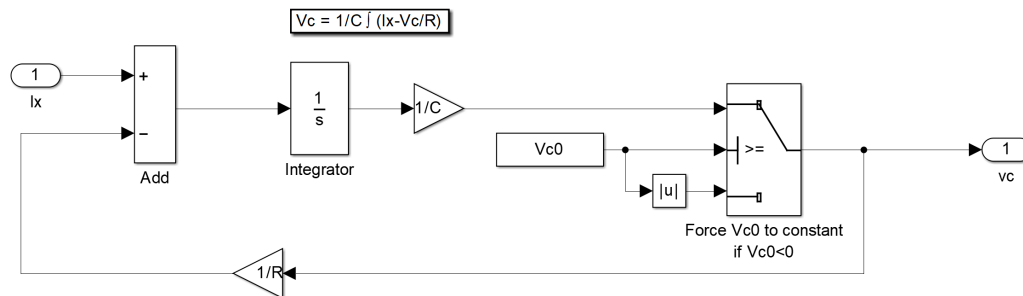
Figure 6.12. Capacitor voltage calculation

6.5. Model verification

Presented model can be initially verified in simple simulation circuits what will be shown in this section.

First, RC circuit will be checked. In case there is zero input current, capacitor bank should be discharged from its initial voltage through discharge resistance. Time constant τ should be equal to $R \cdot C$. That means after $t = 3 \cdot RC$, capacitor voltage should be about $0.05V_{C0}$ (5% of initial voltage).

Fig. 6.13a shows simulation model used to check if the capacitor model is implemented correctly. Zero input current is provided by connecting only passive component (resistor) on the terminal side. Inside the model, following values has been used: $R = 10\Omega$, $C = 20mF$. It leads to time constant $\tau = R \cdot C = 0.2s$. Initial capacitor voltage has been set to $Vc0 = 1000V$.

On the Fig. 6.13b, capacitor discharge curve is presented. As expected, the waveform is exponentially decreasing to zero. Crossing of 95% voltage occurs at $t = 0.6s = 3\tau$, what means following circuit is implemented correctly.

In the next step, passive mode will be checked. In that mode, capacitor charging should be observed. Model behavior will be compared with a simulation model of diode rectifier built in Simscape. Fig. 6.14a presents a test circuit built with an ideal voltage source generating sinusoidal waveform with

(a)   (b)
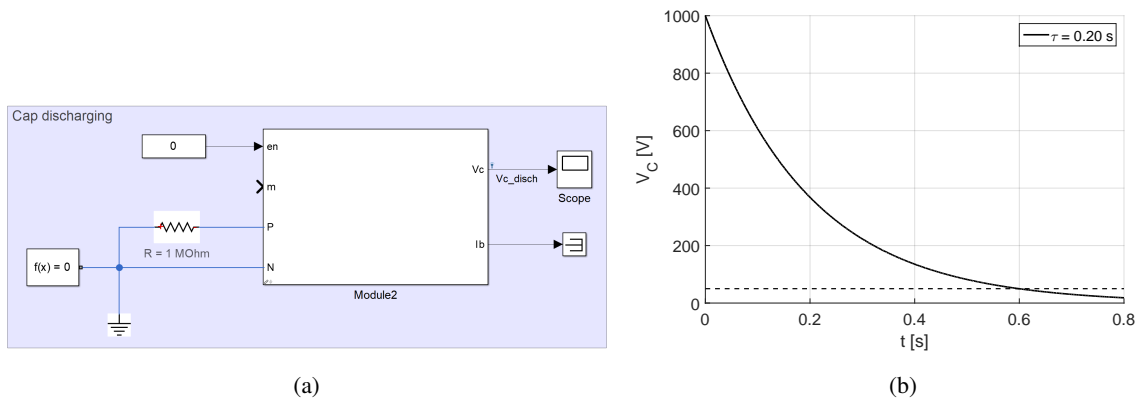
Figure 6.13. Capacitor discharging test circuit (a) and discharging curve for a given
test case (b). Dashed line shows 5% of the initial voltage which is crossed at $t = 3\tau$

$1kV$ amplitude and $50Hz$ frequency. In series with the voltage source, 1Ω, current limiting resistor is
placed.

Top model presents an equivalent model while bottom model is a reference diode rectifier circuit. As
in modeled circuit, capacitor bank with parallel discharge resistor is being implemented.

Fig. 6.14b presents capacitor voltage measurement for modeled circuit (black) and referenced circuit
(red). Additionally, bottom plot presents an absolute error between two measurements calculated for
nominal voltage $V_{nom} = 1000V$ as defined in the Eq. (6.9).

$$\varepsilon = \frac{|V_{C,Model} - V_{C,Simscape}|}{V_{nom}} \tag{6.9}$$

(a)   (b)
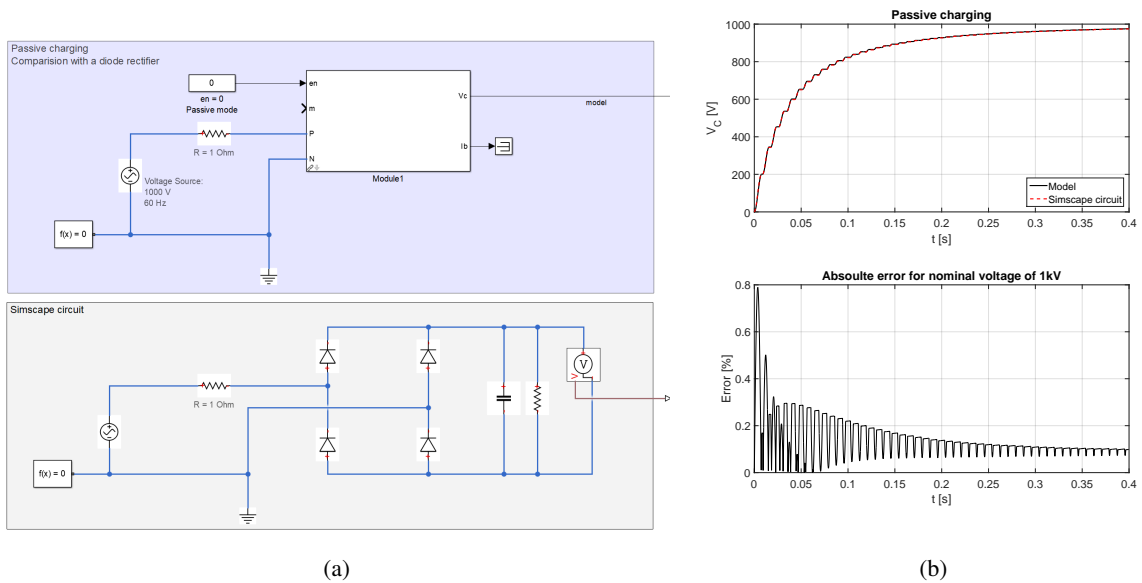
Figure 6.14. Capacitor passive charging test circuit (a) and charging curve (including
absolute error) for a given test case (b).

As the error is below 1% it can be assumed that passive mode in a given model in implemented correctly.

Final step is to check the active mode. To perform that test, enable input `en` should be equal 1. In that mode, modulation index is used to generate output voltage. Sinusoidal waveform with amplitude equal 1 given on the input `m` should result with an output sinusoidal waveform with magnitude equal actual capacitor voltage.

Figure 6.15a presents a test circuit built with a cell model and a resistor connected on the output side. Voltage drop across the resistor should be proportional to modulation index and actual capacitor bank voltage. Resistance will discharge the capacitor. Following phenomenon should be also observed.

Figure 6.15b presents modulation index reference (top plot) and corresponding voltages - capacitor bank (red) and output voltage measured on the terminal outputs of the branch model (black). It can be observed that output voltage follows the reference. Capacitor bank is discharged through connected resistance. Therefore it can be stated that active mode is also implemented correctly.

(a)   (b)
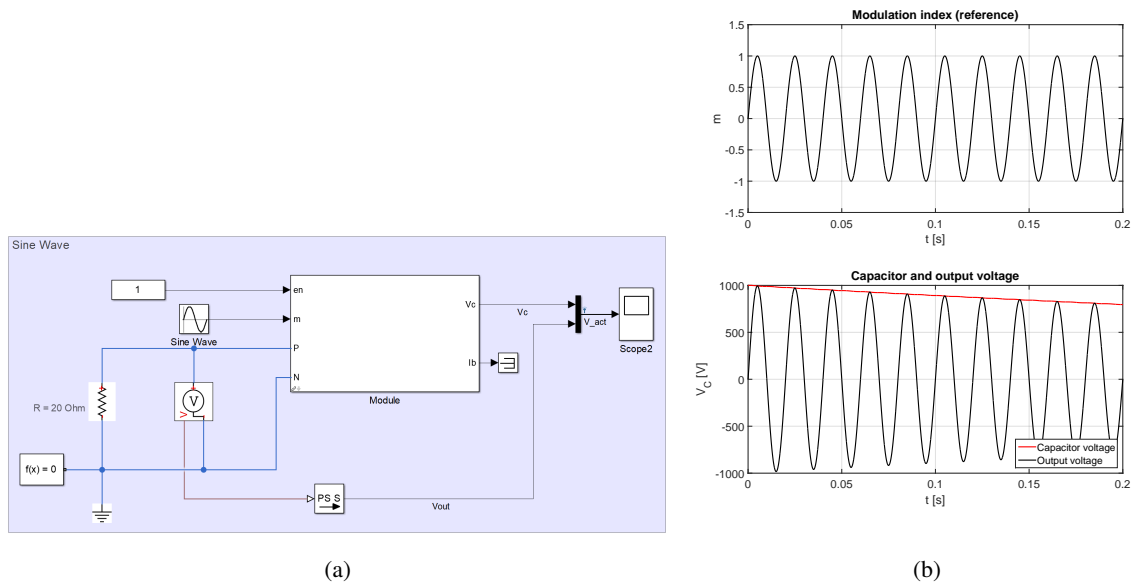
Figure 6.15. Capacitor passive charging test circuit (a) and charging curve (including absolute error) for a given test case (b).

Based on performed tests it can be assumed that given model is implemented correctly and can be used in further simulations.

7. Simulation Results for Real Time Model

Following chapter contains description of simulation model used in the Thesis. Following sections includes summary of performed simulations. The first target to achieve was to show that proposed control loop is working i.e. MMC system follows given setpoints and remains in steady state. The second target was to compare given topology with proposed control loop with an M3C converter topology.

To provide both - detailed analysis and benchmark, three simulation models has been built: one to run at physical controller, and two simplified - one for Hex-Y and one for M3C. Hex-Y simplified model contains the same control blocks as detailed model. The only difference is at the interface level when communication with simulation blocks instead of DSP controller is realized. The purpose of simplified model is benchmark with M3C which is built identically except control at topology level.

Following chapter shows results for Real-Time model. Simplified model description and benchmark is presented in Chapter 8.

Before simulation result presentation, a description of chosen use case is presented.

7.1. Use Case - Direct Drive for Wind Turbine

As it was highlighted in Introduction, there are applications which requires nominal current at low frequencies. Example applications are rolls or lifts for heavy industry. Another branch is hydro and wind power generation. The Thesis use case is wind power generator as well as low speed drive.

In case of wind turbines, there are three basic configurations which use synchronous generators [86]. Low speed direct drive (also called gearless direct drive), which has no gearbox is one. Generator speed is in range up to 30 r.p.m.. Next: medium speed which includes single or two stage gearbox and generator working at speed in range 100-500 r.p.m. The third configuration is high speed built with three-stage gearbox and generator working at speeds in range 1000-2000 r.p.m. Another commonly used generator type is Doubly-Fed Induction Generator (DFIG).

In case of low speed direct drive, a converter which can operate at low frequencies is required. For that application, use of Hex-Y converter can be beneficial. It should be noted, that following system configuration contains least mechanical parts (no gearbox), therefore its volume and weight can be minimized. As mechanical parts requires more maintenance and has lower time-to-service period, use of direct drive turbine is beneficial.

In following Thesis, a system built with Zephyros Z72 turbine is simulated. Details about the turbine can be found in [90]. One line diagram of proposed system is presented on the Figure 7.1.
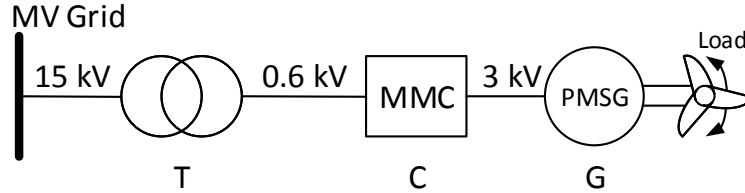
Figure 7.1. Wind Power Converter One Line Diagram. RMS Voltages included.

System is built with transformer (T) which adjust voltage level to required MV grid level. It is possible to built also transformerless system but it will cause MMC converter oversizing. Having transformer also allows to re-use converter in different locations by change transformer ratio instead of converter redesign. Also, if turbine is installed at the location with grid voltage below MMC converter limit (determined by nominal branch voltage), transformer is optional. In given use case, 15/0.6 kV transformer has been proposed. Chosen voltage ratio is present in standard combinations of High Voltages / Low Voltages [90], therefore standard transformer can be used. Required transformer power is at least $1.50 \, MVA$ (determined by generator power).

It must be highlighted that second function of transformer is to provide galvanic insulation which usually is required (by customer and/or by the law regulation), therefore it is anyway required in most cases.

MMC converter (C) is built with PEBB modules described in Chapter 2.2.1. It has been decided to chose a converter built similar to AC/DC rectifier described in [27]. Rectifier parameters and functional lab test results can be found in aforementioned paper as well as in [6, 60, 91, 92]. To meet current rating requirements, four cells in parallel are used [1].

Up to the branch level, the converter is identical. It differs by branch interconnections and branch number (6 in rectifier vs 9 in Hex-Y). For a new topology, with known branch parameters (Table I in [27]), an operation range can be defined as it has been described in Section 2.3.2.4. Branch key parameters are summarized in Table 7.1.

For maximum branch voltage equal $6 \, kV$ (six $1 \, kV$ cells) and generator maximum voltage equal $4.24 \, kV^2$ ($3 \, kV$ RMS), maximum AC input voltage is equal $1.1 \, kV$ RMS - Equation (7.1). As nominal operation point of the converter, $600 \, V$ has been chosen.

$$V_{AC,RMS,max} = \frac{6 - 4.24}{\sqrt{2}} \, [kV] = 1.1 \, [kV] \tag{7.1}$$

---

[1]Based on Eq. (2.16)

[2]What will be described in following paragraph

Table 7.1. MMC Converter Branch Parameters [27]

Description	Symbol	Value [unit]
Number of cells	N	6
Branch nominal voltage	V_b	6 $[kV]$
Branch nominal current	I_b	210 $[A]$

Converter will work at the frequency range from 3 to 9.25 Hz what is defined by generator characteristics. Table 7.2 contains converter nominal parameters.

Table 7.2. MMC Hex-Y Converter Parameters

Description	Symbol	Value [unit]
Input Voltage (max, RMS)	V_1	3 $[kV]$
Output Voltage (RMS)	V_2	0.6 $[kV]$
Branch nominal current (RMS)	I_b	840 $[A]$
Power factor	$cos(\phi_1)$	variable

Generator (G on the Figure 7.1) has nominal voltage equal 3 kV RMS. Nominal power is equal 1.5 MW. Table 7.3 contains generator parameters.

Table 7.3. Zephyros Z72 Parameters [90]

Description	Symbol	Value [unit]
Rated Shaft Power		1.670 $[kW]$
Rated Electrical Power	P_{gen}	1.562 $[kW]$
Rated Voltage	$V_{2,nom}$	3 $[kV]$
Rated Current		327 $[A]$
Rated Frequency		$3 - 9.25$ $[Hz]$
Power factor	$cos(\phi_1)$	0.92

Generator characteristics, i.e. Voltage/frequency curve is presented on the Figure 7.2a. Figure 7.2b shows power-frequency characteristics. In the full system, rotational speed of generator is controlled by blade angle adjustment. This is out of scope in the Thesis. It should be noted that maximum efficiency of the generator is at 9 Hz (95.7 %).

The system will work at frequency range from 3 to 9.25 Hz. It corresponds to AC voltages from 1 up to 3 kV.
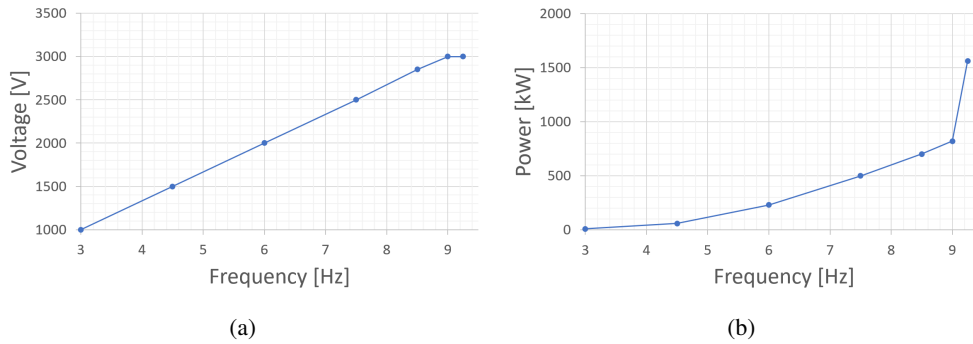
Figure 7.2. Turbine characteristics. V-f (a) and P-f (b).

7.2. Test Cases Description

Control algorithm implemented in the model will be tested for given operation points. Table 7.4 contains test cases summary. Test ID is an internal identification number used by author. Tests starting with first digit ID equal 0 are related to basic functionality. 2 refers to reactive power provision. 3 refers to grid support capability during voltage dips.

Columns RT, SIM and M3C contains information whether test results are summarized in the Thesis or not. RT refers to Real-Time model. Study results can be found in following chapter and Section 9 as well. SIM refers to simplified simulation model of Hex-Y and M3C refers to simplified M3C model. Study results for both can be found in Section 8. As it was said earlier, SIM model is created mainly for benchmark purposes.

Table 7.4. Test Cases Overview

Test ID	RT	SIM	M3C	Description
010	✓			**Open circuit voltage control module.** Check voltage control module - if it follows the reference.
020		✓		**Branch current controller.** Check branch current control by passing non-zero current references. Tune branch current controller if required.
030		✓		**Check balancing modules.** For that test all balancing modules are active. Start from steady state, next change the reference of the converter power and measure capacitor voltages.
040	✓	✓	✓	**Output voltage generation – 0 Hz.** Check if output voltage follows the reference. Check capacitor voltages and branch currents.
041	✓	✓	✓	**Output voltage generation – 3 Hz, 1000 V.**
042	✓	✓	✓	**Output voltage generation – 6 Hz, 2000 V.**
043	✓	✓	✓	**Output voltage generation – 9 Hz, 3000 V.**

045		✓	✓	**Output voltage generation – 0 Hz, 2000 V. Resistive load.** As previous tests but with resistive load to show Hex-Y performance in case of no-zero current at low frequency
046		✓	✓	**Output voltage generation – 3 Hz, 2000 V. Resistive load.**
050	✓	✓	✓	**Reference change 0->9 Hz.** Simulate generator startup sequence.
051	✓	✓	✓	**Reference change 9->0 Hz.** Ramp down frequency.
060	✓			**Charging sequence.** Check state machine by performing full charging sequence (from OFF state to STANDBY).
200		✓	✓	**Reactive power step change 0->1.0 MVA at no AC load.** Check reactive power provision capability.
201		✓	✓	**Reactive power step change 0->1.0 MVA during operation at 6 Hz, 2000 V.**
202	✓	✓	✓	**Reactive power step change 0->1.0 MVA during operation at 9 Hz, 3000 V.**
301	✓			**Voltage dip to 0.15 p.u. for 150 ms.** No power from generator provided. Check output powers, branch currents and branch capacitor voltages.
302	✓			**Voltage dip to 0.80 p.u. for 3 s.** Load as above.
303	✓			**Voltage dip to 0.90 p.u. for 4 s.** Load as above.

7.3. Real Time Model Overview

Proposed control algorithm has been implemented on the test bench containing AC800 PEC controller (top level device). Cell control is implemented on Texas Instruments DSP in PEBBs as it was explained in Chapter 5.2. More details about DPS processor can be found also in Chapter 2.2.1.

Control algorithm for AC800 PEC is prepared in the Matlab/Simulink package what provides not only automated Embedded C code generation but also extensive offline simulation capabilities. That feature has been used by building a test harness around the controller model.

Due to limitations of Real Time Simulator itself, control hardware in the loop testing was not possible. Instead, an extensive simulation model has been built.

The test harness contains interfaces between controller and environment - DSP, measurement devices and overriding control modules. Additionally, a physical model of electric circuit - cells modeled as it has been explained in Chapter 6 and grid/load are present. Atop of that, extensive monitoring, recording, test case generation tools are present. Electric model has been built with Simscape PowerSystems blocks.

Given model is used for verification and validation. For that purpose, a set of test cases with pass/fail criteria has been built. After passing that tests, it can be used in Real-Time Simulations which run

on Opal-RT system. Its specification can be found in [72]. RTS simulations are converged with a phy-sical device what has been proven during laboratory testing of another MMC topology (with identical hardware and control hardware architecture). Experimental results can be found in [6] and [27].

Top level structure of the model is presented on the Figure 7.3. It is built with four main sections. Two sections contains slave controller modules. One is a master systems. Each section includes control parts which are implemented on three separate AC800 PEC controllers (see Chapter 5.1). Fourth section is so-called test harness which contains simulation part: interfaces, DSP simplified control (PWM modulator but without deadtime control) and electric circuit model.
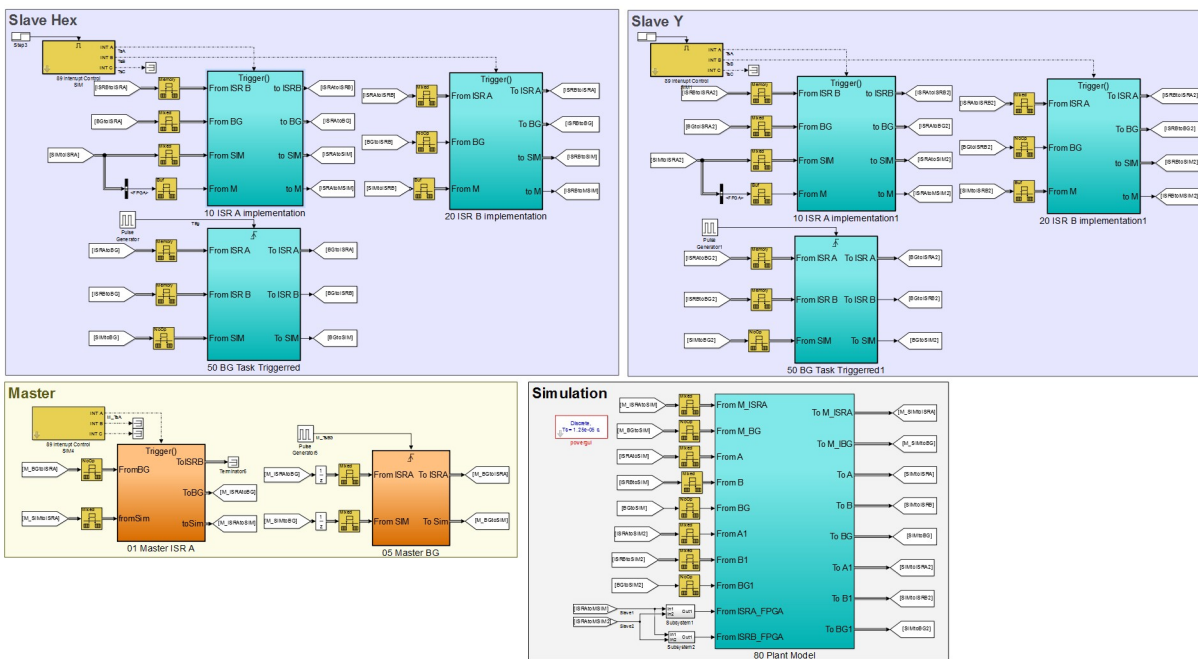
Figure 7.3. Full Simulation Model. On top two Slave controllers. On the bottom left Master controoler. On the bottom right Simulation harness.

Each control module is built with three tasks with different sample time: Task A is executed every 125 μs. Taks B: 500 μs. BG (background task): 1 s.

Task A includes main control algorithm, fast protection and communication with peripheral modules (DSP, master-slave PEC communication and measurement devices). In the Task B, main state machine and slow protection are implemented. BG task is non-deterministic what means 1 s is not guaranteed as this Task is not called by timer interrupt. Therefore it contains only non time-critical activities as cell parameter calculation or some data exchange with monitoring devices.

Communication between PEC controllers is made with PEC PowerLink protocol which has following 10 Mbit/s bandwidth (see Table 5.1 for more detailed specification). On the physical layer, communica-tion is provided by fiber-optic.

7.3.1. Slave Controllers

Both Slaves are built identically. On the Slave controller, branch level functionality is covered, therefore device doesn't have to "know"whether it controls Hex or Y part of the converter. This data is available on the Master controller. On the other side however, Slaves must inform Control hubs about the cell mapping. Therefore Master sends information about the mapping to Control hubs through Slaves.

As it was shown on the Figure 7.3, top level of Slave controller is built with three Tasks (A, B, Background). Task A is presented on the Figure 7.4. Generic structure is identical for all tasks and all PEC models (Slaves and Master), therefore it won't be repeated in the Thesis. On the left, reading interfaces are present. In the middle, data processing is present. On the right, output interfaces are present.
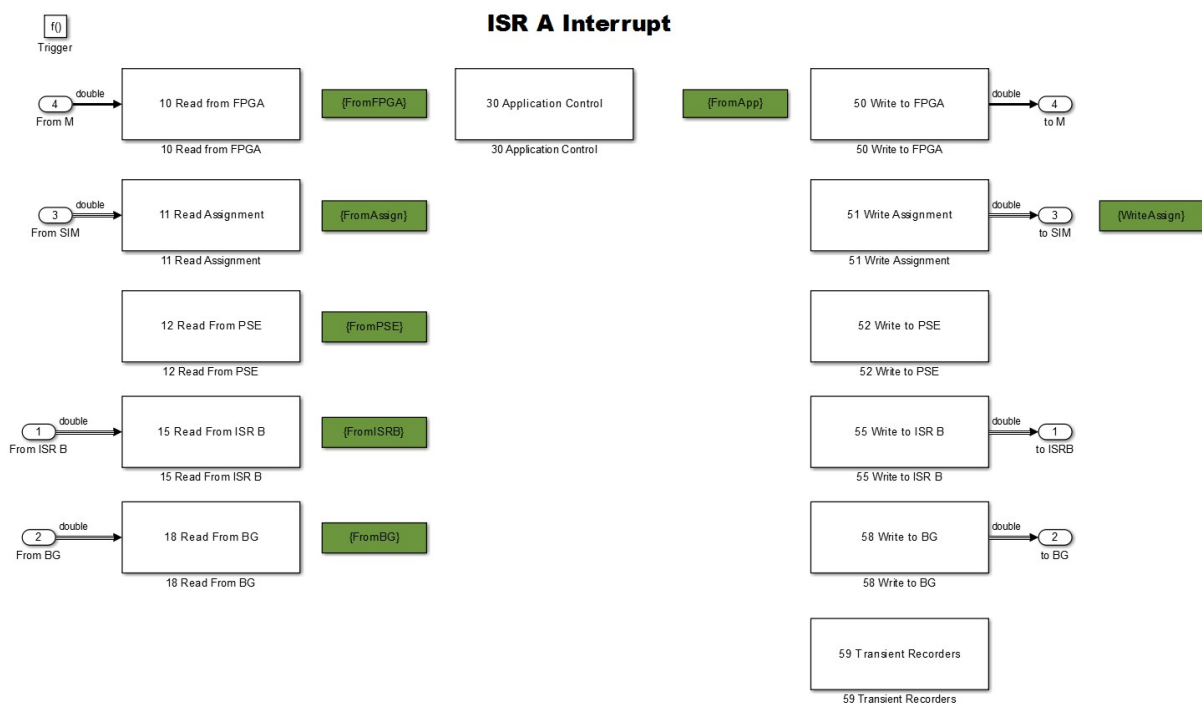
Figure 7.4. PEC Slave Controller, ISR A

Task A contains application control module which includes following modules (described in the section 5.2): PLL, SBV, SBI, BRI and parts of REF and MOD units. Each module functionality and its interconnections has been already described in referenced section.

Task B contains state machine and protection units. In the Table 7.5, all states and possible transitions are presented. In a normal operation, converter goes from state **A** to state **E** by receiving *START* and *ENABLE* commands. Converter stays in **E** state till command *STOP* is received. After that command, converter goes to DISCHARGE state **J** and when cells are off, goes to OFF state (**A**).

Protection module collects measurements, limits and signals and process it by using comparators and timeouts (if applicable). In case of fault detection, it is being reported to the state machine and error code is sent up. It can be read and processed by Master controller.

Table 7.5. State Machine Overview. State names in CAPITAL, Commands in *ITALIC CAPITAL*

State	Description	Possible Transitions
A	OFF - converter is waiting for communication with peripheral modules	**B** - after receiving ON feedback from all Control Hubs
B	ON - converter is initializing cells and waiting for *START* command	**C** - after PLL synchronization and receiving *START* command
		A - after receiving *RESET* command
		J - when fault is present
C	CHARGING - converter starts modulation and is being charged up	**D** - after reaching specified cell voltage level at each of the cells
		A, J - as for the state **B**
D	STANDBY - converter ready for operation. Wating for *ENABLE* command	**E** - after receiving *ENABLE*=1 command
		A, J - as for the state **B**
E	OPERATING - converter is generating output voltage and currents	**D** - after receiving *ENABLE*=0 command
		A - after receiving *RESET* command
		J - after receiving *STOP* command or if fault is present
J	DISCHARGE - converter is being discharged	**A** - after receiving *RESET* command or after converter is being fully discharged

There are two levels of faults - L1 trips the converter (send it to the state **J**). L2 trip sends only a warning. In case of L1 trip, error is coded into binary word which is sent to Master. Table 7.6 contains all processed faults. Bit columns presents at which bit in error code, error is stored.

Background task contains calculations for cell parameters which are sent during startup (state **B**). Key parameters are: cell configuration (full bridge), switching frequency (1 kHz per half bridge unit what gives 2 kHz per cell), current controller proportional gain, nominal cell voltage and current and operation limits (max voltage, current and temperature).

7.3.2. Master Controller

Master controller is built with Task A and BG Task.

Task A contains control modules: CEC, BRB, CCC and REF (see section 5.2). Implementation of Grid Support is also realized here.

Additionally, the main state machine synchronized with slave state machines is present. Its extra functionality is to merge states from both slaves and block *START* and *ENABLE* signals in case they should not be processed. *START* permission depends on feedback signals as „fan ok", „auxilary power supply

Table 7.6. Protection functions in Slave PEC.

Bit	Name	Description	Timeout
	L1 - trip		
0	Overvoltage	At least one cell has voltage above given limit	—
1	Control hub fail	Fault signal from control hub	3 ms
2	PLL fail	PLL synchronization lost	—[a]
3	Overcurrent	Branch current is above given limit	—
4	AC undervoltage	AC side (input) below given limit. Module is disabled as grid support module controls converter behaviour in that fault type	
5	—	*not used*	
6	Overtemperature	At least one cell has temperature above given limit	100 ms
7	PEC Fail	e.g. power supply fail	3 ms
8	Communication fail	Lost communication with Master, PECMI or Control hub	3 ms
	L2 - warning		
—	Overtemperature	At least one cell has temperature above given warning limit	100 ms

[a]PLL module has its internal signal to report syncrhonization loss. It is set to 20 ms

ok" or „communication with Combi I/O is ok". For *ENABLE*, additionally feedback from precharge unit is checked - it should be not possible to transfer power if precharge resistors are not bypassed.

Task A includes also system level protection which complements Slave protection units. It checks system auxiliaries as fan, redundant power supply for control unit etc. Additionally in case of fault in one Slave it sends fault command to the other Slave controller.

BG Task includes communication with optional HMI module. It includes also a module for fan control. Its speed depends on the maximum temperature of cells (broadcaster by Slaves) and branch inductors (measured by Master through Combi IO).

BG Task controls also cabinet door lock. Doors are locked since system is energized till 3 minutes after it is off. Additional delay is dictated by safety precautions. Even though capacitor voltage should not be accessed with opened door (as PEBB module is in cover). In case of double fault, voltage can appear on the PEBB. Within 3 minutes, capacitor should be discharged to the safe level (below 50 V).

7.3.3. Test Harness

Section named Simulation on the Figure 7.3 contains simulation harness built with branch model and electric circuit model.

Branch model is built with four levels: communication, DSP operations (mainly modulator), DSP peripheral operations (measurements, include delays and dead time on the IGBT drivers) and electrical mathematical model including capacitor or switch models. This part of the model is protected by Intellectual Property (IP) of ABB[3], therefore it cannot be described in more detail in the Thesis. In practice, this module calculates what voltage will be generated by the branch for given modulation index. Additionally it calculates what is each cell capacitor voltage for given modulation index and branch current. Simplified model covering the same functionality is being used in simplified simulation model and is described in the Chapter 6.

Output from the branch model are sent to electric model. Top level of that unit is presented on the Figure 7.5. From the left, module is built with grid model, two converter modules (Hex and Y) and load model. Additionally, voltage and current measurement modules are present.
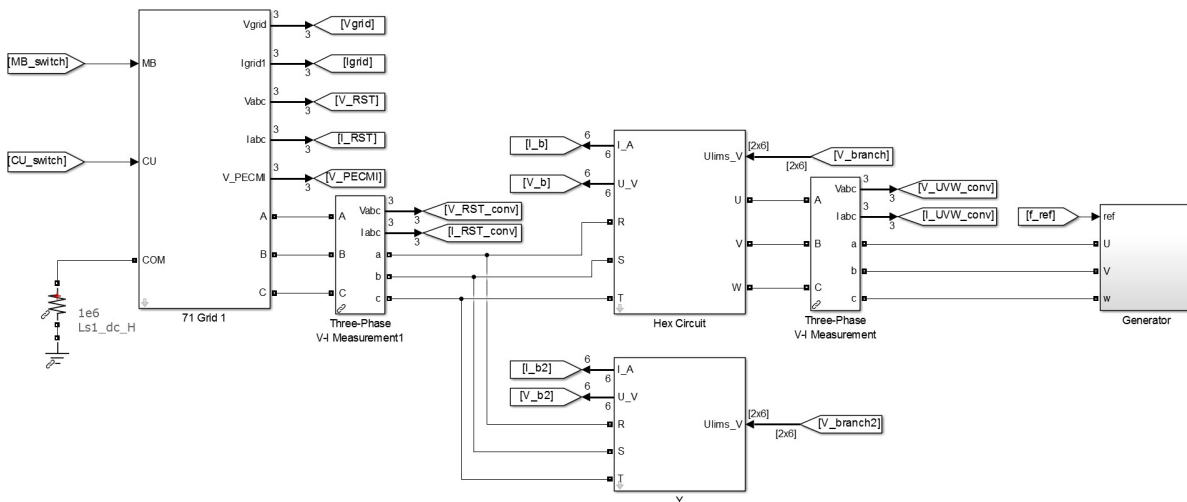
Figure 7.5. Electric circuit. Top level

Grid model is presented on the Figure 7.6. Model is built with an ideal 3-phase voltage source, transformer, main breaker and precharge circuit required to limit inrush current. Resistors, which connects each phase to ground has $1\ M\Omega$ resistance and are present to provide reference for numerical calculations. PECMI block contains High Voltage Divider (HVD). Its output is feed to PECMI measurement board.

The converter is built with branch modules as described in Chapter 6. Figure 7.7 presents Y converter. Hex converter looks the same, but contains six branches. As it is shown, each branch is connected with a branch inductor. Input for the branch is voltage reference. Output is measured current and voltage.

---

[3]as: „keep secret"
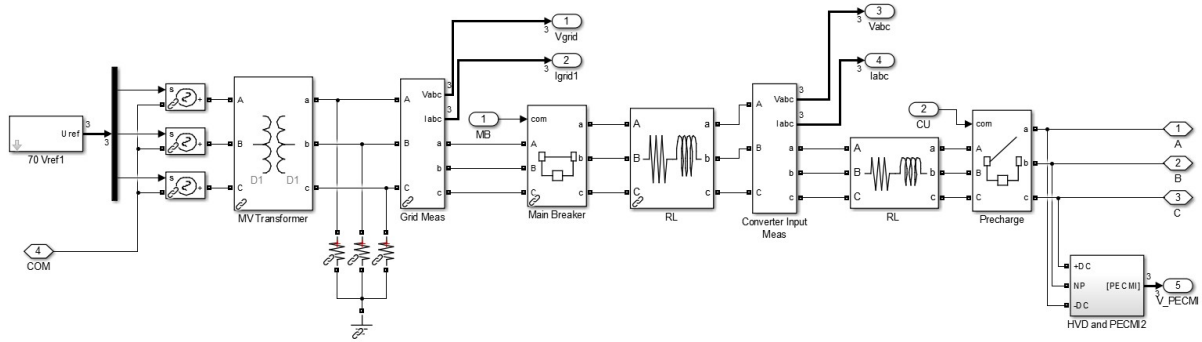
Figure 7.6. Electric circuit. Grid model.
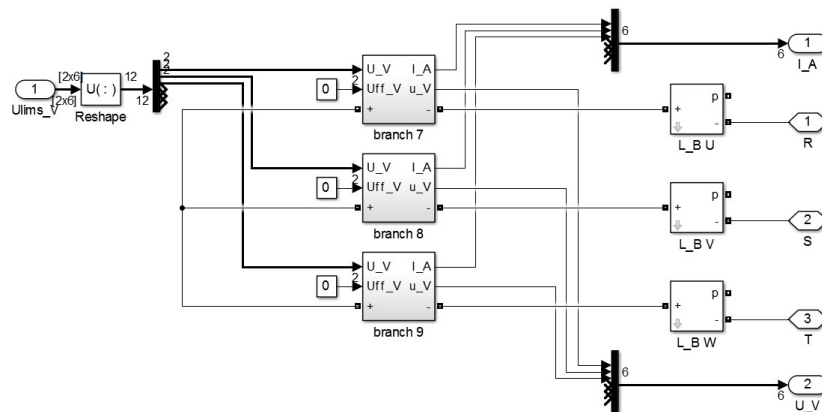
Figure 7.7. Electric circuit. Y converter model.

7.4. Simulation Results

Full model is built with a set of components described with detail in Chapter 5. Before running a full system tests (so called integration tests), unit testing should be performed. As the name says, following tests are focused on given units as e.g. PLL or balancing module. This practice results with more smooth integration tests part as each module has been already tested. Isolation of single modules allows to analyze, tune and check parts of the model - one by one.

RT-010 shows voltage generation capability of the simulation model. As capacitors are not able to be charged from the supply, its voltage will decrease due to the losses and discharge resistors in cells. To not observe this phenomenon, capacitor voltages in this test case are forced to be constant (at nominal voltage level). Also current controller module is disabled to not have influence on the voltage shape.

Next, unit tests checks current control unit. Next, balancing modules one each level are being tested. As for the Thesis, functional tests are more interesting than unit test, those intermediate steps are not described.

Tests RT-04x are focused on steady state behavior of converter. Tests RT-05x checks dynamic response of the converter. RT-060 shows charging sequence for the converter. RT-20x contains reactive

power provision capabilities check and tests RT-3xx included in Chapter 9 checks grid support capability during voltage dips.

7.4.1. RT-010 Open circuit voltage control module

In this unit test, PLL module is being checked. For that test, converter is initially disconnected from the supply grid, but voltage measurements are available. As soon as PLL module is synchronized, converter starts voltage generation and it closes the main breaker. If PLL is correctly synchronized, a low inrush current (below 0.2 p.u.) should be observed. Additionally due to the fact that balancing modules are not active, no current should flow in a steady state (input current reference is equal zero).

Results from this test case are confronted with a wrongly synchronized module to highlight the difference. "Wrong synchronization"was performed by adding 1 deg offset to PLL output. Figure 7.8 shows simulation results. It can be observed that in both cases inrush current is low (on acceptable level). For correctly set PLL module, input current goes to zero.

(a)   (b)
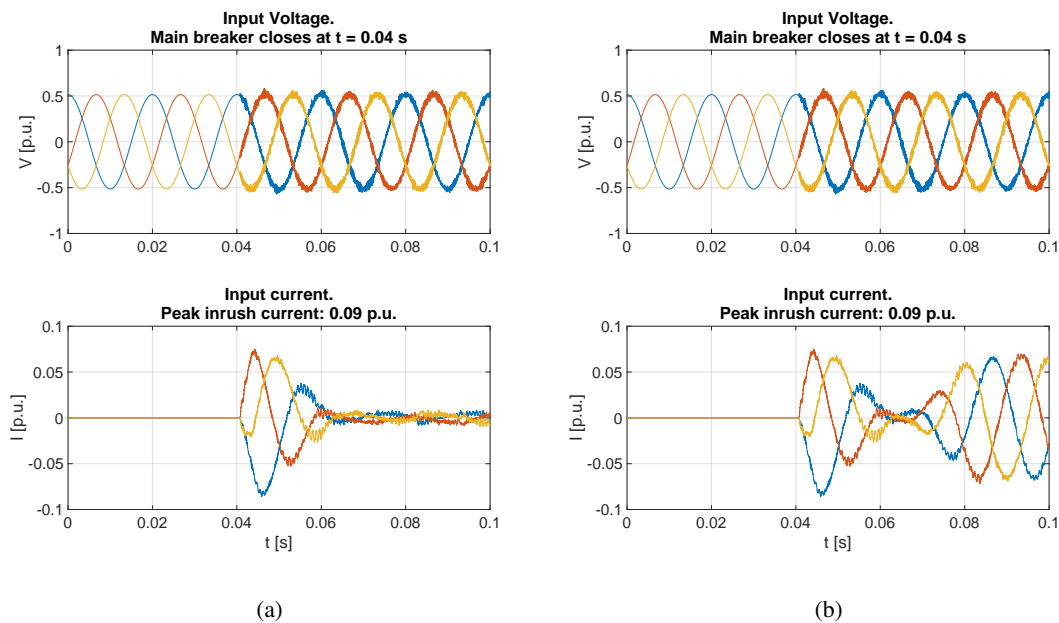
Figure 7.8. Input voltage and current for correctly synchronized PLL (a) and PLL with introduced offset (b)

7.4.2. RT-04x Output Voltage Generation

Following test checks behavior of the converter in a steady state for given operation points. In this test, internal converter parameters i.e. branch current and average cell capacitor voltages in each branch are being measured. Table 7.7 contains summary of research. As it can be observed, for each test case, voltage ripple is below 10% and branch current does not exceed $1\ p.u.$ what are pass criteria for that test.

Table 7.7. Capacitor voltage ripple and branch currents for Hex-Y converter. All quantities in p.u. unless it is specified otherwise.

Test ID	$f_2[Hz]$	Hex-Y		
		$V_{C,rip}[\%]$	$I_{b,RMS}$	$I_{b,max}$
RT-040	0	0.43	0.017	0.065
RT-041	3	0.45	0.020	0.073
RT-042	6	1.59	0.058	0.152
RT-043	9	9.79	0.326	0.759

On the Figure 7.9, waveforms for the test RT-043 with $9\ Hz$ output frequency are shown.
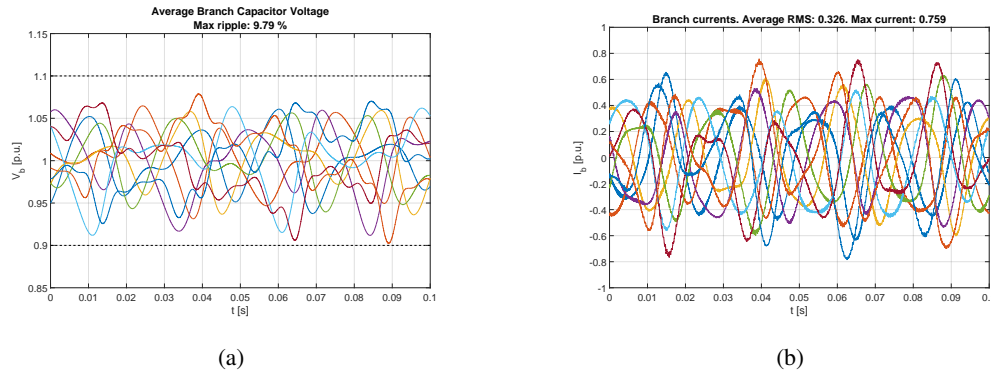
Figure 7.9. Average branch capacitor voltages (a) and branch currents (b) for Test RT-043

Figure 7.10 presents branch voltages and currents for every branch in the converter. Black lines are the references. It can be observed that branch currents follows given setpoints. Branch voltages are correctly generated. Voltage ripples (from PWM modulation) with magnitude of $1/6\ p.u.$ are present.[4]

Figure 7.11 shows output voltage waveforms for all test cases. Reference voltages are marked with a black, dashed line. It can be noticed, that voltage is reproduced correctly.

7.4.3. RT-05x Reference Step Change

Following test checks converter response for the reference setpoint change (dynamic). Change for full range i.e. from 0 to 9 Hz and vice versa has been analyzed. For a change, rise/fall time limit equal $100\ Hz/s$ has been given. It means that change $0 - 9\ Hz$ will take below $0.1\ s$.

Pass criteria for this test are following: average branch capacitor voltage must stay within a range from $0.8\ p.u.$ to $1.2\ p.u.$. Branch currents cannot exceed $1.2\ p.u.$. Table 7.8 contains summary of simulations. According to the Table, pass criteria has been met for both transitions.

---

[4]As $1\ p.u.$ is total branch voltage, voltage steps of $1/N\ p.u.$ are observed for a branch built with N cells. In given test case $N = 6$ (there are six series connected cells in each branch).
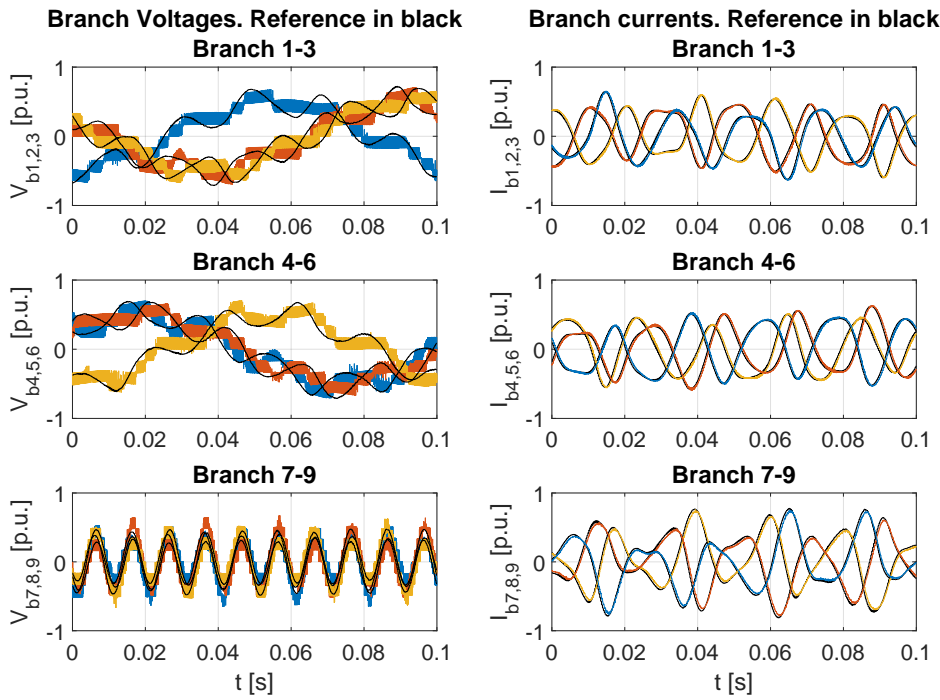
Figure 7.10. Branch voltages (left) and currents (right) for Test RT-043

Table 7.8. RT-05x. Capacitor voltage ripple and branch currents for Hex-Y. All quantities in p.u. unless it is specified otherwise.

		Hex-Y		
Test ID	$f_2[Hz]$	$V_{C,min}$	$V_{C,max}$	$I_{b,max}$
RT-050	$0 \to 9$	0.99	0.81	1.07
RT-051	$9 \to 0$	0.68	0.87	1.08

On the Figure 7.12, average branch capacitor voltage and branch current waveforms for each branch are shown.

Generated (output) voltage waveforms are presented on the Figure 7.13. It can be observed that output voltage follows reference.

Based on simulation results, it can be assumed that dynamics of the converter is at a satisfactory level.

7.4.4. RT-060 Charging Sequence

Following test shows analysis of converter behavior during charging process which can be divided into two steps. In the first stage, so called passive charging is performed. In that time, IGBTs are not active. There is no PWM modulation. Cells are being charged through anti-parallel diodes of transistors.
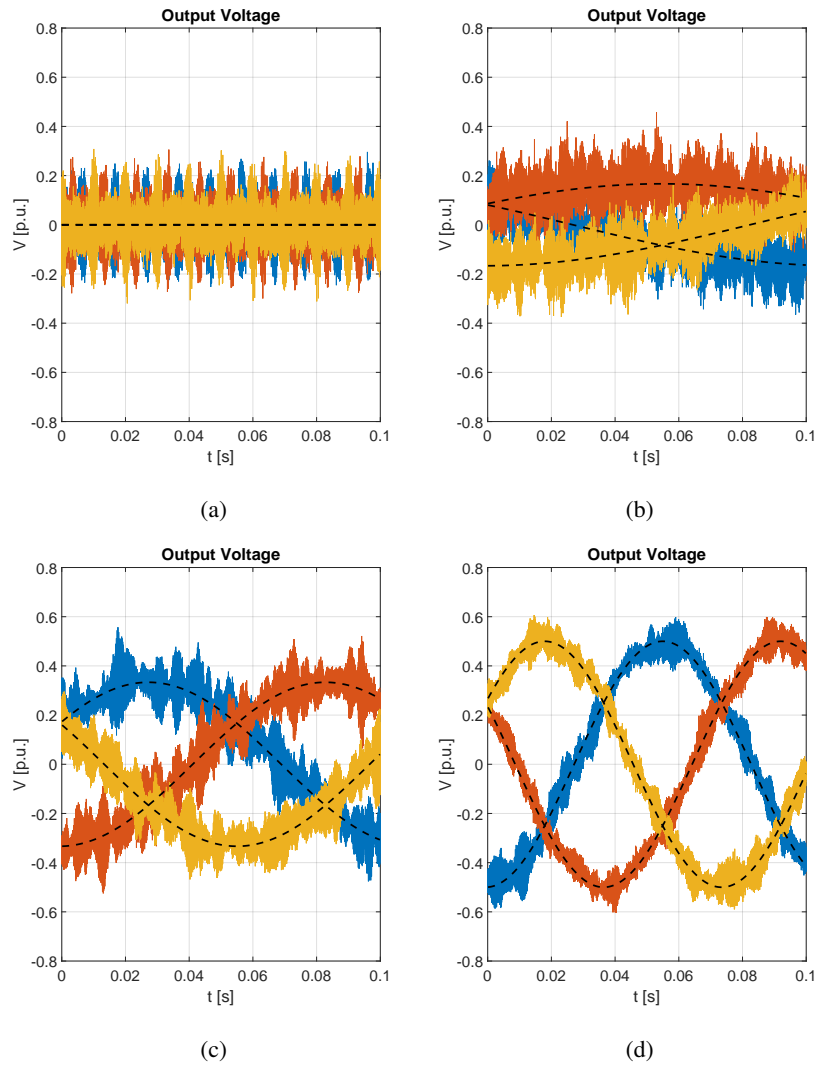
Figure 7.11. Output voltages for tests case RT-040 (a), RT-041 (b), RT-042 (c), RT-043 (d)

Cells can be charged up to maximum voltage given by Eq. (7.2). In given case it leads to the value of c.a. 120 V.

$$V_{Cm-passive} = \frac{V_{1m}}{2 \cdot N} = \frac{600\sqrt{3} \cdot \sqrt{2}}{2 \cdot 6} V \approx 122V \tag{7.2}$$

Number 2 in the equation stands from the fact that between each two phases of the input grid, there are two converter branches connected in series, so the voltage is divided among $2 \cdot N$ cells.

To reduce inrush current, converter should be equipped with precharge circuit, usually built with series connected resistors limiting the current. Resistors are in series with a converter when the main breaker is closed. Later, when capacitors are passively charged, resistors are bypassed (e.g. with use of parallel connected contactors).
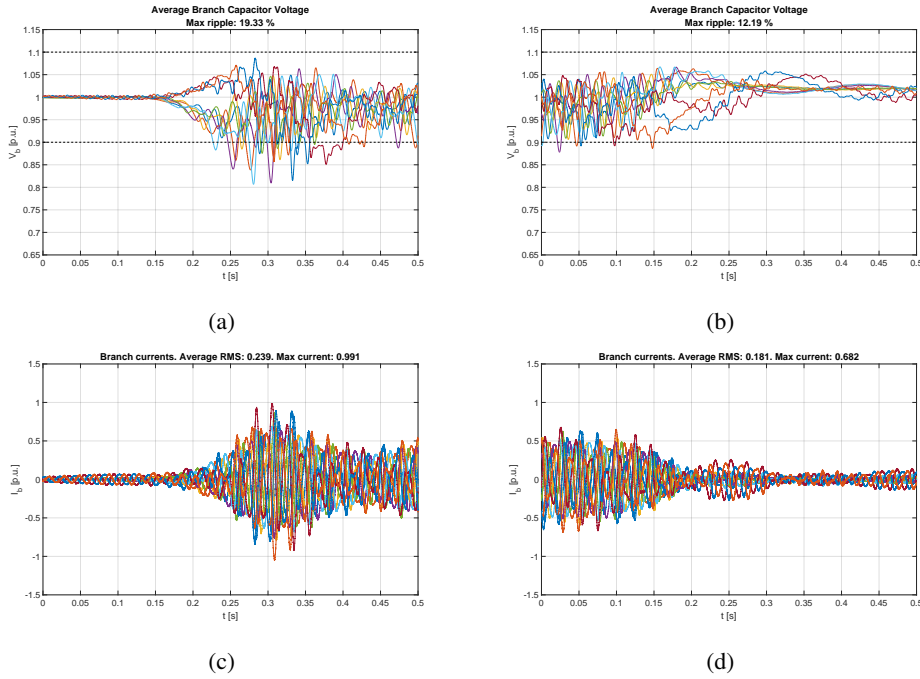
Figure 7.12. Capacitor voltages (a,b) and branch currents (c,d) for refernce step change. Test case RT-050 (a,c) and RT-051 (b,d).

After passive charging, active charging can start. Cells are on and can start modulation to charge up for nominal voltage level what is realized by CEC module which control active power on the input (supply) grid.

Figure 7.14 shows average voltages in each branch capacitor bank during charging. Passive charging has started at $t = 0.05\ s$. Cells are charged for $0.12\ p.u.$ what corresponds with value $120\ V$ calculated in Eq. (7.2). Next, at $t = 0.40\ s$ active charging has started. After c.a. $0.8\ s$ cells reached $90\ \%$ of its nominal voltage what finish charging process.

Charging speed can be controlled by setting current limit in CEC controller. In given case, limit was set to $0.4\ p.u.$.

Figure 7.15 shows input current waveforms. At $t = 0.05\ s$, inrush current can be observed. It can be noticed that due to use of precharge circuit, current is not too high. Precharge resistors are bypassed at $t \approx 0.2\ s$. Next, charging current is observed. Charging current can be controlled by aforementioned limit in CEC controller.

It is clear that higher current during active charging effects with quicker charging. Figure 7.16 shows capacitor voltages and input current for two other charging limits to confirm that assumption.

Based on simulation results it can be assumed that control algorithm behaves correctly and allows to start up the converter. Additionally, charging process can be fully controlled i.e. it is possible to have control over charging speed and maximum current by configuration of CEC module.
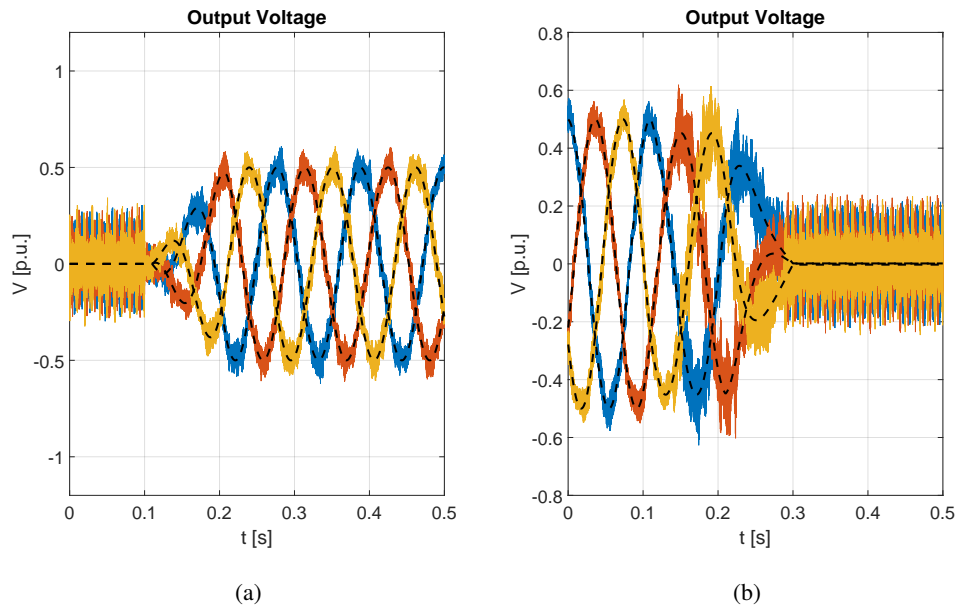
Figure 7.13. Output voltages for test case RT-050 (a) and RT-051 (b). Reference voltage shown with black dashed lines.

7.4.5. RT-202 Reactive Power Provision

Control algorithm allow to independent control of active and reactive power at input terminals. The only coupling factor is the apparent power limitation summarized with Equation (7.3).

$$\sqrt{P_{ref}^2 + Q_{ref}^2} \leq S_{nom} \tag{7.3}$$

Simulation results are investigated to check if converter is able to provide reactive power during nominal operation while power is being transferred between input and output. While the reactive power provision is in use, active power is being limited. As a result, average branch capacitor voltage drift will be observed. However, balancing modules should not be affected, i.e. all voltages will drift in the same direction (either charge or discharge depending on power flow direction).

Figure 7.17 presents branch capacitor voltages during reactive power provision. It can be observed that during that event, branches are being discharged, however after that, they are charged up to its nominal voltage as CEC module is active all the time (even with lower limit during reactive power request).

Input voltages and currents are presented on the Figure 7.18. Figure (b) presents zoom on reactive power provision part. It can be observed that during this event, phase shift between voltage and current is present.

Simulations show that converter is able to provide reactive power for given time with no influence on the system behavior, i.e. converter is not tripped and output voltages are not affected. Figure 7.19 shows voltages at the second terminals set (load side). No interference with reactive power provision can be observed.

Average Branch Capacitor Voltage
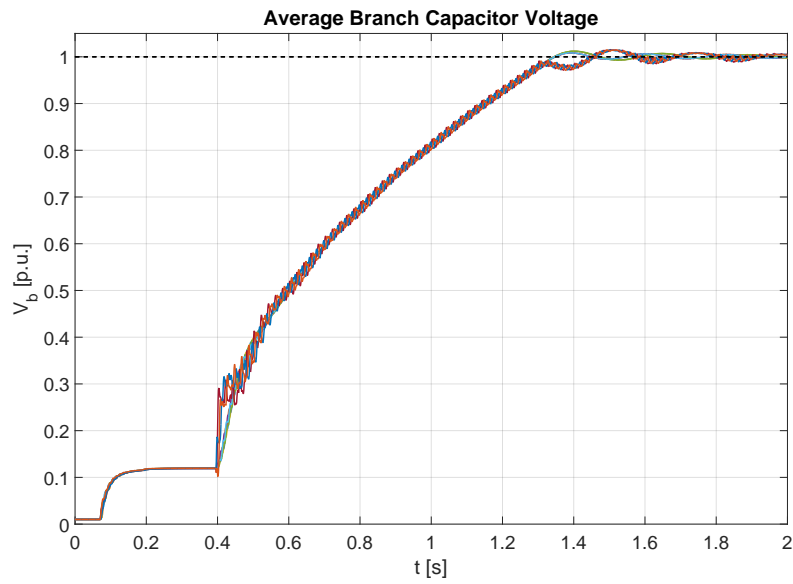
Figure 7.14. Averaged cell voltages in each converter branch during charging process. Black dashed line shows nominal voltage. Passive charging starts at t=0.05 s, active charging starts at t=0.4 s

Input currents during charging.
Max current: 0.601
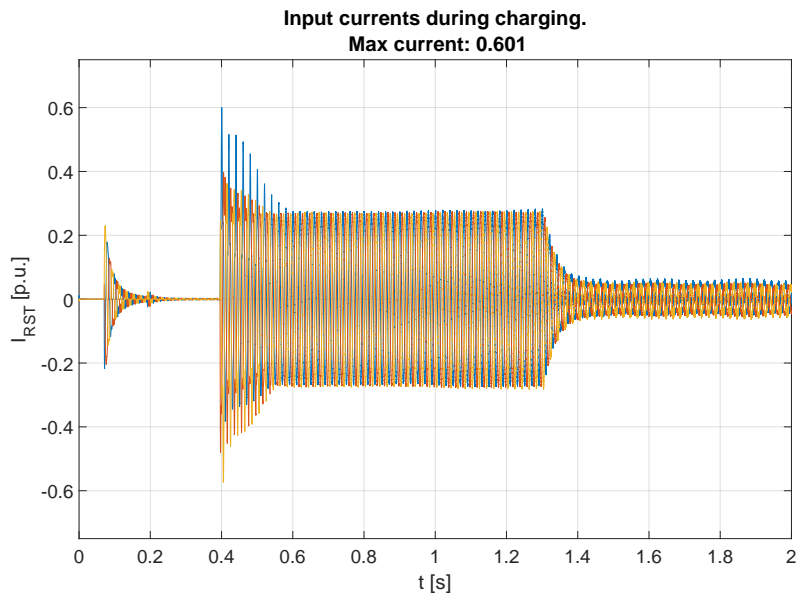
Figure 7.15. Input current during charging process. Passive charging starts at t=0.05 s, active charging starts at t=0.4 s
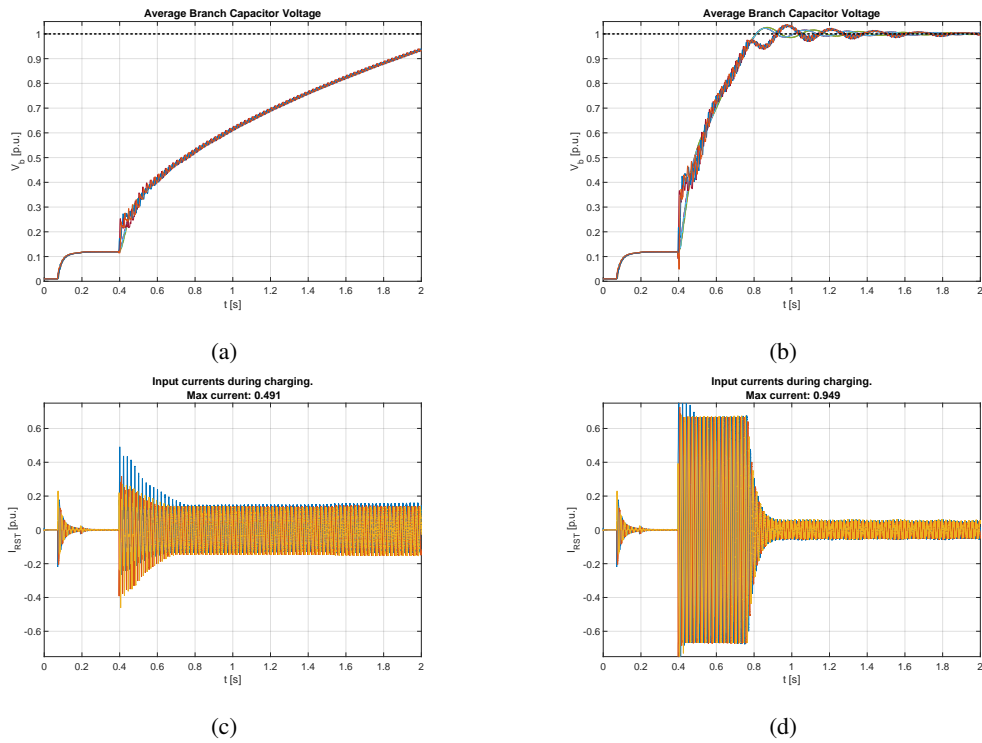
Figure 7.16. Capacitor voltages (a,b) and input currents (c,d) during charging with limit set to 0.2 p.u. (a,c) and 1.0 p.u. (b,d)
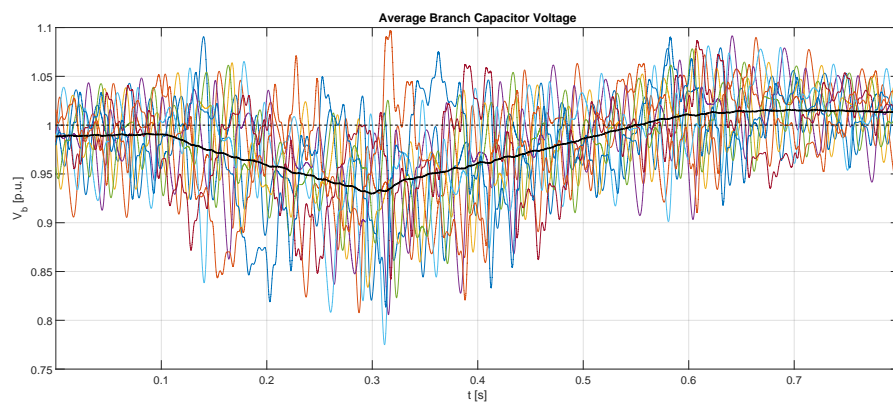
Figure 7.17. Average branch capacitor voltages during nominal operation. Reactive power flow is requested from $t = 0.1\ s$ to $t = 0.3\ s$. Black line shows averaged voltage of all branches.

(a)   (b)
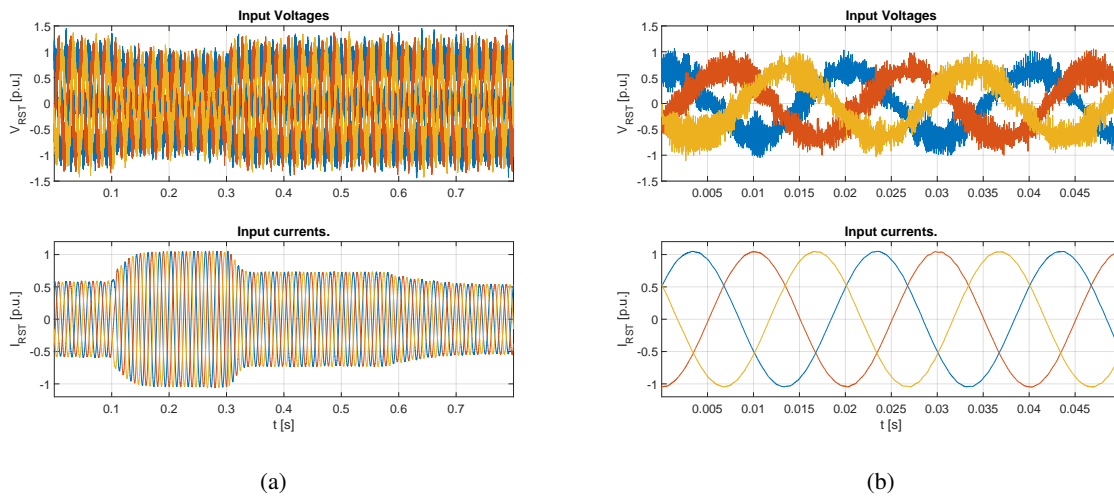
Figure 7.18. Input voltages (top) and currents (bottom) during nominal operation. Reactive power flow is requested from $t = 0.1\ s$ to $t = 0.3\ s$. Figure (b) shows zoom at $t = 0.25\ s - 0.30\ s$
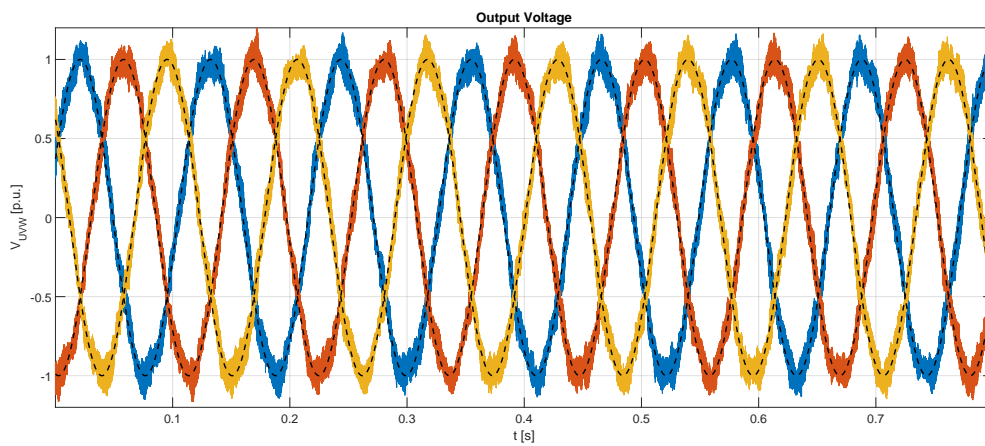
Figure 7.19. Output voltages. Reactive power flow is requested from $t = 0.1\ s$ to $t = 0.3\ s$.

8. Hex-Y Performance Comparison with M3C Topology

Following chapter contains details about simplified model which has been built for two MMC topologies: Hex-Y and M3C. Given models were simulated to highlight differences between state-of-the art and proposed converter topology. Simulation results shows that Hex-Y can be beneficial especially for nominal operation point with low frequency and high current.

8.1. Simplified Model Overview

To compare Hex-Y topology with state-of-the-art, in this case M3C topology, simplified model which contains the same control as Real-Time model has been built. In practice, Simplified model is an extract of Task A from three AC800 PEC controllers, merged into a single model.

Simplified model simulations are much faster (rank of 100-1000). There are two models built - one for Hex-Y and the other one for M3C. In case of M3C, control loop has been realized as it was proposed in [65]. Paper [82] contains detailed model description and summary of models comparison. In the Thesis, more detailed analysis is being performed.

Figure 8.1 presents top level of simulation model of Hex-Y converter. Two main model sections are: distributed control (top) and electric circuit (bottom).

The control system is built with three subsystems representing three AC800 PEC controllers. Additionally, PECMI interface responsible for measurements is implemented.

To be as close to the reality as possible, simulation model contains delay blocks (marked yellow on the Figure). Those blocks represents communication delays present in a physical system. Data exchanged between all modules is also identical to the data available in a real system (resolution and sample time).

8.1.1. Control Section

Master Controller module contains following components: data exchange with Slave Controllers, average capacitor voltage calculation (required by CEC module implemented on the Slave PECs), branch balancing and CCC - Circulating Current Calculation. Additionally, REF module responsible for reference setpoints generation is present.

On the Master Controller, GRI - Grid Support module is present. Following module is responsible for reactive power reference generation. If converter is set to work with unity power factor, GRI reference
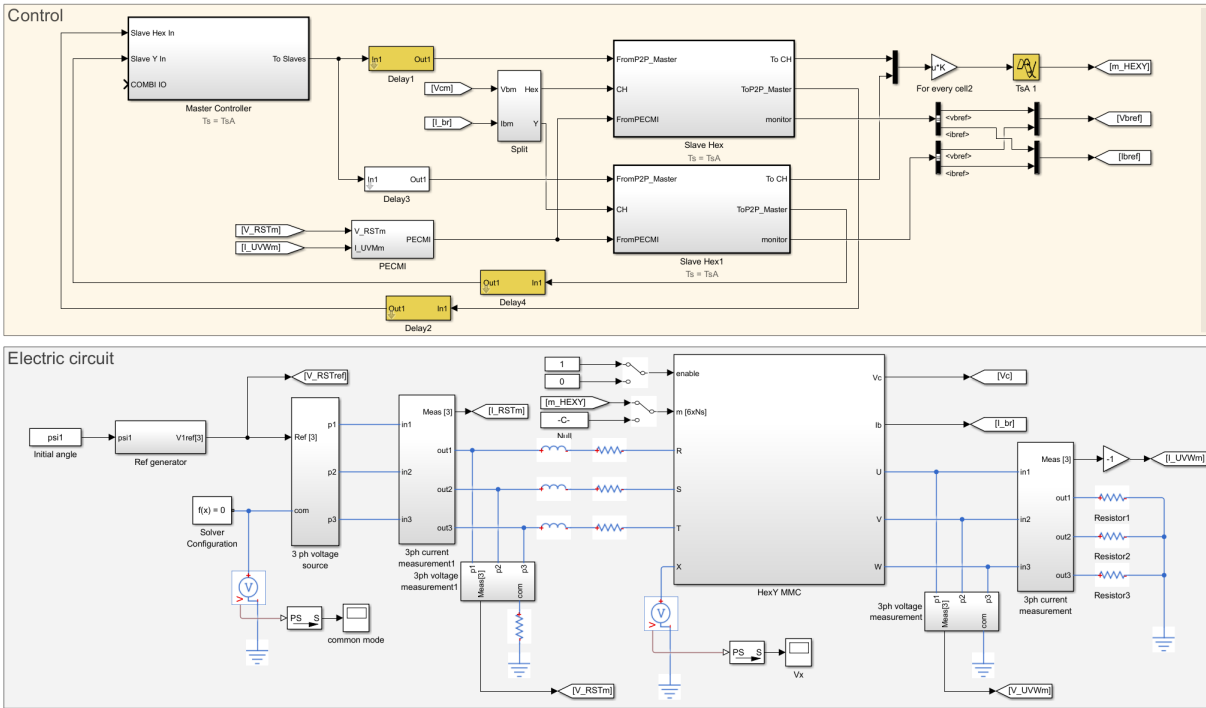
Figure 8.1. Simulation model of Hex-Y converter. Yellow section includes control. Gray section includes electric circuit.

is constant and equal zero. In case of reactive power compensation (e.g. due to voltage sags), non-zero reference can be generated what is explained in Chapter 9.
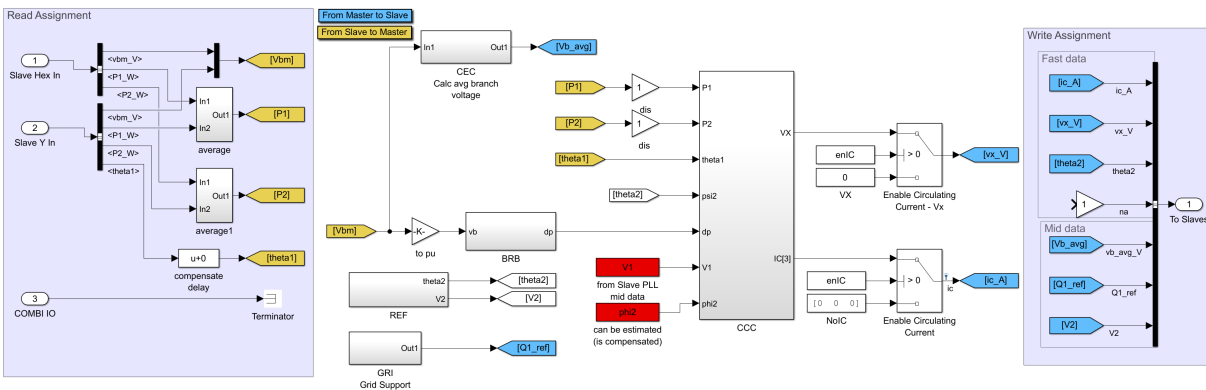
Figure 8.2. Master Controller.

Figure 8.2 shows master control module. Blocks marked with red has different implementation than in a real system. Its influence on simulation results is however negligible.

Additionally, blocks representing communication between Master and Slaves are highlighted with a different color. Blue blocks represents signals sent and yellow blocks represents signals received by Master Controller.

Figure 8.3 shows structure of the Slave controller. Simulation model contains two slave subsystems. They are identical except the blocks with magenta background on the picture. In case of those blocks, its settings must be changed to refer either to branches 1-6 (in case of Hex) or 7-9 (in case of Y).

Other colors has the same meaning as for Master Controllers.
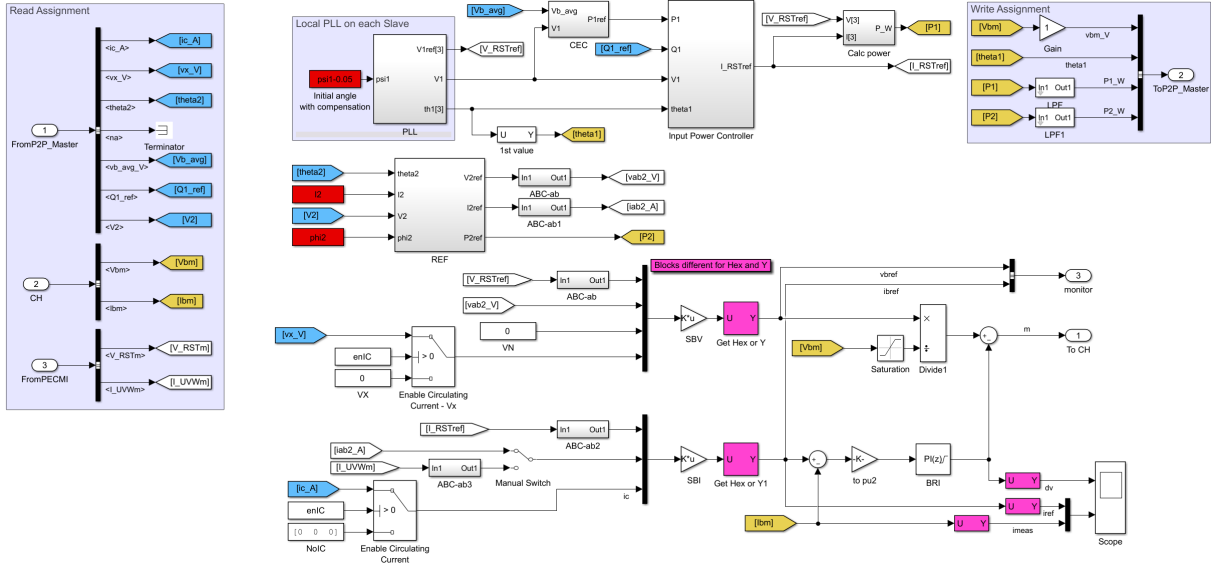
Figure 8.3. Slave Controller.

Slave Controller contains following modules: cascade of PLL, CEC and Input Power Calculation blocks which generates reference input current. REF module calculates three-phase references at converter's output. Slave contains also voltage and current mapping modules (SBV, SBI) and current controller (BRI). As in the Master Controller, communication modules are also present.

8.1.2. Electric Circuit Section

Electric circuit is built with 3-phase voltage source, passive components (resistance, inductance), converter model and measurement units. Simplified one-line diagram is presented on the Figure 8.4.
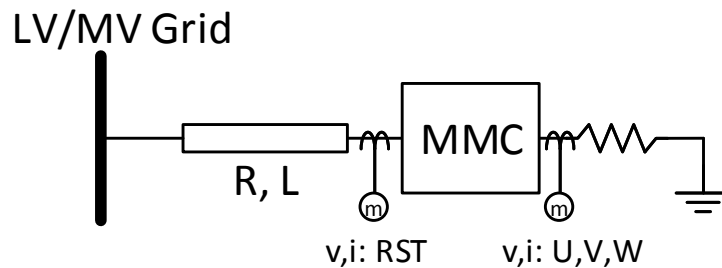
Figure 8.4. One line diagram of electric circuit.

Hex-Y converter is built with nine branches connected as it is proposed in the Thesis. Figure 8.5 shows circuit schematic.
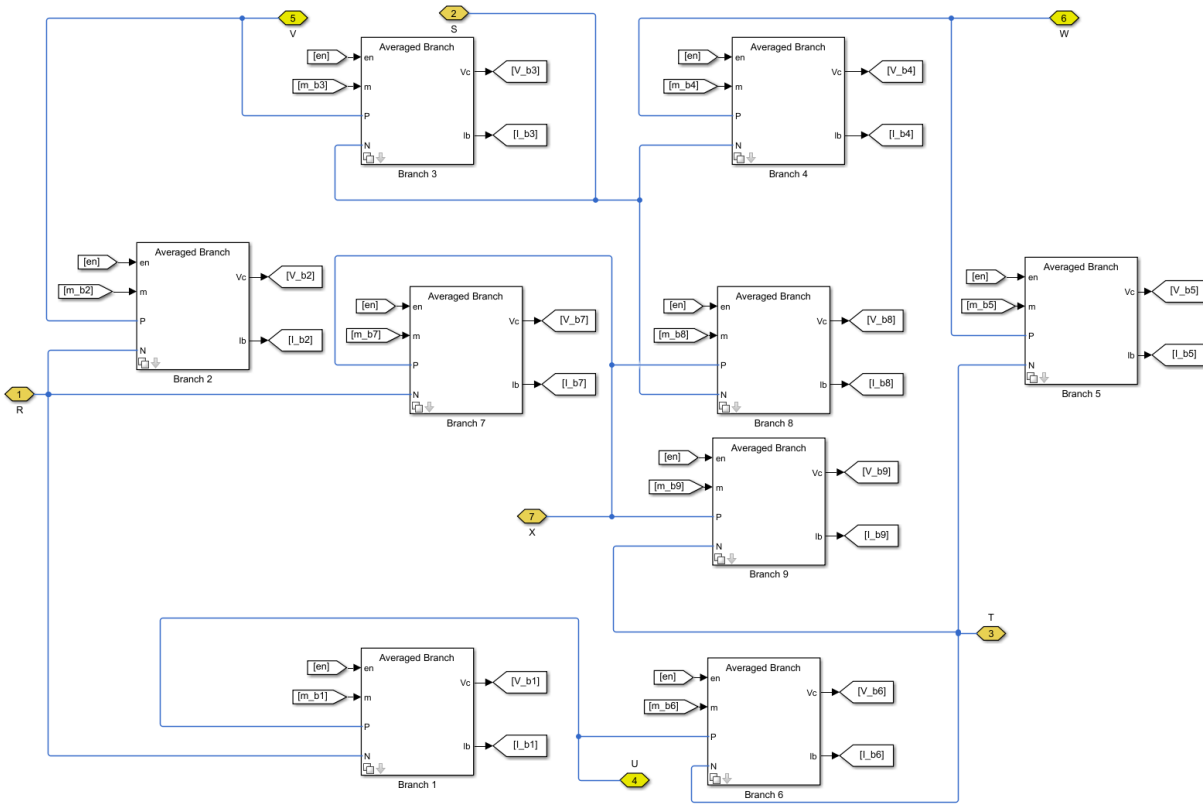
Figure 8.5. Hex-Y Conveter Model.

Each branch is modeled as a resistance, inductance and PEBB module which is modeled as it has been explained in Chapter 6.

To be able to run simulation on the cell level and branch averaged level, a branch system has been designed as a configurable. It means there are two different models which can be switched. Figure 8.6a shows an averaged branch model and Figure 8.6b shows a cell model built with three PEBBs for sake of simplicity. In practice, 6-cell model is being used.

8.1.3. M3C Converter Model

Simulation model for M3C converter topology is presented on the Figure 8.7. Model structure is identical as for Hex-Y converter. Two main sections are control and electric circuit.

Control section contains two subsystems representing two AC800 PEC controllers. As M3C model is not intended to be implemented on the physical control hardware, functionality from Master Controller has been moved to Slave what reduces system complexity. Simplified structure without Master controller is feasible for required simulations scope.

Similar to Hex-Y, PECMI module model and system delays are present in the control loop.
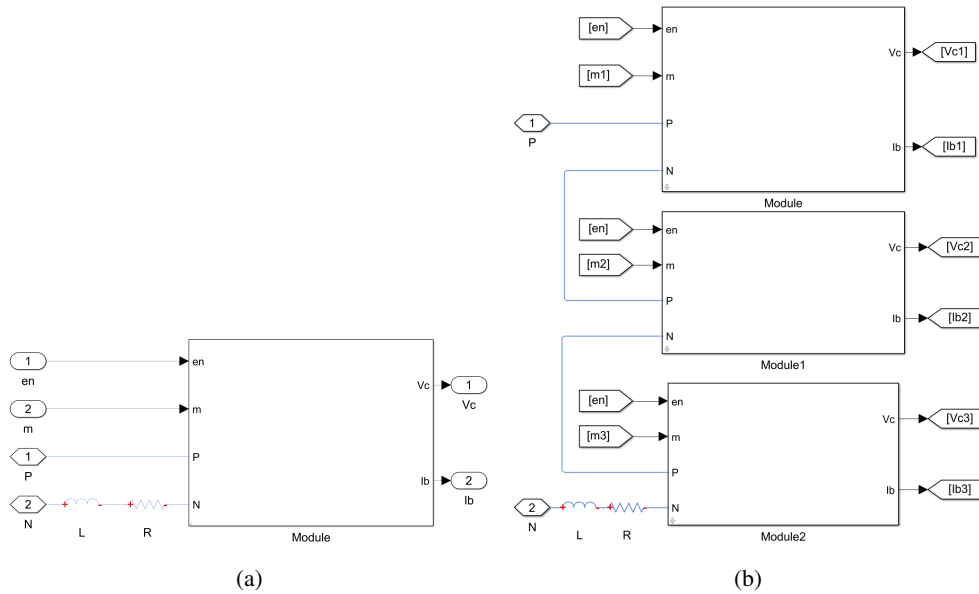
Figure 8.6. Branch averaged (a) and cell level (b) simulation model.

The control algorithm has been realized as it has been proposed in [65]. Both Slave controllers includes control for two three-branch converter sections (called sub-converters).

Figure 8.8 presents Slave controller module. It is built with two separate sub-converter controllers and components responsible for communication with peripheral modules.

Each sub-converter is identical. Its design is shown on the Figure 8.9. Study results for proposed control algorithm can be found in [65] and [82].

Electrical part of the converter is built in the same way as for Hex-Y. The only difference is inter-connection between branches which is presented on the Figure 8.10. Branch is modeled with the same blocks as for another model.

8.2. Test Results

Both models has been tested in given test cases which are being summarized in the Table 7.4.

8.2.1. SIM-020 Branch Current Controller

In this test case, branch current control capability for Hex-Y model is checked. In the first step, branch current controller has been designed as it is described in Chapter 5.3. Next it was tested in open circuit system with forced capacitor voltages to see if controller follows the reference. Next, AC grid and load has been connected. In that case, current flow from grid to the load can be observed.

Because capacitor voltages are forced to constant, nominal voltage all the time, balancing modules are not influencing BRI module. Those modules are enabled in the next test case.
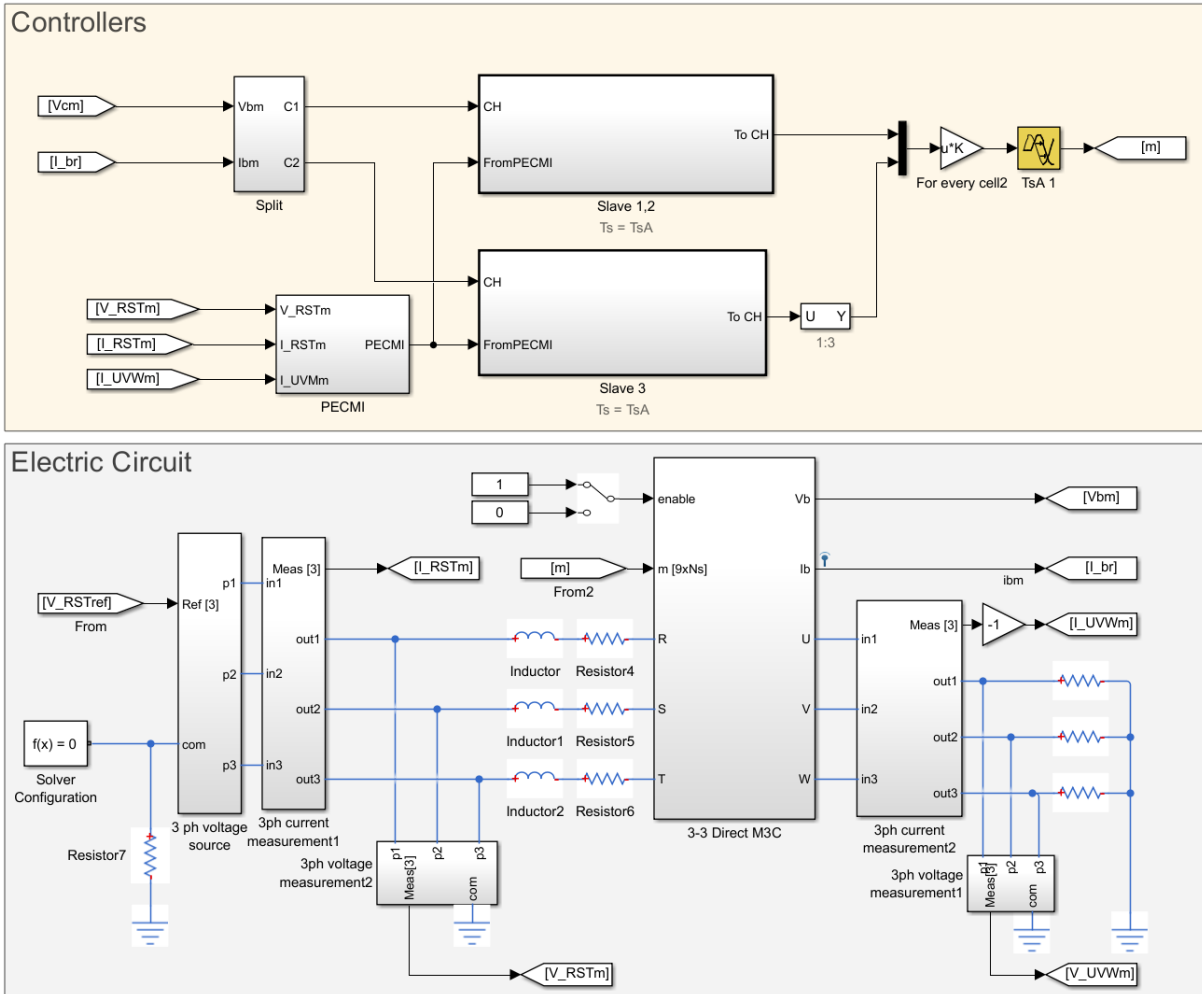
Figure 8.7. Simulation model of M3C converter.

Maximum proportional gain according to Table 5.2 is 20 (sample time $125 \ \mu s$, branch inductance $1.25 \ mH$). Based on simulation results, fine tuning of the controller started with gain equal 2. Finally, proportional gain equal 0.9 has been chosen. Figure 8.11 presents simulation results. It can be noticed that current follows the reference.

8.2.2. SIM-030 Check Balancing Modules

In this test case, converter and branch energy balancing modules can be checked. Low-level cell balancing mode test is not possible as in practice it is implemented on the cell while simulation module is focused on high-level control. Cell balancing has been checked in corresponding test case in Real-Time model.

For that test, initial capacitor voltages are being set to non-equal initial voltage to check branch balancing. Also, average branch energy is below nominal converter energy. Therefore, converter balancing module will take its part.
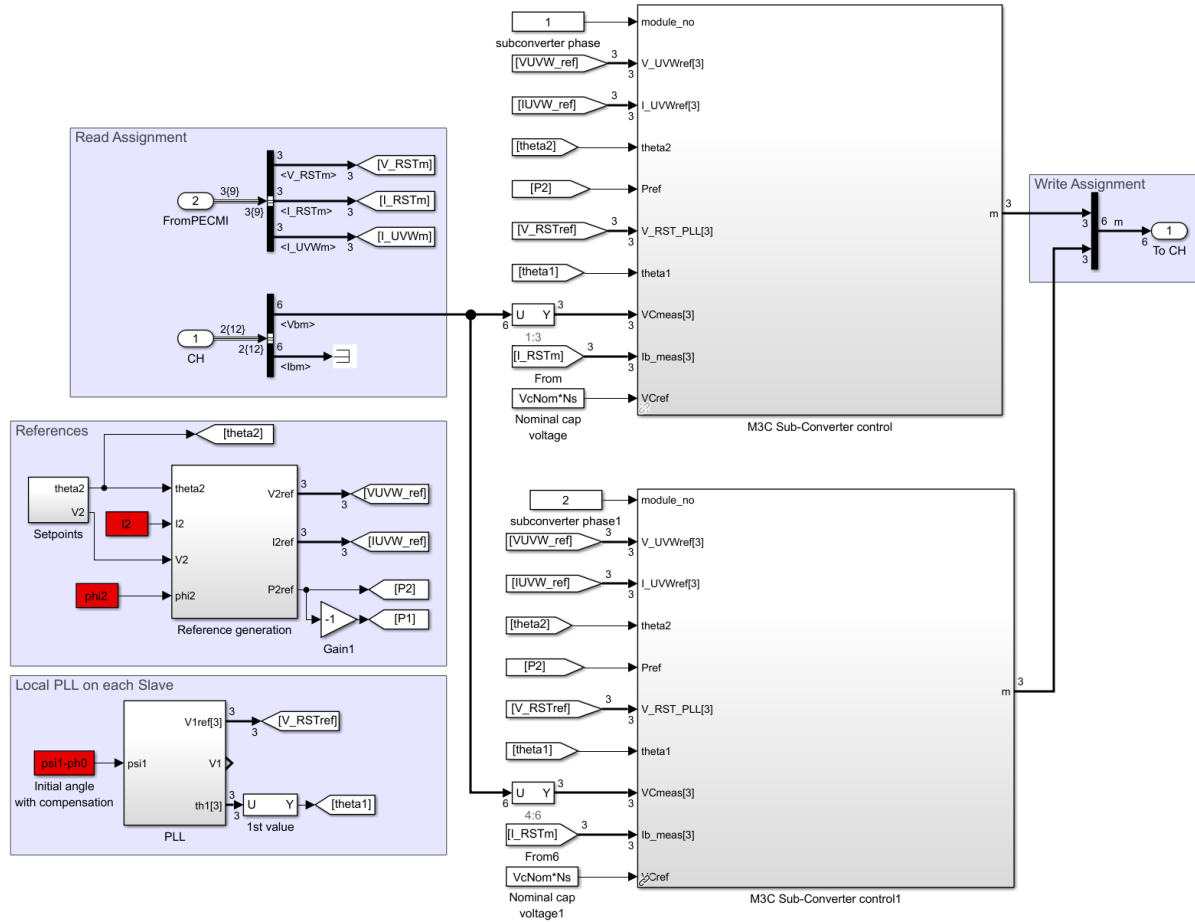
Figure 8.8. Slave Controller module.

Controller tuning was done in two steps. In the first step, converter energy controller has been disabled and only branch energy controller was used. Initial capacitor voltages were different, but its average was equal nominal voltage. Experimental stability region for BRB proportional controller has been defined ($Kp \leq 0.15$).

In the next step, capacitor voltages were randomized with lower average value. In that case, enabled CEC module has to charge converter to its nominal voltage/energy level. As pass/fail criteria for that test following conditions were taken: branch voltages must reach equilibrium point, voltage overshoot should not exceed 10 % of nominal voltage and charging from 50 % of nominal voltage should not take more than 1 s.

Results for tuned controllers are presented on the Figure 8.12. Pass criteria has been met.

8.2.3. SIM-04x Output Voltage Generation

As all basic functional modules has been verified, operation with a load can be studied. This tests are focused on steady state at given operation points. Simulation results from Hex-Y and M3C will be
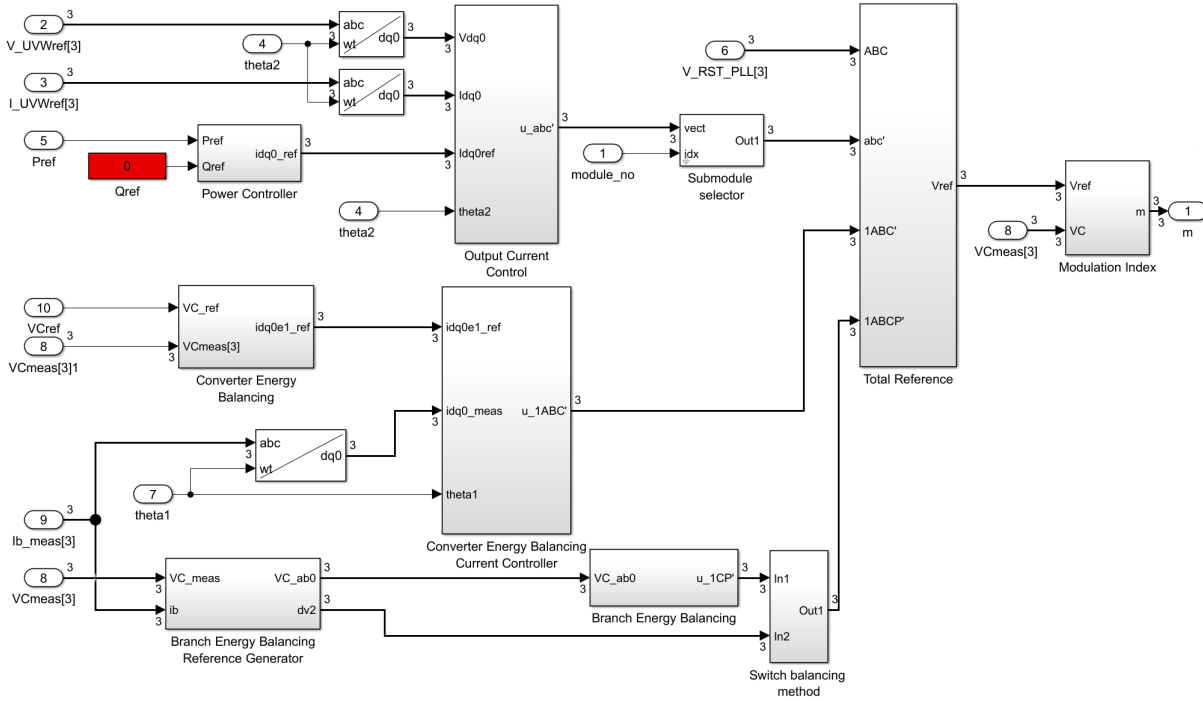
Figure 8.9. Sub-converter control loop.

compared. In total, six operation points are checked within this test case (see Table 7.4). Extra operation points for resistive load are also checked to complete converter characteristics.

First target is to prove that both converters are reaching steady state. The second target is to check converters performance. Two key quantities taken into account are capacitor voltage ripple and branch current. Similar analysis but for a different load has been presented in [82]. First test cases (SIM-040 to SIM-044) are using generator characteristics. Two extra tests (SIM-045 and SIM-046) shows converter performance with resistive load.

Table 8.1 presents simulation results for all test cases.

Table 8.1. Capacitor voltage ripple and branch currents for Hex-Y and M3C. All quantities in p.u. unless it is specified otherwise.

		Hex-Y			M3C		
Test ID	$f_2[Hz]$	$V_{C,rip}[\%]$	$I_{b,RMS}$	$I_{b,max}$	$V_{C,rip}[\%]$	$I_{b,RMS}$	$I_{b,max}$
SIM/M3C-040	0	0.75	0.021	0.056	0.06	0.004	0.005
SIM/M3C-041	3	1.08	0.043	0.168	0.25	0.007	0.015
SIM/M3C-042	6	2.07	0.130	0.338	2.11	0.079	0.159
SIM/M3C-043	9	3.98	0.432	0.818	12.21	0.267	0.477
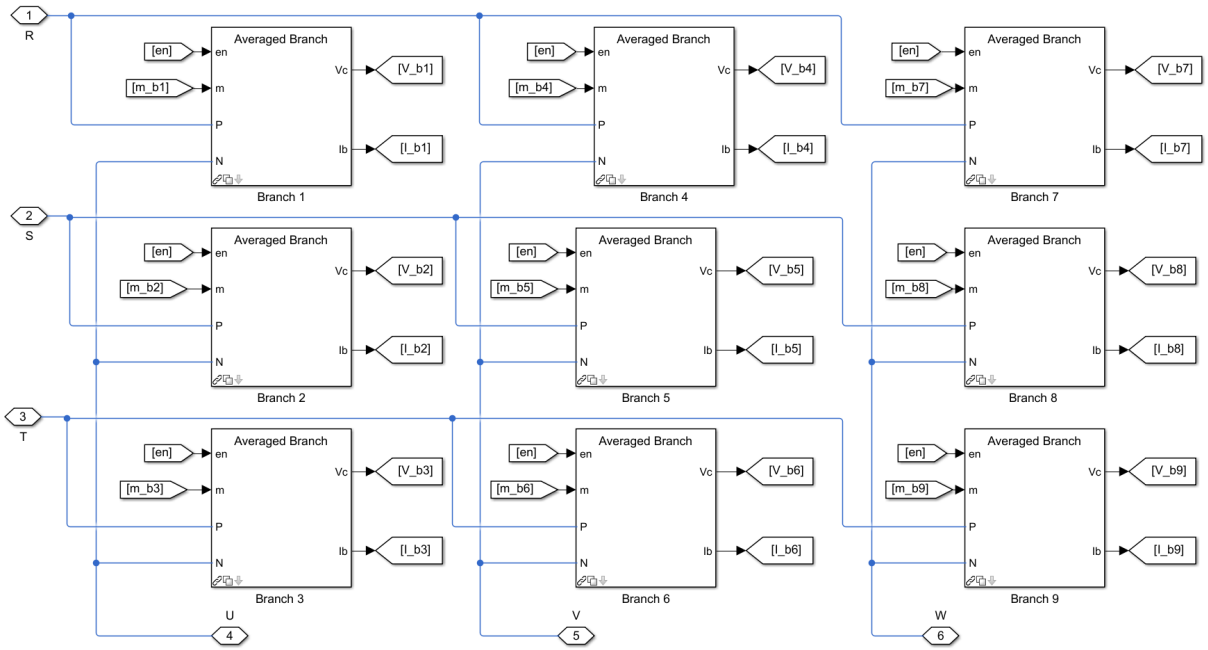
Figure 8.10. M3C Converter Model.

To highlight Hex-Y converter features, tests for resistive load has been also performed. In those test, resistance is equal 65.2 Ω what corresponds to generator impedance at 4.5 Hz. Table 8.2 contains simulation results.

Based on measurements, a graph representing converter characteristics has been built. As for both converters, operation points are identical, comparison is reasonable.

Figure 8.13 presents capacitor voltage ripple for both converter types. As it can be noticed, for a generator type, M3C converter capacitors has lower voltage ripple up to 6 Hz. Hex-Y has much better performance for higher frequencies. In general, Hex-Y characteristics is more flat than M3C. For a full frequency range, voltage ripple is between 1 and 4 Hz.
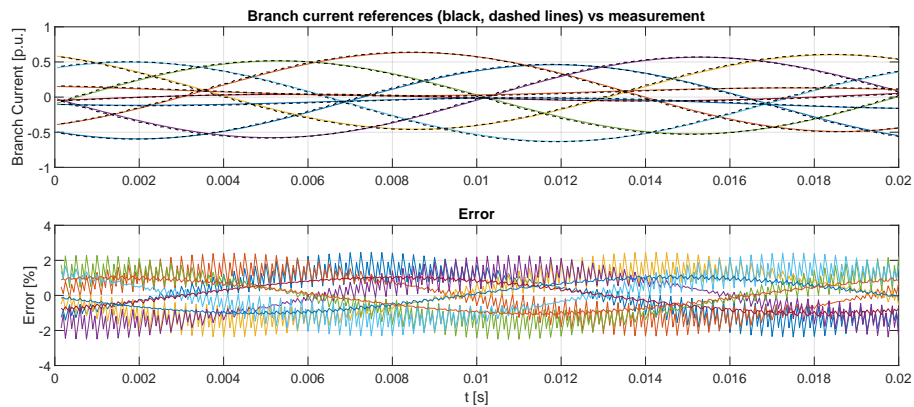
Figure 8.11. Top plot: Branch current references (black, dashed lines) vs branch current. Bottom plot: error
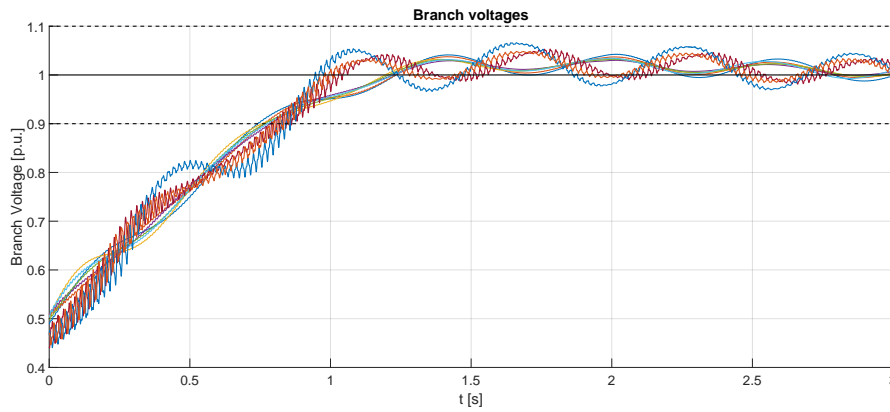
Figure 8.12. Total branch capacitor voltages. Black line shows branch nominal voltage. Dashed lines represents $\pm 10\,\%$ levels

Table 8.2. SIM-04x. Capacitor voltage ripple and branch currents for Hex-Y and M3C. All quantities in p.u. unless it is specified otherwise.

Test ID	$f_2[Hz]$	Hex-Y			M3C		
		$V_{C,rip}[\%]$	$I_{b,RMS}$	$I_{b,max}$	$V_{C,rip}[\%]$	$I_{b,RMS}$	$I_{b,max}$
SIM/M3C-045	0	2.16	0.107	0.430	5.31	0.218	0.578
—	1	2.18	0.102	0.397	4.19	0.189	0.421
—	2	1.79	0.099	0.318	2.01	0.069	0.159
SIM/M3C-046	3	1.87	0.095	0.300	1.52	0.047	0.110
—	4	1.91	0.093	0.296	1.30	0.042	0.090
—	5	1.94	0.098	0.297	1.38	0.047	0.097

If resistive load is used, Hex-Y characteristic is even more flat than for generator. In that case Hex-Y performance is much better also for low frequencies (from 0 to 2 Hz).

Lower capacitor voltage ripple means higher capacitor bank lifetime. On the other hand, branch currents defines level of losses in a converter. Figure 8.14 shows converter characteristics. It can be noticed that in case of generator, Hex-Y converter has higher branch currents than M3C converter due to the fact that for Hex-Y topology circulating currents are required to provide energy balance between the branches.

However, for low frequencies with resistive loads (i.e. non-zero power flow at zero frequency), both capacitors voltage ripple and branch current are lower than for M3C topology. Therefore it can be assumed that Hex-Y converter is more feasible for applications with that operation point. Example applications are lifts, rolls or mills.

Capacitor voltage and branch current waveforms for Test Case no. 43 are presented on the Figure 8.15. Hex-Y has lower capacitor voltage ripple, but higher branch current. It can be also noticed
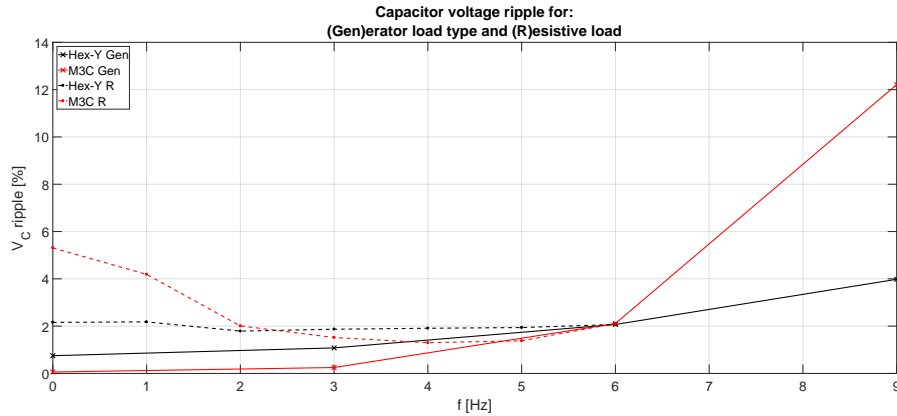
Figure 8.13. Measured capacitor voltage ripple as function of output frequency for generator (solid) and resistive (dashed) load type. Hex-Y black, M3C red

that M3C with lower branch current does not satisfy $\pm 10\%$ tolerance of the voltage ripple for that operation point.

8.2.4. SIM-05x Reference Step Change

Following tests checks system dynamic response for operation point change. The operation point is defined by frequency, but it must be taken into account that for different frequencies, load impedance is changed as well. Figure 7.2b shows the load characteristics.

Tests are performed for a step change with rise/fall time limit set to $100\ Hz/s$. Therefore, change for the full range, i.e. $0 - 9\ Hz$ takes $0.9\ s$. Following limit is implemented only on the impedance model, therefore frequency and magnitude change of generated voltage should be immediate.

For that test, branch capacitor voltages, branch currents, generated voltage and input current are being measured and compared for Hex-Y and M3C converter.

For branch currents, 20 % overshoot is allowed (max branch current should be below 1.2 p.u.). For capacitors, its voltage should remain in a range 0.8-1.2 p.u.

Table 8.3 contains summary of simulation. Results shows that both converters meet given requirements. Hex-Y converter has more dynamic response of branch balancing module: reference change has no significant influence on capacitor voltage. Unfortunately it affects branch current which is higher than for M3C. In case of M3C converter, it can be observed that branch capacitor voltage fluctuations are much higher, however branch current is not changed significantly during the reference change.

On the Figure 8.16, branch voltages and currents for both converters are presented. Figure 8.17 shows output quantities for Hex-Y converter. It can be observed, that generated voltage follows given reference and on the input side no significant transient current is being observed.
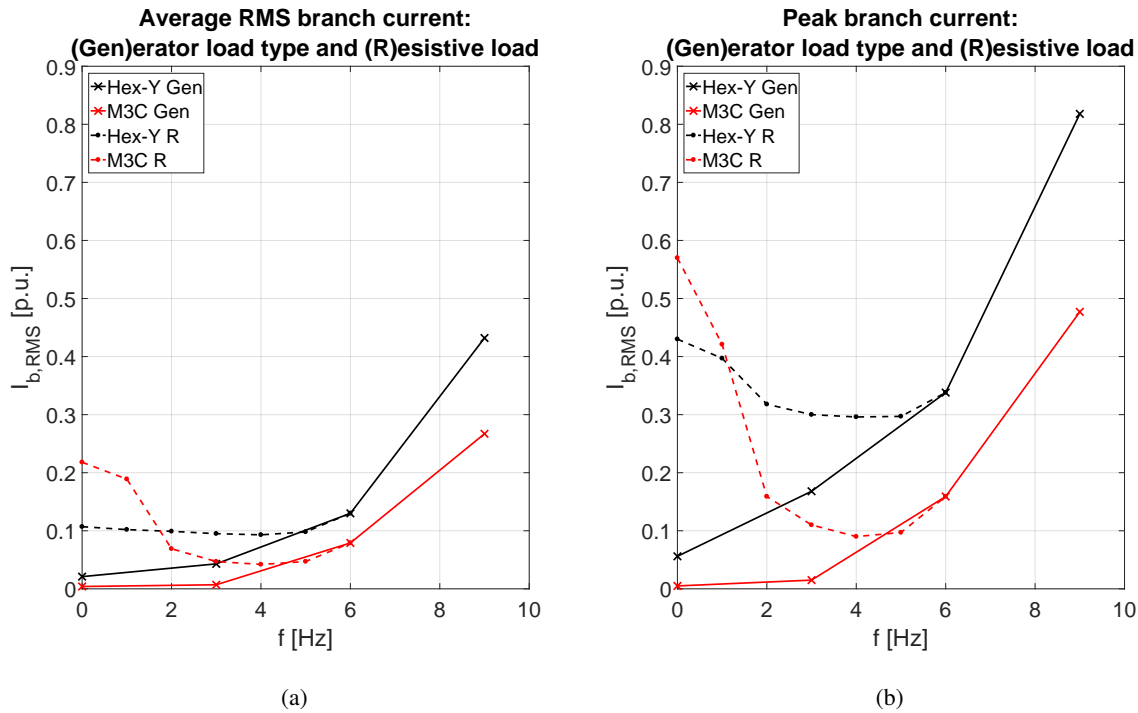
Figure 8.14. Average (a) branch RMS current and peak (b) branch current for Hex-Y (black) and M3C (red).

Table 8.3. SIM-05x. Capacitor voltage ripple and branch currents for Hex-Y and M3C. All quantities in p.u. unless it is specified otherwise.

		Hex-Y			M3C		
Test ID	$f_2[Hz]$	$V_{C,min}$	$V_{C,max}$	$I_{b,max}$	$V_{C,min}$	$V_{C,max}$	$I_{b,max}$
SIM/M3C-050	$0 \to 9$	0.98	1.04	1.15	0.85	1.02	0.56
SIM/M3C-051	$9 \to 0$	0.95	1.03	1.14	0.95	1.13	0.50

8.2.5. SIM-20x Reactive Power Provision

Tests numbered SIM/M3C-20x checks converter behavior while non-zero reactive power is requested. Following functionality is required by grid support module which provides reactive power in case of grid transients as voltage dips or swells.

Test cases check reactive power provision capability during normal converter operation. Different operation points has been checked to confirm that converter is able to support given function. Simulation results for both: Hex-Y and M3C converter are summarized in this section.

Each test was performed by step reference change from $0\ MVAr$ to maximum, $1.0\ MVAr$ at $t = 0.05\ s$ as it is specified in Table 7.4. Given reference is present for $300\ ms$ and set back to 0 afterwards.

Figure 8.18 presents input waveforms (voltages and currents) for a test case with 0 Hz output frequency (SIM/M3C-200) and 9 Hz output frequency (SIM/M3C-202). Line currents are decoupled for
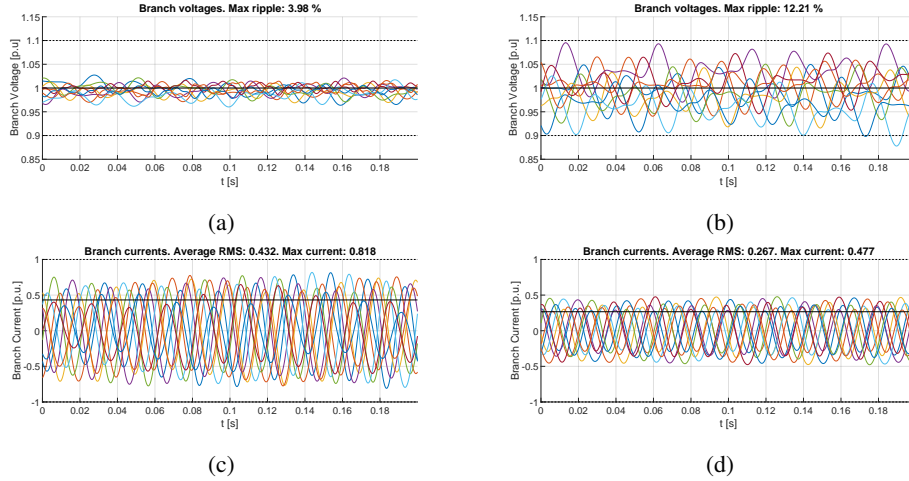
Figure 8.15. Capacitor voltages for Hex-Y (a) and M3C (b) converter. Branch currents for Hex-Y (c) and M3C (d) converter. Test 043 - steady state at 9 Hz output frequency.

active (d) and reactive (q) component by use of Park transformation. For both cases, input voltages looked similar so only SIM result are shown. For comparison, input currents for both SIM and M3C are presented. On presented waveforms, it can be observed that for non-zero reference, reactive power is being provided as requested. During reactive power provision, active current is being limited what was explained in the Section 7.4.5. It can be also noticed, that for given control loops and controller parameters, Hex-Y is more dynamic i.e. setting time is shorter that for M3C converter.

For performed simulations, capacitor branch voltages has been measured. Voltages are kept constant for each operation point: voltage ripple didn't exceed $10\,\%$ of nominal voltage. For cases SIM/M3C-202, a voltage drift (discharge) can be observed. Figure 8.19 presents capacitor voltages for test cases. Cells are being discharged as active power cannot be provided due to introduced apparent power limitations - see Equation (7.3). It was assumed that reactive power has priority: in other words, reactive power will limit maximum active power which can be delivered. The limit is defined by Equation (8.1). For maximum reactive power reference, there is no margin for any active power flow. For no limitation, if the reference is exceeded, overcurrent will be observed.

$$P_{ref} \leq \sqrt{S_{nom}^2 - Q_{ref}^2}$$

(8.1)

Cells will be charged back to nominal voltage when transient is finished and lower reactive power reference is present. In practical cases, grid codes defines for how long given reactive power must be provided. To confirm that converter can meet those requirements, tests with ID SIM-3xx are being performed.

In given tests, branch currents were also measured. Figure 8.20 presents simulation results for test case SIM/M3C-200. The key difference between M3C and Hex-Y can be noticed: for Hex-Y converter, reactive power is provided only by Y-branches (7-9) as it was initially assumed. In case of M3C converter,
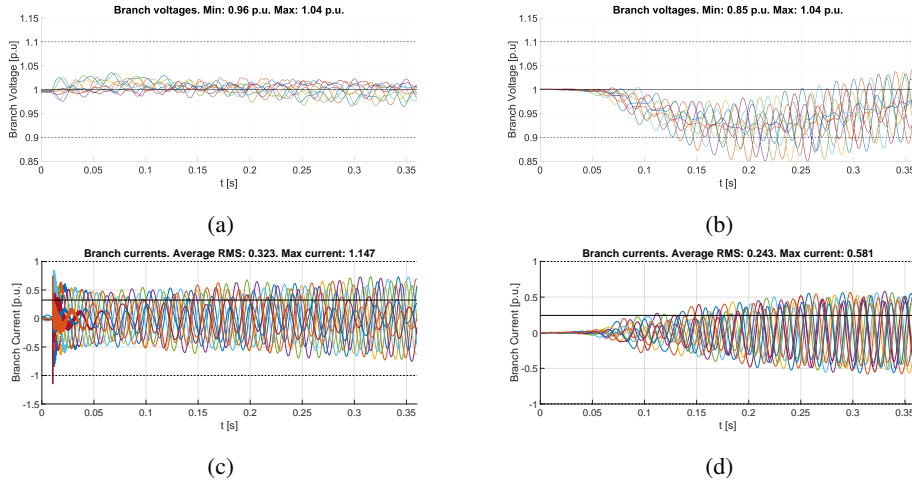
Figure 8.16. Capacitor voltages for Hex-Y (a) and M3C (b) converter. Branch currents for Hex-Y (c) and M3C (d) converter. Test 050 - reference step change from 0 to 9 Hz at t=0.01 s.
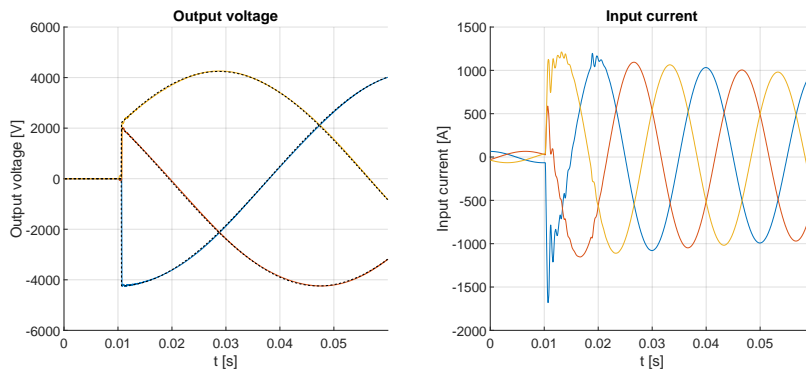
Figure 8.17. Generated output voltage and input grid current. Test 050 - reference step change from 0 to 9 Hz at t=0.01 s.

reactive power is symmetrically provided by all nine branches. For both converters, nominal branch current is within given limits.

8.3. Summary

Simulation results proved that Hex-Y converter can work in given operation point. Its performance has been compared with state-of-the-art M3C converter which is built with the same number of branches. It can be assumed that pricewise and volume wise both converters are similar. Therefore converter behavior for given operation point will define which topology fits better.

From simulations, it can be observed that Hex-Y converter has better performance for low frequencies in case of non-zero load as it is summarized on the Figure 8.13 (dashed lines). For other operation points, Hex-Y converter however has higher branch currents what is summarized on the Figure 8.14. This will cause higher losses in the steady state.
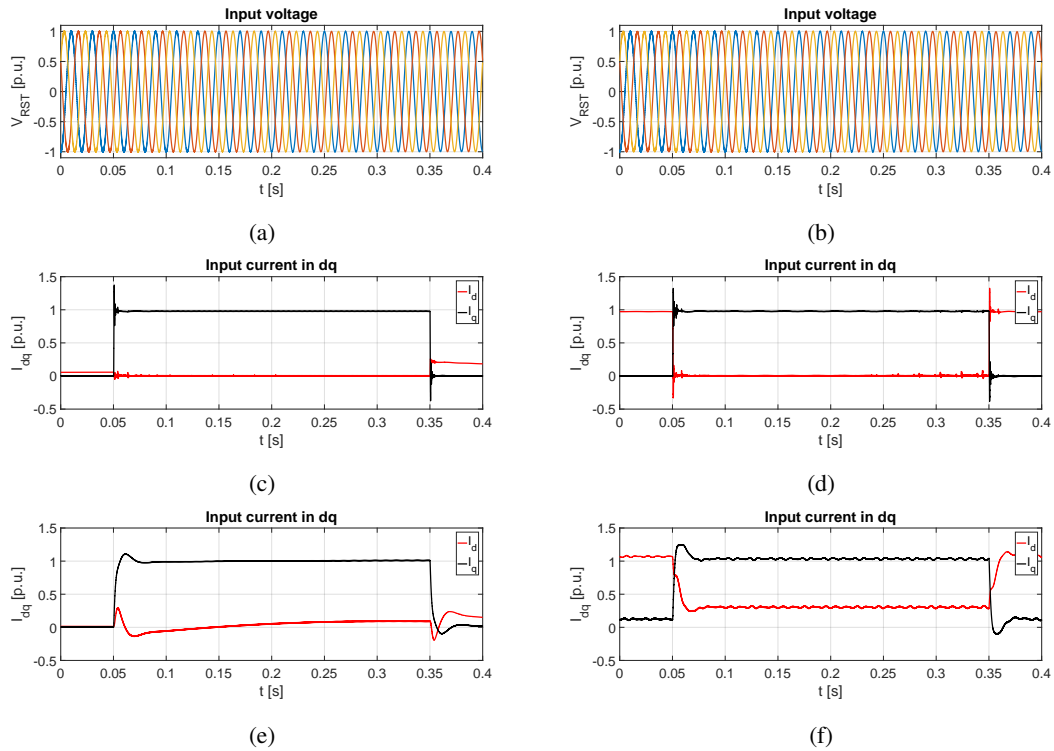
Figure 8.18. Input voltages for test case SIM-200 (a) and SIM-202 (b) and input currents for test cases: SIM-200 (c), SIM-202 (d), M3C-200 (e), M3C-202 (f).

On the other hand, its dynamic response for step reference change is better than M3C. Capacitor voltage ripple is lower than for M3C in given test conditions. Therefore it can be assumed that for systems with required high dynamic response, Hex-Y could be also an interesting solution worth deeper investigation.

Simulations of Hex-Y shows also that given topology is able to provide reactive power. This functionality will be further investigated in Chapter 9 which is focused on grid support capabilities.
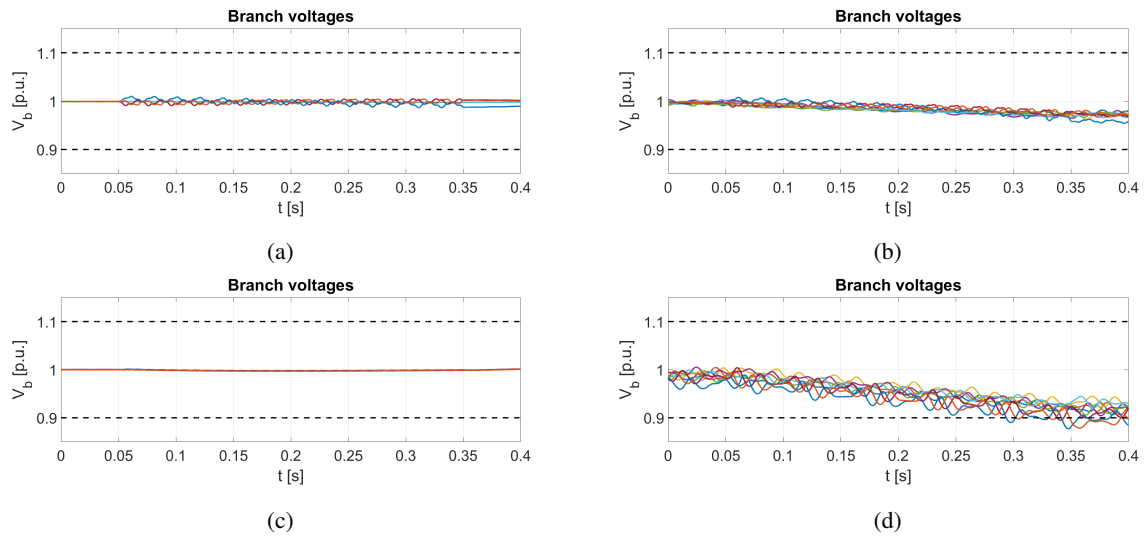
Figure 8.19. Averaged branch capacitor voltages for test cases SIM-200 (a), SIM-202 (b), M3C-200 (c) and M3C-202 (d).
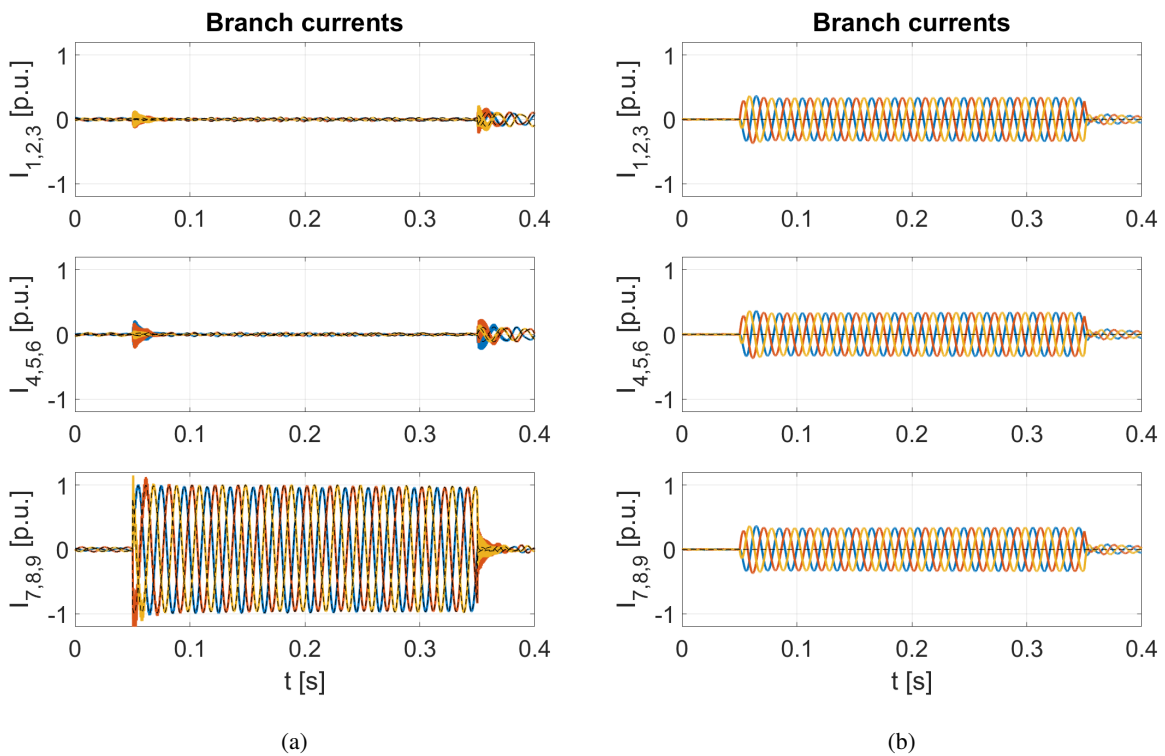
Figure 8.20. Branch currents for a test SIM-200 (a) and M3C-200 (b). Reference in black, dashed lines.

9. Grid Support

Electrical devices connected to the power grid must meet given requirements starting from EMC emission, through safety regulation to functional requirements. In case of power devices, grid codes must be meet to provide that power grid remains stable and fully operational in case of disturbances. Grid codes are standards, requirements and design recommendation specific for a country or region (as e.g. European Union). When the device is designed to operate on given market, grid codes must be met, what means that control algorithm design must take into account given requirements.

Within EU, power generation devices must follow Commission Regulation (EU) 2016/631 [93]. It contains grid codes and information about determination of significance (types A through D) - defined by power levels. Converter presented in the Thesis will fail into type C which covers devices with connection point below $110\ kV$ and maximum capacity between 1 and $50\ MW$[1].

Converter behavior during abnormal grid conditions should not affect grid stability. In fact, power converter is able to improve or make worse the grid quality depending on its design. Grid codes „tells" how a device can help during the transient and how to support recovery afterwards.

In the simplest case, the device can disconnect from the grid when anomaly is detected. However if this will be reaction of all high power converters, it would lead to the chain reaction and finally: blackout. Risk of lost significant power volume will cause also impossibility of recovery without synchronous generators. Therefore, grid codes defines that significant devices (type B to D) must remain active during given transients. Moreover, during given events, they must provide grid support especially to reduce the risk of loosing frequency stability [94, 95].

Grid codes defines minimum time when the converter must remain connected during faults as voltage dip, swell or frequency drift. Additionally, grid support capability realized by reactive power injection are being defined.

In following chapter, converter behavior during voltage dip event is being investigated. Grid support module which detects an event and acts accordingly has been added to the control algorithm. Following functionality is so called Low Voltage Ride Through (LVRT). According to EU regulation, given functionality is required for all generators type B and higher (so for all generators with power above or equal $1\ MW$).

---

[1]Limit defined for Continental Europe

9.1. Low Voltage Ride Through

Within a grid code for LVRT, three key quantities are defined:

1. how long during the transient, converter must remain operational,

2. how much reactive power must be provided during the transient,

3. how fast, after fault clearance, converter should be back at full power.

Figure 9.1a presents LVRT profile defined in the EU regulation. It defines for how long, the converter should be operational as a function of dip depth. Transient starts at $t = 0$. For example, for voltage dip in the range between $U_{ret} - U_{clear}$, converter must remain connected for at least t_{clear}. For voltage dip above U_{rec2} converter must remain operational all the time.

Numerical values of time and voltage levels depends on significance type (A-D) and converter type (synchronous power-generating and power park modules). For power park, type C LVRT profile has been presented on the Figure 9.1b.

Figure 9.1b shows LVRT profile for the test case which will be investigated.
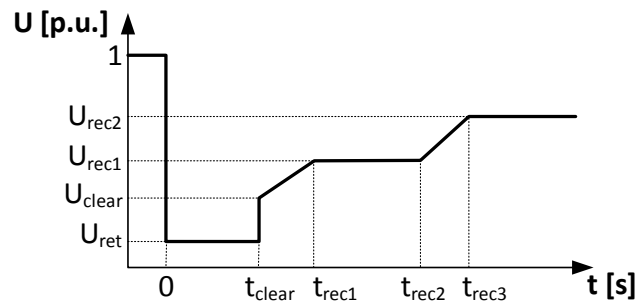
(a)
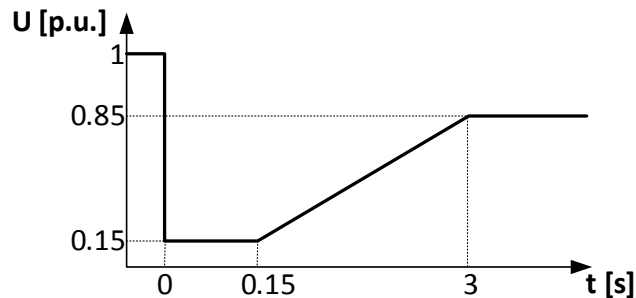
(b)

Figure 9.1. Low Voltage Fault Ride Through profile - generic (a) and specific for given test case (b) [93]

To improve grid stability during the fault, converter shall provide reactive power. Amount of delivered power depends on the dip depth. EU directive however does not define specific number. Given information can be found in the grid codes of specific countries. For example, widely used German BDEW grid code [96, 97] defines linear dependency between dip depth (in p.u.) and required reactive power amount (in p.u. when 1 is nominal power).

Proportional coefficient, called k-factor defines line slope. It takes values from 0 to 10. Usually, value $k = 2$ is chosen [94]. Additionally to k-factor, a range in which reactive power provision is defined as $\pm 10\%$ of nominal voltage range. Figure 9.2 show reactive power profile which will be used in the tests.
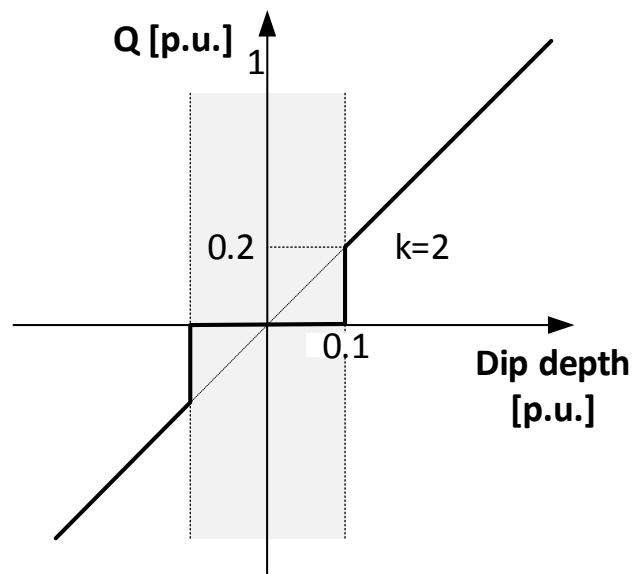
Figure 9.2. Reactive power provision curve. In the gray area reactive power provision is not required.

After fault, recovery time defined in the grid codes. In BDEW it is defined as minimum rise time equal 20 % of P_{nom} per 1 s [96, 97]. It gives 5 s for full operation recovery. For Great Britain and Ireland time is defined as $0.5 - 1$ s depending on the dip depth [98, 99].

For given grid codes for EU, test cases starting with digit 3 has been defined (see Table 7.4). Given tests checks if converter remain operational for given time defined by LVRT profile. During the test, a voltage dip with specific depth and time is generated. Converter parameters as averaged branch voltages during the transient are measured. Converter power (active and reactive) is monitored. System behavior during the transient and afterwards (recovery) is checked. Additionally, it will be verified if converter is tripped for voltage dip which remain for longer time than maximum defined by the LVRT profile.

9.2. Simulation Results

LVRT capability of the converter has been verified for two boundary operation points i.e. deep voltage dip down to 0.15 p.u. for 150 ms (RT-301) and shallow voltage dip to 0.85 p.u. for 3 s (RT-302). Additionally operation at lower grid voltage (0.9 p.u.) for a long time (4 s) has been checked (RT-303). All tests were performed with no-load condition i.e. there were no power from the generator to cover converter losses.

For each test case it was confirmed that converter was not tripped. Active and reactive power during and after fault are shown on the Figure 9.3. It can be observed that for tests RT-301 and RT-302 reactive power was provided. For test RT-303 reactive power provision was not required as it is shown on the Figure 9.2.
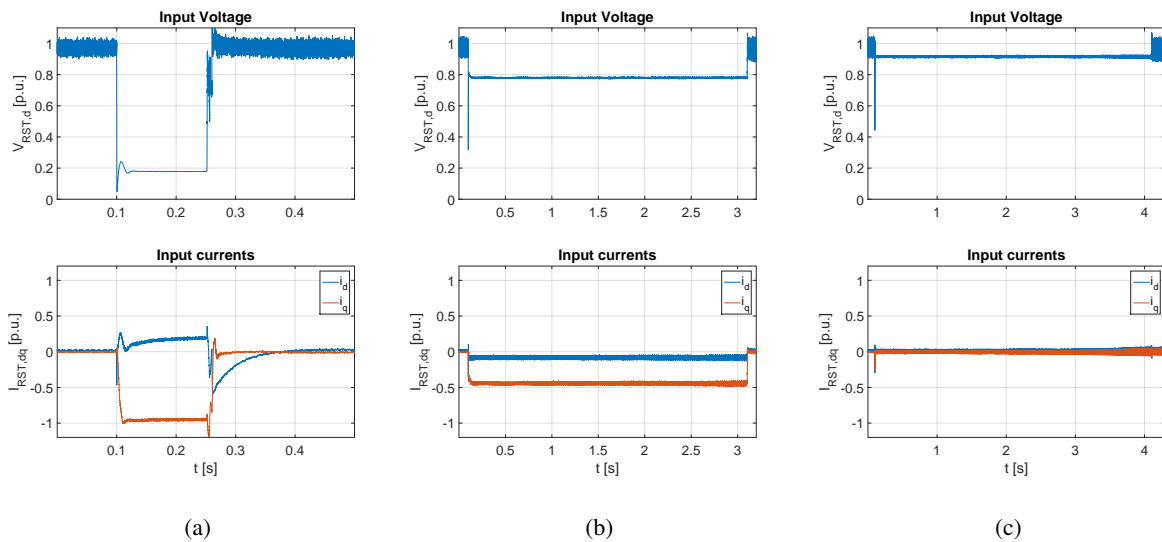
Figure 9.3. Inptut voltage magnitude (top) and active-reactive currents (bottom) for test cases RT-301 (a), RT-302 (b), RT-303 (c). Fault starts at t=0.1 s.

Even though converter functionality during the fault was confirmed it doesn't mean the converter is able to provide given functionality. To prove that converter is working correctly, also branch capacitor voltages has to be checked. Figure 9.4 shows averaged branch capacitor voltages for given test cases. It can be observed that capacitor voltages remains at equilibrium state during the fault and afterwards. Additionally for a deep dip with active power limitation during the transient, capacitors are being charged to its nominal voltage after the fault.

9.3. Summary

Simulation results shows that converter is able to provide reactive power for given time defined by LVRT profile presented on the Figure 9.1. During the deep voltage dip, branch capacitor bank voltage
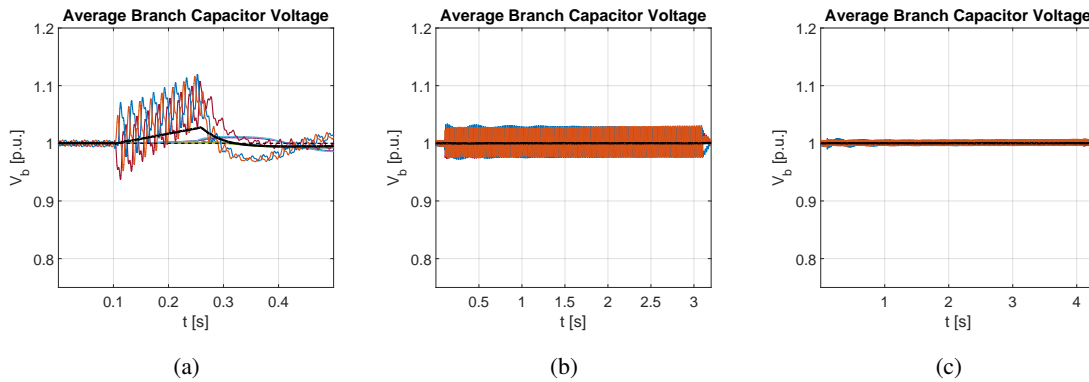
Figure 9.4. Averaged branch capacitor voltages for test cases RT-301 (a), RT-302 (b), RT-303 (c). Fault starts at t=0.1 s. Black line represents average of branch voltages in converter.

drift can be observed but voltages does't exceed 1.2 p.u. so it does not cause converter trip due to overvoltage transient (protection is set at 1.25-1.30 p.u.). For shallow voltage dips no any drift is observed.

For given test cases, reactive power as specified by profile on the Fig. 9.2 has been provided. For RT-301, nominal reactive power was provided as dip depth was above 0.5 p.u. For RT-302, dip depth 0.20 p.u. results with 0.40 p.u. reactive power for k-factor equal 2. In case of RT-303, no reactive current is requested.

Additionally for given test cases different operation points has been checked. Interesting results can be observed in case of drive operation of given topology. In that case, it can be observed that it is possible to provide reactive power also during nominal operation of the converter. Of course, capacitor bank discharge is being observed, but converter remains operational during and after the fault.

Figure 9.5a shows drive operation mode in case of 0.15 p.u. voltage dip (RT-301). For longer transients however, due to active power limitation, converter remains operational but capacitors are discharged to such a low level (see Figure 9.6b) it is not possible to generate valid output waveforms what can be observed on the Figure 9.7.
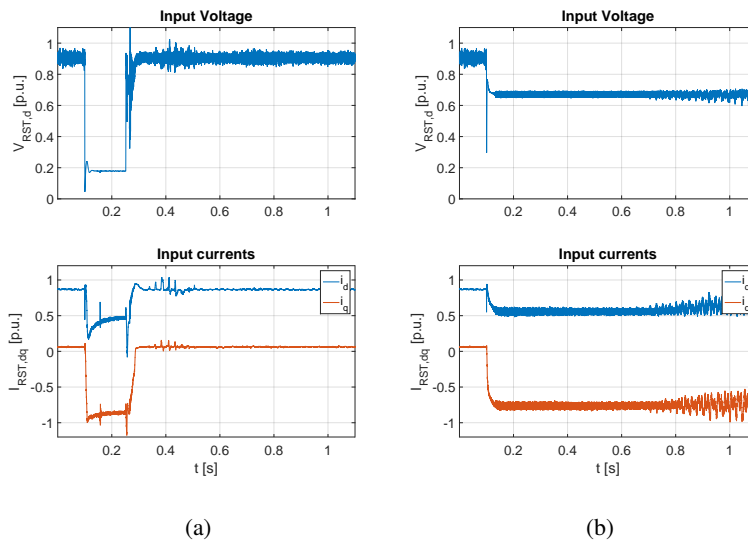
(a)   (b)

Figure 9.5. Inptut voltage magnitude (top) and active-reactive currents (bottom) for test cases RT-301 (a), RT-302 (b) in drive operation mode at nominal power. Fault starts at t=0.1 s.

(a)   (b)
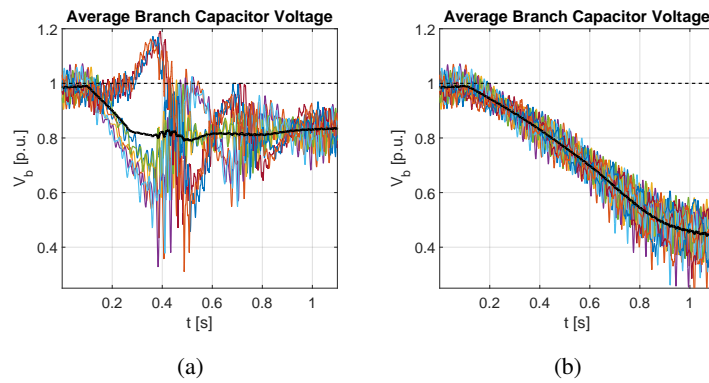
Figure 9.6. Averaged branch capacitor voltages for test cases RT-311 (a), RT-312 (b) in drive operation mode at nominal power. Fault starts at t=0.1 s. Black line represents average of branch voltages in converter.
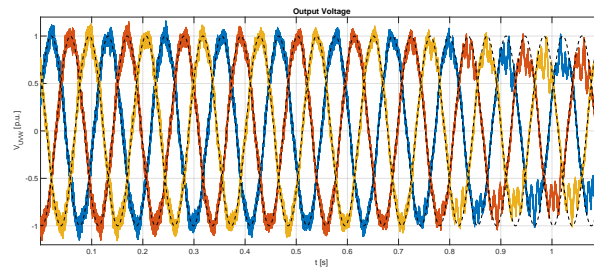
Figure 9.7. Output voltage waveform for test case RT-302 in case of drive operation at nominal power. Black dashed line is the reference voltage.

10. Summary

Thesis content has been summarized in the Introduction chapter. Following section contains summary of key achievements of the author:

– a new topology of MMC converter, so called Hex-Y has been proposed. Given topology differs from existing topologies by branch arrangement,

– internal quantities which can be used as Degrees of Freedom has been identified by electric circuit analysis,

– branch power analysis for proposed topology has been performed to prove it cannot work with zero circulating current as constant components in branch powers will appear,

– specific waveform shapes which cancels out given constant component and prevents branch capacitors voltage drift has been found,

– balancing method which has no influence on output system quantities (as neutral point voltage or line current) has been proposed and tested,

– complete control algorithm has been proposed, explained and used in simulations. Novelty of the solution is an use of circulating currents together with internal star point voltage to provide energy control and energy balancing. Also, due to control hardware limitations, a distributed control has been implemented,

– based on [89], simulation branch model has been build. Author expanded given model by building averaged branch model over given switching model,

– proposed topology has been compared with Matrix M3C. Comparison with other 3 phase to 3 phase topologies has been performed in [4]. Simulation results shows that Hex-Y converter during nominal operation has higher branch current, however voltage ripple in branch capacitors is lower than for given M3C converter. For cases with a load which requires high current also for low frequencies, Hex-Y converter behavior (measured by voltage ripple and branch current) was better than M3C. Given operation point can be found in rolls, lifts or mills. Based on given simulation results author suggests to consider this topology over M3C in those applications,

– study shows also that Hex-Y converter is able to provide reactive power during voltage dips as it is requested by European grid codes.

Author's work summarized in this Thesis has been presented in 11 publications in MMC area during conferences [4, 6, 45, 60, 72, 82, 91, 92] and in Journals [27, 54, 100].

A. Full power equations

Following Appendix contains complete equations which are being used in the Thesis.

A.1. Powers for symmetric voltages and currents. No IC/VN/VX

Branch powers for no circulating current and no common mode / start point voltage.

$$P_{b1} = \tfrac{1}{4}[-P_2 - S_2cos(\phi_2 + 2\psi_2 - 2\omega_2t) + I_2V_1cos(\phi_2 + \psi_2 - \omega_1t - \omega_2t)+ \\ I_2V_1cos(\phi_2 + \psi_2 + \omega_1t - \omega_2t)] \tag{A.1a}$$

$$P_{b2} = \tfrac{1}{8}[-2P_2 + S_2cos(\phi_2 + 2\psi_2 - 2\omega_2t) - I_2V_1cos(\phi_2 + \psi_2 - \omega_1t - \omega_2t) \\ -I_2V_1cos(\phi_2 + \psi_2 + \omega_1t - \omega_2t) - \sqrt{3}S_2sin(\phi_2 + 2\psi_2 - 2\omega_2t) \\ -\sqrt{3}I_2V_1sin(\phi_2 + \psi_2 - \omega_1t - \omega_2t) - \sqrt{3}I_2V_1sin(\phi_2 + \psi_2 + \omega_1t - \omega_2t)] \tag{A.1b}$$

$$P_{b3} = \tfrac{1}{8}[-2P_2 + S_2cos(\phi_2 + 2\psi_2 - 2\omega_2t) - I_2V_1cos(\phi_2 + \psi_2 - \omega_1t - \omega_2t)+ \\ 2I_2V_1cos(\phi_2 + \psi_2 + \omega_1t - \omega_2t) - \sqrt{3}S_2sin(\phi_2 + 2\psi_2 - 2\omega_2t)+ \\ \sqrt{3}I_2V_1sin(\phi_2 + \psi_2 - \omega_1t - \omega_2t)] \tag{A.1c}$$

$$P_{b4} = \tfrac{1}{8}[-2P_2 + S_2cos(\phi_2 + 2\psi_2 - 2\omega_2t) + 2I_2V_1cos(\phi_2 + \psi_2 - \omega_1t - \omega_2t) \\ -I_2V_1cos(\phi_2 + \psi_2 + \omega_1t - \omega_2t) + \sqrt{3}S_2sin(\phi_2 + 2\psi_2 - 2\omega_2t) \\ -\sqrt{3}I_2V_1sin(\phi_2 + \psi_2 + \omega_1t - \omega_2t)] \tag{A.1d}$$

$$P_{b5} = \tfrac{1}{8}[-2P_2 + S_2cos(\phi_2 + 2\psi_2 - 2\omega_2t) - I_2V_1cos(\phi_2 + \psi_2 - \omega_1t - \omega_2t)+ \\ 2I_2V_1cos(\phi_2 + \psi_2 + \omega_1t - \omega_2t) + \sqrt{3}S_2sin(\phi_2 + 2\psi_2 - 2\omega_2t) \\ -\sqrt{3}I_2V_1sin(\phi_2 + \psi_2 - \omega_1t - \omega_2t)] \tag{A.1e}$$

$$P_{b6} = \tfrac{1}{8}[-2P_2 - 2S_2cos(\phi_2 + 2\psi_2 - 2\omega_2t) - I_2V_1cos(\phi_2 + \psi_2 - \omega_1t - \omega_2t) \\ -I_2V_1cos(\phi_2 + \psi_2 + \omega_1t - \omega_2t) + \sqrt{3}I_2V_1sin(\phi_2 + \psi_2 - \omega_1t - \omega_2t) \\ -\sqrt{3}I_2V_1sin(\phi_2 + \psi_2 + \omega_1t - \omega_2t)] \tag{A.1f}$$

$$P_{b7} = \tfrac{1}{8}[-4P_1 - 4S_1cos(\phi_1 - 2\omega_1t) - I_2V_1cos(\phi_2 + \psi_2 - \omega_1t - \omega_2t) \\ -I_2V_1cos(\phi_2 + \psi_2 + \omega_1t - \omega_2t) + \sqrt{3}I_2V_1sin(\phi_2 + \psi_2 - \omega_1t - \omega_2t)+ \\ \sqrt{3}I_2V_1sin(\phi_2 + \psi_2 + \omega_1t - \omega_2t)] \tag{A.1g}$$

$$P_{b8} = \tfrac{1}{8}\left[-4P_1 + 2S_1\cos(\phi_1 - 2\omega_1 t) - I_2 V_1 \cos(\phi_2 + \psi_2 - \omega_1 t - \omega_2 t)\right.$$
$$-I_2 V_1 \cos(\phi_2 + \psi_2 + \omega_1 t - \omega_2 t) - 2\sqrt{3}S_1 \sin(\phi_1 - 2\omega_1 t)$$
$$\left.-\sqrt{3}I_2 V_1 \sin(\phi_2 + \psi_2 - \omega_1 t - \omega_2 t) + \sqrt{3}I_2 V_1 \sin(\phi_2 + \psi_2 + \omega_1 t - \omega_2 t)\right] \tag{A.1h}$$

$$P_{b9} = \tfrac{1}{8}\left[-4P_1 + 2S_1\cos(\phi_1 - 2\omega_1 t) + 2I_2 V_1 \cos(\phi_2 + \psi_2 - \omega_1 t - \omega_2 t)\right.$$
$$-I_2 V_1 \cos(\phi_2 + \psi_2 + \omega_1 t - \omega_2 t) + 2\sqrt{3}S_1 \sin(\phi_1 - 2\omega_1 t) +$$
$$\left.\sqrt{3}I_2 V_1 \sin(\phi_2 + \psi_2 + \omega_1 t - \omega_2 t)\right] \tag{A.1i}$$

A.2. Powers for symmetric voltages and currents. IC/VN/VX given as generic function

If the voltages and currents are defined in generic form as in the Eq. (4.9) and Eq. (4.10) the branch powers are equal:

$$P_1 = \tfrac{1}{4}[-4i_{c1}v_N - I_2 V_2 \cos(\phi_2) + 4i_{c1}V_1\cos(\omega_1 t) - I_2 V_2 \cos(\phi_2 + 2\psi_2 - 2\omega_2 t)$$
$$-4i_{c1}V_2\cos(\psi_2 - \omega_2 t) - 2I_2 v_N \cos(\phi_2 + \psi_2 - \omega_2 t) +$$
$$I_2 V_1\cos(\phi_2 + \psi_2 - \omega_1 t - \omega_2 t) + I_2 V_1\cos(\phi_2 + \psi_2 + \omega_1 t - \omega_2 t)] \tag{A.2a}$$

$$P_2 = \tfrac{1}{8}[8i_{c2}v_N - 2I_2 V_2 \cos(\phi_2) - 8i_{c2}V_1\cos(\omega_1 t) + I_2 V_2 \cos(\phi_2 + 2\psi_2 - 2\omega_2 t)$$
$$-4i_{c2}V_2\cos(\psi_2 - \omega_2 t) + 2I_2 v_N \cos(\phi_2 + \psi_2 - \omega_2 t) - I_2 V_1\cos(\phi_2 + \psi_2 - \omega_1 t - \omega_2 t)$$
$$-I_2 V_1\cos(\phi_2 + \psi_2 + \omega_1 t - \omega_2 t) - \sqrt{3}I_2 V_2 \sin(\phi_2 + 2\psi_2 - 2\omega_2 t)$$
$$-4\sqrt{3}i_{c2}V_2\sin(\psi_2 - \omega_2 t) + 2\sqrt{3}I_2 v_N \sin(\phi_2 + \psi_2 - \omega_2 t)$$
$$-\sqrt{3}I_2 V_1\sin(\phi_2 + \psi_2 - \omega_1 t - \omega_2 t) - \sqrt{3}I_2 V_1\sin(\phi_2 + \psi_2 + \omega_1 t - \omega_2 t)] \tag{A.2b}$$

$$P_3 = \tfrac{1}{8}[-8i_{c2}v_N - 2I_2 V_2 \cos(\phi_2) - 4i_{c2}V_1\cos(\omega_1 t) + I_2 V_2 \cos(\phi_2 + 2\psi_2 - 2\omega_2 t) +$$
$$4i_{c2}V_2\cos(\psi_2 - \omega_2 t) + 2I_2 v_N \cos(\phi_2 + \psi_2 - \omega_2 t) - I_2 V_1\cos(\phi_2 + \psi_2 - \omega_1 t - \omega_2 t) +$$
$$2I_2 V_1\cos(\phi_2 + \psi_2 + \omega_1 t - \omega_2 t) + 4\sqrt{3}i_{c2}V_1\sin(\omega_1 t) - \sqrt{3}I_2 V_2 \sin(\phi_2 + 2\psi_2 -$$
$$2\omega_2 t) + 4\sqrt{3}i_{c2}V_2\sin(\psi_2 - \omega_2 t) + 2\sqrt{3}I_2 v_N \sin(\phi_2 + \psi_2 - \omega_2 t) + \sqrt{3}I_2 V_1\sin(\phi_2 +$$
$$\psi_2 - \omega_1 t - \omega_2 t)] \tag{A.2c}$$

$$P_4 = \tfrac{1}{8}[8i_{c3}v_N - 2I_2 V_2 \cos(\phi_2) + 4i_{c3}V_1\cos(\omega_1 t) + I_2 V_2 \cos(\phi_2 + 2\psi_2 - 2\omega_2 t) -$$
$$4i_{c3}V_2\cos(\psi_2 - \omega_2 t) + 2I_2 v_N \cos(\phi_2 + \psi_2 - \omega_2 t) + 2I_2 V_1\cos(\phi_2 + \psi_2 - \omega_1 t -$$
$$\omega_2 t) - I_2 V_1\cos(\phi_2 + \psi_2 + \omega_1 t - \omega_2 t) - 4\sqrt{3}i_{c3}V_1\sin(\omega_1 t) + \sqrt{3}I_2 V_2 \sin(\phi_2 + 2\psi_2 -$$
$$2\omega_2 t) + 4\sqrt{3}i_{c3}V_2\sin(\psi_2 - \omega_2 t) - 2\sqrt{3}I_2 v_N \sin(\phi_2 + \psi_2 - \omega_2 t) - \sqrt{3}I_2 V_1\sin(\phi_2 +$$
$$\psi_2 + \omega_1 t - \omega_2 t)] \tag{A.2d}$$

$$P_5 = \tfrac{1}{8}[-8i_{c3}v_N - 2I_2 V_2 \cos(\phi_2) - 4i_{c3}V_1\cos(\omega_1 t) + I_2 V_2 \cos(\phi_2 + 2\psi_2 - 2\omega_2 t) +$$
$$4i_{c3}V_2\cos(\psi_2 - \omega_2 t) + 2I_2 v_N \cos(\phi_2 + \psi_2 - \omega_2 t) - I_2 V_1\cos(\phi_2 + \psi_2 - \omega_1 t - \omega_2 t) +$$
$$2I_2 V_1\cos(\phi_2 + \psi_2 + \omega_1 t - \omega_2 t) - 4\sqrt{3}i_{c3}V_1\sin(\omega_1 t) + \sqrt{3}I_2 V_2 \sin(\phi_2 + 2\psi_2 -$$
$$2\omega_2 t) - 4\sqrt{3}i_{c3}V_2\sin(\psi_2 - \omega_2 t) - 2\sqrt{3}I_2 v_N \sin(\phi_2 + \psi_2 - \omega_2 t) - \sqrt{3}I_2 V_1\sin(\phi_2 +$$
$$\psi_2 - \omega_1 t - \omega_2 t)] \tag{A.2e}$$

$$P_6 = \frac{1}{8}[8i_{c1}v_N - 2I_2V_2cos(\phi_2) + 4i_{c1}V_1cos(\omega_1 t) - 2I_2V_2cos(\phi_2 + 2\psi_2 - 2\omega_2 t) + 8i_{c1}V_2cos(\psi_2 - \omega_2 t) - 4I_2v_Ncos(\phi_2 + \psi_2 - \omega_2 t) - I_2V_1cos(\phi_2 + \psi_2 - \omega_1 t - \omega_2 t) - I_2V_1cos(\phi_2 + \psi_2 + \omega_1 t - \omega_2 t) + 4\sqrt{3}i_{c1}V_1sin(\omega_1 t) + \sqrt{3}I_2V_1sin(\phi_2 + \psi_2 - \omega_1 t - \omega_2 t) - \sqrt{3}I_2V_1sin(\phi_2 + \psi_2 + \omega_1 t - \omega_2 t)]$$
(A.2f)

$$P_7 = \frac{1}{8}[8i_{c1}v_X - 8i_{c2}v_X - 4I_1V_1cos(\phi_1) - 8i_{c1}V_1cos(\omega_1 t) + 8i_{c2}V_1cos(\omega_1 t) - 4I_1V_1cos(\phi_1 - 2\omega_1 t) + 8I_1v_Xcos(\phi_1 - \omega_1 t) + 2I_2v_Xcos(\phi_2 + \psi_2 - \omega_2 t) - I_2V_1cos(\phi_2 + \psi_2 - \omega_1 t - \omega_2 t) - I_2V_1cos(\phi_2 + \psi_2 + \omega_1 t - \omega_2 t) - 2\sqrt{3}I_2v_Xsin(\phi_2 + \psi_2 - \omega_2 t) + \sqrt{3}I_2V_1sin(\phi_2 + \psi_2 - \omega_1 t - \omega_2 t) + \sqrt{3}I_2V_1sin(\phi_2 + \psi_2 + \omega_1 t - \omega_2 t)]$$
(A.2g)

$$P_8 = \frac{1}{8}[8i_{c2}v_X - 8i_{c3}v_X - 4I_1V_1cos(\phi_1) + 4i_{c2}V_1cos(\omega_1 t) - 4i_{c3}V_1cos(\omega_1 t) + 2I_1V_1cos(\phi_1 - 2\omega_1 t) - 4I_1v_Xcos(\phi_1 - \omega_1 t) - 4I_2v_Xcos(\phi_2 + \psi_2 - \omega_2 t) - I_2V_1cos(\phi_2 + \psi_2 - \omega_1 t - \omega_2 t) - I_2V_1cos(\phi_2 + \psi_2 + \omega_1 t - \omega_2 t) - 4\sqrt{3}i_{c2}V_1sin(\omega_1 t) + 4\sqrt{3}i_{c3}V_1sin(\omega_1 t) - 2\sqrt{3}I_1V_1sin(\phi_1 - 2\omega_1 t) - 4\sqrt{3}I_1v_Xsin(\phi_1 - \omega_1 t) - \sqrt{3}I_2V_1sin(\phi_2 + \psi_2 - \omega_1 t - \omega_2 t) + \sqrt{3}I_2V_1sin(\phi_2 + \psi_2 + \omega_1 t - \omega_2 t)]$$
(A.2h)

$$P_9 = \frac{1}{8}[-8i_{c1}v_X + 8i_{c3}v_X - 4I_1V_1cos(\phi_1) - 4i_{c1}V_1cos(\omega_1 t) + 4i_{c3}V_1cos(\omega_1 t) + 2I_1V_1cos(\phi_1 - 2\omega_1 t) - 4I_1v_Xcos(\phi_1 - \omega_1 t) + 2I_2v_Xcos(\phi_2 + \psi_2 - \omega_2 t) + 2I_2V_1cos(\phi_2 + \psi_2 - \omega_1 t - \omega_2 t) - I_2V_1cos(\phi_2 + \psi_2 + \omega_1 t - \omega_2 t) - 4\sqrt{3}i_{c1}V_1sin(\omega_1 t) + 4\sqrt{3}i_{c3}V_1sin(\omega_1 t) + 2\sqrt{3}I_1V_1sin(\phi_1 - 2\omega_1 t) + 4\sqrt{3}I_1v_Xsin(\phi_1 - \omega_1 t) + 2\sqrt{3}I_2v_Xsin(\phi_2 + \psi_2 - \omega_2 t) + \sqrt{3}I_2V_1sin(\phi_2 + \psi_2 + \omega_1 t - \omega_2 t)]$$
(A.2i)

A.3. Powers for introduced harmonic circulating currents

If the system voltages and currents are given as symmetric sine waveforms with parameters defined in Table 3.2 and the circulating currents are equal (4.45), branch powers are equal

$$P_1 = \frac{1}{12}[-2\sqrt{3}cos\left(\frac{\pi}{6} - 2\omega_1 t\right) + 3cos(2\omega_2 t) + 2\sqrt{3}cos\left(\frac{\pi}{6} - \omega_1 t - \omega_2 t\right) - 3cos(\omega_1 t - \omega_2 t) + 2\sqrt{3}cos\left(\frac{\pi}{6} - \omega_1 t + \omega_2 t\right) - 3cos(\omega_1 t + \omega_2 t))$$
(A.3a)

$$P_2 = \frac{1}{24}[-4\sqrt{3}cos\left(\frac{\pi}{6} + 2\omega_1 t\right) - 3\sqrt{3}cos\left(\frac{\pi}{6} - 2\omega_2 t\right) - 2\sqrt{3}cos\left(\frac{\pi}{6} + \omega_1 t - \omega_2 t\right) - 2\sqrt{3}cos\left(\frac{\pi}{6} + \omega_1 t + \omega_2 t\right) + 3sin\left(\frac{\pi}{6} - 2\omega_2 t\right) + 6sin\left(\frac{\pi}{6} - \omega_1 t - \omega_2 t\right) + 6sin\left(\frac{\pi}{6} + \omega_1 t + \omega_2 t\right)]$$
(A.3b)

$$P_3 = \frac{1}{24}[-2\sqrt{3}cos\left(\frac{\pi}{6} + 2\omega_1 t\right) - 3\sqrt{3}cos\left(\frac{\pi}{6} - 2\omega_2 t\right) + 3\sqrt{3}cos\left(\frac{\pi}{6} - \omega_1 t - \omega_2 t\right) - \sqrt{3}cos\left(\frac{\pi}{6} + \omega_1 t - \omega_2 t\right) + 2\sqrt{3}cos\left(\frac{\pi}{6} + \omega_1 t + \omega_2 t\right) + 6sin\left(\frac{\pi}{6} + 2\omega_1 t\right) + 3sin\left(\frac{\pi}{6} - 2\omega_2 t\right) - 3sin\left(\frac{\pi}{6} - \omega_1 t - \omega_2 t\right) + 3sin\left(\frac{\pi}{6} + \omega_1 t - \omega_2 t\right) - 6sin\left(\frac{\pi}{6} + \omega_1 t + \omega_2 t\right)]$$
(A.3c)

$$P_4 = \tfrac{1}{24}[6cos(2\omega_1 t) - 6cos(\omega_1 t - \omega_2 t) + 3\sqrt{3}cos\left(\tfrac{\pi}{6} - \omega_1 t + \omega_2 t\right) + 6cos(\omega_1 t + \omega_2 t) - 3\sqrt{3}cos\left(\tfrac{\pi}{6} + \omega_1 t + \omega_2 t\right) - 3\sqrt{3}cos\left(\tfrac{\pi}{6} + 2\omega_2 t\right) + 2\sqrt{3}sin(2\omega_1 t) - 2\sqrt{3}sin(\omega_1 t - \omega_2 t) - 3sin\left(\tfrac{\pi}{6} - \omega_1 t + \omega_2 t\right) - 2\sqrt{3}sin(\omega_1 t + \omega_2 t) - 3sin\left(\tfrac{\pi}{6} + \omega_1 t + \omega_2 t\right) + 3sin\left(\tfrac{\pi}{6} + 2\omega_2 t\right)] \tag{A.3d}$$

$$P_5 = \tfrac{1}{24}[6cos(2\omega_1 t) + 6cos(\omega_1 t - \omega_2 t) - 3\sqrt{3}cos\left(\tfrac{\pi}{6} - \omega_1 t + \omega_2 t\right) - 6cos(\omega_1 t + \omega_2 t) + 3\sqrt{3}cos\left(\tfrac{\pi}{6} + \omega_1 t + \omega_2 t\right) - 3\sqrt{3}cos\left(\tfrac{\pi}{6} + 2\omega_2 t\right) - 2\sqrt{3}sin(2\omega_1 t) + 2\sqrt{3}sin(\omega_1 t - \omega_2 t) - 3sin\left(\tfrac{\pi}{6} - \omega_1 t + \omega_2 t\right) + 2\sqrt{3}sin(\omega_1 t + \omega_2 t) - 3sin\left(\tfrac{\pi}{6} + \omega_1 t + \omega_2 t\right) + 3sin\left(\tfrac{\pi}{6} + 2\omega_2 t\right)] \tag{A.3e}$$

$$P_6 = \tfrac{1}{24}[-2\sqrt{3}cos\left(\tfrac{\pi}{6} - 2\omega_1 t\right) + 6cos(2\omega_2 t) - 4\sqrt{3}cos\left(\tfrac{\pi}{6} - \omega_1 t - \omega_2 t\right) + 3cos(\omega_1 t - \omega_2 t) - 4\sqrt{3}cos\left(\tfrac{\pi}{6} - \omega_1 t + \omega_2 t\right) + 3cos(\omega_1 t + \omega_2 t) + 6sin\left(\tfrac{\pi}{6} - 2\omega_1 t\right) + 3\sqrt{3}sin(\omega_1 t - \omega_2 t) + 3\sqrt{3}sin(\omega_1 t + \omega_2 t)] \tag{A.3f}$$

$$P_7 = \tfrac{1}{4}[sin\left(\tfrac{\pi}{6} - \omega_1 t + \omega_2 t\right) + sin\left(\tfrac{\pi}{6} + \omega_1 t + \omega_2 t\right)] \tag{A.3g}$$

$$P_8 = \tfrac{1}{8}[cos(\omega_1 t - \omega_2 t) + cos(\omega_1 t + \omega_2 t) - \sqrt{3}sin(\omega_1 t - \omega_2 t) - \sqrt{3}sin(\omega_1 t + \omega_2 t)] \tag{A.3h}$$

$$P_9 = \tfrac{1}{8}[-\sqrt{3}cos\left(\tfrac{\pi}{6} - \omega_1 t - \omega_2 t\right) + \sqrt{3}cos\left(\tfrac{\pi}{6} + \omega_1 t - \omega_2 t\right) - sin\left(\tfrac{\pi}{6} - \omega_1 t - \omega_2 t\right) - sin\left(\tfrac{\pi}{6} + \omega_1 t - \omega_2 t\right)] \tag{A.3i}$$

It should be noted that there is no any constant component in a given equations.

A.4. Powers for charging scenario

For symmetric charging, circulating currents with ω_1 frequency are being used. Total branch powers are equal (A.5). It should be noted that for every branch, the same constant component can be found: $\frac{1 + \sqrt{3}I_{C1m}}{4}$ or $\frac{-3 - 2\sqrt{3}}{4}$. Note that both components are equal for selected voltages:

$$P_1 = 1.5$$
$$P_2 = -1.0 \tag{A.4}$$
$$I_{C1m} = \frac{P_2 - 2P_1}{3\sqrt{3}} = -\frac{4}{3\sqrt{3}}$$

$$P_1 = \tfrac{1}{4}[1 + \sqrt{3}i_{C1m} + 2i_{C1m}cos\left(\tfrac{\pi}{6} - 2\omega_1 t\right) + cos(2\omega_2 t) - 2i_{C1m}cos\left(\tfrac{\pi}{6} - \omega_1 t - \omega_2 t\right) - cos(\omega_1 t - \omega_2 t) - 2i_{C1m}cos\left(\tfrac{\pi}{6} - \omega_1 t + \omega_2 t\right) - cos(\omega_1 t + \omega_2 t)] \tag{A.5a}$$

$$P_2 = \tfrac{1}{8}[2 + 2\sqrt{3}i_{C1m} + 4i_{C1m}cos\left(\tfrac{\pi}{6} + 2\omega_1 t\right) - \sqrt{3}cos\left(\tfrac{\pi}{6} - 2\omega_2 t\right) +$$
$$2i_{C1m}cos\left(\tfrac{\pi}{6} + \omega_1 t - \omega_2 t\right) + 2i_{C1m}cos\left(\tfrac{\pi}{6} + \omega_1 t + \omega_2 t\right) + sin\left(\tfrac{\pi}{6} - 2\omega_2 t\right) +$$
$$2sin\left(\tfrac{\pi}{6} - \omega_1 t - \omega_2 t\right) + 2sin\left(\tfrac{\pi}{6} + \omega_1 t - \omega_2 t\right) + 2\sqrt{3}i_{C1m}sin\left(\tfrac{\pi}{6} + \omega_1 t - \omega_2 t\right) -$$
$$2\sqrt{3}i_{C1m}sin\left(\tfrac{\pi}{6} + \omega_1 t + \omega_2 t\right)] \tag{A.5b}$$

$$P_3 = \tfrac{1}{8}[2 + 2\sqrt{3}i_{C1m} + 2i_{C1m}cos\left(\tfrac{\pi}{6} + 2\omega_1 t\right) - \sqrt{3}cos\left(\tfrac{\pi}{6} - 2\omega_2 t\right) +$$
$$\sqrt{3}cos\left(\tfrac{\pi}{6} - \omega_1 t - \omega_2 t\right) - \sqrt{3}cos\left(\tfrac{\pi}{6} + \omega_1 t - \omega_2 t\right) - 2i_{C1m}cos\left(\tfrac{\pi}{6} + \omega_1 t - \omega_2 t\right) -$$
$$2i_{C1m}cos\left(\tfrac{\pi}{6} + \omega_1 t + \omega_2 t\right) - 2\sqrt{3}i_{C1m}sin\left(\tfrac{\pi}{6} + 2\omega_1 t\right) + sin\left(\tfrac{\pi}{6} - 2\omega_2 t\right) -$$
$$sin\left(\tfrac{\pi}{6} - \omega_1 t - \omega_2 t\right) - sin\left(\tfrac{\pi}{6} + \omega_1 t - \omega_2 t\right) - 2\sqrt{3}i_{C1m}sin\left(\tfrac{\pi}{6} + \omega_1 t - \omega_2 t\right) +$$
$$2\sqrt{3}i_{C1m}sin\left(\tfrac{\pi}{6} + \omega_1 t + \omega_2 t\right)] \tag{A.5c}$$

$$P_4 = \tfrac{1}{8}[2 + 2\sqrt{3}i_{C1m} - 2\sqrt{3}i_{C1m}cos(2\omega_1 t) + 2\sqrt{3}i_{C1m}cos(\omega_1 t - \omega_2 t) +$$
$$\sqrt{3}cos\left(\tfrac{\pi}{6} - \omega_1 t + \omega_2 t\right) - 2\sqrt{3}i_{C1m}cos(\omega_1 t + \omega_2 t) - \sqrt{3}cos\left(\tfrac{\pi}{6} + \omega_1 t + \omega_2 t\right) -$$
$$\sqrt{3}cos\left(\tfrac{\pi}{6} + 2\omega_2 t\right) - 2i_{C1m}sin(2\omega_1 t) + 2i_{C1m}sin(\omega_1 t - \omega_2 t) -$$
$$sin\left(\tfrac{\pi}{6} - \omega_1 t + \omega_2 t\right) + 2i_{C1m}sin(\omega_1 t + \omega_2 t) - sin\left(\tfrac{\pi}{6} + \omega_1 t + \omega_2 t\right) +$$
$$sin\left(\tfrac{\pi}{6} + 2\omega_2 t\right)] \tag{A.5d}$$

$$P_5 = \tfrac{1}{8}[2 + 2\sqrt{3}i_{C1m} - 2\sqrt{3}i_{C1m}cos(2\omega_1 t) - 2\sqrt{3}i_{C1m}cos(\omega_1 t - \omega_2 t) -$$
$$\sqrt{3}cos\left(\tfrac{\pi}{6} - \omega_1 t + \omega_2 t\right) + 2\sqrt{3}i_{C1m}cos(\omega_1 t + \omega_2 t) + \sqrt{3}cos\left(\tfrac{\pi}{6} + \omega_1 t + \omega_2 t\right) -$$
$$\sqrt{3}cos\left(\tfrac{\pi}{6} + 2\omega_2 t\right) + 2i_{C1m}sin(2\omega_1 t) - 2i_{C1m}sin(\omega_1 t - \omega_2 t) -$$
$$sin\left(\tfrac{\pi}{6} - \omega_1 t + \omega_2 t\right) - 2i_{C1m}sin(\omega_1 t + \omega_2 t) - sin\left(\tfrac{\pi}{6} + \omega_1 t + \omega_2 t\right) +$$
$$sin\left(\tfrac{\pi}{6} + 2\omega_2 t\right)] \tag{A.5e}$$

$$P_6 = \tfrac{1}{8}[2 + 2\sqrt{3}i_{C1m} + 2i_{C1m}cos\left(\tfrac{\pi}{6} - 2\omega_1 t\right) + 2cos(2\omega_2 t) +$$
$$4i_{C1m}cos\left(\tfrac{\pi}{6} - \omega_1 t - \omega_2 t\right) + cos(\omega_1 t - \omega_2 t) + 4i_{C1m}cos\left(\tfrac{\pi}{6} - \omega_1 t + \omega_2 t\right) +$$
$$cos(\omega_1 t + \omega_2 t) - 2\sqrt{3}i_{C1m}sin\left(\tfrac{\pi}{6} - 2\omega_1 t\right) + \sqrt{3}sin(\omega_1 t - \omega_2 t) + \sqrt{3}sin(\omega_1 t + \omega_2 t)] \tag{A.5f}$$

$$P_7 = \tfrac{1}{4}[-3 - 2\sqrt{3}i_{C1m} - 3cos(2\omega_1 t) - 2i_{C1m}cos\left(\tfrac{\pi}{6} - 2\omega_1 t\right) - 2i_{C1m}cos\left(\tfrac{\pi}{6} + 2\omega_1 t\right) +$$
$$sin\left(\tfrac{\pi}{6} - \omega_1 t + \omega_2 t\right) + sin\left(\tfrac{\pi}{6} + \omega_1 t + \omega_2 t\right)] \tag{A.5g}$$

$$P_8 = \tfrac{1}{8}[-6 - 4\sqrt{3}i_{C1m} + 2\sqrt{3}i_{C1m}cos(2\omega_1 t) + 3\sqrt{3}cos\left(\tfrac{\pi}{6} - 2\omega_1 t\right) -$$
$$2i_{C1m}cos\left(\tfrac{\pi}{6} + 2\omega_1 t\right) + cos(\omega_1 t - \omega_2 t) + cos(\omega_1 t + \omega_2 t) + 2i_{C1m}sin(2\omega_1 t) -$$
$$3sin\left(\tfrac{\pi}{6} - 2\omega_1 t\right) + 2\sqrt{3}i_{C1m}sin\left(\tfrac{\pi}{6} + 2\omega_1 t\right) - \sqrt{3}sin(\omega_1 t - \omega_2 t) - \sqrt{3}sin(\omega_1 t +$$
$$\omega_2 t)] \tag{A.5h}$$

$$
\begin{aligned}
P_9 = \ \frac{1}{8}[& -6 \quad - \quad 4\sqrt{3}i_{C1m} \quad + \quad 2\sqrt{3}i_{C1m}cos(2\omega_1 t) \quad - \quad 2i_{C1m}cos\left(\tfrac{\pi}{6} - 2\omega_1 t\right) \quad + \\
& 3\sqrt{3}cos\left(\tfrac{\pi}{6} + 2\omega_1 t\right) \quad - \quad \sqrt{3}cos\left(\tfrac{\pi}{6} - \omega_1 t - \omega_2 t\right) \quad + \quad \sqrt{3}cos\left(\tfrac{\pi}{6} + \omega_1 t - \omega_2 t\right) \quad - \\
& 2i_{C1m}sin(2\omega_1 t) \quad + \quad 2\sqrt{3}i_{C1m}sin\left(\tfrac{\pi}{6} - 2\omega_1 t\right) \quad - \quad 3sin\left(\tfrac{\pi}{6} + 2\omega_1 t\right) \quad - \\
& sin\left(\tfrac{\pi}{6} - \omega_1 t - \omega_2 t\right) - sin\left(\tfrac{\pi}{6} + \omega_1 t - \omega_2 t\right)]
\end{aligned}
\tag{A.5i}
$$

Bibliography

[1] H. J. Knaak. "Modular Multilevel Converters and HVDC / FACTS : a success story The modular multilevel technology". In: *Proceedings of the 14th European Conference on Power Electronics and Applications (EPE 2011)* Lcc (2011), pp. 1 –6.

[2] D. Jovcic. *High Voltage Direct Current Transmission: Converters, Systems and DC Grids*. Ed. by John Wiley & Sons. 2019.

[3] R. W. Erickson and O. A. Al-Naseem. "A new family of matrix converters". In: *IECON'01 - 27th Annual Conference of the IEEE Industrial Electronics Society*. Vol. 2. Xcx. Denver, CO, USA: IEEE, 2001, pp. 1515–1520. ISBN: 0-7803-7108-9. DOI: *10.1109/IECON.2001.976015*.

[4] **P. Blaszczyk**. "Hex-Y – A New Modular Multilevel Converter Topology for a Direct AC-AC Power Conversion". In: *EPE'18 ECCE Europe*. 2018, pp. 1–10. ISBN: 9789075815290.

[5] M. Malinowski. "Cascaded multilevel converters in recent research and applications". In: *Bulletin of the Polish Academy of Sciences Technical Sciences* 65.5 (2017), pp. 567–578. ISSN: 2300-1917. DOI: *10.1515/bpasts-2017-0062*.

[6] M. Winkelnkemper, L. Schwager, **P. Blaszczyk**, M. Steurer, and D. Soto. "Short circuit output protection of MMC in voltage source control mode". In: *2016 IEEE Energy Conversion Congress and Exposition (ECCE)*. IEEE, 2016, pp. 1–6. ISBN: 978-1-5090-0737-0. DOI: *10.1109/ECCE.2016.7855427*.

[7] F. J. Rodriguez, J. S. Lai, and F. Z. Peng. "Multilevel inverters: A survey of topologies, controls, and applications". In: *IEEE Transactions on Industrial Electronics* 49.4 (2002), pp. 724–738. ISSN: 02780046. DOI: *10.1109/TIE.2002.801052*.

[8] P.W. Hammond. "A new approach to enhance power quality for medium voltage drives". In: *Industry Applications Society 42nd Annual Petroleum and Chemical Industry Conference*. IEEE, 1995, pp. 231–235. ISBN: 0-7803-2909-0. DOI: *10.1109/PCICON.1995.523958*.

[9] K. Wang, Y. Li, Z. Zheng, and Lie Xu. "Voltage balancing and fluctuation-suppression methods of floating capacitors in a new modular multilevel converter". In: *IEEE Transactions on Industrial Electronics* 60.5 (2013), pp. 1943–1954. ISSN: 02780046. DOI: *10.1109/TIE.2012.2201433*.

[10] T. Noguchi and S. Suroso. "Review of novel multilevel current-source inverters with H-bridge and common-emitter based topologies". In: *2010 IEEE Energy Conversion Congress and Exposition*. IEEE, 2010, pp. 4006–4011. ISBN: 978-1-4244-5286-6. DOI: *10.1109/ECCE.2010.5617804*.

[11] S. Suroso and T. Noguchi. "Multilevel Current Waveform Generation Using Inductor Cells and H-Bridge Current-Source Inverter". In: *IEEE Transactions on Power Electronics* 27.3 (2012), pp. 1090–1098. ISSN: 0885-8993. DOI: *10.1109/TPEL.2010.2056933*.

[12] M. A. Perez, S. Bernet, F. J. Rodriguez, S. Kouro, and R. Lizana. "Circuit Topologies, Modeling, Control Schemes, and Applications of Modular Multilevel Converters". In: *IEEE Transactions on Power Electronics* 30.1 (2015), pp. 4–17. ISSN: 0885-8993. DOI: *10.1109/TPEL.2014.2310127*.

[13] A. Nami, J. Liang, F. Dijkhuizen, and G. D. Demetriades. "Modular Multilevel Converters for HVDC Applications: Review on Converter Cells and Functionalities". In: *IEEE Transactions on Power Electronics* 30.1 (2015), pp. 18–36. ISSN: 0885-8993. DOI: *10.1109/TPEL.2014.2327641*.

[14] S. Aubert, C. Hillberg, and P. K. Steimer. "Variable speed pumped storage with converter-fed synchronous machines (CFSM): advanced grid services in a network with large penetration of wind and solar generation". In: *Proc. Hydro* (2014).

[15] M. Vasiladiotis, R. Baumann, C. Haderli, and J. Steinke. "IGCT-Based Direct AC/AC Modular Multilevel Converters for Pumped Hydro Storage Plants". In: *2018 IEEE Energy Conversion Congress and Exposition (ECCE)*. IEEE, 2018, pp. 4837–4844. ISBN: 978-1-4799-7312-5. DOI: *10.1109/ECCE.2018.8557594*.

[16] A. Hillers, M. Stojadinovic, and J. Biela. "Systematic comparison of modular multilevel converter topologies for battery energy storage systems based on split batteries". In: *2015 17th European Conference on Power Electronics and Applications (EPE'15 ECCE-Europe)*. IEEE, 2015, pp. 1–9. ISBN: 978-9-0758-1522-1. DOI: *10.1109/EPE.2015.7309385*.

[17] H. Akagi. "Multilevel Converters: Fundamental Circuits and Systems". In: *Proceedings of the IEEE* 105.11 (2017), pp. 2048–2065. ISSN: 0018-9219. DOI: *10.1109/JPROC.2017.2682105*.

[18] E. Kontos, G. Tsolaridis, R. Teodorescu, and P. Bauer. "Full-bridge MMC DC fault ride-through and STATCOM operation in multi-terminal HVDC grids". In: *Bulletin of the Polish Academy of Sciences Technical Sciences* 65.5 (2017), pp. 1–6. ISSN: 2300-1917. DOI: *10.1515/bpasts-2017-0070*.

[19] A. J. Korn, M. Winkelnkemper, and P. K. Steimer. "Low output frequency operation of the Modular Multi-Level Converter". In: *2010 IEEE Energy Conversion Congress and Exposition*. IEEE, 2010, pp. 3993–3997. ISBN: 978-1-4244-5286-6. DOI: *10.1109/ECCE.2010.5617802*.

[20] G. J. M. De Sousa and M. L. Heldwein. "Three-phase unidirectional modular multilevel converter". In: *2013 15th European Conference on Power Electronics and Applications, EPE 2013* Dcc (2013), pp. 1–10. DOI: *10.1109/EPE.2013.6634676*.

[21] C. Rech and J. R. Pinheiro. "Hybrid multilevel converters: Unified analysis and design considerations". In: *IEEE Transactions on Industrial Electronics* 54.2 (2007), pp. 1092–1104. ISSN: 02780046. DOI: *10.1109/TIE.2007.892255*.

[22] A. Nabae, I. Takahashi, and H. Akagi. "A New Neutral-Point-Clamped PWM Inverter". In: *IEEE Transactions on Industry Applications* IA-17.5 (1981), pp. 518–523. ISSN: 0093-9994. DOI: *10.1109/TIA.1981.4503992*.

[23] T. B. Soeiro and J. W. Kolar. "Novel 3-level Hybrid Neutral-Point-Clamped Converter". In: *IECON 2011 - 37th Annual Conference of the IEEE Industrial Electronics Society*. c. IEEE, 2011, pp. 4457–4462. ISBN: 978-1-61284-972-0. DOI: *10.1109/IECON.2011.6120042*.

[24] A. Nami, L. Wang, F. Dijkhuizen, and A. Shukla. "Five level cross connected cell for cascaded converters". In: *2013 15th European Conference on Power Electronics and Applications (EPE)*. IEEE, 2013, pp. 1–9. ISBN: 978-1-4799-0116-6. DOI: *10.1109/EPE.2013.6631941*.

[25] R. Marquardt. "Modular Multilevel Converter: An universal concept for HVDC-Networks and extended DC-Bus-applications". In: *The 2010 International Power Electronics Conference - ECCE ASIA -*. IEEE, 2010, pp. 502–507. ISBN: 978-1-4244-5394-8. DOI: *10.1109/IPEC.2010.5544594*.

[26] B. S. Riar, U. K. Madawala, and D. J. Thrimawithana. "Analysis and control of a three-phase Modular Multi-level Converter based on Inductive Power Transfer technology (M2LC-IPT)". In: *2013 IEEE International Conference on Industrial Technology (ICIT)*. IEEE, 2013, pp. 475–480. ISBN: 978-1-4673-4569-9. DOI: *10.1109/ICIT.2013.6505718*.

[27] M. Steurer, K. Schoder, O. Faruque, D. Soto, M. Bosworth, M. Sloderbeck, F. Bogdan, J. Hauer, M. Winkelnkemper, L. Schwager, and **P. Blaszczyk**. "Multifunctional Megawatt-Scale Medium Voltage DC Test Bed Based on Modular Multilevel Converter Technology". In: *IEEE Transactions on Transportation Electrification* 2.4 (2016), pp. 597–606. ISSN: 2332-7782. DOI: *10.1109/TTE.2016.2582561*.

[28] B. Karanayil, V. G. Agelidis, and J. Pou. "Performance Evaluation of Three-Phase Grid-Connected Photovoltaic Inverters Using Electrolytic or Polypropylene Film Capacitors". In: *IEEE Transactions on Sustainable Energy* 5.4 (2014), pp. 1297–1306. ISSN: 1949-3029. DOI: *10.1109/TSTE.2014.2347967*.

[29] M. Moranchel, E. J. Bueno, F. J. Rodriguez, and I. Sanz. "Implementation of nearest level modulation for Modular Multilevel Converter". In: *2015 IEEE 6th International Symposium on Power Electronics for Distributed Generation Systems (PEDG)*. Vol. 00. c. IEEE, 2015, pp. 1–5. ISBN: 978-1-4799-8586-9. DOI: *10.1109/PEDG.2015.7223079*.

[30] L. Franquelo, F. J. Rodriguez, J. Leon, S. Kouro, R. Portillo, and M. Prats. "The age of multilevel converters arrives". In: *IEEE Industrial Electronics Magazine* 2.2 (2008), pp. 28–39. ISSN: 1932-4529. DOI: *10.1109/MIE.2008.923519*.

[31] M. Jussila, M. Salo, and H. Tuusa. "Induction motor drive fed by a vector modulated indirect matrix converter". In: *2004 IEEE 35th Annual Power Electronics Specialists Conference (IEEE Cat. No.04CH37551)*. Vol. 4. IEEE, 2004, pp. 2862–2868. ISBN: 0-7803-8399-0. DOI: *10.1109/PESC.2004.1355288*.

[32] S. F. Pinto and J. F. Silva. "Direct control method for matrix converters with input power factor regulation". In: *2004 IEEE 35th Annual Power Electronics Specialists Conference (IEEE Cat. No.04CH37551)*. Vol. 3. I. IEEE, 2004, pp. 2366–2372. ISBN: 0-7803-8399-0. DOI: *10.1109/PESC.2004.1355492*.

[33] J. E. Huber and A. J. Korn. "Optimized pulse pattern modulation for modular multilevel converter high-speed drive". In: *15th International Power Electronics and Motion Control Conference and Exposition, EPE-PEMC 2012 ECCE Europe* (2012), pp. 1–7. DOI: *10.1109/EPEPEMC.2012.6397383*.

[34] Q. Li, Z. He, and G. Tang. "Investigation of the Harmonic Optimization Approaches in the New Modular Multilevel Converters". In: *2010 Asia-Pacific Power and Energy Engineering Conference* (2010), pp. 1–6. ISSN: 21574839. DOI: *10.1109/APPEEC.2010.5449299*.

[35] F. Gao and R. Iravani. "Dynamic Model of a Space Vector Modulated Matrix Converter". In: *IEEE Transactions on Power Delivery* 22.3 (2007), pp. 1696–1705. ISSN: 0885-8977. DOI: *10.1109/TPWRD.2007.899609*.

[36] F. Bradaschia, E. Ibarra, J. Andreu, I. Kortabarria, E. Ormaetxea, and M. Cavalcanti. "Matrix Converter: Improvement of the Space Vector Modulation via a new double-sided generalized Scalar PWM". In: *2009 35th Annual Conference of IEEE Industrial Electronics*. IEEE, 2009, pp. 4511–4516. ISBN: 978-1-4244-4648-3. DOI: *10.1109/IECON.2009.5414878*.

[37] S. Raju and N. Mohan. "Space vector modulated hybrid indirect multilevel matrix converter". In: *IECON Proceedings (Industrial Electronics Conference)*. 2013. ISBN: 9781479902248. DOI: *10.1109/IECON.2013.6699933*.

[38] Y. Miura, T. Fujikawa, T. Yoshida, and T. Ise. "Control scheme of the modular multilevel matrix converter using space vector modulation for wide frequency range operation". In: *2017 IEEE Energy Conversion Congress and Exposition (ECCE)*. Vol. 2017-Janua. IEEE, 2017, pp. 1084–1091. ISBN: 978-1-5090-2998-3. DOI: *10.1109/ECCE.2017.8095908*.

[39] S. Rohner, S. Bernet, M. Hiller, and R. Sommer. "Modelling, simulation and analysis of a Modular Multilevel Converter for medium voltage applications". In: *2010 IEEE International Conference on Industrial Technology*. IEEE, 2010, pp. 775–782. ISBN: 978-1-4244-5695-6. DOI: *10.1109/ICIT.2010.5472634*.

[40]   D. Guanjun, T. Guangfu, H. Zhiyuan, and D. Ming. "New technologies of voltage source con-
        verter (VSC) for HVDC transmission system based on VSC". In: *2008 IEEE Power and Energy
        Society General Meeting - Conversion and Delivery of Electrical Energy in the 21st Century.*
        IEEE, 2008, pp. 1–8. ISBN: 978-1-4244-1905-0. DOI: *10.1109/PES.2008.4596399.*

[41]   S. Kenzelmann, A. Rufer, D. Dujic, F. Canales, and Y. R. Novaes. "A versatile DC/DC converter
        based on modular multilevel converter for energy collection and distribution". In: *IET Conference
        on Renewable Power Generation (RPG 2011).* Mv. IET, 2011, pp. 71–71. ISBN: 978-1-84919-
        536-2. DOI: *10.1049/cp.2011.0126.*

[42]   S. Norrga, L. Angquist, and A. Antonopoulos. "The polyphase cascaded-cell DC/DC converter".
        In: *2013 IEEE Energy Conversion Congress and Exposition.* IEEE, 2013, pp. 4082–4088. ISBN:
        978-1-4799-0336-8. DOI: *10.1109/ECCE.2013.6647243.*

[43]   L. Baruschka, D. Karwatzki, M. Von Hofen, and A. Mertens. "A new modular multilevel AC/DC
        converter topology applied to a modular multilevel DC/DC converter". In: *2014 16th European
        Conference on Power Electronics and Applications.* IEEE, 2014, pp. 1–10. ISBN: 978-1-4799-
        3015-9. DOI: *10.1109/EPE.2014.6910842.*

[44]   T. Luth, M. M. C. Merlin, T. C. Green, F. Hassan, and C. D. Barker. "High-Frequency Operation
        of a DC/AC/DC System for HVDC Applications". In: *IEEE Transactions on Power Electronics*
        29.8 (2014), pp. 4107–4115. ISSN: 0885-8993. DOI: *10.1109/TPEL.2013.2292614.*

[45]   K. Koska, **P. Blaszczyk**, R. Jez, and P. Klimczak. "Double Wye Modular Multilevel Converter -
        Direct DC-DC Topology". In: *8th IET International Conference on Power Electronics, Machines
        and Drives (PEMD 2016).* Institution of Engineering and Technology, 2016, pp. 6 .–6 . ISBN:
        978-1-78561-188-9. DOI: *10.1049/cp.2016.0185.*

[46]   M. Hagiwara, K. Nishimura, and H. Akagi. "A modular multilevel PWM inverter for medium-
        voltage motor drives". In: *2009 IEEE Energy Conversion Congress and Exposition, ECCE 2009*
        1.c (2009), pp. 2557–2564. DOI: *10.1109/ECCE.2009.5316479.*

[47]   A. Antonopoulos, K. Ilves, L. Angquist, and H. P. Nee. "On interaction between internal con-
        verter dynamics and current control of high-performance high-power AC motor drives with mod-
        ular multilevel converters". In: *2010 IEEE Energy Conversion Congress and Exposition.* IEEE,
        2010, pp. 4293–4298. ISBN: 978-1-4244-5286-6. DOI: *10.1109/ECCE.2010.5618474.*

[48]   A. Antonopoulos, L. Angquist, S. Norrga, K. Ilves, L. Harnefors, and H. P. Nee. "Modular Mul-
        tilevel Converter AC Motor Drives With Constant Torque From Zero to Nominal Speed". In:
        IEEE Transactions on Industry Applications 50.3 (2014), pp. 1982–1993. ISSN: 0093-9994. DOI:
        10.1109/TIA.2013.2286217.

[49] A. Marzoughi, R. Burgos, D. Boroyevich, and Y. Xue. "Investigation and comparison of cascaded H-bridge and modular multilevel converter topologies for medium-voltage drive application". In: *IECON 2014 - 40th Annual Conference of the IEEE Industrial Electronics Society*. IEEE, 2014, pp. 1562–1568. ISBN: 978-1-4799-4032-5. DOI: *10.1109/IECON.2014.7048710*.

[50] M. Hagiwara, R. Maeda, and H. Akagi. "Theoretical Analysis and Control of the Modular Multilevel Cascade Converter Based on Double-Star Chopper-Cells (MMCC-DSCC)". In: *IEEE Transactions on Power Electronics* (2010). ISSN: 08858993.

[51] A. J. Korn, M. Winkelnkemper, P. K. Steimer, and J. W. Kolar. "Direct modular multi-level converter for gearless low-speed drives". In: *Power Electronics and Applications (EPE 2011), Proceedings of the 2011-14th European Conference on* direct MMC (2011), pp. 1–7.

[52] P. K. Steimer, S. Aubert, and S. Linder. "New dimensions in converter fed synchronous machines: (CFSM) for pumped storage plants". In: *HYDRO 2013 - Promoting the Versatile Role of Hydro* (2013).

[53] Y. Wang, W. Zhao, G. Chen, Y. Hu, and M. Wang. "Application of modular multilevel converter in medium voltage high power permanent magnet synchronous generator wind energy conversion systems". In: *IET Renewable Power Generation* 10.6 (2016), pp. 824–833. ISSN: 1752-1416. DOI: *10.1049/iet-rpg.2015.0444*.

[54] **P. Blaszczyk**, K. Koska, and P. Klimczak. "Energy balancing in modular multilevel converter systems". In: *Bulletin of the Polish Academy of Sciences Technical Sciences* 65.5 (2017), pp. 685–694. ISSN: 2300-1917. DOI: *10.1515/bpasts-2017-0073*.

[55] D. Karwatzki and A. Mertens. "Generalized Control Approach for a Class of Modular Multilevel Converter Topologies". In: *IEEE Transactions on Power Electronics* 33.4 (2017), pp. 1–1. ISSN: 0885-8993. DOI: *10.1109/TPEL.2017.2703917*.

[56] H. Akagi. "Classification, Terminology, and Application of the Modular Multilevel Cascade Converter (MMCC)". In: *IEEE Transactions on Power Electronics* 26.11 (2011), pp. 3119–3130. ISSN: 0885-8993. DOI: *10.1109/TPEL.2011.2143431*.

[57] S. Liu, J. Jiang, and Y. Wan. "Generalised analytical methods and current-energy control design for modular multilevel cascade converter". In: *IET Power Electronics* 6.3 (2013), pp. 495–504. ISSN: 1755-4535. DOI: *10.1049/iet-pel.2012.0494*.

[58] M. Winkelnkemper, A. J. Korn, and P. K. Steimer. "A modular direct converter for transformerless rail interties". In: *2010 IEEE International Symposium on Industrial Electronics*. IEEE, 2010, pp. 562–567. ISBN: 978-1-4244-6390-9. DOI: *10.1109/ISIE.2010.5637826*.

[59] M. Glinka and M. Rainer. "A New Single-Phase Multilevel-Converter for Traction Vehicles operating on AC Line Voltage". In: *EPE Journal (European Power Electronics and Drives Journal)* (2003), p. 132.

[60] **P. Blaszczyk**, M. Steurer, D. Soto, F. Bogdan, J. Hauer, M. Sloderbeck, and K. Schoder. "Modular multilevel converter based test bed for mvdc applications — A case study with a 12 kV, 5 MW setup". In: *2016 IEEE International Power Electronics and Motion Control Conference (PEMC)*. IEEE, 2016, pp. 139–145. ISBN: 978-1-5090-1798-0. DOI: *10.1109/EPEPEMC.2016.7751988*.

[61] J. Kucka, D. Karwatzki, and A. Mertens. "AC/AC modular multilevel converters in wind energy applications: Design considerations". In: *2016 18th European Conference on Power Electronics and Applications, EPE 2016 ECCE Europe* (2016), pp. 1–10. DOI: *10.1109/EPE.2016.7695542*.

[62] S. Angkititrakul and R. W. Erickson. "Control and Implementation of a New Modular Matrix Converter". In: *Nineteenth Annual IEEE Applied Power Electronics Conference and Exposition, 2004. APEC '04.* 00.C (2004), pp. 813–819. DOI: *10.1109/APEC.2004.1295916*.

[63] P. W. Wheeler, F. J. Rodriguez, J. C. Clare, L. Empringham, and A. Weinstein. "Matrix converters: a technology review". In: *IEEE Transactions on Industrial Electronics* 49.2 (2002), pp. 276–288. ISSN: 0278-0046. DOI: *10.1109/41.993260*.

[64] K. Ilves, L. Bessegato, and S. Norrga. "Comparison of cascaded multilevel converter topologies for AC/AC conversion". In: *2014 International Power Electronics Conference, IPEC-Hiroshima - ECCE Asia 2014* (2014), pp. 1087–1094. DOI: *10.1109/IPEC.2014.6869722*.

[65] J. Ma, M. Dahidah, V. Pickert, and J. Yu. "Modular multilevel matrix converter for offshore low frequency AC transmission system". In: *2017 IEEE 26th International Symposium on Industrial Electronics (ISIE)*. IEEE, 2017, pp. 768–774. ISBN: 978-1-5090-1412-5. DOI: *10.1109/ISIE.2017.8001343*.

[66] L. Baruschka and A. Mertens. "A new 3-phase direct modular multilevel converter". In: *Proceedings of the 2011 14th European Conference on Power Electronics and Applications* 2.2 (2011), pp. 1–10. ISSN: 0095-3997. DOI: *10.1177/0095399703256775*.

[67] D. Karwatzki, L. Baruschka, and A. Mertens. "Survey on the Hexverter topology - A modular multilevel AC/AC converter". In: *2015 9th International Conference on Power Electronics and ECCE Asia (ICPE-ECCE Asia)*. IEEE, 2015, pp. 1075–1082. ISBN: 978-8-9570-8254-6. DOI: *10.1109/ICPE.2015.7167914*.

[68] J. M. Erdman, R. J. Kerkman, D. W. Schlegel, and G. L. Skibinski. "Effect of PWM inverters on AC motor bearing currents and shaft voltages". In: *IEEE Transactions on Industry Applications* 32.2 (1996), pp. 250–259. ISSN: 00939994. DOI: *10.1109/28.491472*.

[69] D. Karwatzki, L. Baruschka, J. Kucka, M. Von Hofen, and A. Mertens. "Improved hexverter topology with magnetically coupled branch inductors". In: *2014 16th European Conference on Power Electronics and Applications, EPE-ECCE Europe 2014* Mmmc (2014). DOI: *10.1109/EPE.2014.6910845*.

[70] K. Koska. "Nieizolowany Wielopoziomowy Przekształtnik Modułowy DC/DC typu YY". PhD thesis. AGH University of Science and Technology, 2017.

[71]   C. D. Barker, C. C. Davidson, D. R. Trainer, and R. S. Whitehouse. "Requirements of DC-DC converters to facilitate large DC grids (B4-204)". In: *CIGRE , Bologna, Paris* Lcc (2012), pp. 1–10. DOI: *10.1152/ajpregu.00362.2004*.

[72]   K. Koska, **P. Blaszczyk**, P. Klimczak, P. Halat, and R. Jez. "Branch energy balancing of double wye DC-DC Modular Multilevel Converter". In: *2017 19th European Conference on Power Electronics and Applications (EPE'17 ECCE Europe)*. IEEE, 2017, P.1–P.10. ISBN: 978-90-75815-27-6. DOI: *10.23919/EPE17ECCEEurope.2017.8098932*.

[73]   L. Baruschka and A. Mertens. "Comparison of Cascaded H-Bridge and Modular Multilevel Converters for BESS application". In: *2011 IEEE Energy Conversion Congress and Exposition*. IEEE, 2011, pp. 909–916. ISBN: 978-1-4577-0542-7. DOI: *10.1109/ECCE.2011.6063868*.

[74]   P. Himmelmann. "A Generalized Approach to the Analysis and Control of Modular Mul- tilevel Converters". In: *PCIM Europe 2017*. May. 2017, pp. 16–18. ISBN: 9783800744244.

[75]   T. D. Nguyen and H. H. Lee. "Development of a Three-to-Five-Phase Indirect Matrix Converter With Carrier-Based PWM Based on Space-Vector Modulation Analysis". In: *IEEE Transactions on Industrial Electronics* 63.1 (2016), pp. 13–24. ISSN: 0278-0046. DOI: *10.1109/TIE.2015.2472359*.

[76]   S. Bolkowski. *Teoria Obwodów Elektrycznych*. Wydawnictwo Naukowe PWN SA, 2017.

[77]   Robert Meyers, ed. *Encyclopedia of Physical Science and Technology 3rd Edition*. Academic Press, 2001.

[78]   J. Wang, R. Burgos, and D. Boroyevich. "Switching-Cycle State-Space Modeling and Control of the Modular Multilevel Converter". In: *Emerging and Selected Topics in Power Electronics, IEEE Journal of* PP.99 (2014), p. 1. ISSN: 2168-6777. DOI: *10.1109/JESTPE.2014.2354393*.

[79]   S. Rohner, S. Bernet, M. Hiller, and R. Sommer. "Analysis and Simulation of a 6 kV, 6 MVA Modular Multilevel Converter". In: *2009 35th Annual Conference of IEEE Industrial Electronics*. IEEE, 2009, pp. 225–230. ISBN: 978-1-4244-4648-3. DOI: *10.1109/IECON.2009.5414775*.

[80]   MICROSEMI. *Park, Inverse Park And Clarke, Inverse Clarke Software, Transformations MSS Implementation. User Guide*. 2013.

[81]   N. Oo. "On Harmonic Addition Theorem". In: *International Journal of Computer and Communication Engineering* 1.3 (2012), pp. 200–202. ISSN: 20103743. DOI: *10.7763/IJCCE.2012.V1.52*.

[82]   **P. Blaszczyk**. "Low Frequency Mode Operation for Direct ac-ac Modular Multilevel Converter Systems. A Comparison of M3C and Hex-Y Topology". In: *2019 21st European Conference on Power Electronics and Applications (EPE '19 ECCE Europe)*. IEEE, 2019, P.1–P.10. ISBN: 978-9-0758-1531-3. DOI: *10.23919/EPE.2019.8915378*.

[83] ABB. "Control IT AC 800PEC Control System The modular controller for high-speed performance". In: *Online - http://www04.abb.com/global/seitp/seitp202.nsf/0/5e16be0cfa73bc6bc125714e00501c63/ $file/AC+800PEC+control+system.pdf* (2004).

[84] ABB. "AC 800PEC The high-performance control system for model-based design". In: *Online - https://library.e.abb.com/public/a7566254919255a0c12578c3003355f7/AC 800PEC Sales Brochure.pdf* (2011).

[85] ABB. "UA D144 A01 AC 800PEC Measurement Interface UA D144 A01 AC 800PEC Measurement Interface". In: *ABB Switzerland Ltd, Power Electronics* (2003), pp. 1–2.

[86] ABB. "ABB Review 1/14". In: *ABB* 1 (2014), pp. 24–27.

[87] ABB. "UA D142 AC 800PEC Combi IO Mixed Module Data Sheet". In: *ABB Switzerland Ltd, Power Electronics* (2004).

[88] M. Nowak and S. Piróg. "Simulation studies of the proportional resonant controller". In: *Przeglad Elektrotechniczny* 94.6 (2018), pp. 128–131. ISSN: 24499544. DOI: *10.15199/48.2018.06.24*.

[89] W. Li and J. Belanger. "An Equivalent Circuit Method for Modelling and Simulation of Modular Multilevel Converters in Real-Time HIL Test Bench". In: *IEEE Transactions on Power Delivery* 31.5 (2016), pp. 2401–2409. ISSN: 0885-8977. DOI: *10.1109/TPWRD.2016.2541461*.

[90] C. Versteegh and G. Hassan. "Design of the Zephyros Z72 wind turbine with emphasis on the direct drive PM generator". In: *Proc. of the Nordic workshop on power and industrial electronics (NORPIE)* 31.0 (2004), pp. 14–16.

[91] **P. Blaszczyk**, M. Winkelnkemper, and L. Schwager. "Converter energy balancing in MMC system energy sharing using master controller". In: *2015 International Conference on Electrical Drives and Power Electronics (EDPE)*. IEEE, 2015, pp. 30–37. ISBN: 978-1-4673-7376-0. DOI: *10.1109/EDPE.2015.7325265*.

[92] **P. Blaszczyk**, M. Steurer, D. Soto, M. Bosworth, and M. Winkelnkemper. "Power balancing in multi-converter systems composed of modular multilevel converters (MMCs)". In: *2016 18th European Conference on Power Electronics and Applications (EPE'16 ECCE Europe)*. IEEE, 2016, pp. 1–10. ISBN: 978-9-0758-1524-5. DOI: *10.1109/EPE.2016.7695321*.

[93] European Union. "Commission Regulation (EE) 2016/631 establishing a network code on requirements for grid connection of generators". In: *Official Journal of the European Union* 14 April 2016 (2016), p. 68.

[94] B. Weise. "Impact of K-factor and active current reduction during fault-ride-through of generating units connected via voltage-sourced converters on power system stability". In: *IET Renewable Power Generation* 9.1 (2015), pp. 25–36. ISSN: 1752-1416. DOI: *10.1049/iet-rpg.2014.0116*.

[95]   Deutsche Energie-Agentur GmbH (dena). "Zusammenfassung der wesentlichen Ergebnisse der Studie „Energiewirtschaftliche Planung für die Netzintegration von Windenergie in Deutschland an Land und Offshore bis zum Jahr 2020"". In: *Online* (2005), pp. 1–23.

[96]   H. Berndt, M. Hermann, H. Kreye, R. Reinisch, U. Scherer, and J. Vanzetta. "TransmissionCode 2007 Network and System Rules of the German Transmission System Operators". In: *VDN* August (2007).

[97]   SDL WindV. *Ordinance on System Services by Wind Energy Plants (System Service Ordinance – SDLWindV) A*. 2020.

[98]   EirGrid. *Ireland Grid Code*. 2013.

[99]   T. Heir. *The grid code - Issue 5, Revision 21*. 5. National Grid, 2017. ISBN: 7977433974.

[100] M. Florkowski, **P. Blaszczyk**, and P. Klimczak. "Partial discharges in twisted-pair magnet wires subject to multilevel PWM pulses". In: *IEEE Transactions on Dielectrics and Electrical Insulation* 24.4 (2017), pp. 2203–2210. ISSN: 1070-9878. DOI: *10.1109/TDEI.2017.006313*.

Anti Plagiarism Notice